NEW INSIGHTS IN *MYCOBACTERIUM TUBERCULOSIS*

EDITED BY: Natarajaseenivasan Kalimuthusamy
PUBLISHED IN: Frontiers in Cellular and Infection Microbiology

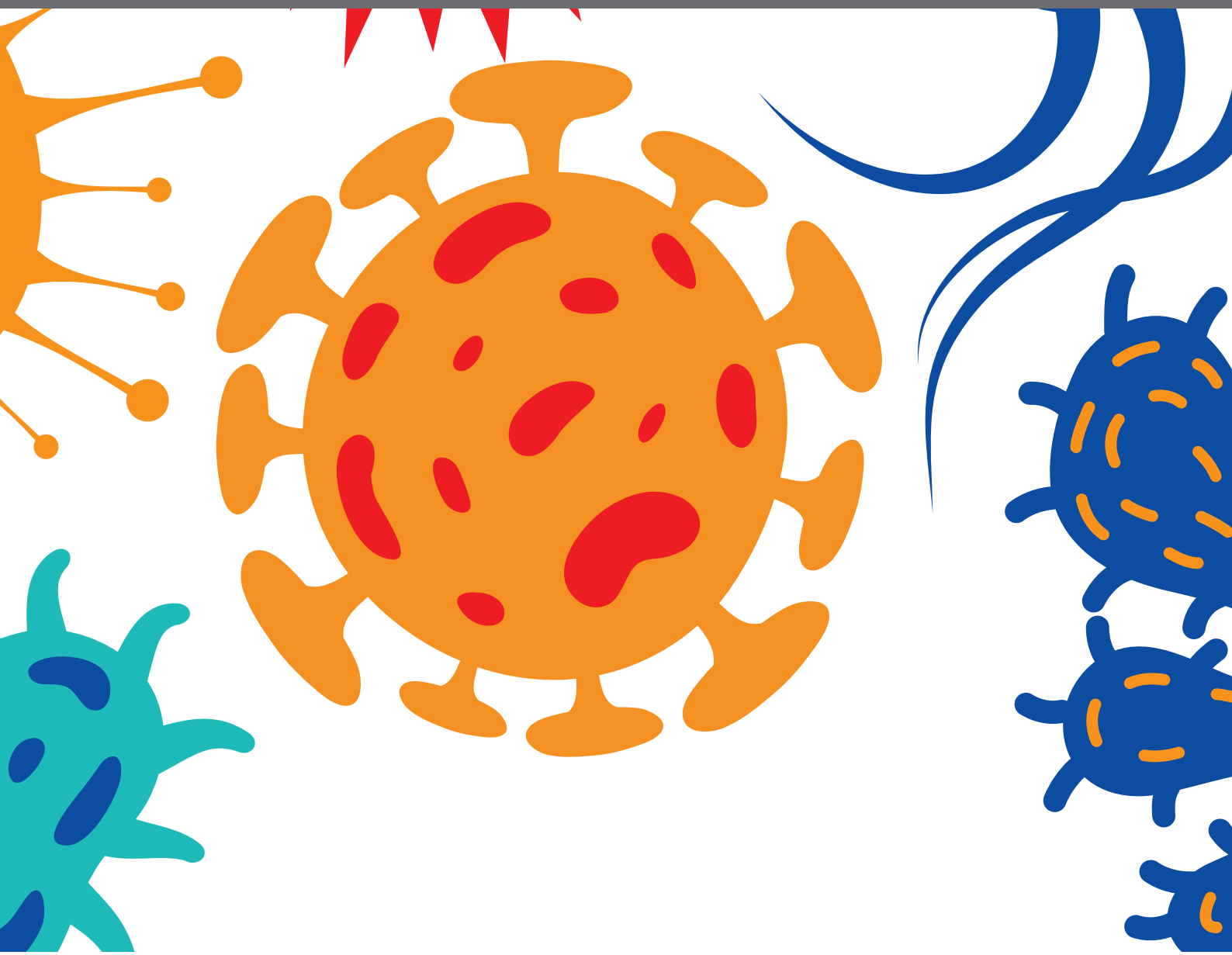

frontiers Research Topics

frontiers

ISSN 1664-8714
ISBN 978-2-83250-611-0
DOI 10.3389/978-2-83250-611-0

About Frontiers

Frontiers is more than just an open-access publisher of scholarly articles: it is a pioneering approach to the world of academia, radically improving the way scholarly research is managed. The grand vision of Frontiers is a world where all people have an equal opportunity to seek, share and generate knowledge. Frontiers provides immediate and permanent online open access to all its publications, but this alone is not enough to realize our grand goals.

Frontiers Journal Series

The Frontiers Journal Series is a multi-tier and interdisciplinary set of open-access, online journals, promising a paradigm shift from the current review, selection and dissemination processes in academic publishing. All Frontiers journals are driven by researchers for researchers; therefore, they constitute a service to the scholarly community. At the same time, the Frontiers Journal Series operates on a revolutionary invention, the tiered publishing system, initially addressing specific communities of scholars, and gradually climbing up to broader public understanding, thus serving the interests of the lay society, too.

Dedication to Quality

Each Frontiers article is a landmark of the highest quality, thanks to genuinely collaborative interactions between authors and review editors, who include some of the world's best academicians. Research must be certified by peers before entering a stream of knowledge that may eventually reach the public - and shape society; therefore, Frontiers only applies the most rigorous and unbiased reviews.
Frontiers revolutionizes research publishing by freely delivering the most outstanding research, evaluated with no bias from both the academic and social point of view. By applying the most advanced information technologies, Frontiers is catapulting scholarly publishing into a new generation.

What are Frontiers Research Topics?

Frontiers Research Topics are very popular trademarks of the Frontiers Journals Series: they are collections of at least ten articles, all centered on a particular subject. With their unique mix of varied contributions from Original Research to Review Articles, Frontiers Research Topics unify the most influential researchers, the latest key findings and historical advances in a hot research area! Find out more on how to host your own Frontiers Research Topic or contribute to one as an author by contacting the Frontiers Editorial Office: frontiersin.org/about/contact

NEW INSIGHTS IN *MYCOBACTERIUM TUBERCULOSIS*

Topic Editor:
Natarajaseenivasan Kalimuthusamy, Bharathidasan University, India

Citation: Kalimuthusamy, N., ed. (2022). New Insights in *Mycobacterium Tuberculosis*. Lausanne: Frontiers Media SA. doi: 10.3389/978-2-83250-611-0

Table of Contents

frontiers | Frontiers in Cellular and Infection Microbiology

TYPE Editorial
PUBLISHED 13 October 2022
DOI 10.3389/fcimb.2022.1020267

OPEN ACCESS

EDITED BY
Mariola J. Edelmann,
University of Florida, United States

REVIEWED BY
Md. Aejazur Rahman,
Africa Health Research Institute (AHRI), South Africa
Marta Alonso-Hearn,
Basque Institute for Agricultural Research and Development-Basque Research and Technology Alliance (BRTA), Spain

*CORRESPONDENCE
Kalimuthusamy Natarajaseenivasan
natarajaseenivasan@bdu.ac.in

SPECIALTY SECTION
This article was submitted to Bacteria and Host, a section of the journal Frontiers in Cellular and Infection Microbiology

RECEIVED 16 August 2022
ACCEPTED 30 September 2022
PUBLISHED 13 October 2022

CITATION
Natarajaseenivasan K (2022) Editorial: New insights in *Mycobacterium tuberculosis*. *Front. Cell. Infect. Microbiol.* 12:1020267. doi: 10.3389/fcimb.2022.1020267

Editorial: New insights in *Mycobacterium tuberculosis*

Kalimuthusamy Natarajaseenivasan[1,2]*

[1]Department of Microbiology, Bharathidasan University, Tiruchirappalli, India, [2]Department of Neural Sciences, Lewis Katz School of Medicine, Temple University, Philadelphia, PA, United States

KEYWORDS

***Mycobacterium tuberculosis*, risk factors, diagnosis, biomarkers, therapy**

Editorial on the Research Topic
New insights in *Mycobacterium tuberculosis*

Tuberculosis (TB), resulting from infection by the bacterium *Mycobacterium tuberculosis (Mtb)*, is one of the top 10 causes of death worldwide as per the World Health Organization (WHO). Approximately one-third of the World's population is latently infected with *Mtb*, and this has a dramatic impact on the quality of life of the patients. To improve the battle against *Mtb*, we first need to understand the host-pathogen interactions. Secondly, developing new diagnostic tools or improving the sensitivity of the one already existing will help diagnose the disease in patients effectively, this will allow early treatment of the infected persons to avoid the late stage of the disease and its spread to others. This should be followed by developing some improvised therapeutic approaches.

Our Research Topic entitled "*New Insights in Mycobacterium tuberculosis*" emphasized the submission of original research papers describing novel approaches to understanding molecular pathogenesis, improvised diagnosis, and therapeutics with clinical trials. The overwhelming response from the authors indeed excited us and resulted in 10 articles with more than 12,000 views so far. These interesting novel works will benefit the readers and society.

Our collection includes exciting work about relapse, re-infection, and the current situation of recurrence of TB in Jiangsu, China (Shao et al.). In this work, they adapted population-based surveillance on culture-positive TB cases and systematically implemented MIRU-VNTR for drug resistance and genotype detection. The outcome of the study revealed that relapse and re-infection contributed equally to the situation of recurrence of TB in Jiangsu, China.

Ning et al. practiced the subunit vaccine ESAT-6:c-di-AMP through the intranasal route, which elicited a significant immune response to protect against *M. tuberculosis* infection. The developed subunit vaccine could elicit innate and adaptive immune responses and protected against *Mtb* challenges and c-di-AMP being a mucosal adjuvant enhanced the innate immunity and is a preferred candidate for a mucosal vaccine against TB.

Since the speedy diagnosis of pulmonary tuberculosis (PTB) remains a task during clinical practice. Peng et al. addressed this issue by optimizing an algorithm for rapid diagnosis of PTB in a real-world setting. Their significant contribution by concurrently performing AFB smear and Xpert MTB/RIF assay on sputum and/or BALF could aid in rapid diagnosis of PTB and nontuberculous mycobacteria (NTM) infections in a real-world high-burden setting using reasonable sample replicates.

A few bacilli can hide and live inside the host mesenchymal stem cells (MSC) and that leads to futile therapeutics often. Aqdas et al. presented an exhilarating work to clear this cellular bacillus using immunotherapy-based approaches. Cumulative signaling through NOD-2 and TLR-4 could eliminate *M. tuberculosis* and significantly reduce the intracellular survival of *Mtb* in the MSC. Overall, their results suggest that the triggering through N2.T4 can be a future method of immunotherapy to eliminate the *Mtb* concealed inside the MSC.

STAT3 had a great effect on fast-acting innate immunity against *Mtb* and it also has an important role in biological balance. Wang et al. hypothesized that STAT3 SNP down-regulation of STAT3 leads to a change in susceptibility to TB in humans. They experimented with their hypothesis in a case-control study of TB patients and healthy control (HC) subjects, then conducted a functional analysis using cellular models. Their innovative finding suggests that low constitutive STAT3 derived from the T/A genotype/T-A haplotype acts to down-regulate STAT3, depressing multiple anti-mycobacterial pathways/mechanisms downstream, which leads to an enhanced mycobacterial infection or TB in high-risk individuals.

Jorgensen et al. explored the effect of cyclooxygenase 2 inhibitor (COX-2i) treatment on eicosanoid levels and signaling pathways in monocytes. Eicosanoids and intracellular signaling pathways are potential targets for host-directed therapy (HDT) in TB. The systematic outcome of this study showed that COX-2i may reduce excess inflammation in TB *via* the lipoxygenase (LOX) pathway in addition to modulation of phosphorylation patterns in monocytes. Immunomodulatory effects of adjunctive COX-2i in TB may be used as an HDT strategy.

Indeed, *Mtb* inhibits autophagy to support its survival in host cells, even though the molecular mechanisms behind this process are not well established. Sengupta et al. magnificently established the mechanistic way of the *Mtb* inhibition of autophagy. They identified the *Mtb* phosphoribosyltransferase (MTB-PRT) inhibits autophagy in an mTOR-independent manner in *Mtb* infected macrophages.

People with type 2 diabetes (T2D) are a known risk factor for TB. Therefore, T2D increases the individual's susceptibility to incident TB. Sinha et al. attentively developed a preclinical model of pre-diabetes and TB. The developed murine model offers the opportunity to further study the underlying immunological, metabolic, and endocrine mechanisms of the association between T2D and TB. Their finding demonstrated that pre-diabetes increases susceptibility to TB, but a high body mass index without dysglycemia is protective.

Chen et al. systematically discovered novel potential diagnostic serum biomarkers of metabolomics in osteoarticular TB patients. Osteoarticular TB is one of the forms of extrapulmonary TB. As it is already described above that TB is caused by Mtb infection. Since metabolomics is used to study the changes in the body's metabolites during different states, it is important means of discovery of disease-related metabolic biomarkers and the corresponding mechanism research. This group has identified several biomarkers and they had high diagnostic values.

Miliary pulmonary TB in pregnant women after *in vitro* fertilization-embryo transfer (IVF-ET) leads to poor outcomes, which needs more emphasis. Dong et al. analyzed the clinical features and risk factors in pregnant women with miliary pulmonary TB after IVF-ET. Their finding denotes that tube infertility with underscreened or untreated TB is a risk factor for miliary TB during pregnancy after IVF-ET.

This exceptional compilation of articles on our Research Topic gives new insights into the risk factors associated with *Mtb*, molecular pathogenesis, improvised diagnosis, and therapeutics. This also offers novel approaches to fight this notorious pathogen *Mtb*. We thank all the reviewers for their comments that improvised the manuscripts, and we also thank all the authors for their novel exceptional contributions.

Author contributions

The author confirms being the sole contributor of this work and has approved it for publication.

Conflict of interest

The author declares that the research was conducted in the absence of any commercial or financial relationships that could be construed as a potential conflict of interest.

Publisher's note

frontiers in Cellular and Infection Microbiology

ORIGINAL RESEARCH
published: 17 March 2021
doi: 10.3389/fcimb.2021.638990

Relapse or Re-Infection, the Situation of Recurrent Tuberculosis in Eastern China

Yan Shao[1], Honghuan Song[1], Guoli Li[1], Yan Li[1], Yishu Li[2], Limei Zhu[1], Wei Lu[1] and Cheng Chen[1]**

[1] Department of Chronic Communicable Disease, Center for Disease Control and Prevention of Jiangsu Province, Nanjing, China, [2] Department of Epidemiology and Statistics, School of Public Health, Southeast University, Nanjing, China

Purpose: Recurrent tuberculosis (TB) is defined by more than one TB episode per patient and is caused by re-infection with a new *Mycobacterium tuberculosis* (Mtb) strain or relapse with the previous strain. Recurrence of TB is one important obstacle for End TB strategy in the world and elucidating the triggers of recurrence is important for the current TB control strategy in China. This study aimed to analyze the sources of recurrent TB by the molecular genotyping method.

Method: A population-based surveillance was undertaking on all culture-positive TB cases in Jiangsu province, China from 2013 to 2019. Phenotypic drug susceptibility test (DST) by proportion method and mycobacterial interspersed repetitive units-variable number of tandem repeat (MIRU-VNTR) were adopted for drug resistance and genotype detection.

Results: A total of 1451 culture-positive TB patients were collected and 30 (2.06%, 30/1451) TB cases had recurrent TB episodes. Except 7 isolates were failed during subculture, 23 paired isolates were assessed. After genotyping by MIRU-VNTR, 12 (52.17%, 12/23) paired recurrence TB were demonstrated as relapse and 11 (47.83%,11/23) paired cases were identified as re-infection. The average interval time for recurrence was 24.04 (95%CI: 19.37-28.71) months, and there was no significant difference between relapse and re-infection. For the relapsed cases, two paired isolates exhibited drug resistance shifting, while four paired isolates revealed inconsistent drug resistance among the re-infection group including two multidrug-resistant tuberculosis (MDR-TB) at the second episode.

Conclusion: Relapse and re-infection contributed equally to the current situation of recurrence TB in Jiangsu, China. Besides, more efficient treatment assessment, specific and vigorous interventions are urgently needed for MDR-TB patients, considering obvious performance among re-infection cases.

Keywords: recurrence, relapse, re-infection, MIRU-VNTR, tuberculosis

OPEN ACCESS

Edited by:
Rodnei Dennis Rossoni, Sao Paulo State University, Brazil

Reviewed by:
Deepak Saxena, New York University, United States
Troels Lillebaek, Statens Serum Institut (SSI), Denmark

****Correspondence:***
Cheng Chen
chencheng128@gmail.com
orcid.org/0000-0002-6663-3113
Wei Lu
weiluxx@163.com

Specialty section:
This article was submitted to Bacteria and Host, a section of the journal Frontiers in Cellular and Infection Microbiology

Received: *08 December 2020*
Accepted: *01 March 2021*
Published: *17 March 2021*

Citation:
Shao Y, Song H, Li G, Li Y, Li Y, Zhu L, Lu W and Chen C (2021) Relapse or Re-Infection, the Situation of Recurrent Tuberculosis in Eastern China. Front. Cell. Infect. Microbiol. 11:638990. doi: 10.3389/fcimb.2021.638990

INTRODUCTION

Tuberculosis (TB) is an old communicable disease and the leading cause of death from a single infectious agent. Globally, it was estimated 10.0 million people fell ill with TB in 2018, and only 7.0 million TB patients were notified and reported to WHO as new or relapse cases. China still ranks in the 30 high TB burden countries with a total incidence rate of 61 per 100000 population in 2018 (WHO, 2019). Although China obtained tremendous successes in controlling the TB epidemic in the past years, it is not on track to reach the target of End TB Strategy yet. There are many challenges faced by clinical and national TB control programs to achieve the targets even with improvements in TB diagnosis, treatment and prevention. One such obstacle is the recurrence of TB which varied by country and region according to previous studies (Hozbor et al., 2017; Wingfield et al., 2019). A combined analysis of the mathematical model revealed that further reducing new TB cases only has a modest effect on disease burden, but interventions that restrain reactivation have a greater improvement on disease burden in China (Houben et al., 2016).

Either endogenous reactivation or exogenous infection could result in a new episode of TB even after a complete anti-TB treatment. Comparing the isolates from the first and second episodes of TB could distinguish such two different causes. It was commonly considered that two episodes with identical isolates as a relapse, otherwise, it means exogenous infection or namely re-infection. However, under special circumstances with a dominant cluster of TB strain, the possibility of a re-infection by identical genotypes could not be overlooked as well (Folkvardsen et al., 2020). In this study, patients with identical strain genotype were considered a potential relapse, otherwise a re-infection. In the high TB incidence region, re-infection would be the principal reason for recurrent TB (Bryant et al., 2013a). Genotyping methods for *Mycobacterium tuberculosis complex* (MTBC), such as spoligotyping and mycobacterial interspersed a repetitive units-variable number of tandem repeat (MIRU-VNTR) typing, which utilize variations in repetitive sequences in MTBC strains, enable researchers to discriminate relapse and re-infection (Oelemann et al., 2007). The different type of recurrent TB requires a specific control strategy. If re-infection accounted for the majority of TB recurrence, a powerful control strategy of infection control should be adopted. Otherwise, effective treatment of TB should be reinforced. Some studies have demonstrated recurrent TB in China by molecular epidemiology, but they proposed quite different results about the proportion of re-infection (Nsofor et al., 2017; Zong et al., 2018). So we conduct this retrospective study to evaluate relapse and re-infection among those recurrent TB patients in eastern China. Meanwhile, we adopted the profiles of demographic characteristics of TB cases and drug-resistant patterns of isolates to explore the potential effect on the recurrent TB.

METHODS

Study Population

This study was undertaken in TB drug resistance surveillance spots in Jiangsu Province which were established according to national survey of drug-resistant TB (Zhao et al., 2012). During 2013-2019, all newly registered pulmonary TB patients with either sputum smear-positive or molecular testing positive were consecutively collected after an informed consent was obtained. Furthermore, sputum samples were performed culture on Lowenstein-Jensen (LJ) media as well. Finally, a total of 1451 culture-positive TB patients were collected, including new cases and previously treated cases (WHO, 2009). Those TB patients were followed up by the National Health Management and Information System (HMIS), and we found that 30 patients presented the second episode of TB. The isolates from recurrent TB patients which conserved with cryoprotectant at -80°C were thawed and re-cultured on L-J media in our provincial TB laboratory. Except 7 isolates were failed in the subculture, twenty-three pairs of cases were finally enrolled for further analysis. Meanwhile, the interval time between the first and second episodes and the demographic features were collected.

Treatment and Follow-Up

Without obtaining the drug-resistant information, the treatment regimen was prescribed based on the history of TB treatment, and all the cases were classified into new cases and previously treated cases. All recruited new cases were treated with standard 2HRZE/4HR regimens, which started with 2 months of daily isoniazid (H), rifampicin (R), pyrazinamide (Z), and ethambutol (E), then followed by daily isoniazid (H) and rifampicin (R) for another 4 months. Meanwhile, for previously treated cases, streptomycin (S) was added to the four drugs (HRZE) daily for 2 months and then three drugs (HRE) daily lasting to 6 months (2HRZES/6HRE) (WHO, 2010). The detailed treatment regimens and durations were list in **Table 1**. We followed up all cases from treatment initiate to recurrence of TB during the study period.

Drug Susceptibility Test

All subcultured positive isolates were analyzed by phenotypic drug susceptibility test (DST) by proportion method on Lowenstein–Jensen (L-J) media (Baso, Zhuhai, China). The p-nitrobenzoic acid (PNB) test was adopted for *non-tuberculosis* mycobacterium (NTM) identification. DST performed on L-J media adopted the following critical drug concentrations: rifampicin 40μg/ml, isoniazid 0.2μg/mL, streptomycin 4μg/mL, and ethambutol 2μg/mL respectively (WHO, 2009).

DNA Extraction

About two loops of the bacterial growth were scraped from L-J media (Baso, Zhuhai, China) and placed into the 500μl of 75% ethanol bath in a microcentrifuge tube. Then, the sample was sterilized in the 75% ethanol bath for 1 hour after 5 minutes of ultrasound. After centrifuging with 12,000 g for 3 min, the supernatant was discarded. The sample was resuspended in 200μl of 20mg/ml lysozyme solution (Sangon Biotech, Shanghai, China) with glass powder for DNA releasing thoroughly. The following steps were referred to chemical lysis with cetyltrimethylammonium bromide (CTAB) method. In general, CTAB-NaCl solution was added and incubated at 65°C

TABLE 1 | Drug resistance status and clinical information depending on recurrence type.

Recurrence type	NO. pair	Interval time (month)	Treatment regimen for the first episode	Drug Resistance Status		Chest X-ray of the first episode: cavitation
				First episode	Second episode	
re-infection	2	10	2HRZE/4HR	susceptible	susceptible	Yes
	3	33	2HRZES/6HRE	resistant to R,H, S	susceptible	Yes
	5	23	2HRZES/6HRE	susceptible	susceptible	No
	8	21	2HRZE/4HR	susceptible	susceptible	Yes
	11	22	2HRZES/6HRE	susceptible	susceptible	Yes
	14	45	2HRZE/4HR	susceptible	resistant to R,H, S	Yes
	15	16	2HRZES/6HRE	susceptible	resistant to R,H, S	No
	16	19	2HRZE/4HR	susceptible	susceptible	No
	18	38	2HRZE/4HR	resistant to H	resistant to H	No
	20	25	2HRZE/4HR	susceptible	resistant to H,S	Yes
	22	11	2HRZE/4HR	susceptible	susceptible	No
relapse	1	9	2HRZES/6HRE	susceptible	susceptible	No
	4	22	2HRZES/6HRE	susceptible	susceptible	Yes
	6	54	2HRZE/4HR	resistant to R	susceptible	No
	7	26	2HRZE/4HR	susceptible	susceptible	Yes
	9	26	2HRZE/4HR	susceptible	susceptible	Yes
	10	16	2HRZE/4HR	susceptible	susceptible	No
	12	26	2HRZE/4HR	susceptible	susceptible	No
	13	26	2HRZE/4HR	susceptible	susceptible	No
	17	24	2HRZE/4HR	susceptible	susceptible	Yes
	19	13	2HRZES/6HRE	resistant to H	resistant to R,H, E	No
	21	29	2HRZES/6HRE	susceptible	susceptible	Yes
	23	19	2HRZE/4HR	susceptible	susceptible	No

R, rifampicin; H, isoniazid; S, streptomycin; Z, pyrazinamide; E, ethambutol.

for 10 minutes, then the mixture of Chloroform: isoamyl alcohol (24:1) mixture was added followed by a centrifuge of 12000 g for 5 min. Wash the sample again with Chloroform: isoamyl alcohol mixture and remove the upper phase to a new tube with cold isopropanol, after gentle mixture and the solution was frozen for at least 30 min. After thawing and washed with 70% cold ethanol, the solution was centrifuged for 20 minutes at 12000g. Finally, the supernatant was discarded and dried pellets were resuspended in 50μl of Tris-EDTA (TE) buffer (Yates et al., 2002).

MIRU-VNTR Analysis

The standard 24 loci were performed for genotyping of *Mycobacterium tuberculosis* according to Supply et al. (2006) After amplification of extracted DNA, PCR products were examined by 1.5% agarose gel. To analyze the genetic relationship between the first and second episodes, the web application MIRU-VNTRplus was adopted, and the re-infection case was defined as paired isolates with different MIRU-VNTR patterns at two or more than two loci according to phylogenetic lineage identification (Interrante et al., 2015; Maghradze et al., 2019).

Statistical Analysis

The questionnaire was double entered in EpiData 3.1 (EpiData Association, Odense, Denmark). Person chi-square test or Fisher's exact test were used to compare the categorical variables, and *t*-test was applied for the continuous variables. All analyses were performed using SAS 9.3 software (SAS Institute, Inc., Cary, NC, USA) and $P<0.05$ was considered statistically significant.

RESULTS

During the study period, a total of 1451 TB patients from tertiary hospitals provided positive cultures and up to 2% (30/1451) were observed recurrence after completion of anti-TB treatment. Except 7 isolates failed in the subculture, 23 pairs of isolates were undergoing the MIRU-VNTR method to distinguish the genotypes (**Figure 1**). For the 23 recurrent patients, the mean age was 49.48 ± 22.71 years, and the male gender accounted 82.60% (19/23). According to the treatment history, new cases accounted 65.22% (15/23) of the total. The chest X-ray indicated that 47.83% (11/23) recurrent TB patients had cavitation for the first episodes.

Considering the power of discrimination, 24 loci were adopted in this study, and the genotype results based on MIRU-VNTR of each isolate were demonstrated in **Figure 2**. Out of 23 pairs of isolates, 12 (52.17%, 12/23) pairs exhibited consistent genotype patterns by the minimum spanning tree algorithm, while another 11 (47.83%,11/23) pairs of isolates exhibited different MIRU-VNTR patterns at more than two loci (**Figure 2**). There is no significant difference between

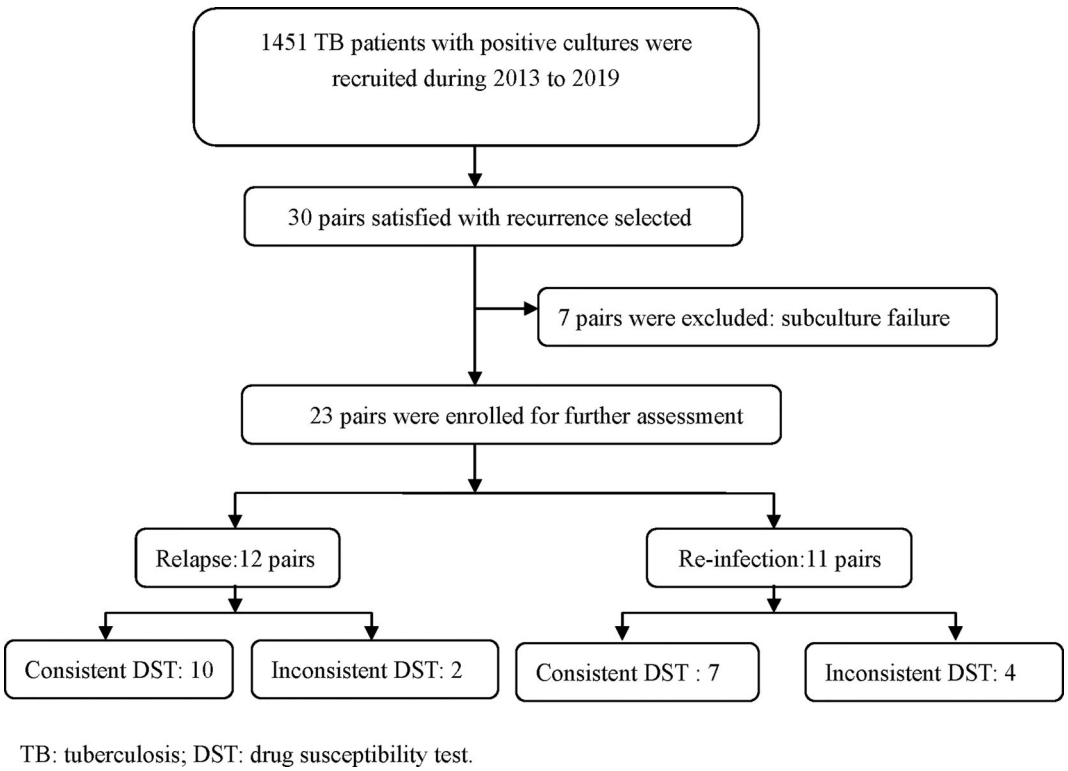

FIGURE 1 | Study flow for case enrollment.

relapse and re-infection for age (t=0.835, P=0.413), gender (P=0.640), and cavitation (P=0.381).

For those 23 TB cases, the average interval time between the first and second episodes was 24.04 months (95%CI:19.37-28.71). Meanwhile, the average interval periods between the first and second episodes for the relapsed cases and re-infected cases were 24.17 and 23.91 months, respectively (P=0.7) (**Figure 3**).

We further compared drug susceptibility profiles between relapsed and re-infected TB cases. Out of those 12 relapsed cases, there were two pairs detected with inconsistent DST results, one exhibited change from isoniazid-resistance to MDR, while another rifampicin-resistant isolate was transformed to susceptible isolate in the second episode. Meanwhile, there were four inconsistent drug-susceptibility results among the re-infection group. In general, two susceptible isolates were replaced by MDR isolates, and one another susceptible isolate was replaced by isoniazid and streptomycin-resistant isolate. Besides, one MDR patient was found reverted to susceptible in the second episode (**Table 1**).

DISCUSSION

The emerging of recurrent TB posed a great challenge for the national TB elimination program in China. Previous studies indicated that recurrent TB patients required longer diagnostic delay time compared to new cases, which increased the opportunity of transmission (Nsofor et al., 2017; Xie et al., 2020). Meanwhile, the unfavorable treatment outcome and poor management were usually accompanied by the recurrence of TB (Nakanwagi-Mukwaya et al., 2013; Dedefo et al., 2019).

In this study, the rate of recurrence TB was up 2%, which was a little higher than that of Europe (Millet et al., 2013) and distinctly lower than that of India (Cardona et al., 2018). It seems that TB recurrence declined with the decreasing incidence of TB. However, it was still reported a reverse relationship between TB recurrence and incidence (Lambert et al., 2003).In Korea, the recurrence rate declined yearly from 2005-2010 along with an increased TB notification. In our study, we found that relapse and re-infection contributed equally to TB recurrence. A previous surveillance study conducted in London during 2002-2015 revealed that the rate of re-infection was much higher than that of relapse (Wingfield et al., 2019), but an opposite result was raised by another study carried out in Beijing, which indicated that recurrent TB was dominated by relapse cases (Nsofor et al., 2017). Several reasons could be responsible for such variation of the proportion of recurrence. First, the varied study observation length might result in different proportion of recurrence. Commonly, relapse occurred earlier than re-infection (Luzze et al., 2013), if the study tracked cases in a relatively shorter

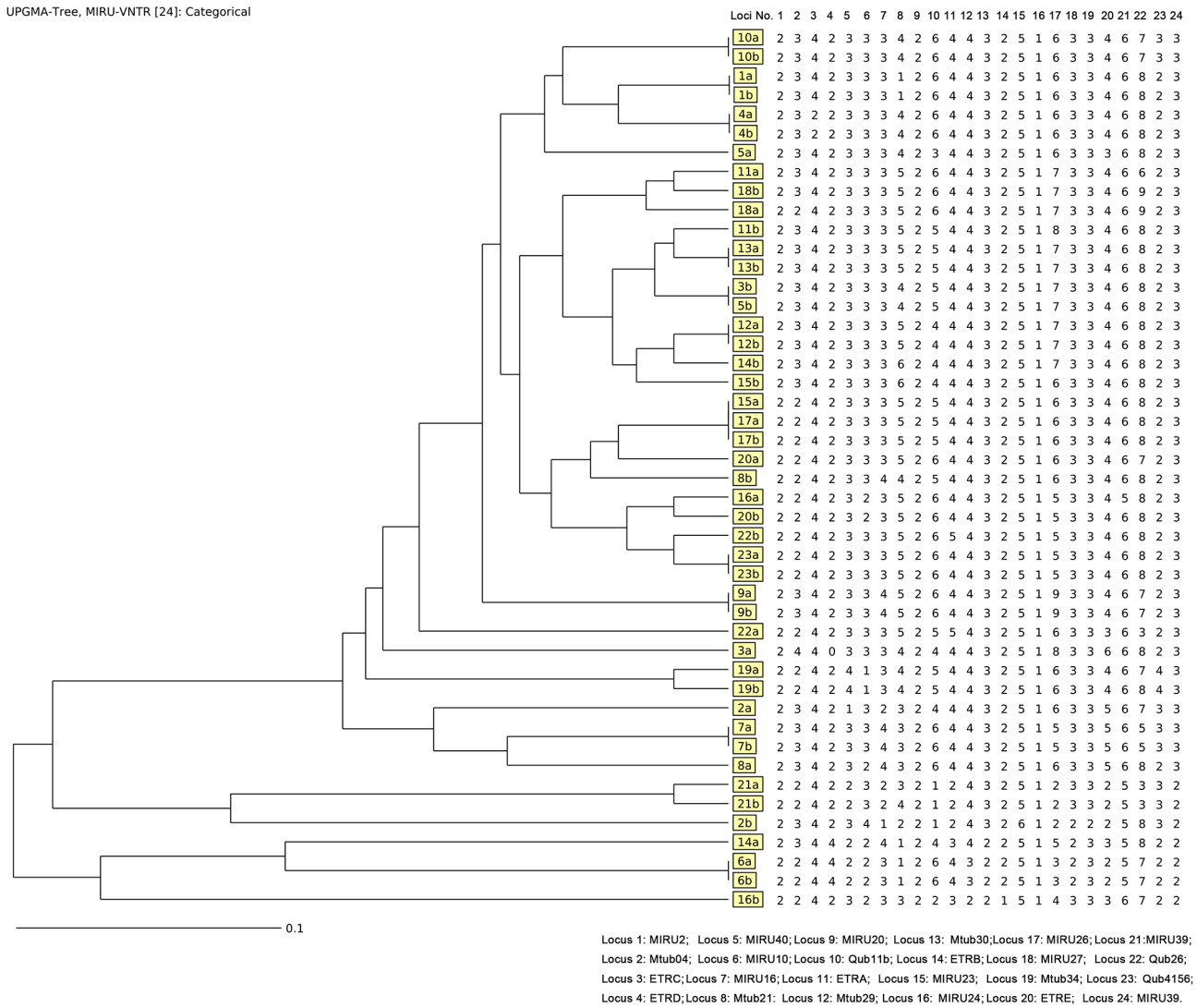

FIGURE 2 | Genotype results for the 23 paired isolates by MIRU-VNTR.

period, re-infection cases would be missed, resulting in a relatively lower re-infection rate (Marx et al., 2014) Besides, different genotyping methods, such as MIRU-VNTR and whole-genome sequencing (WGS), qualified as disparate discriminatory power that would make difference in classification of recurrence (Kruuner et al., 2002; Bryant et al., 2013b). Moreover, human immunodeficiency virus (HIV) and MDR, could increase the likelihood from infection to disease and generate more re-infection cases (Cox et al., 2006; Pettit et al., 2011). Therefore, the rate of reported relapse or re-infection varied widely in different studies. The relationship between the risk factors, such as age, gender, and cavitation on chest X-ray, and recurrence were controversial in past studies (Moosazadeh et al., 2015; Silva et al., 2017; Cudahy et al., 2020), in our study there was no significant association between those factors and different recurrence types.

In general, the rate of relapse due to inadequate treatment or ineffective human immunity is important to evaluate TB treatment regimen and patient management (Lambert et al., 2003). Considering the directly observed therapy (DOT) was fundamentally implemented in China for many years, the treatment outcome assessment might not be effective as expected. Currently, sputum smear was taken as one of the main methods to evaluate the treatment outcome of TB. However, most patients could not provide sputum samples at the end of treatment. Thus, treatment outcome was mainly assessed by chest X-ray examination. Meanwhile, previous studies had revealed that chest X-ray result was weakly related to bacteria grade before the treatment, and limited in the assessment of the outcome after treatment (Murthy et al., 2018; Lee et al., 2020). So a feasible and robust assessment of treatment efficacy should be established to solve such a dilemma.

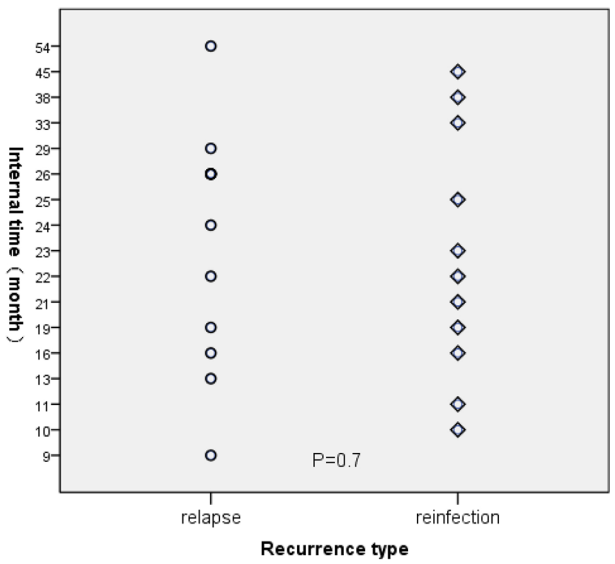

FIGURE 3 | The interval time for recurrent TB.

Acquired drug resistance for relapsed TB should be concerned, especially for acquired MDR-TB. A previous study indicated recurrence of TB was a risk factor for rifampicin-resistance (Chen et al., 2019). In our study, there was an isoniazid- resistant TB (Hr-TB) developed into MDR-TB in the second episode of the relapse group. Nowadays, isoniazid-resistance detection was not prioritized for TB drug-resistance detection, where GeneXpert MTB/RIF was extensively used for rifampicin-resistant screening. Thus, most Hr-TB patients were not detected and prescribed a standard anti-TB regimen. A previous study had revealed that inappropriate treatment of Hr-TB would result in MDR as well (Murray et al., 2009). Meanwhile, the treatment failure and relapse rates for Hr-TB were significantly higher than drug-susceptible TB (Gegia et al., 2012; Gegia et al., 2017). Thus, we suggested drug susceptibility test of isoniazid should be carried out, and appropriate treatment regimens should be adopted for Hr-TB.

At the same time, a rifampicin-resistant TB prescribed with a 6-month treatment regimen reached a treatment success in the first episode of TB. The reason for prescribing the first-line anti-TB drugs because the culture-based anti-TB drug susceptibility test usually came out the results three months later. However, the clinical symptom and X-ray examination demonstrated an effective treatment under this 6-month treatment regimen. Thus, 6-month treatment was prescribed until a successful treatment was reached. Previous studies indicated first-line anti-TB drugs might be helpful for MDR-TB treatment in this region (Zheng et al., 2020)The second TB episode of this case was happened 54 months after successful treatment of the first episode as shown in **Table 1**, and the MIRU data demonstrated an identical genotype but the drug resistant testing demonstrated rifampicin-susceptible. A previous study had revealed drug resistant changes between the two episodes for relapsed TB cases (Zong et al., 2018).

On the other hand, re-infection from an exogenous pathogen is associated with the recent spread of TB which required high-quality public health programs to restrict transmission. Notably, re-infected cases harbored more MDR than relapsed cases, although there was no significant difference. Therefore, further interventions for re-infection should focus on the management of MDR patients, and early detection of drug-susceptible character for the clinical patient.

Several limitations should be mentioned. First, compared to the whole genome sequencing, the discrimination power was relatively lower for 24 loci MIRU-VNTR, the genetic diversity of relapse and re-infection cases might be overlapped, but MIRU-VNTR was still a major molecular method for strain identification. Second, identical genotypes caused by re-infection can't be overlooked, especially those identical genotypes belong to the main clusters of the area. Third, the number of recurrent TB in this study was relatively small, the drug-resistant profile was limited to explore the transmission model of drug resistance for recurrent TB.

CONCLUSION

This study illustrated that endogenous relapse and exogenous re-infection contributed equally to the recurrence of TB, while re-infection cases were more likely to exhibit MDR in a second episode. Distinguishing between relapse and re-infection would be very necessary for design a more efficient TB control strategy. Meanwhile, the acquired drug resistance for relapsed cases should be concerned as well, especially for the first incident of isoniazid resistance.

DATA AVAILABILITY STATEMENT

The raw data supporting the conclusions of this article will be made available by the authors, without undue reservation.

ETHICS STATEMENT

The studies involving human participants were reviewed and approved by the institutional review board of Jiangsu province center for disease control and prevention. The patients/participants provided their written informed consent to participate in this study.

AUTHOR CONTRIBUTIONS

YS wrote the draft of the manuscript. CC designed and edited the manuscript. YS, HS, GL, YL, and YSL conducted the experiments. WL, LZ, and CC reviewed the data collection. All authors contributed to the article and approved the submitted version.

FUNDING

This work was supported by the National Major Science & Technology Projects for Infectious Disease Control and Prevention [grant number 2018ZX10715002], Jiangsu Commission of Health [grant number M2020040], Center for Disease Control and Prevention of Jiangsu Province [grant number JKRC2016006]. The funders had no role in study design, data collection, and analysis, decision to publish, or preparation of the manuscript.

REFERENCES

Bryant, J. M., Harris, S. R., Parkhill, J., Dawson, R., Diacon, A. H., van Helden, P., et al. (2013a). Whole-genome sequencing to establish relapse or re-infection with Mycobacterium tuberculosis: a retrospective observational study. *Lancet Respir. Med.* 1 (10), 786–792. doi: 10.1016/S2213-2600(13)70231-5

Bryant, J. M., Harris, S. R., Parkhill, J., Dawson, R., Diacon, A. H., van Helden, P., et al. (2013b). Whole-genome sequencing to establish relapse or re-infection with Mycobacterium tuberculosis: a retrospective observational study. *Lancet Respir. Med.* 1 (10), 786–792. doi: 10.1016/S2213-2600(13)70231-5

Cardona, P.-J., Velayutham, B., Chadha, V. K., Singla, N., Narang, P., Gangadhar Rao, V., et al. (2018). Recurrence of tuberculosis among newly diagnosed sputum positive pulmonary tuberculosis patients treated under the Revised National Tuberculosis Control Programme, India: A multi-centric prospective study. *PLoS One* 13 (7), e0200150. doi: 10.1371/journal.pone.0200150

Chen, Q., Peng, L., Xiong, G., Peng, Y., Luo, D., Zou, L., et al. (2019). Recurrence Is a Noticeable Cause of Rifampicin-Resistant Mycobacterium tuberculosis in the Elderly Population in Jiangxi, China. *Front. Public Health* 7, 182. doi: 10.3389/fpubh.2019.00182

Cox, H., Kebede, Y., Allamuratova, S., Ismailov, G., Davletmuratova, Z., Byrnes, G., et al. (2006). Tuberculosis recurrence and mortality after successful treatment: impact of drug resistance. *PloS Med.* 3 (10), e384. doi: 10.1371/journal.pmed.0030384

Cudahy, P. G. T., Wilson, D., and Cohen, T. (2020). Risk factors for recurrent tuberculosis after successful treatment in a high burden setting: a cohort study. *BMC Infect. Dis.* 20 (1), 789. doi: 10.1186/s12879-020-05515-4

Dedefo, M. G., Sirata, M. T., Ejeta, B. M., Wakjira, G. B., Fekadu, G., and Labata, B. G. (2019). Treatment Outcomes of Tuberculosis Retreatment Case and Its Determinants in West Ethiopia. *Open Respir. Med. J.* 13, 58–64. doi: 10.2174/1874306401913010058

Folkvardsen, D. B., Norman, A., Rasmussen, E. M., Lillebaek, T., Jelsbak, L., and Andersen, A. B. (2020). Recurrent tuberculosis in patients infected with the predominant Mycobacterium tuberculosis outbreak strain in Denmark. New insights gained through whole genome sequencing. *Infect. Genet. Evol.* 80, 104169. doi: 10.1016/j.meegid.2020.104169

Gegia, M., Cohen, T., Kalandadze, I., Vashakidze, L., and Furin, J. (2012). Outcomes among tuberculosis patients with isoniazid resistance in Georgia, 2007–2009. *Int. J. Tuberc. Lung Dis.* 16 (6), 812–816. doi: 10.5588/ijtld.11.0637

Gegia, M., Winters, N., Benedetti, A., van Soolingen, D., and Menzies, D. (2017). Treatment of isoniazid-resistant tuberculosis with first-line drugs: a systematic review and meta-analysis. *Lancet Infect. Dis.* 17 (2), 223–234. doi: 10.1016/S1473-3099(16)30407-8

Houben, R. M. G. J., Menzies, N. A., Sumner, T., Huynh, G. H., Arinaminpathy, N., Goldhaber-Fiebert, J. D., et al. (2016). Feasibility of achieving the 2025 WHO global tuberculosis targets in South Africa, China, and India: a combined analysis of 11 mathematical models. *Lancet Global Health* 4 (11), e806–e815. doi: 10.1016/S2214-109X(16)30199-1

Hozbor, D. F., Gadoev, J., Asadov, D., Harries, A. D., Parpieva, N., Tayler-Smith, K., et al. (2017). Recurrent tuberculosis and associated factors: A five - year countrywide study in Uzbekistan. *PLoS One* 12 (5), e0176473. doi: 10.1371/journal.pone.0176473

Interrante, J. D., Haddad, M. B., Kim, L., and Gandhi, N. R. (2015). Exogenous Reinfection as a Cause of Late Recurrent Tuberculosis in the United States. *Ann. Am. Thoracic Soc.* 12 (11), 1619–1626. doi: 10.1513/AnnalsATS.201507-429OC

Kruuner, A., Pehme, L., Ghebremichael, S., Koivula, T., Hoffner, S. E., and Mikelsaar, M. (2002). Use of molecular techniques to distinguish between treatment failure and exogenous reinfection with Mycobacterium tuberculosis. *Clin. Infect. Dis.* 35 (2), 146–155. doi: 10.1086/340980

Lambert, M.-L., Hasker, E., Deun, A. V., Roberfroid, D., Boelaert, M., and Van der Stuyft, P. (2003). Recurrence in tuberculosis: relapse or reinfection? *Lancet Infect. Dis.* 3 (5), 282–287. doi: 10.1016/s1473-3099(03)00607-8

Lee, J. H., Kim, O.-H., Kim, Y. J., Shim, T. S., and Jo, K.-W. (2020). Changes in chest X-ray findings in 1- and 2-month group after treatment initiation for suspected pulmonary tuberculosis. *Korean J. Internal Med.* 35 (5), 1145–1153. doi: 10.3904/kjim.2019.036

Luzze, H., Johnson, D. F., Dickman, K., Mayanja-Kizza, H., Okwera, A., Eisenach, K., et al. (2013). Relapse more common than reinfection in recurrent tuberculosis 1-2 years post treatment in urban Uganda. *Int. J. Tuberc. Lung Dis.* 17 (3), 361–367. doi: 10.5588/ijtld.11.0692

Maghradze, N., Jugheli, L., Borrell, S., Tukvadze, N., Aspindzelashvili, R., Avaliani, Z., et al. (2019). Classifying recurrent Mycobacterium tuberculosis cases in Georgia using MIRU-VNTR typing. *PLoS One* 14 (10), e0223610. doi: 10.1371/journal.pone.0223610

Marx, F. M., Dunbar, R., Enarson, D. A., Williams, B. G., Warren, R. M., van der Spuy, G. D., et al. (2014). The temporal dynamics of relapse and reinfection tuberculosis after successful treatment: a retrospective cohort study. *Clin. Infect. Dis.* 58 (12), 1676–1683. doi: 10.1093/cid/ciu186

Millet, J. P., Shaw, E., Orcau, A., Casals, M., Miro, J. M., and Cayla, J. A. (2013). Tuberculosis recurrence after completion treatment in a European city: reinfection or relapse? *PLoS One* 8 (6), e64898. doi: 10.1371/journal.pone.0064898

Moosazadeh, M., Bahrampour, A., Nasehi, M., and Khanjani, N. (2015). The incidence of recurrence of tuberculosis and its related factors in smear-positive pulmonary tuberculosis patients in Iran: A retrospective cohort study. *Lung India* 32 (6), 557–560. doi: 10.4103/0970-2113.168113

Murray, M., Menzies, D., Benedetti, A., Paydar, A., Martin, I., Royce, S., et al. (2009). Effect of Duration and Intermittency of Rifampin on Tuberculosis Treatment Outcomes: A Systematic Review and Meta-Analysis. *PLoS Med.* 6 (9), e1000146. doi: 10.1371/journal.pmed.1000146

Murthy, S. E., Chatterjee, F., Crook, A., Dawson, R., Mendel, C., Murphy, M. E., et al. (2018). Pretreatment chest x-ray severity and its relation to bacterial burden in smear positive pulmonary tuberculosis. *BMC Med.* 16 (1), 73. doi: 10.1186/s12916-018-1053-3

Nakanwagi-Mukwaya, A., Reid, A. J., Fujiwara, P. I., Mugabe, F., Kosgei, R. J., Tayler-Smith, K., et al. (2013). Characteristics and treatment outcomes of tuberculosis retreatment cases in three regional hospitals, Uganda. *Public Health Action* 3 (2), 149–155. doi: 10.5588/pha.12.0105

Nsofor, C. A., Jiang, Q., Wu, J., Gan, M., Liu, Q., Zuo, T., et al. (2017). Transmission is a Noticeable Cause of Resistance Among Treated Tuberculosis Patients in Shanghai, China. *Sci. Rep.* 7 (1), 7691. doi: 10.1038/s41598-017-08061-3

Oelemann, M. C., Diel, R., Vatin, V., Haas, W., Rusch-Gerdes, S., Locht, C., et al. (2007). Assessment of an optimized mycobacterial interspersed repetitive- unit-variable-number tandem-repeat typing system combined with spoligotyping for population-based molecular epidemiology studies of tuberculosis. *J. Clin. Microbiol.* 45 (3), 691–697. doi: 10.1128/JCM.01393-06

Pettit, A. C., Kaltenbach, L. A., Maruri, F., Cummins, J., Smith, T. R., Warkentin, J. V., et al. (2011). Chronic lung disease and HIV infection are risk factors for recurrent tuberculosis in a low-incidence setting. *Int. J. Tuberc. Lung Dis.* 15 (7), 906–911. doi: 10.5588/ijtld.10.0448

Silva, V., Mello, F., and Figueiredo, S. (2017). Estimated rates of recurrence, cure, and treatment abandonment in patients with pulmonary tuberculosis treated with a four-drug fixed-dose combination regimen at a tertiary health care facility in the city of Rio de Janeiro, Brazil. *J. Brasileiro Pneumol.* 43 (2), 113–120. doi: 10.1590/s1806-37562016000000204

Supply, P., Allix, C., Lesjean, S., Cardoso-Oelemann, M., Rusch-Gerdes, S., Willery, E., et al. (2006). Proposal for standardization of optimized mycobacterial interspersed repetitive unit-variable-number tandem repeat typing of Mycobacterium tuberculosis. *J. Clin. Microbiol.* 44 (12), 4498–4510. doi: 10.1128/JCM.01392-06

WHO (2009). *Guidelines for surveillance of drug resistance in TB WHO 4th version* (Geneva: World Health Organization).

WHO (2010). *Treatment of tuberculosis guidelines Fourth edition* (Geneva: World Health Organization).

WHO (2019). *Global tuberculosis report 2019* (Geneva: World Health Organization).

Wingfield, T., Afshar, B., Carless, J., Roche, A., Balasegaram, S., and Anderson, C. (2019). Surveillance of tuberculosis (TB) cases attributable to relapse or reinfection in London, 2002-2015. *PLoS One* 14 (2), e0211972. doi: 10.1371/journal.pone.0211972

Xie, Z., Wang, T., Chen, H., Wang, D., Gao, X., and Hui, Y. (2020). Factors associated with diagnostic delay in recurrent TB. *BMC Public Health* 20 (1), 1207. doi: 10.1186/s12889-020-09005-9

Yates, M. D., Drobniewski, F. A., and Wilson, S. M. (2002). Evaluation of a Rapid PCR-Based Epidemiological Typing Method for Routine Studies of Mycobacterium tuberculosis. *J. Clin. Microbiol.* 40 (2), 712–714. doi: 10.1128/JCM.40.2.712-714.2002

Zhao, Y., Xu, S., Wang, L., Chin, D. P., Wang, S., Jiang, G., et al. (2012). National survey of drug-resistant tuberculosis in China. *N. Engl. J. Med.* 366 (23), 2161–2170. doi: 10.1056/NEJMoa1108789

Zheng, X. B., Diwan, V. K., Zhao, Q., Hu, Y., Bruchfeld, J., Jiang, W. L., et al. (2020). Treatment quality and outcome for multidrug-resistant tuberculosis patients in four regions of China: a cohort study. *Infect. Dis. Poverty* 9 (1), 97. doi: 10.1186/s40249-020-00719-x

Zong, Z., Huo, F., Shi, J., Jing, W., Ma, Y., Liang, Q., et al. (2018). Relapse Versus Reinfection of Recurrent Tuberculosis Patients in a National Tuberculosis Specialized Hospital in Beijing, China. *Front. Microbiol.* 9, 1858. doi: 10.3389/fmicb.2018.01858

Conflict of Interest: The authors declare that the research was conducted in the absence of any commercial or financial relationships that could be construed as a potential conflict of interest.

frontiers in Cellular and Infection Microbiology

ORIGINAL RESEARCH
published: 18 March 2021
doi: 10.3389/fcimb.2021.650163

Harnessing Big Data to Optimize an Algorithm for Rapid Diagnosis of Pulmonary Tuberculosis in a Real-World Setting

Jing Peng[1†], Juan Song[2†], Feng Wang[1†], Peng Zuo[3], Yanjun Lu[1], Weiyong Liu[1], Lei Tian[1], Zhongju Chen[1], Yaowu Zhu[1], Xiong Wang[1], Na Shen[1], Xu Wang[1], Shiji Wu[4], Qin Yu[4], Bruce A. Vallance[5], Kevan Jacobson[5], Ziyong Sun[1‡] and Hong Bing Yu[5*]*

[1] Department of Laboratory Medicine, Tongji Hospital, Tongji Medical College, Huazhong University of Science and Technology, Wuhan, China, [2] Department of Gastroenterology & Endocrinology, Wuhan No. 9 Hospital, Wuhan, China, [3] Department of Respiratory Medicine, Tongji Hospital, Tongji Medical College, Huazhong University of Science and Technology, Wuhan, China, [4] Department of Gastroenterology, Tongji Hospital, Tongji Medical College, Huazhong University of Science and Technology, Wuhan, China, [5] Department of Pediatrics, BC Children's Hospital Research Institute, University of British Columbia, Vancouver, BC, Canada

OPEN ACCESS

Edited by:
Natarajaseenivasan Kalimuthusamy, Bharathidasan University, India

Reviewed by:
Ni Made Mertaniasih, Airlangga University, Indonesia
Amit Singh, All India Institute of Medical Sciences, India

***Correspondence:**
Ziyong Sun
zysun@tjh.tjmu.edu.cn
Hong Bing Yu
hby@mail.ubc.ca

[†]These authors have contributed equally to this work

[‡]Lead contact

Specialty section:
This article was submitted to Bacteria and Host, a section of the journal Frontiers in Cellular and Infection Microbiology

Received: *06 January 2021*
Accepted: *01 March 2021*
Published: *18 March 2021*

Citation:
Peng J, Song J, Wang F, Zuo P, Lu Y, Liu W, Tian L, Chen Z, Zhu Y, Wang X, Shen N, Wang X, Wu S, Yu Q, Vallance BA, Jacobson K, Sun Z and Yu HB (2021) Harnessing Big Data to Optimize an Algorithm for Rapid Diagnosis of Pulmonary Tuberculosis in a Real-World Setting. Front. Cell. Infect. Microbiol. 11:650163. doi: 10.3389/fcimb.2021.650163

Background: The prompt diagnosis of pulmonary tuberculosis (PTB) remains a challenge in clinical practice. The present study aimed to optimize an algorithm for rapid diagnosis of PTB in a real-world setting.

Methods: 28,171 adult inpatients suspected of having PTB in China were retrospectively analyzed. Bronchoalveolar lavage fluid (BALF) and/or sputum were used for acid-fast bacilli (AFB) smear, Xpert MTB/RIF (Xpert), and culture. A positive mycobacterial culture was used as the reference standard. Peripheral blood mononuclear cells (PBMC) were used for T-SPOT.*TB*. We analyzed specimen types' effect on these assays' performance, determined the number of smears for diagnosing PTB, and evaluated the ability of these assays performed alone, or in combination, to diagnose PTB and nontuberculous mycobacteria (NTM) infections.

Results: Sputum and BALF showed moderate to substantial consistency when they were used for AFB smear or Xpert, with a higher positive detection rate by BALF. 3-4 smears had a higher sensitivity than 1-2 smears. Moreover, simultaneous combination of AFB and Xpert correctly identified 44/51 of $AFB^+/Xpert^+$ and 6/7 of $AFB^+/Xpert^-$ cases as PTB and NTM, respectively. Lastly, when combined with AFB/Xpert sequentially, T-SPOT showed limited roles in patients that were either AFB^+ or $Xpert^+$. However, $T\text{-}SPOT^{MDC}$ (manufacturer-defined cut-off) showed a high negative predicative value (99.1%) and suboptimal sensitivity (74.4%), and TBAg/PHA (ratio of *Mycobacterium tuberculosis*-specific antigens to phytohaemagglutinin spot-forming cells, which is a modified method calculating T-SPOT.*TB* assay results) ≥0.3 demonstrated a high specificity (95.7%) and a relatively low sensitivity (16.3%) in $AFB^-/Xpert^-$ patients.

Conclusions: Concurrently performing AFB smear (at least 3 smears) and Xpert on sputum and/or BALF could aid in rapid diagnosis of PTB and NTM infections in a real-world high-burden setting. If available, BALF is preferred for both AFB smear and Xpert. Expanding this algorithm, PBMC T-SPOT^{MDC} and TBAg/PHA ratios have a supplementary role for PTB diagnosis in AFB$^-$/Xpert$^-$ patients (moderately ruling out PTB and ruling in PTB, respectively). Our findings may also inform policy makers' decisions regarding prevention and control of TB in a high burden setting.

Keywords: Xpert MTB/RIF, smear microscopy, T-SPOT.*TB*, diagnostic algorithm, real-world study

INTRODUCTION

Tuberculosis (TB) caused by the pathogen *Mycobacterium tuberculosis* (*M. tuberculosis*, MTB) continues to pose a major threat to public health. It is estimated that about one quarter of the world's population is infected with MTB, and 5–10% of those infected will develop TB disease throughout their lifetime (WHO, 2020). While progress has been made in reducing the TB burden worldwide, it has been insufficient to reach the first milestones of the End TB Strategy (WHO, 2018; WHO, 2020). One of the key hurdles to achieving these milestones is the high prevalence of drug resistant TB (Zhao et al., 2012). Moreover, MTB and nontuberculous mycobacteria (NTM) infections often cause indistinguishable clinical symptoms, but their treatment can be vastly different (Forbes et al., 2018).

Rapid and accurate diagnosis of TB is required for effective TB control. Typical TB diagnostic tools include acid-fast bacilli (AFB) smear microscopy, culture, Xpert MTB/RIF (Xpert), and interferon gamma (IFN-γ) releasing assays (IGRAs) (Theron et al., 2012; Forbes et al., 2018). Sputum AFB smear microscopy is the most widely used TB diagnostic test (Forbes et al., 2018). A positive culture of MTB from clinical samples is the gold standard for diagnosing active TB (ATB) infections. However, due to its time-consuming and laborious nature, culture is not often implemented in routine practice. Xpert is a PCR-based test that simultaneously detects MTB and rifampin resistance (Forbes et al., 2018). It is highly sensitive and specific. IGRAs, such as T-SPOT.*TB* [T-SPOT], are T-cell based assays that measure IFN-γ release in response to MTB-specific antigens (Sester et al., 2011) and can yield relatively fast results (usually within one day). IGRAs can be used for diagnosing latent TB infections (LTBI), but cannot be used to rule in or rule out ATB (Mazurek et al., 2010; Sester et al., 2011). Intriguingly, we found that TBAg/PHA ratios (the larger of ESAT-6/PHA and CFP-10/PHA ratios) in the T-SPOT.*TB* assay could be used to distinguish between ATB and LTBI (Wang et al., 2016). Whether TBAg/PHA ratios can be used to diagnose ATB in a real-world setting remains unclear.

There are many different algorithms that integrate the above assays for diagnosing pulmonary TB (PTB). However, this can also complicate health providers' decisions in choosing optimal PTB diagnostic assays, and sometimes create a "know-do gap" scenario where health providers generally know which algorithms are recommended but in practice use something different (Datta et al., 2017). Moreover, the performance of these algorithms can be affected by the types of specimens (such as sputum vs. BALF), the number of AFB smears and other factors (Conde et al., 2000; Monkongdee et al., 2009). Therefore, it is necessary to identify an optimal algorithm for rapid diagnosis of PTB in a real-world setting.

We retrospectively analyzed a large real-world data set on the diagnosis of PTB. This included assessing the effect of specimen types on the performance of PTB diagnostic assays, determining the number of smears for diagnosing PTB, and evaluating the ability of these assays performed alone, or in combination, to diagnose PTB and NTM infections. Through these rigorous analyses, we were able to identify an optimal algorithm for rapid diagnosis of PTB and NTM infections in a real-world setting.

METHODS

Study Population

Between January 2016 and March 2019, data from inpatients (≥18 years) undergoing evaluation for PTB (having PTB-related symptoms and/or signs, or unexplained cough lasting ≥2 weeks, or unexplained findings on chest radiographs suggestive of PTB) in Tongji Hospital (Wuhan, China) were included. Tongji hospital is the sixth largest hospital (with 5000 beds) in China, and has been certified by both ISO 15189 (Medical Laboratories-Particular Requirements for Quality and Competence) and CAP (College of American Pathologists).

Specimen Collection and Processing

Bronchoscopy-derived BALF and expectoration-derived unconcentrated sputum were used for AFB smear, Xpert, and culture tests. About 40 ml of BALF was collected after instilling 30-50 ml of sterile saline (0.9%) into the airway of the affected lung segment. AFB smears and mycobacterial cultures were conducted as previously described (Forbes et al., 2018), but with minor modifications. Briefly, AFB smears on unconcentrated sputum and concentrated BALF (pelleted after centrifugation) were screened using the auramine fluorescence staining method (Baso Diagnostics Inc. Zhuhai, China). Auramine positive AFB smears were also confirmed by Ziehl–Neelsen staining (Baso Diagnostics Inc. Zhuhai, China), a method that appears to have a high specificity for diagnosing ATB (Tarhan et al., 2003; Lee et al., 2018). As for cultures, all sputum and BALF samples were

mixed with an equal volume of a 0.5% N-acetyl-L-cysteine-2.0% NaOH and incubated at 37°C for 15-20 min. The mixture was then neutralized by the addition of phosphate buffer (pH 6.8), followed by centrifugation at 3,000 × g for 15 min. After resuspending the pellet in 2 ml of the phosphate buffer, 0.5 ml of the suspension was inoculated into liquid medium (BACTEC 960/MGIT, Becton Dickinson Diagnostic Instrument Systems, Sparks, MD) and 0.2 ml of the suspension was inoculated onto solid medium (Lowenstein-Jensen, Baso Diagnostics Inc. Zhuhai, China). Cultures were grown for 8 weeks. To distinguish between MTB and NTM, positive cultures were tested using the TBAg MPT64 assay (a MPT64-based rapid immunochromatographic kit, GENESIS, Kaibili, China). Cultures negative for TBAg MPT64 were reported as NTM, or subjected to 16S rRNA sequencing to identify the mycobacterial species.

PTB was defined as at least one of the BALF and/or sputum specimens having a positive culture result for *M. tuberculosis* from liquid and/or solid media. A similar approach was used to define active NTM and Nocardia infections.

Xpert was conducted according to the manufacturer's instructions (Cepheid, Sunnyvale, California). Briefly, untreated sputum samples or BALF samples that were pelleted after centrifugation were mixed with the sample reagent at 1:2 ratio (vol/vol), and incubated at 20–30°C for about 15 min (the mixtures were vortexed for at least 10 seconds between 5 and 10 minutes). About 2 ml of the sample reagent-treated sample was then transferred into the sample chamber of the Xpert cartridge. Xpert results were reported according to the manufacturer's recommended semi-quantitative classification of the cycle-threshold (Ct) values: high ($Ct \leq 16$), medium ($16<Ct \leq 22$), low ($22<Ct \leq 28$), and very low ($Ct>28$). If initial Xpert results were non-determinate (error, invalid or no result), testing was repeated with the leftover sample reagent-treated sample (at least 2 ml). In case there was less than 2 ml of sample-reagent-treated sample left, the leftover from the original sample was treated with sample reagent and re-tested as above.

Peripheral blood mononuclear cell (PBMC) T-SPOT.*TB* assay was performed with the T-SPOT ELISpot assay according to the manufacturer's instructions (Oxford Immunotec Ltd., Oxford, England). Briefly, 2.5×10^5 PBMCs were added to 96-well plates pre-coated with anti-IFN-γ antibody. After incubation for 16–20 h at 37°C with 5% CO2, plates were washed with phosphate buffered saline and developed using an anti-IFN-γ antibody conjugate and substrate, and detected for the presence of secreted IFN-γ. Spot-forming cells (sfc) were counted with an automated ELISpot reader (CTL Analyzers, Cleveland, OH, USA). To report a case of PTB, we used two different methods. One was to use the manufacturer-defined cut-off (T-SPOT^{MDC}), and the other was to use ratios of *Mycobacterium tuberculosis*-specific antigens (TBAg) to phytohaemagglutinin (PHA) sfc (TBAg/PHA) as previously described (Wang et al., 2016). Briefly, the ratios of ESAT-6 sfc to PHA sfc and CFP-10 sfc to PHA sfc were calculated, with the larger of the two values representing the TBAg/PHA ratio of one sample.

Statistical Analysis

AFB smear-positive (AFB$^+$) status was based on per-person results (defined as at least one of the BALF and/or sputum specimens having a positive AFB smear), unless otherwise stated. Culture-confirmed PTB and NTM infections were defined as at least one of the BALF and/or sputum specimens having a positive MTB or NTM culture. A positive mycobacterial culture from solid and/or liquid media was used as the reference standard. Comparisons of sensitivities and specificities between independent subgroups of interest were assessed using $\chi 2$ test. The *kappa* coefficients were calculated to determine the agreement between BALF and sputum. The agreement of the results (*kappa* value) was categorized as near perfect (0.8–1.0), substantial (0.6–0.8), moderate (0.4–0.6), fair (0.2–0.4), slight (0–0.2), or poor (<0) (Roberts, 2008). All analyses were performed using SPSS version 19 (IBM, Chicago, Illinois), with results considered significantly different at $p<0.05$.

RESULTS

Demographic and Clinical Characteristics of Study Population

A total of 28,192 inpatients were screened for eligibility. 21 patients received TB treatment 1 month before hospitalization and were not included (**Supplementary Table S1**). Sputum and/or BALF culture results were available for 7,528 patients, with 8.9% and 1.2% being positive for MTB and NTM, respectively. Among the cultured NTM strains, 25 were identified to species level: 12 *M. avium-intracellulare* complex, 8 *M. fortuitum*, 4 *M.abscessus*, and 1 *M. kansasii*.

Preferences in Choosing PTB Diagnostic Assays in Real Practice

TB tests ordered by clinicians were variable, including 8,866 AFB, 9,388 AFB/T-SPOT, and many other combinations of tests (**Supplementary Figure S1** and **Table S2**). While AFB and T-SPOT were the first and second most frequently ordered tests, respectively, the percentage of patients undergoing Xpert increased rapidly from 0.8% in 2016 to 17.3% in 2019.

Consistency Between Sputum and BALF for Diagnosing PTB

In a real-world setting, very few patients had their sputum and BALF collected simultaneously for single PTB diagnostic assay. We determined the consistency between sputum and BALF when they were used for AFB smear, culture, and Xpert. Patients having both sputum and BALF collected within one week of hospitalization for AFB smear (n=3,975), culture (n=109), and Xpert (n=181) analysis were included (**Supplementary Table S3**). Sputum and BALF showed moderate to substantial consistency when used for AFB smear, culture, and Xpert. The positive detection rate by BALF was higher than that by sputum, when they were used for AFB smear or Xpert. The positive detection rate by sputum culture was slightly but insignificantly higher than that by BALF culture.

Number of Smears to Diagnose PTB

A total of 7,155 patients had 1-8 BALF and/or sputum AFB smears tested within one week of hospitalization (**Supplementary Table S4**). The overall sensitivity of 1-4 AFB smears was 24.6%, 33.4%, 36.2%, and 37.3%, respectively (**Table 1**). While one AFB

smear was able to detect 64.7% of AFB$^+$ patients with positive MTB culture, two AFB smears increased the detection rate to 88.0% (**Supplementary Table S5**). Three AFB smears detected a further 7.4% of AFB$^+$ TB patients as compared to two AFB smears. Four smears detected 98.3% of AFB$^+$ TB patients.

Performance of AFB Smear, Xpert, or T-SPOT Alone in Diagnosing PTB

A total of 2,044 patients had their respiratory samples tested for AFB smear, culture, Xpert, and T-SPOT (**Table 2**). Both AFB smear and Xpert showed great specificity (>95%), but the sensitivity of AFB smear was much lower than that of Xpert (19.8% vs. 79.7%). Depending on AFB smear status, Xpert performance was different. Xpert was able to identify 97.8% of AFB$^+$/culture-positive (culture$^+$) TB patients, but only 75.3% of AFB smear-negative (AFB$^-$)/culture$^+$ TB patients (**Supplementary Table S6**). Despite these findings, Xpert was not performed in 4,252 patients who had both AFB smear and culture results available (**Supplementary Table S7**). Of these patients, 326 (7.7%) were MTB culture$^+$, including 212 (65.0%) that were AFB$^-$ (**Supplementary Table S8**).

In addition to AFB smear and Xpert, T-SPOT performance was analyzed. We used two different methods in the T-SPOT assay to define a PTB case, with one method using the manufacturer-defined cut-off (T-SPOT^{MDC}), and the other using the TBAg/PHA ratios as previously described (Wang et al., 2016). While T-SPOT^{MDC} and Xpert demonstrated similar sensitivity (**Table 2**), T-SPOT^{MDC} had much lower specificity (69.1%) than Xpert (95.3%). When TBAg/PHA ratios were used, the specificity increased significantly, but at the expense of reduced sensitivity. For instance, TBAg/PHA ≥0.3 demonstrated an overall sensitivity of 37.3% and specificity of 94.8% (**Table 2**). TBAg/PHA ≥0.5 gave an overall sensitivity of 17.3% and specificity of 97.1%. Increasing the TBAg/PHA cut-off to 1.0 decreased the sensitivity to 9.1%, but increased the specificity to 99.0% (**Supplementary Table S9**).

Use AFB Smear and Xpert to Distinguish Between PTB and NTM Infections

While combining AFB smear and Xpert did not further increase their sensitivity and specificity in diagnosing PTB compared to Xpert alone (**Table 2**), they were able to differentiate PTB and NTM cases more effectively (**Table 3**). The majority (44/51) of AFB$^+$/Xpert-positive (Xpert$^+$) patients were MTB culture$^+$, and the remaining seven patients were culture$^-$ but diagnosed as having TB disease based on clinical presentations. Of the 216 AFB$^-$/Xpert$^+$ patients, 137 and 73 were MTB culture$^+$ and culture$^-$/clinically active TB, respectively. Six of seven AFB$^+$/Xpert$^-$ patients were NTM culture$^+$. Of 1,770 AFB$^-$/Xpert$^-$ patients, the majority (1,710) were negative for both MTB and NTM culture. Together, a combination of AFB and Xpert was able to detect 80.2% of patients with culture-proven PTB, and 28.6% of patients with culture-proven NTM.

Use T-SPOT in Conjunction With AFB Smear and/or Xpert to Diagnose PTB

We asked if combining T-SPOT with AFB smear and/or Xpert would improve PTB diagnosis. The sensitivity and specificity of AFB/T-SPOT^{MDC} combination was comparable to those of T-SPOT^{MDC} alone, suggesting this combination does not improve PTB diagnosis (**Table 2**). However, when T-SPOT^{MDC} was used together with Xpert, the sensitivity and negative predictive value (NPV) increased to 95.0% and 99.1%, respectively, much higher than those of Xpert or T-SPOT^{MDC} alone (**Table 2**). Adding AFB smear into Xpert/T-SPOT^{MDC} combination did not further increase the sensitivity and NPV. Notably, although combining T-SPOT^{MDC} with Xpert or AFB/Xpert greatly increased sensitivity, it was at the expense of reduced specificity (<67.6%). When TBAg/PHA≥0.3 (**Table 2**) (compared to T-SPOT^{MDC}) was used in conjunction with AFB smear and/or Xpert, the specificity increased significantly. These results suggest that TBAg/PHA≥0.3 have some added values for PTB diagnosis when combined with AFB smear and/or Xpert.

T-SPOT Performance in Diagnosing PTB When Stratified by AFB Smear and Xpert Status

While the above results analyzed the performance of T-SPOT in the overall population, it remained unclear if T-SPOT would perform differently among patients with different AFB smear and Xpert status. We first defined T-SPOT performance based on AFB

TABLE 1 | Performance of acid-fast bacilli smears for diagnosing pulmonary tuberculosis.

Accumulated AFB smears (N)	Accumulated samples (N)	Sensitivity % (95% CI)	Positive/ total	Specificity% (95% CI)	Negative/ total	PPV % (95% CI)	NPV % (95% CI)
1	7,155	24.6 (21.2-27.9)	156/635	99.6 (99.4-99.7)	6,492/6,520	84.8 (79.6-90.0)	93.1 (92.5-93.7)
2	10,688	33.4 (29.7-37.1)	212/635	99.5 (99.3-99.7)	6,487/6,520	86.5 (82.3-90.8)	93.9 (93.3-94.4)
3	12,160	36.2 (32.5-40.0)	230/635	99.5 (99.3-99.6)	6,485/6,520	86.8 (82.7-90.9)	94.1 (93.6-94.7)
4	12,993	37.3 (33.6-41.1)	237/635	99.5 (99.3-99.6)	6,484/6,520	86.8 (82.8-90.8)	94.2 (93.7-94.8)
5	13,282	37.6 (33.9-41.4)	239/635	99.4 (99.2-99.6)	6,482/6,520	86.3 (82.2-90.3)	94.2 (93.7-94.8)
6	13,419	38.0 (34.2-41.7)	241/635	99.4 (99.2-99.6)	6,481/6,520	86.1 (82.1-90.1)	94.3 (93.7-94.8)
7	13,488	38.0 (34.2-41.7)	241/635	99.4 (99.2-99.6)	6,481/6,520	86.1 (82.1-90.1)	94.3 (93.7-94.8)
8	13,526	38.0 (34.2-41.7)	241/635	99.4 (99.2-99.6)	6,481/6,520	86.1 (82.1-90.1)	94.3 (93.7-94.8)

A total of 7,155 patients, who had 1-8 BALF and/or sputum AFB smears, as well as BALF and/or sputum cultures (single or multiple per person) performed simultaneously during hospitalization, were included in the analysis. Pulmonary tuberculosis was defined as at least one of the BALF and/or sputum specimens having one positive culture result for M. tuberculosis. AFB, acid-fast bacilli; PPV, positive predictive value; NPV, negative predictive value; CI, confidence interval; BALF, bronchoalveolar lavage fluid.

TABLE 2 | Performance of acid-fast bacilli smear, Xpert MTB/RIF, and T-SPOT.*TB*, alone or in combination, in diagnosing pulmonary tuberculosis.

Methodology	T-SPOT status	Sensitivity % (95% CI)†	Positive/total	Specificity%(95% CI)‡	Negative/total	PPV %(95% CI)	NPV %(95% CI)§
AFB	.	19.8 (14.7-25.0)[1]	45/227	99.3 (98.9-99.7)[2]	1,804/1,817	77.6 (66.9-88.3)	90.8 (89.6-92.1)[3]
Xpert	.	79.7 (74.5-85.0)	181/227	95.3 (94.3-96.0)	1,731/1,817	67.8 (62.2-73.4)	97.4 (96.7-98.2)
T-SPOT¶	T-SPOT^{MDC}	81.4 (76.2-86.5)[4]	179/220	69.1 (66.9-71.2)[5]	1,240/1,795	24.4 (21.3-27.5)	96.8 (95.8-97.8)[6]
	TBAg/PHA≥0.3	37.3 (30.9-43.7)[7]	82/220	94.8 (93.7-95.8)[8]	1,701/1,795	46.6 (39.2-54.0)	92.5 (91.3-93.7)[9]
AFB/Xpert	.	80.2 (75.0-85.4)[10]	182/227	94.9 (93.9-95.9)[11]	1,725/1,817	66.4 (60.8-72.1)	97.5 (96.7-98.2)[12]
AFB/T-SPOT¶	T-SPOT^{MDC}	84.6 (79.8-89.3)[13]	186/220	68.9 (66.8-71.1)[14]	1,237/1,795	25 (21.9-28.1)	97.3 (96.4-98.2)[15]
	TBAg/PHA≥0.3	43.2 (36.6-49.7)[16]	95/220	94.2 (93.1-95.3)[17]	1,691/1,795	47.7 (40.8-54.7)	93.1 (92.0-94.3)[18]
Xpert/T-SPOT¶	T-SPOT^{MDC}	95 (92.1-97.9)[19]	209/220	67.6 (65.4-69.7)[20]	1,213/1,795	26.4 (23.4-29.5)	99.1 (98.6-99.6)[21]
	TBAg/PHA≥0.3	83.6 (78.8-88.5)[22]	184/220	91.1 (89.8-92.5)[23]	1,636/1,795	53.6 (48.4-58.9)	97.9 (97.2-98.5)[24]
AFB/Xpert/T-SPOT¶	T-SPOT^{MDC}	95.0 (92.1-97.9)[25]	209/220	67.4 (65.2-69.6)[26]	1,210/1,795	26.3 (23.3-29.4)	99.1 (98.6-99.6)[27]
	TBAg/PHA≥0.3	84.1 (79.3-88.9)[28]	185/220	90.4 (89.1-91.8)[29]	1,623/1,795	51.8 (46.6-57)	97.9 (97.2-98.6)[30]

A total of 2,044 patients had BALF and/or sputum AFB, culture, and Xpert assays, as well as peripheral blood mononuclear cell T-SPOT performed simultaneously. For strict comparison of the performance of AFB, Xpert, and T-SPOT, alone or in combination, only the first AFB, Xpert, and T-SPOT test results were used in the analysis. Pulmonary tuberculosis was defined as at least one of the BALF and/or sputum specimens having one positive culture result for M. tuberculosis. ¶Twenty-nine patients with invalid T-SPOT results (PHA spot forming cells <20) were excluded from the analysis, including 7 culture-confirmed MTB cases (1 AFB$^+$/Xpert$^-$, 4 AFB$^-$/Xpert$^+$, and 2 AFB$^-$/Xpert$^-$), 1 NTM cases with AFB$^+$/Xpert$^-$, and 21 culture-negative cases (1 AFB$^-$/Xpert$^+$ and 20 AFB$^-$/Xpert$^-$). PPV=positive predictive value; NPV=negative predictive value; CI=confidence interval; AFB=acid-fast bacilli smear; Xpert=Xpert MTB/RIF; T-SPOT=T-SPOT.TB; T-SPOT^{MDC}=manufacturer-defined cutoff; TBAg=Mycobacterium tuberculosis-specific antigen; PHA=phytohaemagglutinin; BALF=bronchoalveolar lavage fluid.†Sensitivity comparison with Xpert: [1]p<0.0001. [4]p=0.664. [7]p=0.0001. [10]p<0.907. [19]p<0.0001. [22]p=0.287. Sensitivity comparison with AFB: [13]p<0.0001. [16]p<0.0001. Sensitivity comparison with AFB/Xpert: [25]p<0.0001. [28]p=0.280. ‡Specificity comparison with Xpert: [2]p<0.0001. [5]p<0.0001. [8]p=0.487. [11]p=0.645. [20]p<0.0001. [23]p<0.0001. Specificity comparison with AFB: [14]p<0.0001. [17]p<0.0001. Specificity comparison with AFB/Xpert: [26]p<0.0001. [29]p<0.0001. §NPV comparison with Xpert: [3]p<0.0001. [6]p=0.315. [9]p<0.0001. [12]p=0.931. [21]p=0.001. [24]p=0.401. NPV comparison with AFB: [15]p<0.0001. [18]p=0.01. NPV comparison with AFB/Xpert: [27]p=0.001. [30]p=0.403.

TABLE 3 | Culture results of patients with different acid-fast bacilli smear and Xpert MTB/RIF status.

Culture	AFB$^+$/Xpert$^+$	AFB$^+$/Xpert$^-$	AFB$^-$/Xpert$^+$	AFB$^-$/Xpert$^-$	Total
MTB	44	1	137	45*	227
NTM	0	6†	0	15‡	21
Nocardia	0	0	0	3	3
Negative	7†	0	79¶	1,707	1,793
Total	51	7	216	1,770	2,044

*A total of 2,044 patients had BALF and/or sputum AFB smear, culture, Xpert assays, and peripheral blood mononuclear cell T-SPOT performed simultaneously. For strict comparison, only the first AFB smear and Xpert test results were used in the analysis. Culture results were per-patient results (i.e., MTB positivity was defined as at least one of the BALF and/or sputum specimens having one positive culture result for M. tuberculosis. A similar approach was used to define active NTM and Nocardia infections). *None of them were clinically diagnosed as having active tuberculosis. †All of them were clinically diagnosed as having definite or probable tuberculosis. ‡None of them were clinically diagnosed as having NTM infections. ¶Six of them had no tuberculosis-related diagnosis. AFB, acid-fast bacilli; AFB$^+$, AFB smear positive; AFB$^-$, AFB smear negative; Xpert. Xpert MTB/RIF; Xpert$^+$, Xpert positive; Xpert$^-$, Xpert negative; MTB, M. tuberculosis; NTM, nontuberculous mycobacteria; T-SPOT, T-SPOT.TB; BALF, bronchoalveolar lavage fluid.*

smear or Xpert results. For AFB$^+$ or Xpert$^+$ patient populations, T-SPOT^{MDC} showed suboptimal sensitivities (84.1% vs. 83.1%) and very low NPVs (30.0% vs. 47.4%) (**Table 4**). For AFB$^-$ or Xpert$^-$ patient populations, T-SPOT^{MDC} also showed suboptimal sensitivities (74.4-80.7%), but much higher NPVs (97.3-99.1%). When TBAg/PHA≥0.3 was used, the specificities increased significantly but at the cost of decreased sensitivities (**Table 2**).

We then defined T-SPOT performance based on the status of both AFB smear and Xpert. Accordingly, patients were grouped into four populations: AFB$^-$/Xpert$^-$, AFB$^+$/Xpert$^+$, AFB$^+$/Xpert$^-$, and AFB$^-$/Xpert$^+$ (**Table 4**). For AFB$^-$/Xpert$^-$ patients, T-SPOT^{MDC} demonstrated a high NPV (99.1%) and a suboptimal sensitivity (74.4%) and specificity (71.0%). When TBAg/PHA≥0.3 was used, the specificity was significantly increased to 95.7% but with a decreased sensitivity (16.3%). In contrast, T-SPOT^{MDC} and TBAg/PHA showed no added values in 51 AFB$^+$/Xpert$^+$ patients and 211 AFB$^-$/Xpert$^+$ patients who were either MTB culture$^+$ or clinically diagnosed as having PTB. T-SPOT performance was inconclusive in AFB$^+$/Xpert$^-$ patients (n=5), although it ruled out PTB in three NTM culture$^+$ cases.

TABLE 4 | Performance of T-SPOT.*TB* in detecting pulmonary tuberculosis patients with different acid-fast bacilli smear and/or Xpert MTB/RIF status.

AFB smear/Xpert status (N)*	T-SPOT status	Sensitivity % (95% CI)	Positive/total	Specificity% (95% CI)	Negative/total	PPV % (95% CI)	NPV % (95% CI)	Specificity in NTM cases %(n/N)
AFB$^+$ (56)	T-SPOT^{MDC}	84.1 (73.3-94.9)	37/44	25 (0.5-49.5)	3/12	80.4 (69.0-91.9)	30 (1.6-58.4)	60.0 (3/5)
	TBAg/PHA≥0.3	20.5 (8.5-32.4)	9/44	83.3 (62.3-104.4)	10/12	81.8 (59.0-104.6)	22.2 (10.1-34.4)	100 (5/5)
AFB$^-$ (1,959)	T-SPOT^{MDC}	80.7 (74.9-86.5)	142/176	69.4 (67.2-71.5)	1,237/1,783	20.6 (17.6-23.7)	97.3 (96.4-98.2)	100 (15/15)
	TBAg/PHA≥0.3	29.0 (22.3-35.7)	51/176	94.8 (93.8-95.9)	1,691/1,783	35.7 (27.8-43.5)	93.1 (92.0-94.3)	100 (15/15)
Xpert$^+$ (262)	T-SPOT^{MDC}	83.1 (77.5-88.6)	147/177	31.8 (21.9-41.7)	27/85	71.7 (65.5-77.9)	47.4 (34.4-60.3)	No NTM
	TBAg/PHA≥0.3	29.9 (23.2-36.7)	53/177	76.5 (67.5-85.5)	65/85	72.6 (62.4-82.8)	34.4 (27.6-41.2)	No NTM
Xpert$^-$ (1,753)	T-SPOT^{MDC}	74.4 (61.4-87.5)	32/43	71.0 (68.8-73.1)	1,213/1,710	6.1 (4.0-8.1)	99.1 (98.6-99.6)	90.0 (18/20)
	TBAg/PHA≥0.3	16.3 (5.2-27.3)	7/43	95.7 (94.7-96.6)	1,636/1,710	8.6 (2.5-14.8)	97.9 (97.2-98.5)	100 (20/20)
AFB$^-$/Xpert$^-$ (1,748)	T-SPOT^{MDC}	74.4 (61.4-87.5)	32/43	71.0 (68.8-73.1)	1,210/1,705	6.1 (4.0-8.1)	99.1 (98.6-99.6)	100 (20/20)
	TBAg/PHA≥0.3	16.3 (5.2-27.3)	7/43	95.7 (94.7-96.6)	1,631/1,705	8.6 (2.5-14.8)	97.8 (97.1-98.5)	100 (15/15)
AFB$^+$/Xpert$^+$ (51)	T-SPOT^{MDC}	84.1 (73.3-94.9)	37/44	0.0 (0.0-0.0)	0/7	84.1 (73.3-94.9)	0.0 (0.0-.00)	No NTM
	TBAg/PHA≥0.3	20.5 (8.5-32.4)	9/44	71.4 (38.0-104.9)	5/7	81.8 (59.0-104.6)	12.5 (2.3-22.8)	No NTM
AFB$^+$/Xpert$^{-\dagger}$ (5)	T-SPOT^{MDC}	N/A	.	60 (17.1-102.9)	3/5	0 (0-0)	100 (100-100)	60 (3/5)
	TBAg/PHA≥0.3	N/A	.	100 (100-100)	5/5	N/A	100 (100-100)	100 (5/5)
AFB$^-$/Xpert$^+$ (211)	T-SPOT^{MDC}	82.7 (76.3-89.1)	110/133	34.6 (24.1-45.2)	27/78	68.3 (61.1-75.5)	54 (40.2-67.8)	No NTM
	TBAg/PHA≥0.3	33.1 (25.1-41.1)	44/133	59.1 (44.6-73.6)	26/44	71.0 (59.7-82.3)	22.6 (15.0-30.3)	No NTM

*A total of 2,044 patients had BALF and/or sputum AFB smear, culture, and Xpert assays, as well as peripheral blood mononuclear cell T-SPOT performed concurrently. For strict comparison of the performance of T-SPOT in patients with different AFB smear and Xpert status, only the first AFB smear, Xpert, and T-SPOT results were used in the analysis. Twenty-nine patients with invalid T-SPOT results (PHA spot forming cells <20) were excluded from the analysis, including 7 culture-confirmed MTB cases (1 AFB$^+$/Xpert$^-$, 4 AFB$^-$/Xpert$^+$, and 2 AFB$^-$/Xpert$^-$), 1 NTM cases with AFB$^+$/Xpert$^-$, and 21 culture-negative cases (1 AFB$^-$/Xpert$^+$ and 20 AFB$^-$/Xpert$^-$). Pulmonary tuberculosis was defined as at least one of the BALF and/or sputum specimens having one positive culture result for M. tuberculosis. *Number of patients with different AFB smear and Xpert status. †No tuberculosis cases. AFB, acid-fast bacilli; AFB$^+$, AFB smear positive; AFB$^-$, AFB smear negative; Xpert, Xpert MTB/RIF; Xpert$^+$, Xpert positive; Xpert$^-$, Xpert negative; PPV, positive predictive value; NPV, negative predictive value; NTM, nontuberculous mycobacteria; CI, confidence interval; N/A, not applicable; T-SPOT, T-SPOT.TB; BALF, bronchoalveolar lavage fluid; MTB, M. tuberculosis.*

DISCUSSION

While there are many meta-analyses and pro/retrospective studies addressing the performance of individual TB tests (AFB smear, Xpert, and T-SPOT), very few studies compared the performance of these tests in a holistic view in a real-world setting. Moreover, there are no real-world studies deciphering how these individual tests should be integrated into an optimal algorithm for rapid diagnosis of PTB.

To identify such a potential algorithm, we retrospectively analyzed a large real-world data set from a tertiary referral hospital. We found a much higher sensitivity of 3-4 AFB smears compared to 1-2 AFB smears. We also demonstrated the superiority of BALF to sputum for both AFB smear and Xpert, the higher sensitivity of Xpert compared to AFB smear, as well as the significantly improved accuracy of combining Xpert and AFB smear to diagnose MTB and NTM infections. Lastly, we showed that T-SPOT^{MDC} and TBAg/PHA ratios have a supplementary role for PTB diagnosis in AFB$^-$/Xpert$^-$ patients. These findings led us to propose an optimal algorithm, whereby AFB smear (≥3 smears) and Xpert should be performed first on sputum and/or BALF for rapid diagnosis of MTB and NTM infections in a high-burden setting (**Figure 1**). If available, BALF is preferred for both AFB smear and Xpert. T-SPOT^{MDC} and TBAg/PHA ratios may be useful for diagnosing PTB in AFB$^-$/Xpert$^-$ patients (moderately ruling out PTB and ruling in PTB, respectively).

Our recommendation that 3-4 AFB smears should be performed is based on two observations: (1) 3-4 smears showed high sensitivities and were capable of identifying >95% of AFB$^+$/culture$^+$ TB patients; and (2) the quality of respiratory samples in real practice may not be always ideal. Similar to our study, a US algorithm recommended three consecutive sputum smears for AFB staining (Jensen et al., 2005). In contrast, WHO and European Union recommended two consecutive sputum smears in settings with appropriate external quality assurance and high-quality microscopy (Migliori et al., 2018).

The higher sensitivity of Xpert (compared to AFB smear) and lower specificity of T-SPOT^{MDC} (compared to AFB smear and

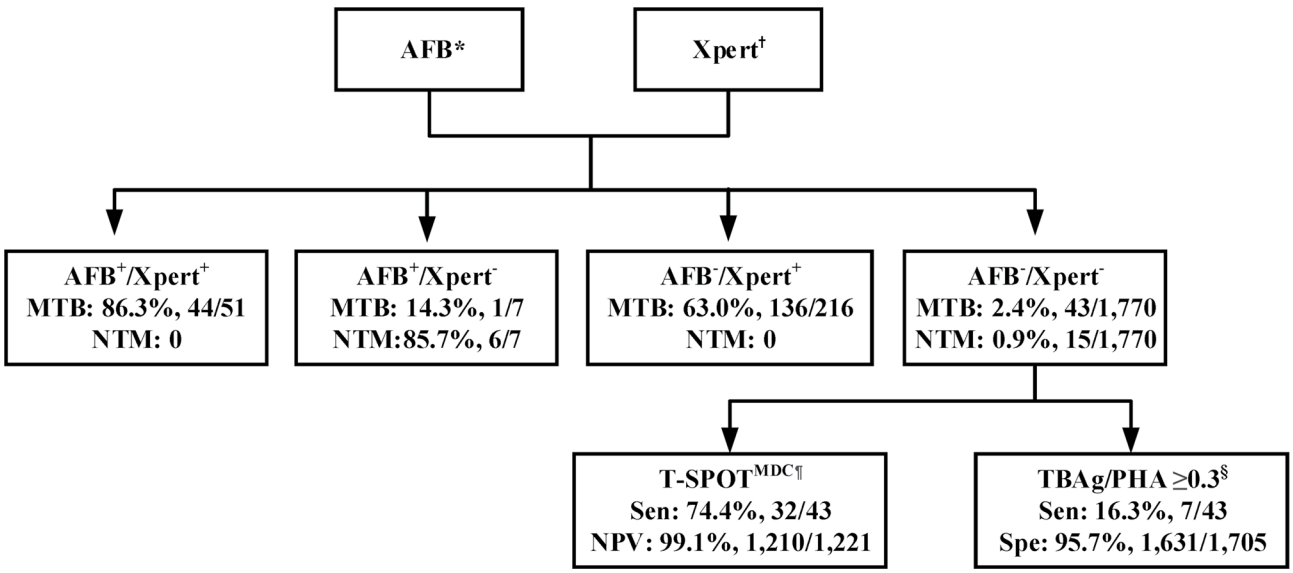

FIGURE 1 | Recommended algorithm for accurate and rapid diagnosis of pulmonary tuberculosis in a real-world setting with high prevalence of *M. tuberculosis* and nontuberculous mycobacterium infections. *Three to four respiratory samples are recommended for AFB smear microscopy, with bronchoalveolar lavage liquid (BALF) preferred. †BALF preferred. ¶T-SPOT^{MDC} (manufacturer-defined cutoff) has a supplementary role in ruling out pulmonary tuberculosis among AFB$^-$/Xpert$^-$ patients. §TBAg/PHA (ratio of TBAg to PHA spot-forming cells, which is modified method calculating T-SPOT.*TB* assay results) ≥0.3 has a supplementary role in ruling in pulmonary tuberculosis among AFB$^-$/Xpert$^-$ patients. AFB, acid-fast bacilli smear; AFB$^+$, AFB smear positive; AFB$^-$, AFB smear negative; Xpert, Xpert MTB/RIF; Xpert$^+$, Xpert positive; Xpert$^-$, Xpert negative; MTB, *Mycobacterium tuberculosis*; NTM, nontuberculous mycobacterium; T_SPOT, T-SPOT.*TB*; MDC, manufacturer-defined cutoff; TBAg, *Mycobacterium tuberculosis*-specific antigens; PHA, phytohaemagglutinin; Sen, sensitivity; PPV, positive predictive value; Spe, specificity.

Xpert) for detecting PTB in this study are consistent with those reported by other prospective/retrospective studies (Ling et al., 2011; Metcalfe et al., 2011; Theron et al., 2011; Lee et al., 2013). While this may not be unexpected, it suggests that Xpert is the preferred assay in real practice. Moreover, when Xpert was used in combination with AFB smear, it significantly improved the diagnostic accuracy for PTB and NTM infections. These findings are consistent with the recommendation by US CDC that participants with AFB$^+$/nucleic acid amplification test (NAAT) positive and AFB$^+$/NAAT-negative respiratory samples are presumable ATB and NTM cases, respectively (Forbes et al., 2018).

Our real-world data also showed that T-SPOT^{MDC} or TBAg/PHA ratio alone was unable to rule in or rule out PTB. When combined with AFB smear or Xpert, they also did not improve the performance compared to AFB smear or Xpert alone. This agrees with findings from other studies (Ling et al., 2011; Metcalfe et al., 2011; Forbes et al., 2018), and supports the WHO policy that IGRAs should not be used for diagnosing active TB (Sester et al., 2011). However, upon stratifying the results of AFB smear and Xpert, T-SPOT^{MDC} and TBAg/PHA ratios showed added values in AFB$^-$/Xpert$^-$ patients (moderately ruling out and ruling in PTB, respectively), but not in AFB$^+$ or Xpert$^+$ patients. Similarly, IGRAs showed a moderate performance in ruling out ATB in Xpert$^-$ individuals in a high-TB/HIV burden setting (Theron et al., 2012). Intriguingly, a recent study showed that T-SPOT with BALF with a cut-off of >4000 early secretory antigenic target-6- or culture filtrate protein-10-specific interferon-γ-producing lymphocytes per 10^7 lymphocytes was able to identify 88.9% of AFB$^-$/Xpert$^-$ patients with culture-proven MTB (Jafari et al., 2018), although the sample size of this study is small. It will be interesting to determine if BALF-based T-SPOT^{MDC} and TBAg/PHA ratios can better predict TB disease within a large AFB$^-$/Xpert$^-$ population.

Although T-SPOT^{MDC} or the TBAg/PHA ratio alone was unable to rule in or rule out PTB, the TBAg/PHA ratio (≥0.3) showed increased specificity (albeit at the cost of decreased sensitivity) for diagnosing PTB as compared to T-SPOT^{MDC} (**Table 2**). Traditional T-SPOT^{MDC} measures IFN-γ release in response to MTB-specific antigens, but its performance can be greatly affected by host immune status. Interestingly, we found reduced IFN-γ release in response to PHA in active TB (Wang et al., 2016), although the mechanism underlying this remains unclear. By normalizing TBAg IFN-γ release against PHA IFN-γ release (*i.e.* TBAg/PHA ratio), the impact of host immune status appears to be minimized. In fact, this TBAg/PHA ratio was able to outperform T-SPOT^{MDC} in differentiating between ATB and LTBI (Wang et al., 2016).

Thus, our analyses not only validated the performance of individual tests in a real-world setting, but also provided the basis of integrating these tests in a single algorithm to diagnose PTB and NTM infections. Prior to this study, no formal evidence-based PTB diagnostic algorithms have been developed in a real-world setting. As a result, clinicians from this study tended to have different decisions in choosing TB tests. For instance, only 26.7% of patients underwent culture tests (**Supplementary Table S2**), probably reflecting the fact that clinicians prefer to order TB assays with fast turnaround time (such as AFB smear). Indeed,

we noticed about 1/3 patients were ordered for AFB smear alone, and another 1/3 of patients were ordered for AFB/T-SPOT. Less than 1/5 of patients were ordered for AFB/Xpert.

Our study has several strengths. All data were collected from a large heterogeneous population, allowing the generation of real-world evidence that confirms findings from studies with selected populations. Furthermore, our diagnostic algorithm included both PTB and NTM infections. A few prospective/retrospective studies have demonstrated improved accuracy of combining AFB smear and PCR-based tests for diagnosing PTB (Tueller et al., 2005; Roberts, 2008; Pan et al., 2018), but did not include NTM diagnosis in their algorithms. Lastly, this algorithm recommends T-SPOT assay only for AFB^-/$Xpert^-$ patients. Benefiting from this algorithm, AFB^+ or $Xpert^+$ patients will not have to undergo T-SPOT assay or pay additional costs.

Our study also has some limitations. We did not include children, for whom PTB diagnosis is more challenging. We also did not evaluate the performance of diagnostic tests in patients with different immune status, such as those co-infected with HIV or having diabetes. This is largely due to insufficient numbers of these patients in a very heterogeneous population. The sample size of NTM infections in this study is still too small. Additionally, fast tests for drug resistance (such as the line probe assay GenoType MTBDRplus) should be incorporated into the algorithm in the future study.

In summary, extensive analyses of a large real-world data set allowed us to identify an optimal algorithm for fast diagnosis of PTB and NTM infections in a high-burden setting (such as China, and probably other lower middle-income countries with a similar situation). Findings from this study may also inform policy makers' decisions regarding prevention and control of TB at a local and national level. Nevertheless, our future work will be to validate the proposed algorithm through multi-center prospective studies and analyze its cost-effectiveness.

DATA AVAILABILITY STATEMENT

The raw data supporting the conclusions of this article will be made available by the authors, without undue reservation.

ETHICS STATEMENT

The studies involving human participants were reviewed and approved by Tongji Medical College, Huazhong University of Science & Technology, Wuhan, China. Written informed consent for participation was not required for this study in accordance with the national legislation and the institutional requirements.

AUTHOR CONTRIBUTIONS

JP, JS, ZS, and HY conceived and designed the study. JP, FW, WL, YL, FW, LT, ZC, YZ, and TL performed the experiments. JP, JS, XiW, NS, XuW, SW, QY, BAV, KJ, ZS, and HBY interpreted the data. ZS contributed reagents and materials. ZS and HBY supervised this study. JP and HBY wrote the manuscript. All authors contributed to the article and approved the submitted version.

FUNDING

This work was supported in part by grants from National Mega Project on Major Infectious Disease Prevention (grant no. 2017ZX10103005-007-001, 2017ZX10103005-007-002).

ACKNOWLEDGMENTS

We thank doctors and nurses at the participating departments for inclusion and following up of patients. We also thank all the participants for sample contribution.

SUPPLEMENTARY MATERIAL

The Supplementary Material for this article can be found online at: https://www.frontiersin.org/articles/10.3389/fcimb.2021.650163/full#supplementary-material

REFERENCES

Conde, M. B., Soares, S. L., Mello, F. C., Rezende, V. M., Almeida, L. L., Reingold, A. L., et al. (2000). Comparison of sputum induction with fiberoptic bronchoscopy in the diagnosis of tuberculosis: experience at an acquired immune deficiency syndrome reference center in Rio de Janeiro, Brazil. *Am. J. Respir. Crit. Care Med.* 162, 2238–2240. doi: 10.1164/ajrccm.162.6.2003125

Datta, S., Saunders, M. J., Tovar, M. A., and Evans, C. A. (2017). Improving tuberculosis diagnosis: Better tests or better healthcare? *PloS Med.* 14, e1002406. doi: 10.1371/journal.pmed.1002406

Forbes, B. A., Hall, G. S., Miller, M. B., Novak, S. M., Rowlinson, M. C., Salfinger, M., et al. (2018). Practice Guidelines for Clinical Microbiology Laboratories: Mycobacteria. *Clin. Microbiol. Rev.* 31, e00038-17. doi: 10.1128/CMR.00038-17

Jafari, C., Olaru, I. D., Daduna, F., Ernst, M., Heyckendorf, J., Lange, C., et al. (2018). Rapid diagnosis of pulmonary tuberculosis by combined molecular and immunological methods. *Eur. Respir. J.* 51. doi: 10.1183/13993003.02189-2017

Jensen, P. A., Lambert, L. A., Iademarco, M. F., and Ridzon, R. (2005). Guidelines for preventing the transmission of Mycobacterium tuberculosis in health-care settings 2005. *MMWR Recomm. Rep.* 54, 1–141.

Lee, H. Y., Seong, M. W., Park, S. S., Hwang, S. S., Lee, J., Park, Y. S., et al. (2013). Diagnostic accuracy of Xpert(R) MTB/RIF on bronchoscopy specimens in patients with suspected pulmonary tuberculosis. *Int. J. Tuberc. Lung Dis.* 17, 917–921. doi: 10.5588/ijtld.12.0885

Lee, H. S., Kee, S. J., Shin, J. H., Kwon, Y. S., Chun, S., Lee, J. H., et al. (2018). Xpert MTB/RIF Assay as a Substitute for Smear Microscopy in an Intermediate Burden Setting. *Am. J. Respir. Crit. Care Med.* 199, 784–794. doi: 10.1164/rccm.201804-0654OC

Ling, D. I., Pai, M., Davids, V., Brunet, L., Lenders, L., Meldau, R., et al. (2011). Are interferon-gamma release assays useful for diagnosing active tuberculosis in a high-burden setting? *Eur. Respir. J.* 38, 649–656. doi: 10.1183/09031936.00181610

Mazurek, G. H., Jereb, J., Vernon, A., Lobue, P., Goldberg, S., Castro, K., et al. (2010). Updated guidelines for using Interferon Gamma Release Assays to detect Mycobacterium tuberculosis infection - United States 2010. *MMWR Recomm. Rep.* 59, 1–25. doi: 10.1093/infdis/jir410

Metcalfe, J. Z., Everett, C. K., Steingart, K. R., Cattamanchi, A., Huang, L., Hopewell, P. C., et al. (2011). Interferon-gamma release assays for active pulmonary tuberculosis diagnosis in adults in low- and middle-income countries: systematic review and meta-analysis. *J. Infect. Dis.* 204 Suppl 4, S1120–S1129.

Migliori, G. B., Sotgiu, G., Rosales-Klintz, S., Centis, R., D'ambrosio, L., Abubakar, I., et al. (2018). ERS/ECDC Statement: European Union standards for tuberculosis care 2017 update. *Eur. Respir. J.* 51, 1702678. doi: 10.1183/13993003.02678-2017

Monkongdee, P., Mccarthy, K. D., Cain, K. P., Tasaneeyapan, T., Nguyen, H. D., Nguyen, T. N., et al. (2009). Yield of acid-fast smear and mycobacterial culture for tuberculosis diagnosis in people with human immunodeficiency virus. *Am. J. Respir. Crit. Care Med.* 180, 903–908. doi: 10.1164/rccm.200905-0692OC

Pan, X., Yang, S., Deighton, M. A., Qu, Y., Hong, L., and Su, F. (2018). A Comprehensive Evaluation of Xpert MTB/RIF Assay With Bronchoalveolar Lavage Fluid as a Single Test or Combined With Conventional Assays for Diagnosis of Pulmonary Tuberculosis in China: A Two-Center Prospective Study. *Front. Microbiol.* 9, 444. doi: 10.3389/fmicb.2018.00444

Roberts, C. (2008). Modelling patterns of agreement for nominal scales. *Stat. Med.* 27, 810–830. doi: 10.1002/sim.2945

Sester, M., Sotgiu, G., Lange, C., Giehl, C., Girardi, E., Migliori, G. B., et al. (2011). Interferon-gamma release assays for the diagnosis of active tuberculosis: a systematic review and meta-analysis. *Eur. Respir. J.* 37, 100–111. doi: 10.1183/09031936.00114810

Tarhan, G., Ordulu, L., Gumuslu, F., Ceyhan, I., and Cesur, S. (2003). [Comparison of auramine-rhodamine and Erlich-Ziehl-Neelsen staining methods for the diagnosis of tuberculosis]. *Mikrobiyol. Bul.* 37, 131–136.

Theron, G., Peter, J., Van Zyl-Smit, R., Mishra, H., Streicher, E., Murray, S., et al. (2011). Evaluation of the Xpert MTB/RIF assay for the diagnosis of pulmonary tuberculosis in a high HIV prevalence setting. *Am. J. Respir. Crit. Care Med.* 184, 132–140. doi: 10.1164/rccm.201101-0056OC

Theron, G., Pooran, A., Peter, J., Van Zyl-Smit, R., Kumar Mishra, H., Meldau, R., et al. (2012). Do adjunct tuberculosis tests, when combined with Xpert MTB/RIF, improve accuracy and the cost of diagnosis in a resource-poor setting? *Eur. Respir. J.* 40, 161–168. doi: 10.1183/09031936.00145511

Tueller, C., Chhajed, P. N., Buitrago-Tellez, C., Frei, R., Frey, M., and Tamm, M. (2005). Value of smear and PCR in bronchoalveolar lavage fluid in culture positive pulmonary tuberculosis. *Eur. Respir. J.* 26, 767–772. doi: 10.1183/09031936.05.00046105

Wang, F., Hou, H. Y., Wu, S. J., Zhu, Q., Huang, M., Yin, B., et al. (2016). Using the TBAg/PHA ratio in the T-SPOT((R)).TB assay to distinguish TB disease from LTBI in an endemic area. *Int. J. Tuberc. Lung Dis.* 20, 487–493. doi: 10.5588/ijtld.15.0756

Who (2018). *Global tuberculosis report 2018* (Geneva, Switzerland: Geneva: World Health Organization).

Who (2020). "WHO consolidated guidelines on tuberculosis: tuberculosis preventive treatment: Module 1: prevention," in *WHO consolidated guidelines on tuberculosis: tuberculosis preventive treatment: Module 1: prevention* (Geneva: WHO).

Zhao, Y., Xu, S., Wang, L., Chin, D. P., Wang, S., Jiang, G., et al. (2012). National survey of drug-resistant tuberculosis in China. *N. Engl. J. Med.* 366, 2161–2170. doi: 10.1056/NEJMoa1108789

Conflict of Interest: The authors declare that the research was conducted in the absence of any commercial or financial relationships that could be construed as a potential conflict of interest.

frontiers in Cellular and Infection Microbiology

ORIGINAL RESEARCH
published: 22 March 2021
doi: 10.3389/fcimb.2021.647220

Subunit Vaccine ESAT-6:c-di-AMP Delivered by Intranasal Route Elicits Immune Responses and Protects Against *Mycobacterium tuberculosis* Infection

Huanhuan Ning[1,2†], Wei Zhang[3†], Jian Kang[2†], Tianbing Ding[4], Xuan Liang[1], Yanzhi Lu[2], Chengxuan Guo[5], Wenjie Sun[5], Huapeng Wang[5], Yinlan Bai[2] and Lixin Shen[1*]*

[1] Key Laboratory of Resources Biology and Biotechnology in Western China, College of Life Sciences, Northwest University, Xi'an, China, [2] Department of Microbiology and Pathogen Biology, Basic Medical School, Air Force Medical University, Xi'an, China, [3] Department of Paediatrics, TangDu Hospital, Air Force Medical University, Xi'an, China, [4] Medical College, Xijing University, Xi'an, China, [5] Student Brigade, Basic Medical School, Air Force Medical University, Xi'an, China

OPEN ACCESS

Edited by:
Xihui Shen,
Northwest A and F University, China

Reviewed by:
Hongxia Niu,
Lanzhou University, China
Farzad Khademi,
Ardabil University of Medical Sciences, Iran

***Correspondence:**
Lixin Shen
shenlx@nwu.edu.cn
Yinlan Bai
yinlanbai@fmmu.edu.cn

[†]These authors have contributed equally to this work

Specialty section:
This article was submitted to Bacteria and Host, a section of the journal Frontiers in Cellular and Infection Microbiology

Received: 29 December 2020
Accepted: 01 March 2021
Published: 22 March 2021

Citation:
Ning H, Zhang W, Kang J, Ding T, Liang X, Lu Y, Guo C, Sun W, Wang H, Bai Y and Shen L (2021) Subunit Vaccine ESAT-6:c-di-AMP Delivered by Intranasal Route Elicits Immune Responses and Protects Against Mycobacterium tuberculosis Infection. Front. Cell. Infect. Microbiol. 11:647220. doi: 10.3389/fcimb.2021.647220

Tuberculosis (TB), caused by *Mycobacterium tuberculosis* (Mtb) infection, remains the most common cause of death from a single infectious disease. More safe and effective vaccines are necessary for preventing the prevalence of TB. In this study, a subunit vaccine of ESAT-6 formulated with c-di-AMP (ESAT-6:c-di-AMP) promoted mucosal and systemic immune responses in spleen and lung. ESAT-6:c-di-AMP inhibited the differentiations of $CD8^+$ T cells as well as macrophages, but promoted the differentiations of ILCs in lung. The co-stimulation also enhanced inflammatory cytokines production in MH-S cells. It was first revealed that ESAT-6 and c-di-AMP regulated autophagy of macrophages in different stages, which together resulted in the inhibition of Mtb growth in macrophages during early infection. After Mtb infection, the level of ESAT-6-specific immune responses induced by ESAT-6:c-di-AMP dropped sharply. Finally, inoculation of ESAT-6:c-di-AMP led to significant reduction of bacterial burdens in lungs and spleens of immunized mice. Our results demonstrated that subunit vaccine ESAT-6:c-di-AMP could elicit innate and adaptive immune responses which provided protection against Mtb challenge, and c-di-AMP as a mucosal adjuvant could enhance immunogenicity of antigen, especially for innate immunity, which might be used for new mucosal vaccine against TB.

Keywords: ***Mycobacterium tuberculosis*, subunit vaccine, ESAT-6, c-di-AMP, mucosal adjuvant**

INTRODUCTION

Tuberculosis (TB) remains the most common cause of death from a single infectious disease. Approximately two billion people worldwide are infected with *Mycobacterium tuberculosis* (Mtb), with around 10 million new cases of TB emerging each year and approximately 1.4 million deaths in 2019 (WHO, 2020). Bacillus Calmette-Guerin (BCG) is the only licensed TB vaccine, and provides

effective protection against TB meningitis and miliary TB when inoculated *via* the intradermal route in children, but its efficacy is variable against pulmonary diseases in adults and does not confer long-lasting protection (Mangtani et al., 2014). As of 2020, there are 14 new TB vaccines in clinical trials, and four of those are subunit vaccines composed of serial Mtb antigens with different adjuvants (WHO, 2020). Subunit vaccine exhibits superior safety and activates stronger antigens-specific immune response compared with other vaccines such as DNA vaccine and attenuated live mycobacterial vaccine (Zhu et al., 2018). More efforts are being made in the formulation, adjuvants, and delivery methods of subunit vaccine to improve the protection against Mtb infection.

The 6 kDa early secretory antigenic target (ESAT-6), an abundantly secreted protein identified from the secreted culture filtrate of Mtb, is a promising candidate antigen for subunit vaccine (Unnikrishnan et al., 2017). ESAT-6 is encoded by *esxA*, a gene in a genetic locus known as region of difference 1 (RD1), which is absent in BCG (Abdallah et al., 2007). Until now, two subunit vaccines composed of ESAT-6, GamTBvac (containing Ag85a and ESAT6-CFP10) and H56:IC31 (containing Ag85B, ESAT-6 and Rv2660c), are now being tested in Phase IIa and IIb trails respectively (WHO, 2020). Our previous work showed that fusion protein Ag85B-ESAT-6 adjuvanted with monophosphoryl lipid A (MPLA) induces significant humoral and cellular immune response by subcutaneous (s.c.) vaccination (Xu, 2014). While, ESAT-6 alone exhibits insufficient immunogenicity either immunized by s.c. or intramuscular (i.m.) route (Lu et al., 2018).

It is widely agreed that the mucosal immune response is vital for protecting against respiratory pathogens including Mtb (Copland et al., 2018; Paquin-Proulx et al., 2018). Mucosal vaccination leads to both mucosal and systemic responses due to dendritic cells (DCs) carrying the immunized antigen to systemic inductive sites such as the lymph nodes and spleen (Macpherson et al., 2008; Lycke, 2012). Several successful mucosal vaccines against diseases have been widely used, indicating the feasibility and safety of this approach. Vaccines against polio, cholera, rotavirus, as well as salmonella are administrated through the oral route (Stylianou et al., 2019). It was also found that intranasal (i.n.) administration of ESAT-6-CFP-10 was inclined to reinforcement of cellular immune responses than that of by i.m. and s.c. immunization (Namvarpour et al., 2019). Hence, mucosal vaccination of ESAT-6 with safe adjuvant may provide improved immune responses against Mtb.

Currently, there is no approved safe and reliable mucosal adjuvant for subunit vaccine. Cyclic dimeric adenosine monophosphate (c-di-AMP), a bacterial second messenger, regulates the cellular physiologies including bacterial growth, biofilm formation, potassium homeostasis, fatty acid metabolism, and virulence (Devaux et al., 2018; Commichau et al., 2019; Zarrella and Bai, 2020). Moreover, c-di-AMP from bacteria activates the cytosolic surveillance pathway leading to the induction of type I interferons (IFNs) during infection (Woodward et al., 2010; Yang et al., 2014; Dey et al., 2015), which is mediated by the stimulator of interferon genes (STING) (Burdette et al., 2011). c-di-AMP derived from Mtb elicits increased autophagy, which restricts the intracellular bacteria growth (Dey et al., 2015).

Additionally, both model antigens β-galactosidase and ovalbumin co-administrated with c-di-AMP induced antigen-specific secreted IgA (sIgA) and balanced Th1/Th2/Th17 response pattern (Ebensen et al., 2011; Skrnjug et al., 2014). Pathogen specific antigens with c-di-AMP as a mucosal adjuvant conferred protection against influenza virus (Sanchez et al., 2014) or *Trypanosoma cruzi* (Matos et al., 2017). Our previous work demonstrated that c-di-AMP as endogenous adjuvant of recombinant BCG (rBCG) induced stronger immune responses in mice after Mtb infection, which was related to trained immunity (Ning et al., 2019). Another report of this rBCG enhanced the protective efficacy against TB in a guinea pig model (Dey et al., 2020). Thus, c-di-AMP exhibits a promising potential as an adjuvant for the development of subunit vaccines, especially for mucosal inoculation.

In this study, a subunit vaccine of ESAT-6 with c-di-AMP as an adjuvant (ESAT-6:c-di-AMP) was administrated by intranasal route *in vivo*, as well as macrophages *in vitro*, to be evaluated for its immune properties and protection against Mtb infection.

MATERIALS AND METHODS

Bacteria Strains, Cell Lines, and Animals

Mycobacterium tuberculosis H37Ra were obtained from National Institute for Food and Drug Control (China) and grown in Middlebrook 7H9 medium (BD) supplemented with 10% oleic acid-albumin-dextrose-catalase (OADC) (BD) and 0.05% Tween 80, or 7H10 medium (BD) for plate. Murine alveolar macrophage cell line MH-S and monocyte/macrophages RAW 264.7 cells were purchased from Procell Life Science & Technology Co., Ltd. (China). SPF mice were purchased from Animal Center of Air Force Medical University.

Animal Groups, Immunization, and Infection

Female BALB/c mice aged from 6 to 8 weeks were anesthetized and treated by intranasal immunization in 50 μl PBS containing c-di-AMP (5 μg/mouse), ESAT-6 (30 μg/mouse), or ESAT-6 (30 μg/mouse) with c-di-AMP (5 μg/mouse) for three times at 2-week intervals. ESAT-6 dose was reduced to 15 μg/mouse in the third immunization. PBS (50 μl/mouse) were used as a control [Naïve and un-vaccinated (UN)]. After 4-week immunization, mice were challenged with 5×10^4 CFU of Mtb H37Ra intravenously in 100 μl PBS.

Detection Antibodies by ELISA

Antibodies in sera and bronchoalveolar lavage fluid (BALF) were detected by enzyme-linked immunosorbent assay (ELISA). Recombinant ESAT-6 was coated to 96-well plate according to the procedures in our previous work (Lu et al., 2018). HRP-conjugated goat anti-mouse IgG, IgG1, IgG2a, IgG2b, IgG3, and

IgA were used, respectively, as secondary antibodies. Subsequently, 3,3′,5,5′-tetramethylbenzidine (TMB) substrate solution was added for detection. The absorbance was determined at an optical density of 450 nm (OD_{450}) using microplate reader (BioTek).

Preparation of Single Cell Suspension From Lung

Lung tissues were cut into small pieces with sterilized scissors on ice, and then digested in 3 ml digestion media [RPMI 1640 media containing 5% fetal bovine serum (FBS) with 50 μg/ml DNase I (Sigma), 1 mg/ml collagenase V (Sigma), 100 U/ml penicillin, and 100 μg/ml streptomycin (Solarbio)] for 1h at 37°C with 5% CO_2. The digested suspension was passed through 70 μm cell strainer and pelleted by centrifugation, then erythrocytes were lysed through osmotic shock buffer (150 mM NH_4Cl, 10 mM $KHCO_3$, and 0.1 mM EDTA, pH 7.2) for 1 min at room temperature. Cells were resuspended and adjusted to the appropriate densities for use.

Measurement of Splenocytes Proliferation

Mouse spleen was aseptically removed and homogenized with 40 μm cell strainers. Single cell suspension was prepared as our previous work (Ning et al., 2019). Splenocytes were seeded in 96-well microplates at 2×10^5 cells/well and stimulated with 5 μg/ml ESAT-6 at the indicated timepoints. MTS reagent was then added and incubated for another 3 h. The absorbance was determined at OD_{490} using microplate reader.

Flow Cytometry

Cells were resuspended in 100 μl PBS containing viability stain Zombie NIR dye (BioLegend) and incubated for 20 min at room temperature in the dark. To avoid unspecific antibody binding, Fc receptors were blocked by anti-mouse CD16/32 mAb in Cell Staining Buffer (BioLegend) for 15 min on ice. Cells were then incubated in 100 μl Cell Staining Buffer with fluorochrome-conjugated cell surface antibodies for 15 min on ice shielded from light. Eventually, cells were washed and resuspended in 500 μl of Cell Staining Buffer for flow cytometry detection.

Intracellular cytokine staining was performed after surface molecule staining as described above. Cells were stimulated with ESAT-6 for 72 h and protein transport inhibitors Brefeldin A Solution (BioLegend) were added to culture in the last 12 h of stimulation prior to harvest. Cells were fixed and permeabilized according to the instructions of Cytofix/Cytoperm Fixation/Permeabilization Kit (BD). Then cells were resuspended in 50 μl of BD Perm/Wash buffer (BD) containing fluorochrome-conjugated antibodies and incubated at 4°C for 30 min in the dark. Finally, cells were washed with Perm/Wash buffer and resuspend in Staining Buffer for flow cytometric analysis. All labeled antibodies were listed in **Table S1**.

Flow cytometry was performed using a BD FACSAria and analyzed with FlowJo software version 10.0 (TreeStar, Ashland).

qRT-PCR Analysis

Total RNA was extracted by TRIZol reagent (TaKaRa) according to the manufacturer's instruction. cDNA was obtained by reverse transcription of 500 ng total RNA using PrimeScript RT reagent Kit with gDNA Eraser (TaKaRa). The primers for qRT-PCR synthesized by Tsingke Biological Technology of China. The sequences of primers were listed in **Table S2**. The fold change of target gene transcription was calculated by $2^{-\Delta\Delta Ct}$.

Cytokine Secretion Assays

Splenocytes were seeded in 96-well microplate 1×10^6 cells/well and stimulated with 5 μg/ml ESAT-6 protein for 72 h. Cell supernatants were collected to measure cytokine secretion by mouse ELISA kits for IFN-γ, IL-2, IL-10, IL-17, IL-1β, IL-18, IL-6, and TNF-α (eBioscience) according to the manufacturer's instructions.

Generation of Bone Marrow-Derived Macrophages (BMDMs)

Bone marrow from both femurs and tibiae of mice was harvested in RPMI 1640. Cells were subsequently resuspended in RPMI 1640 supplemented with 15% FBS, 100 U/ml penicillin, 100 μg/ml streptomycin, and 25% L929-conditioned media in petri dishes (100 mm) and incubated for 3 d at 37°C with 5% CO_2, replaced the medium with the same fresh media. Cells were cultured for another 2 days allowing to differentiation. At day 5, cells were removed using 0.25% trypsin supplemented with 0.02% EDTA and cell scraper. Cells were harvested and resuspended in complete RPMI 1640 medium for *in vitro* assays.

Stimulation of Macrophage Cell Line *In Vitro*

Mouse alveolar macrophage line MH-S cells, RAW264.7 macrophages, and BMDMs were seeded in six-well plates at 1×10^6 cells/well in complete RPMI 1640 medium with Penicillin and Streptomycin solution and incubated overnight. Cells were stimulated by adding c-di-AMP and ESAT-6 with concentration and the duration of stimulation shown in the corresponding figure legends (Jung et al., 2017; Rueckert et al., 2017).

Western Blot Analysis

Cells were lysed using RIPA buffer (Solarbio) supplemented with protease inhibitor cocktail complete (Roche) and phosphatase inhibitor cocktail (Roche) after treatment *in vitro*. LC3 (Sigma) and p62/SQSTM (Proteintech) antibodies were incubated respectively, β-actin (Proteintech) was detected as an internal reference protein.

Immunofluorescence

Cells were fixed with 4% paraformaldehyde and permeabilized with 0.5% Triton X-100 and blocked with 3% BSA. LC3 puncta were stained with LC3 antibody, detected by FITC conjugated goat anti-rabbit antibody. Cell nucleus were stained with Hoechst 33342 for observation under Olympus fluorescence microscope. Extent of autophagy inductions were represented by the percentages of LC3 aggregates puncta-positive cells referring to previous study (Dey et al., 2015).

Bacteria Survival in Macrophages

MH-S cells were stimulated by adding c-di-AMP (10 μg/ml) referred to the previous study (Rueckert et al., 2017), ESAT-6

(10 μg/ml), or ESAT-6 combined with c-di-AMP for 24 h. Log-phase cultures of Mtb H37Ra was washed and diluted in antibiotic-free RPMI, and then were added to the cells with a multiplicity of infection (MOI) at 2:1 for 4 h. The extracellular bacteria were removed by washing with sterile PBS three times, and this time point marked as "0 h" post infection. After infection, cells were washed thoroughly with PBS and lysed by 0.025% SDS at indicated time points. Lysis solutions were diluted and spread on 7H10 agar plates for 3-week of incubation at 37°C for bacteria CFUs counting.

CFU Enumeration

After Mtb challenge, mice spleens and lungs were aseptically removed and homogenized with 40 μm strainer. Serial dilutions of tissue homogenates were spread on 7H10 agar plates, and CFUs were numerated after 3-week of incubation at 37°C.

Statistical Analysis

Statistical analysis was performed using Graph Pad Prism 5.0. All measurements were replicated at least three times and the results expressed as mean ± SEM. The variance differences were compared by Student's *t*-test or for multiple comparisons by analysis of variance (ANOVA). Significant differences were established if $P < 0.05$. "*/$^{\#}$" $P < 0.05$, "**/$^{\#\#}$" $P < 0.01$, "***/$^{\#\#\#}$" $P < 0.001$.

RESULTS

ESAT-6:c-di-AMP Induced Systemic IgG and Higher Local Mucosal sIgA

Our previous work found that ESAT-6 specific antibodies were relatively low in both Mtb-infected mice and guinea pig, which exhibited poor immunogenicity (Lu et al., 2018). Anti-ESAT-6 antibody titer exhibited only 1.13-fold higher in sera of TB patients than healthy control (**Figure S1**). In this study, mice were vaccinated with ESAT-6:c-di-AMP by i.n. route, and the immunization strategy scheme was shown in **Figure 1A**. ESAT-6 alone induced significant elevated total IgG response than Naïve mice ($P < 0.01$) (**Figure 1B**). ESAT-6:c-di-AMP vaccination induced comparable IgG with the antigen alone (**Figure 1B**). For antibody isotypes, either ESAT-6:c-di-AMP or ESAT-6 alone could induce increased IgG2b (**Figure 1C**). Humoral immune responses in the local mucosa are mainly mediated by sIgA, which is considered the hallmark antibody (Stylianou et al., 2019). ESAT-6 alone did not induce significant alteration of sIgA compared with Naïve mice in BALF ($P > 0.05$). Noticeably, c-di-AMP enhanced local mucosal sIgA secretion in BALF induced by ESAT-6 compared to that detected from Naïve mice ($P < 0.01$) (**Figure 1D**). These results indicated that subunit vaccine ESAT-6:c-di-AMP induces high systemic IgG and higher local mucosal sIgA, and c-di-AMP as a mucosal

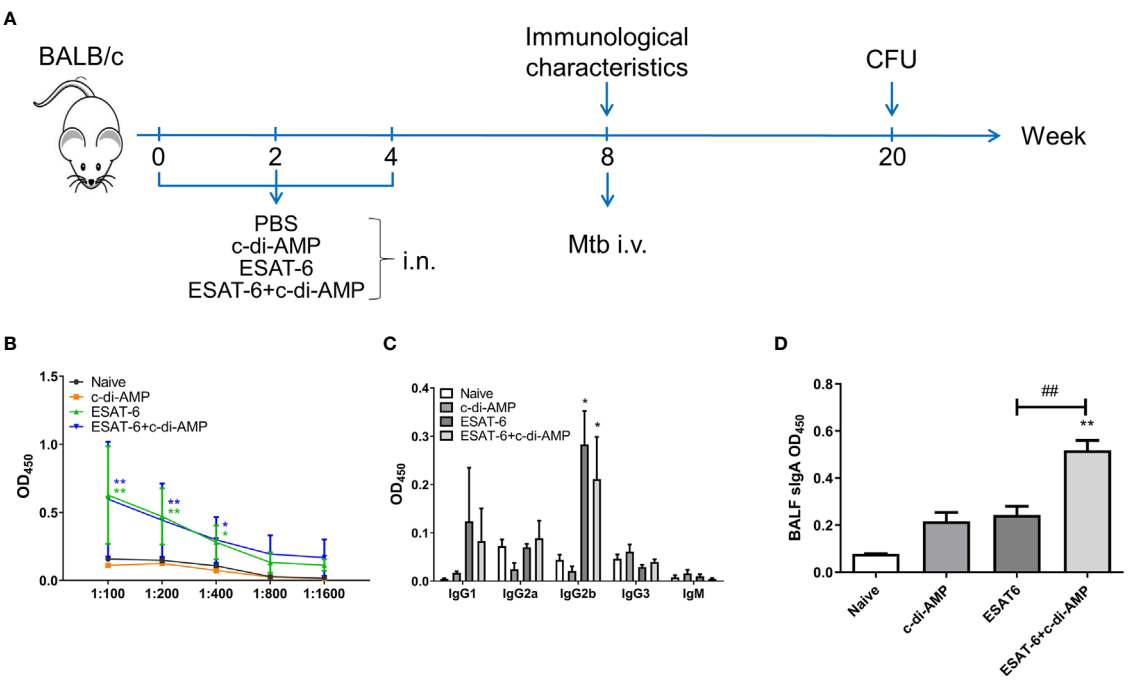

FIGURE 1 | The subunit vaccine ESAT-6:c-di-AMP induced systemic IgG and enhanced mucosal sIgA. **(A)** The immunization and Mtb infection strategy scheme. Female BALB/c mice were immunized intranasally (i.n.) with PBS (Naïve group), c-di-AMP, ESAT-6, or ESAT-6 co-administrated with c-di-AMP, respectively. Mice were boosted twice at 2-week internals. Four weeks after the last immunization, mice were challenged intravenously (i.v.) with Mtb H37Ra at 5×10^4 CFU. **(B)** ESAT-6-specific total IgG in sera at a series of dilutions from 1:100 to 1:1 600. **(C)** ESAT-6-specific subclasses of antibody in sera (1:200) of immunized mice. **(D)** ESAT-6-specific sIgA in BALF of immunized mice were determined using ELISA. "*," compared with the control group (Naïve). *P<0.05, **/##P<0.01, ***P<0.001.

adjuvant enhances humoral immune response induced by ESAT-6.

ESAT-6:c-di-AMP Promoted Th1/Th2/Th17 Immune Responses and Inflammatory Cytokines in Spleen

Cytokines play a crucial role both in controlling initial infection and in promoting as well as maintaining adaptive T-cell responses that mediate host resistance to pathogen (Shaw et al., 2018). Our data showed that immunization of mice with ESAT-6 alone stimulated 2.0-fold splenocytes proliferation than the Naïve group (**Figure 2A**), and c-di-AMP enhanced the proliferation induced by ESAT-6 ($P < 0.01$) (**Figure 2A**). It has been reported that c-di-AMP as a mucosal adjuvant enhances Th1/Th2/Th17 responses of antigen in mice (Ebensen et al., 2011). In this study, we did not find differences in the proportions of $CD4^+$ and $CD8^+$ T cells secreting IFN-γ, IL-2, and IL-10 between different groups after 72 h stimulation *in vitro* (**Figures 2B, C**). Splenocytes from mice immunized with ESAT-6 alone produced increased IL-2 ($P < 0.05$) and IL-17 ($P < 0.05$) than Naïve mice (**Figures 2E, G**). Moreover, c-di-AMP enhanced the secretions of IFN-γ ($P < 0.05$), IL-2 ($P < 0.01$), and IL-17 ($P < 0.05$) in splenocytes of ESAT-6:c-di-AMP immunized mice compared to the vaccination with ESAT-6 alone (**Figures 2D–G**).

In our previous work we found that rBCG with elevated c-di-AMP induced more cytokines related to trained immunity such as IL-1β, IL-6, and TNF-α in splenocytes (Ning et al., 2019). Both IL-1 and IL-18 belong to the interleukin-1 family of cytokines and were secreted following inflammasome activation, which involved in innate and adaptive immune system (Mantovani et al., 2019). It was showed that ESAT-6:c-di-AMP inoculation had no effect on IL-1β (**Figure 2H**), and slightly stimulated IL-18 secretion (**Figure 2I**) ($P < 0.01$). However, we found that ESAT-6:c-di-AMP induced highest levels of IL-6 ($P < 0.01$) and TNF-α ($P < 0.01$) compared to the control mice (**Figures 2H–K**). Overall, ESAT-6:c-di-AMP could potently induce the Th1/Th2/Th17

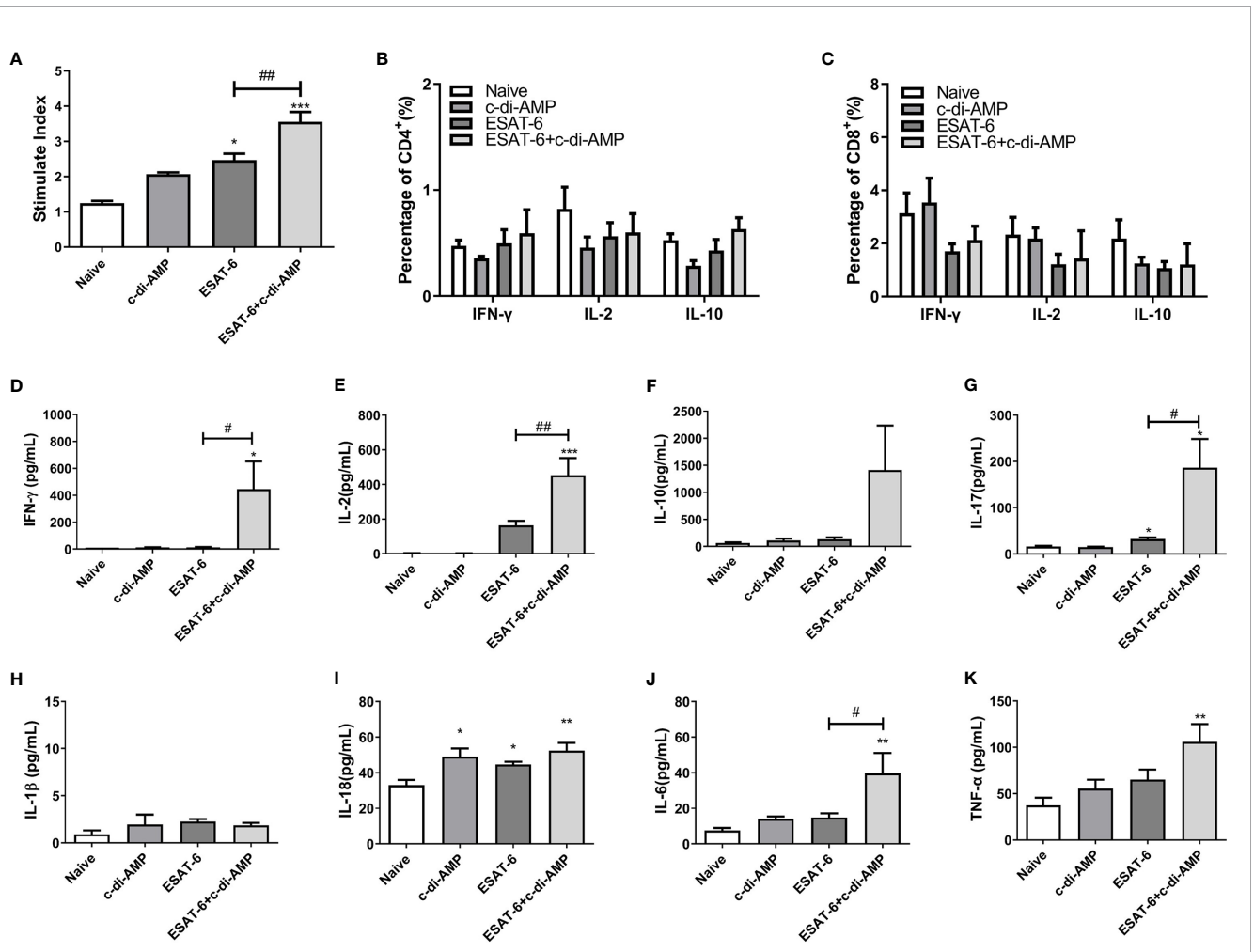

FIGURE 2 | The subunit vaccine ESAT-6:c-di-AMP elicited stronger cellular responses in spleen. **(A)** Splenocyte proliferation of immunized mice stimulated by ESAT-6 (5 μg/ml) *in vitro*. IFN-γ, IL-2, IL-10 secreting splenocytes of $CD4^+$ **(B)** and $CD8^+$ **(C)** T cells detected by FCM after stimulated with ESAT-6 (5 μg/ml) *in vitro*. IFN-γ **(D)**, IL-2 **(E)**, IL-10 **(F)**, IL-17 **(G)**, IL-1β **(H)**, IL-18 **(I)**, IL-6 **(J)**, and TNF-α **(K)** release in supernatant of splenocytes detected using ELISA after stimulated with ESAT-6 (5 μg/ml) *in vitro*. "*," compared with the control group (Naïve) $^{*/\#}P<0.05$, $^{**/\#\#}P<0.01$, $^{***}P<0.001$.

cellular immune responses and inflammatory cytokines release in spleen by mucosal inoculation, indicating a predictive protection against Mtb infection.

ESAT-6:c-di-AMP Promoted Cytokine Responses in Lung

We showed that ESAT-6:c-di-AMP promoted Th1/Th2/Th17 as well as inflammatory cytokines response systematically in spleen (**Figure 2**). Mice inoculated with ESAT-6:c-di-AMP also displayed similar mRNA levels of IFN-γ and IL-2 but decreased IL-10 ($P < 0.05$) and IL-17 ($P < 0.01$) in lungs compared to those vaccinated with ESAT-6 alone (**Figures 3A–D**), which suggested that c-di-AMP prevented increases of IL-10 and IL-17 in lung. For inflammatory cytokines, ESAT-6:c-di-AMP inoculation resulted in elevated IL-18 ($P < 0.05$) and TNF-α ($P < 0.01$) mRNA levels in lung than those in Naïve mice, but not significantly different from the group vaccinated with ESAT-6 alone (**Figures 3E–I**). IFN-β levels were induced mainly by c-di-AMP in ESAT-6:c-di-AMP immunization group ($P < 0.01$), consistent with studies of c-di-AMP on IFN-β response in macrophages (Dey et al., 2015; Rueckert et al., 2017; Ning et al., 2019). Taken together, inoculation ESAT-6:c-di-AMP elicited Th17 and inflammatory cytokine responses in lung. ESAT-6 and c-di-AMP in subunit vaccine played respective roles through distinct mechanisms on immune cells in lung, which were different from that in spleen.

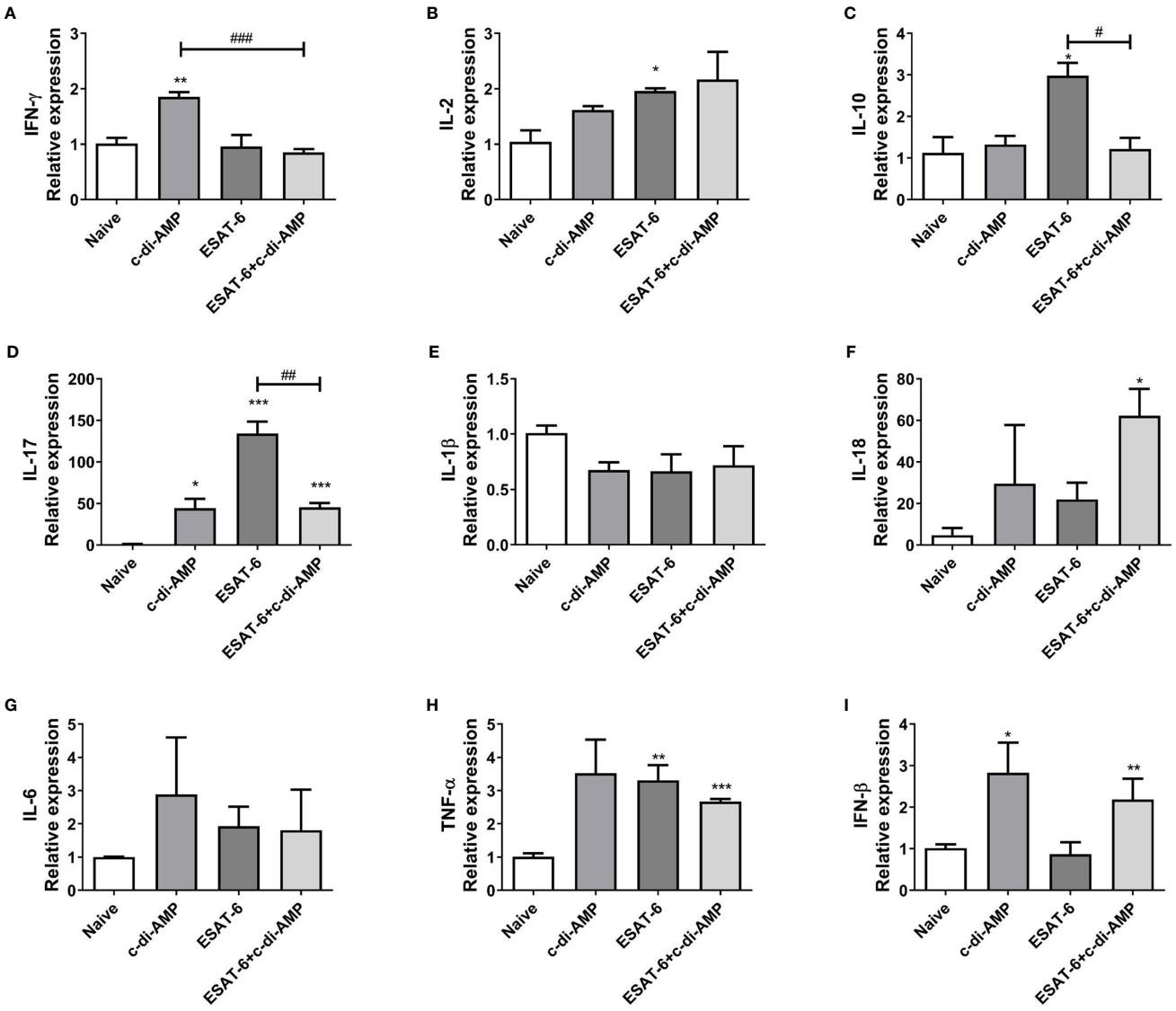

FIGURE 3 | Subunit vaccine ESAT-6:c-di-AMP induced cytokines response in lung. mRNA levels of IFN-γ **(A)**, IL-2 **(B)**, IL-10 **(C)**, IL-17 **(D)**, IL-1β **(E)**, IL-18 **(F)**, IL-6 **(G)**, TNF-α **(H)**, and IFN-β **(I)** in lungs of immunized mice were examined using qRT-PCR. "*," compared with the control group (Naïve) $^{*/\#}P<0.05$, $^{**/\#\#}P<0.01$, $^{***/\#\#\#}P<0.001$.

ESAT-6:c-di-AMP Inhibited the Differentiation of CD8$^+$T Cells in Lung

Further, the proportions of cell subsets in lungs were detected by FCM. ESAT-6 tended to induce cell proliferation of T and B cells, though no difference among all the groups ($P > 0.05$) (**Figure 4A**). To our surprise, it showed that c-di-AMP alone significantly inhibited CD4$^+$ T cells ($P < 0.001$), and ESAT-6 inhibited CD8$^+$ T cells ($P < 0.01$) in lung compared with Naïve group (**Figure 4B**). In contrast, the decline of CD8$^+$ T cells induced by ESAT-6 ($P < 0.01$), and this trend further exacerbated by ESAT-6:c-di-AMP inoculation ($P < 0.001$) (**Figure 4B**).

ESAT-6:c-di-AMP Inhibited the Differentiation of Macrophages in Lung

It has been identified that ESAT-6 is a key mycobacterial effector induced metabolic perturbations to drive the differentiation of macrophage into lipid loaded foamy macrophage (Singh et al., 2015). We found that both ESAT-6 alone and c-di-AMP alone markedly reduced the proportions of lung macrophages than the Naïve group ($P < 0.05$) (**Figure 4C**), and ESAT-6:c-di-AMP resulted in an 11.2% reduction in macrophages than Naïve mice ($P < 0.01$) (**Figure 4C**). Neutrophils, belong to phagocytes as macrophages, are the most abundant cell type in the bronchoalveolar lavage of the active pulmonary TB patients (Liu et al., 2017). However, ESAT-6:c-di-AMP had no effect on the proportion of neutrophils, so did vaccination with ESAT-6 alone and c-di-AMP alone (**Figure 4C**).

ESAT-6:c-di-AMP Induced the Differentiation of Lung ILCs

Innate lymphoid cells (ILCs) are located at mucosal site that respond quickly to invading pathogens (Liu et al., 2017; Gupta et al., 2018; Ardain et al., 2019). ILCs share features of both the innate and adaptive immune systems, and are categorized into three main subsets, ILC1, ILC2, and ILC3

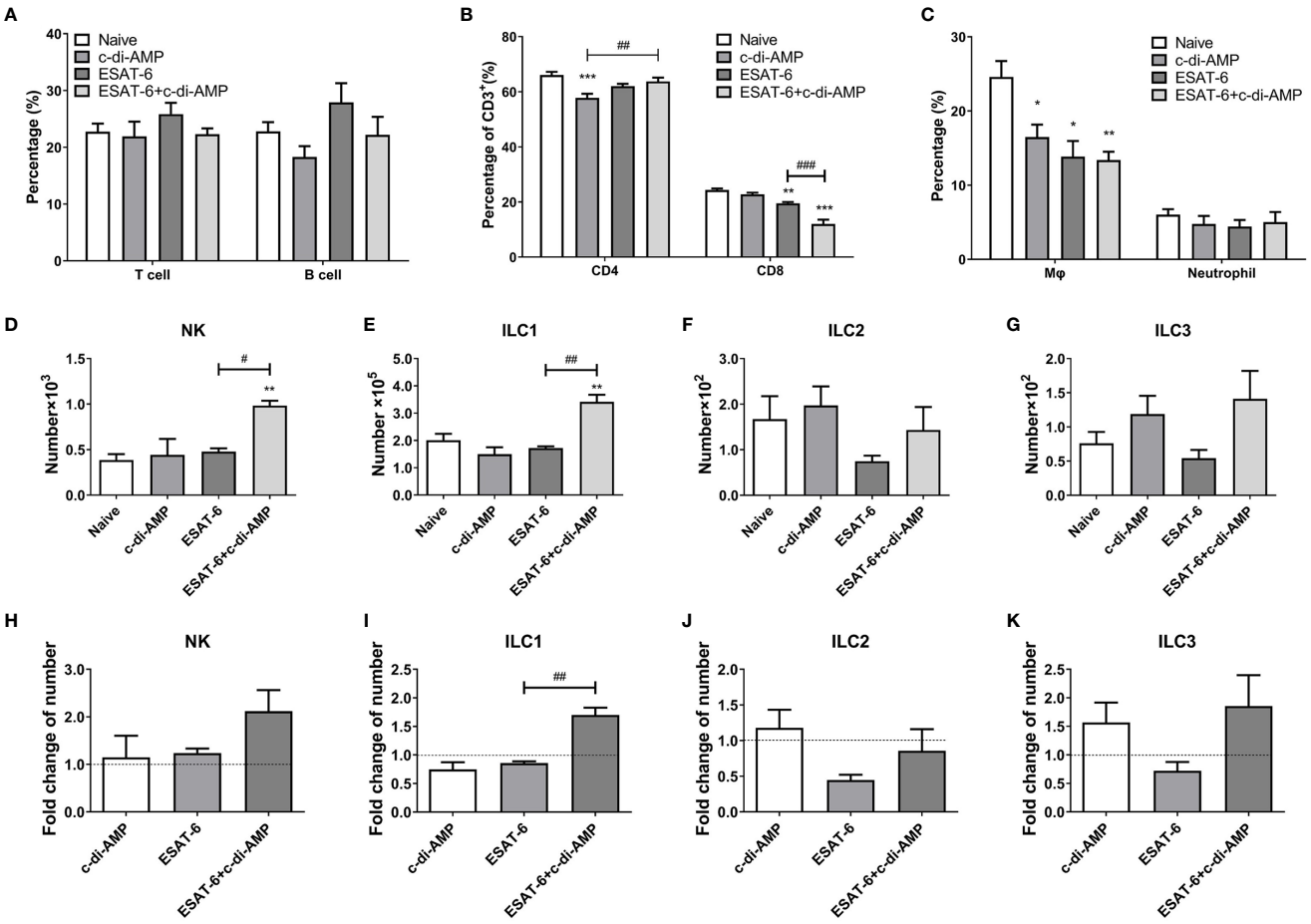

FIGURE 4 | Subunit vaccine ESAT-6:c-di-AMP inoculation affected the differentiations of cell subsets in lung. Proportions of T and B cells **(A)**, CD4$^+$ and CD8$^+$ T cells **(B)**, and macrophages and neutrophils **(C)** in lungs of immunized mice. ILCs numbers of NK cells **(D)**, ILC1 **(E)**, ILC2 **(F)**, and ILC3 **(G)** in lungs of immunized mice 4-week after final immunization. **(H–K)** Fold changes of ILCs cells number related to Naïve mice in **(D–G)**. "*," compared with the control group (Naïve) */#P<0.05, **/##P<0.01, ***/###P<0.001.

(Geremia and Arancibia-Carcamo, 2017; Steigler et al., 2018). NK cells are included in ILC1 group now, and close to killer T cells, while other types of ILC executes similarly to helper T cells. Lung cells were stained for FCM and gated the cells referred to a previous reported study (Steigler et al., 2018) as shown in **Figure S2**. At 4 weeks after intranasal immunization, ESAT-6 alone had no effect on NK and ILC1, but inhibited ILC2 and ILC3 numbers (**Figures 4D–K**). However, ESAT-6:c-di-AMP induced significant increase of NK cells and ILC1 subset compared with ESAT-6 alone group ($P < 0.05$) (**Figures 4D, E, H, I**), which strongly inferred the synergy between ESAT-6 and c-di-AMP. In subunit vaccine group, ILC2 and ILC3 numbers elevated 1.9-fold and 2.6-fold than the group vaccinated with ESAT-6 respectively, which was mainly due to c-di-AMP (**Figures 4F, G, J, K**). Thus, ESAT-6:c-di-AMP induced the differentiations of ILCs in lung and may enhance the immune responses against Mtb infection.

ESAT-6 and c-di-AMP Regulated Autophagy of Macrophages in Different Stages

Autophagy is increasingly appreciated as a pivotal mechanism by which macrophages defense intracellular bacteria including Mtb (Racanelli et al., 2018; Chai et al., 2019). It was reported that ESAT-6 inhibited autophagic flux by impeding autophagosome-lysosome fusion which involved in Mtb immune escape from macrophages (Dong et al., 2016; Peng and Sun, 2016; Wong, 2017). However, recombinant Mtb (rMtb) secreting more c-di-AMP could induce higher autophagy compared with wildtype, which resulted in attenuation of the intracellular growth of rMtb in macrophages J774.1 (Dey et al., 2015). By immunofluorescence staining, we detected an increasing of LC3 puncta formation induced by c-di-AMP, and a mild rise induced by ESAT-6 after 24 h treatment (**Figures 5A, B**). We found that in BMDMs and MH-S cells, ESAT-6 blocked autophagic flux by inhibiting p62 degradation, and c-di-AMP obviously initiated autophagy with an increasing of symbolic autophagy LC3 II after 6 h treatment (**Figures 5C, D**). LC3 II formation induced by c-di-AMP was smoothed by increasing of p62 degradation induced by ESAT-6 after 24 h treatment (**Figures 5C, D**). In ESAT-6 plus c-di-AMP treated cells, autophagy was inhibited with p62 accumulation after 48 h treatment (**Figure 5D**). These observations suggested that ESAT-6 strongly induced the inhibition of p62 degradation at early stage of treatment, which seemed to stock the excessive autophagy of LC3 II formation co-induced by ESAT-6 and c-di-AMP as treatment time prolonged.

ESAT-6 Combined With c-di-AMP Promoted Inflammatory Cytokine Releases in MH-S Cells

c-di-AMP derived from mycobacteria triggers a type I IFN responses *via* the STING-TBK1-IRF3 axis in macrophages, which facilitates host resistance and clears intracellular bacterial infections (Yang et al., 2014; Dey et al., 2015). In our study, c-di-AMP induced IFN-β transcription after 6 h treatment at a dose-dependent manner and lasted at least 24 h (**Figure 6A**). It was reported that ESAT-6 induced IFN-β response *via* TLRs-mediated signaling in BMDMs and MH-S cells (Jang et al., 2018). We found that ESAT-6 induced IFN-β transcription (**Figure 6B**), but not secretion after 24 h treatment (**Figure 6C**). As a result, ESAT-6 with c-di-AMP

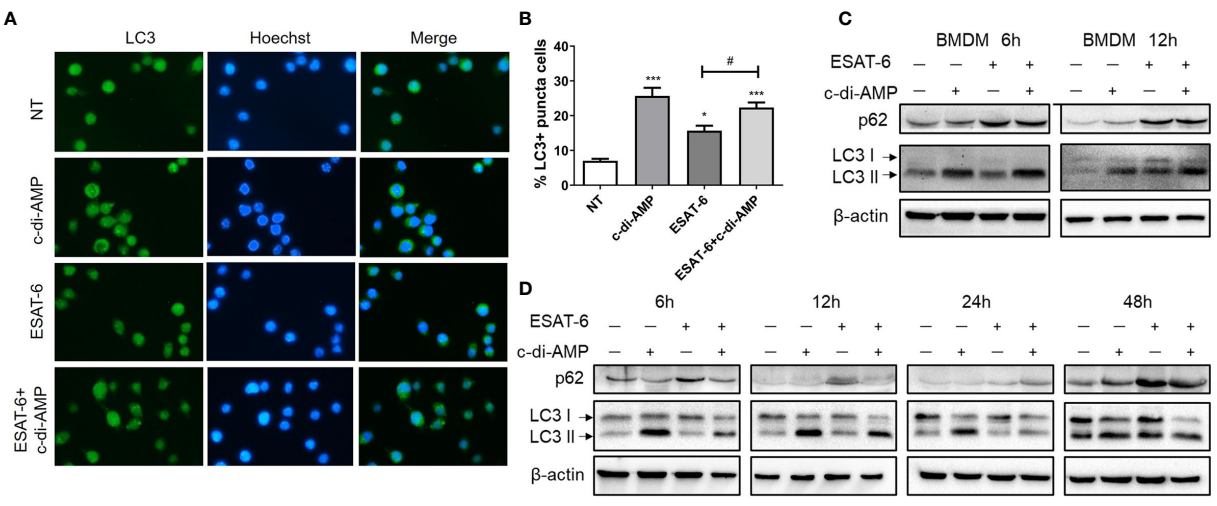

FIGURE 5 | ESAT-6 and c-di-AMP regulated autophagy activation in macrophage. **(A)** Detection of LC3 puncta in RAW264.7 cells after cells were treated with c-di-AMP (10 μg/ml), ESAT-6 (10 μg/ml), and ESAT-6 co-administrated with c-di-AMP for 12 h by immunofluorescence staining. **(B)** Quantitative analysis of the cell proportion of LC3 puncta positive cells in **(A).** LC3 and p62/SQSTM expression in BMDMs **(C)** and MH-S cells **(D)** after cells were treated with c-di-AMP (10 μg/ml), ESAT-6 (10 μg/ml), or ESAT-6 co-stimulated with c-di-AMP at indicated time points. "*," compared with the non-treatment group (NT) */#P<0.05, ***P<0.001.

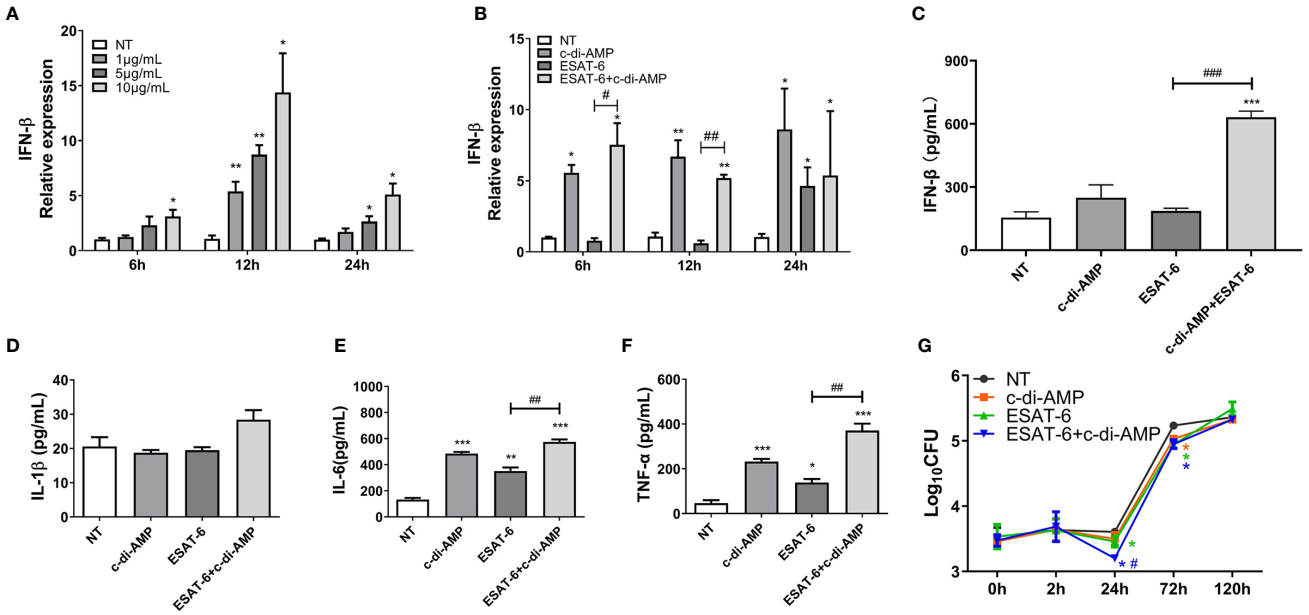

FIGURE 6 | ESAT-6 combined with c-di-AMP promoted cytokine responses and inhibited Mtb survival in macrophages in early stage. **(A)** IFN-β mRNA levels of MH-S cells stimulated by c-di-AMP at different concentrations for indicated time period. **(B)** IFN-β mRNA levels of MH-S cells stimulated by c-di-AMP (10 μg/ml), ESAT-6 (10 μg/ml), or ESAT-6 co-stimulated with c-di-AMP for indicated time period. Cytokine secretions of IFN-β **(C)**, IL-β **(D)**, IL-6 **(E)**, and TNF-α **(F)** in the supernatants of MH-S cells stimulated by c-di-AMP (10 μg/ml), ESAT-6 (10 μg/ml), or ESAT-6 co-stimulated with c-di-AMP for 24 h. **(G)** Mtb H37Ra CFUs within MH-S cells post treatment with c-di-AMP (10 μg/ml), ESAT-6 (10 μg/ml), or ESAT-6 co-administrated with c-di-AMP for 24 h. Bacteria CFUs were determined at indicated time points. "*," compared with the non-treatment group (NT); "#," comparison between experimental groups as indicated in panels **(A–F)**. In panel **(G)**, "#" stands for comparison between ESAT-6+c-di-AMP and ESAT-6 treatments. */#P<0.05, **/##P<0.01, ***/###P<0.001.

induced significant IFN-β secretion after 24 h treatment in MH-S cells which suggested that c-di-AMP had additive effect on ESAT-6 induced IFN-β response (**Figure 6C**). Neither ESAT-6 nor c-di-AMP stimulated IL-1β secretion in MH-S cells after 24 h treatment (**Figure 6D**), similarly to that of in lung and spleen of mice (**Figures 2H**, **3E**). Additionally, co-stimulation with ESAT-6 and c-di-AMP triggered elevated IL-6 and TNF-α secretions than ESAT-6 alone (**Figures 6E, F**), consistent with the results obtained in mice (**Figures 2J, K**). Stimulation of c-di-AMP or ESAT-6 alone induced significant IL-6 and TNF-α secretion (**Figures 6E, F**).

c-di-AMP Enhanced the Restriction of Mtb Survival Induced by ESAT-6 at Early Infection Stage

We wondered whether ESAT-6 and c-di-AMP treatment affects the intracellular growth of Mtb in MH-S cells. After 24 h treatment, ESAT-6 could significantly inhibit Mtb survivals in MH-S cells by 0.15 Log_{10}CFU reduction (**Figure 6G**). c-di-AMP enhanced the inhibition of ESAT-6 on Mtb survivals by 0.26 Log_{10}CFU reduction, and the difference was significant between ESAT-6 and combined treatment, suggesting a synergy of ESAT-6 and c-di-AMP (**Figure 6G**). What is noticeable is that Mtb survivals significantly increased after 24 h of infection, and the inhibition effect of all treatment groups were vanished after 120 h of infection (**Figure 6G**). It suggested that the rapidly activated innate immune response in macrophages could effectively resist early infection, while it was not enough for sustained Mtb infection. Thus, the activated adaptive immune response is needed to clear the infection finally.

ESAT-6 Specific Antibody Declined in Immunized Mice After Mtb Infection

After Mtb infection, ESAT-6 specific IgG level of sera declined in immunized mice (**Figure 7A**), and IgG subclasses were almost undetectable in most groups, excepted IgG1 (**Figure 7B**). Mucosal local humoral response of specific sIgA levels were higher in ESAT-6 alone immunized mice in BALF compared with the un-immunized group after Mtb infection ($P < 0.05$) (**Figure 7C**). Still, ESAT-6:c-di-AMP immunized mice exhibited higher sIgA levels than those of ESAT-6 group ($P < 0.05$) (**Figure 7C**), which showed similar trend as that of after immunization (**Figure 1D**).

Splenocytes of ESAT-6 Immunized Mice Exhibited Anergic Cytokine Response After Mtb Infection

It was obviously that ESAT-6 induced splenocytes proliferation after Mtb infection ($P < 0.05$), and the proliferation stimulated

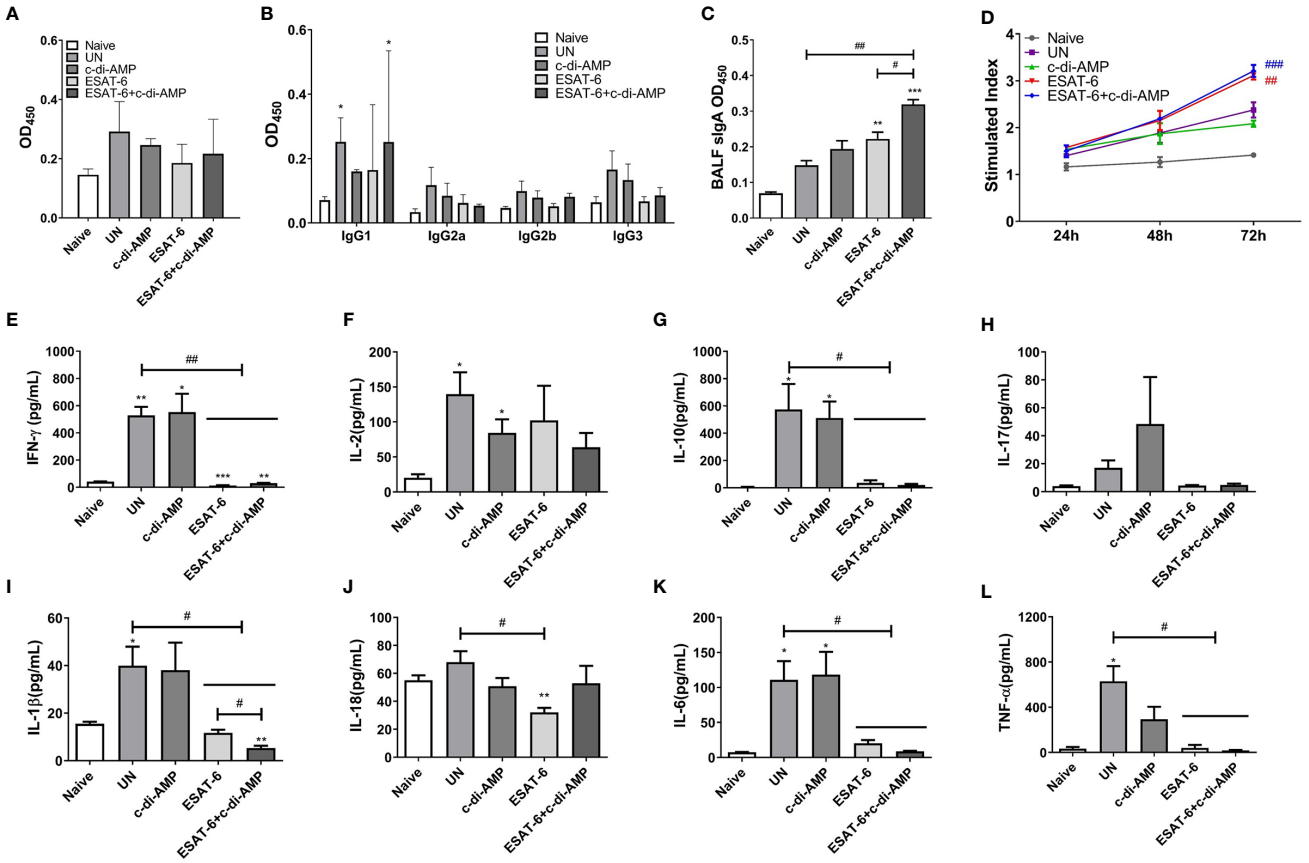

FIGURE 7 | Subunit vaccine ESAT-6:c-di-AMP elicited mucosal sIgA *in vivo* and resulted in restricted cellular immune response *in vitro* after Mtb infection. ESAT-6 specific IgG **(A)** and antibody subclass **(B)** in sera (1:200) of immunized mice after Mtb infection. **(C)** ESAT-6 specific sIgA in BALF of immunized mice after Mtb infection. **(D)** Splenocytes proliferation after cells stimulated with ESAT-6 (5 μg/ml) at indicated time points *in vitro*. **(E–L)** Splenocytes stimulated by ESAT-6 (5 μg/ml) for 72 h *in vitro* and supernatants were examined for cytokines using ELISA. "*," compared with the control group (Naïve); "#," comparison between experimental groups as indicated in panels **(A, C, E–L)**. In panel **(D)**, "#" stands for compared with UN group. */#P<0.05, **/##P<0.01, ***/###P<0.001.

by c-di-AMP faded away after Mtb infection (**Figure 7D**). Splenocytes from Mtb infection mice without vaccination produced significant Th1/Th2 and inflammatory cytokines after re-stimulated with ESAT-6 (**Figures 7E–L**). To our surprise, splenocytes from ESAT-6 and ESAT-6:c-di-AMP immunization groups were not responsive to the re-stimulation of ESAT-6 *in vitro* (**Figures 7E–L**). Almost all cytokine levels detected, except for IL-2, were similarly to that of Naïve mice in supernatants of splenocytes from ESAT-6 and ESAT-6:c-di-AMP immunization mice. At the meantime, c-di-AMP did not affect the productions of cytokines after Mtb infection (**Figures 7E–L**). Our study showed that splenocytes were initially activated by ESAT-6:c-di-AMP immunization in mice (**Figures 2D–K**), and then re-activated by Mtb infection *in vivo*. After Mtb challenge, splenocytes showed not responsive to antigen re-stimulation *in vitro*, concluded with low levels of cytokine releases. Besides, c-di-AMP as adjuvant exacerbated the inhibitory of splenocytes on IL-1β release (**Figure 7I**).

ESAT-6:c-di-AMP Conferred Protection Against Mtb Infection by Vein

In lung, vaccination of ESAT-6:c-di-AMP reduced bacterial load by 0.57 Log_{10}CFU than UN ($P < 0.01$) (**Figure 8A**). In spleen, ESAT-6:c-di-AMP vaccination group showed 1.06 Log_{10}CFU ($P < 0.001$) reduction in bacterial load than the UN group (**Figure 8B**). And ESAT-6 vaccination alone exhibited 0.78 Log_{10}CFU ($P < 0.01$) reduction in bacterial load than UN mice (**Figure 8B**). Overall, ESAT-6 immunization by mucosal route could reduce Mtb CFUs in lung ($P < 0.05$) and in spleen ($P < 0.01$) (**Figures 8A, B**). While, c-di-AMP immunization alone could not provide significant protection against Mtb infection intravenously (**Figure 8A**), which was similar with our results from rBCG with elevated c-di-AMP (Ning et al., 2019). Though no differences were found between subunit vaccine ESAT-6:c-di-AMP and ESAT-6 alone immunization, there exhibited a further downward trend in ESAT-6:c-di-AMP immunized group. These results proved that subunit vaccine ESAT-6:c-di-AMP inoculation by mucosal route might provide

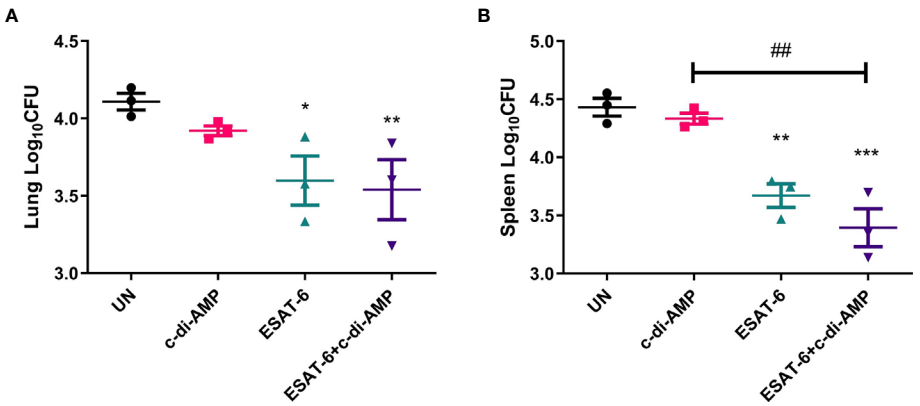

FIGURE 8 | Bacterial burdens in mice after Mtb challenge. After 12-week of Mtb infection, bacterial burdens in the lungs **(A)** and spleens **(B)** of un-immunized (UN), c-di-AMP or ESAT-6 alone, and ESAT-6:c-di-AMP, respectively, were counted by plating. "*," compared with un-immunized group (UN) *P<0.05, **/##P<0.01, ***P<0.001.

protection against Mtb infection intravenously, which was from synergistic effects of ESAT-6 and c-di-AMP.

DISCUSSION

Several prophylactic subunit vaccines for TB have been tested in multiple animal models of mouse, guinea pig, and non-human primate. ESAT-6 is one of the most promising candidates for TB vaccine design. Previously, we have demonstrated that Ag85B-ESAT-6 adjuvanted with MPLA induces significant humoral and cellular immune response *via* s.c. administration, which mainly caused by Ag85B (Xu, 2014). We found that levels of anti-ESAT-6 antibody were increased, but very low in infected animals, as well as in patients (**Figure S1**), and adjuvant enhanced immunogenicity of ESAT-6 either *via* s.c. or i.m. route (Lu et al., 2018). A vaccine formulated with ESAT-6 adjuvanted with both aluminum hydroxide and TLR8 agonist immunized by i.m. route provided protection against Mtb challenge in vein (Tang et al., 2017). Subunit vaccine based on Ag85B-Acr-ESAT6-HBHA intranasal boost administration provided protection against Mtb infection in BCG-primed mice (Hart et al., 2018). Moreover, a mucosal vaccine based on $ESAT6_{1-20}$ peptide delivered through the mucosal route inducing IL-17-dependent induction of CXCL13 and provide protection against Mtb infection in mice (Gopal et al., 2013). These studies show that ESAT-6 as component of subunit vaccine could provide protection against Mtb infection, but requires adjuvant or vaccination through mucosal route to enhance its effects.

Recent study reported that Ag85B-ESAT-6 antigen, delivered by immunogenic carrier of *Lactobacillus plantarum* adjuvanted with poly(I:C) through a primary subcutaneous immunization followed by intranasal boosters, led to slightly elevated IgG levels in serum, and significantly increased levels of antigen-specific mucosal IgA in mice (Kuczkowska et al., 2019). In this study, we composed of a subunit vaccine ESAT-6:c-di-AMP for mucosal immunization. Though IgG were not elevated significantly by addition of c-di-AMP (**Figure 1B**), our study showed that subunit vaccine ESAT-6:c-di-AMP administrated by intranasal route induced higher mucosal sIgA in BALF (**Figure 1C**), which means protection against respiratory pathogens.

ESAT-6 is potent antigen for human T cells and is a putative vaccine candidate against Mtb infection. In this study, ESAT-6:c-di-AMP dramatically improved the production of Th1/Th2/Th17 as well as inflammatory cytokines responses by mucosal inoculation (**Figures 2D–K**), which is in line of previous study of c-di-AMP as mucosal adjuvant (Ebensen et al., 2011). However, it seemed that the profile of cytokine responses was different between lung (**Figure 3**) and spleen (**Figures 2D–K**). From these results, we proposed that ESAT-6 and c-di-AMP may have direct effects on immune cells at mucosal site. $CD4^+$ T cells is more sensitive to recognize Mtb-infected macrophages than $CD8^+$ T cells in lungs, which could correlate with protective immunity (Patankar et al., 2020). The proportions of cell subsets in mice lungs showed that ESAT-6 inhibited $CD8^+$ T cells, and c-di-AMP exacerbate the decline of $CD8^+$ T cells induced by ESAT-6 in ESAT-6:c-di-AMP group (**Figure 4B**). $CD8^+$ T cells, also named cytotoxic T lymphocytes (CTL), killing mechanism is generally dependent on the production of perforin (Lin and Flynn, 2015). While, perforin knockout mice were not more susceptible to Mtb infection (Cooper et al., 1997), but had higher overall IFN-γ production (Serbina et al., 2001), which could compensate for the lack of $CD8^+$ T cell cytotoxicity. As a result, we found that ESAT-6:c-di-AMP inoculation triggered enhanced overall IFN-γ response. Animal model data support a non-redundant role for $CD8^+$ T cells in control of Mtb infection (Lin and Flynn, 2015). Besides, ESAT-6:c-di-AMP induced significant increase of NK cells, which belong to ILC1 subsets, a group of quick response immune cells at mucosal site. Thus, ESAT-6 and c-di-AMP may stimulate immune cells through the same or different mechanisms.

The mechanism study with murine alveolar macrophage cell line MH-S also found the divergence of ESAT-6 and c-di-AMP on immune responses. ESAT-6 alone unable to induce IFN-β production, which was inconsistent with report of ESAT-6 alone promoted IFN-β mRNA level in MH-S cells (Jang et al., 2018). Co-stimulation with ESAT-6 and c-di-AMP promoted IFN-β response, which was mainly due to c-di-AMP (**Figure 3I**). Autophagy is an important innate immune mechanism against intracellular bacteria such as Mtb. ESAT-6 inhibited autophagic flux as reported before (Dong et al., 2016; Peng and Sun, 2016; Wong, 2017). However, c-di-AMP induced increasing of autophagy-associated genes expression in RAW264.7 (Ning et al., 2019), and LC3 II formation in J774.1 (Dey et al., 2015) with elevated c-di-AMP in mycobacteria. In this study, we found that c-di-AMP could triggered LC3 II formation at early stage, but enhanced the p62 degradation inhibition by ESAT-6 and finally inhibited autophagy with the decrease of LC3 II formation after long-term stimulation (**Figures 5C, D**) with more IL-1β, IL-6, and TNF-α secretions (**Figures 6D–F**). The survival trends were similarly to that of autophagy activated with either ESAT-6 or c-di-AMP alone or combined, consistent with the consensus that autophagy plays a major role in restricting bacterial replication (Paik et al., 2019).

After Mtb infection, ESAT-6 specific IgG levels declined in immunized groups compared to those of Naïve mice (**Figures 7A, B**), but high sIgA maintained in ESAT-6 alone and ESAT-6:c-di-AMP immunized mice (**Figure 7C**). Though ESAT-6 induced splenocytes proliferation after Mtb infection, ESAT-6 immunized mice showed no response to antigen re-stimulation and almost no longer secreted cytokines, including Th1/Th2/Th17 as well as inflammatory cytokines *in vitro* (**Figures 7E–H**). It was reported that ESAT-6 treated human T cells, pre-activated with anti-CD3/CD28 mAbs or heat-killed Mtb, produced less IFN-γ compared with non-treatment (Wang et al., 2009). It was also revealed that ESAT-6 can directly bind to T cells and subsequently inhibits the production of IFN-γ by activated T cells through p38 mitogen-activated protein kinase (MAKP)-dependent pathway (Wang et al., 2009). ESAT-6 also inhibited the production of IL-10, IL-17, and TNF-α, but did not affect IL-2 production (Wang et al., 2009; Peng et al., 2011). Besides, ESAT-6 primes DC to stimulate Th17 and inhibits Th1 immune responses, and effects of ESAT-6 were not mediated through cAMP or p38 MAPK pathway (Wang et al., 2012). These observations may partly explain the unresponsive state of splenocytes from ESAT-6:c-di-AMP immunized mice after Mtb infection.

For the evaluation of protection efficiency, we chose Mtb H37Ra strain, a risk group (RG2) pathogen of H37Rv relevant, which has also been extensive used as a surrogate to study the virulence of Mtb in Biosafety Level 2 (BSL2) facilities (Ning et al., 2017; Yang et al., 2020). Mucosal vaccination can induce local mucosal and systemic immune responses. Both ESAT-6 and ESAT-6:c-di-AMP subunit vaccines provided protection against intravenous Mtb H37Ra infection by intranasally in mice. C-di-AMP as adjuvant could improve the protection efficiency of ESAT-6 to a certain extent, while no significant differences were found between two ESAT-6 groups (**Figure 8A**). Our previous study showed that rBCG with c-di-AMP as adjuvant could induce higher immune responses, but provided similar protection as BCG did against Mtb infection intravenously (Ning et al., 2019). However, a similar rBCG conferred improved protection than BCG after respiratory infection of Mtb in guinea pig (Dey et al., 2020). Another study suggested that c-di-AMP as a relatively new immunomodulatory molecule exhibits great potential to promote protective immunity and as an immune-adjuvant to enhance vaccine potency (Libanova et al., 2012). Additionally, another inoculation route of s.c. were applied which c-di-AMP exhibited superior properties in targeting DC (Volckmar et al., 2019). Based on multiple functions that c-di-AMP involved, we will further evaluate the immune protection of these subunit vaccine through more susceptible animals, such as guinea pigs, aerosol challenge of Mtb, or different immunization pathways and strategies.

In this study, there were no adverse reactions observed in the mice throughout the experiments. Of note, ESAT-6 is considered as a virulence factor of Mtb since its knock-out strain showed attenuated virulence in animal infection models. And c-di-AMP promoted a self-limited immune activation by targeting STING degradation, which is a prerequisite for designing the vaccines with predictable efficacy and safety profiles (Rueckert et al., 2017). Nevertheless, subunit vaccine delivered by mucosal route needs a more careful assessment of their safety profile and their capacity to promote potential adverse effects. In this study, we demonstrated that intranasal inoculation of a subunit vaccine ESAT-6:c-di-AMP promoted humoral and cellular immune response, which provided preliminary evidences that antigen adjuvanted with c-di-AMP might be used to formulate mucosal vaccines against Mtb infection.

DATA AVAILABILITY STATEMENT

The original contributions presented in the study are included in the article/**Supplementary Material**. Further inquiries can be directed to the corresponding authors.

ETHICS STATEMENT

The animal studies were conducted under the approval of the Institutional Ethics Committee of Tangdu Hospital, Second Affiliated Hospital of Air Force Medical University, according to the recommendations from the Guide for the Care and Use of Laboratory Animals of the Institute (Approval No. TDLL-2016325).

AUTHOR CONTRIBUTIONS

HN, WZ, and JK performed most experiments. XL, YL, CG, WS, and HW conducted several experiments. HN, WZ, and TD analyzed the data. HN and YB wrote the manuscript. YB and

LS conceived and designed the research. YB supervised this work. All authors contributed to the article and approved the submitted version.

FUNDING

This study was funded by National Major Special Projects of 13th Five-year Plan (No. 2018ZX10302302002004), National Natural Science Foundation (No. 81671638, 81971560), Provincial Natural Science Foundation of Shaanxi Province (No. 2018ZDXM-SF-004).

ACKNOWLEDGMENTS

We thank Dr. Guangchun Bai (Albany Medical College, Albany, NY, USA) for reading the manuscript.

SUPPLEMENTARY MATERIAL

The Supplementary Material for this article can be found online at: https://www.frontiersin.org/articles/10.3389/fcimb.2021.647220/full#supplementary-material

REFERENCES

Abdallah, A. M., Gey van Pittius, N. C., Champion, P. A., Cox, J., Luirink, J., Vandenbroucke-Grauls, C. M., et al. (2007). Type VII secretion–mycobacteria show the way. *Nat. Rev. Microbiol.* 5, 883–891. doi: 10.1038/nrmicro1773

Ardain, A., Domingo-Gonzalez, R., Das, S., Kazer, S. W., Howard, N. C., Singh, A., et al. (2019). Group 3 innate lymphoid cells mediate early protective immunity against tuberculosis. *Nature* 570, 528–532. doi: 10.1038/s41586-019-1276-2

Burdette, D. L., Monroe, K. M., Sotelo-Troha, K., Iwig, J. S., Eckert, B., Hyodo, M., et al. (2011). STING is a direct innate immune sensor of cyclic di-GMP. *Nature* 478, 515–518. doi: 10.1038/nature10429

Chai, Q., Wang, X., Qiang, L., Zhang, Y., Ge, P., Lu, Z., et al. (2019). A *Mycobacterium tuberculosis* surface protein recruits ubiquitin to trigger host xenophagy. *Nat. Commun.* 10, 1973. doi: 10.1038/s41467-019-09955-8

Commichau, F. M., Heidemann, J. L., Ficner, R., and Stulke, J. (2019). Making and Breaking of an Essential Poison: the Cyclases and Phosphodiesterases That Produce and Degrade the Essential Second Messenger Cyclic di-AMP in Bacteria. *J. Bacteriol.* 201, e00462–18. doi: 10.1128/JB.00462-18

Cooper, A. M., D'Souza, C., Frank, A. A., and Orme, I. M. (1997). The course of *Mycobacterium tuberculosis* infection in the lungs of mice lacking expression of either perforin- or granzyme-mediated cytolytic mechanisms. *Infect. Immun.* 65, 1317–1320. doi: 10.1128/IAI.65.4.1317-1320.1997

Copland, A., Diogo, G. R., Hart, P., Harris, S., Tran, A. C., Paul, M. J., et al. (2018). Mucosal Delivery of Fusion Proteins with *Bacillus subtilis* Spores Enhances Protection against Tuberculosis by Bacillus Calmette-Guerin. *Front. Immunol.* 9:346:346. doi: 10.3389/fimmu.2018.00346

Devaux, L., Kaminski, P. A., Trieu-Cuot, P., and Firon, A. (2018). Cyclic di-AMP in host-pathogen interactions. *Curr. Opin. Microbiol.* 41, 21–28. doi: 10.1016/j.mib.2017.11.007

Dey, B., Dey, R. J., Cheung, L. S., Pokkali, S., Guo, H., Lee, J. H., et al. (2015). A bacterial cyclic dinucleotide activates the cytosolic surveillance pathway and mediates innate resistance to tuberculosis. *Nat. Med.* 21, 401–406. doi: 10.1038/nm.3813

Dey, R. J., Dey, B., Singh, A. K., Praharaj, M., and Bishai, W. (2020). Bacillus Calmette-Guerin Overexpressing an Endogenous Stimulator of Interferon Genes Agonist Provides Enhanced Protection Against Pulmonary Tuberculosis. *J. Infect. Dis.* 221, 1048–1056. doi: 10.1093/infdis/jiz116

Dong, H., Jing, W., Runpeng, Z., Xuewei, X., Min, M., Ru, C., et al. (2016). ESAT6 inhibits autophagy flux and promotes BCG proliferation through MTOR. *Biochem. Biophys. Res. Commun.* 477, 195–201. doi: 10.1016/j.bbrc.2016.06.042

Ebensen, T., Libanova, R., Schulze, K., Yevsa, T., Morr, M., and Guzman, C. A. (2011). Bis-(3',5')-cyclic dimeric adenosine monophosphate: strong Th1/Th2/Th17 promoting mucosal adjuvant. *Vaccine* 29, 5210–5220. doi: 10.1016/j.vaccine.2011.05.026

Geremia, A., and Arancibia-Carcamo, C. V. (2017). Innate Lymphoid Cells in Intestinal Inflammation. *Front. Immunol.* 8:1296:1296. doi: 10.3389/fimmu.2017.01296

Gopal, R., Rangel-Moreno, J., Slight, S., Lin, Y., Nawar, H. F., Fallert Junecko, B. A., et al. (2013). Interleukin-17-dependent CXCL13 mediates mucosal vaccine-induced immunity against tuberculosis. *Mucosal Immunol.* 6, 972–984. doi: 10.1038/mi.2012.135

Gupta, N., Kumar, R., and Agrawal, B. (2018). New Players in Immunity to Tuberculosis: The Host Microbiome, Lung Epithelium, and Innate Immune Cells. *Front. Immunol.* 9:709:709. doi: 10.3389/fimmu.2018.00709

Hart, P., Copland, A., Diogo, G. R., Harris, S., Spallek, R., Oehlmann, W., et al. (2018). Nanoparticle-Fusion Protein Complexes Protect against *Mycobacterium tuberculosis* Infection. *Mol. Ther.* 26, 822–833. doi: 10.1016/j.ymthe.2017.12.016

Jang, A. R., Choi, J. H., Shin, S. J., and Park, J. H. (2018). *Mycobacterium tuberculosis* ESAT6 induces IFN-beta gene expression in Macrophages via TLRs-mediated signaling. *Cytokine* 104, 104–109. doi: 10.1016/j.cyto.2017.10.006

Jung, B. G., Wang, X., Yi, N., Ma, J., Turner, J., and Samten, B. (2017). Early Secreted Antigenic Target of 6-kDa of *Mycobacterium tuberculosis* Stimulates IL-6 Production by Macrophages through Activation of STAT3. *Sci. Rep.* 7:40984. doi: 10.1038/srep40984

Kuczkowska, K., Overland, L., Rocha, S. D. C., Eijsink, V. G. H., and Mathiesen, G. (2019). Comparison of eight *Lactobacillus* species for delivery of surface-displayed mycobacterial antigen. *Vaccine* 37, 6371–6379. doi: 10.1016/j.vaccine.2019.09.012

Libanova, R., Becker, P. D., and Guzman, C. A. (2012). Cyclic di-nucleotides: new era for small molecules as adjuvants. *Microbial. Biotechnol.* 5, 168–176. doi: 10.1111/j.1751-7915.2011.00306.x

Lin, P. L., and Flynn, J. L. (2015). CD8 T cells and *Mycobacterium tuberculosis* infection. *Semin. Immunopathol.* 37, 239–249. doi: 10.1007/s00281-015-0490-8

Liu, C. H., Liu, H., and Ge, B. (2017). Innate immunity in tuberculosis: host defense vs pathogen evasion. *Cell Mol. Immunol.* 14, 963–975. doi: 10.1038/cmi.2017.88

Lu, Y., Kang, J., Ning, H., Wang, L., Xu, Y., Xue, Y., et al. (2018). Immunological characteristics of *Mycobacterium tuberculosis* subunit vaccines immunized through different routes. *Microb. Pathog.* 125, 84–92. doi: 10.1016/j.micpath.2018.09.009

Lycke, N. (2012). Recent progress in mucosal vaccine development: potential and limitations. *Nat. Rev. Immunol.* 12, 592–605. doi: 10.1038/nri3251

Macpherson, A. J., McCoy, K. D., Johansen, F. E., and Brandtzaeg, P. (2008). The immune geography of IgA induction and function. *Mucosal Immunol.* 1, 11–22. doi: 10.1038/mi.2007.6

Mangtani, P., Abubakar, I., Ariti, C., Beynon, R., Pimpin, L., Fine, P. E., et al. (2014). Protection by BCG vaccine against tuberculosis: a systematic review of randomized controlled trials. *Clin. Infect. Dis. Off. Publ. Infect. Dis. Soc. America* 58, 470–480. doi: 10.1093/cid/cit790

Mantovani, A., Dinarello, C. A., Molgora, M., and Garlanda, C. (2019). Interleukin-1 and Related Cytokines in the Regulation of Inflammation and Immunity. *Immunity* 50, 778–795. doi: 10.1016/j.immuni.2019.03.012

Matos, M. N., Cazorla, S. I., Schulze, K., Ebensen, T., Guzman, C. A., and Malchiodi, E. L. (2017). Immunization with Tc52 or its amino terminal domain adjuvanted with c-di-AMP induces Th17+Th1 specific immune responses and confers protection against *Trypanosoma cruzi*. *PloS Negl. Trop. Dis.* 11, e0005300. doi: 10.1371/journal.pntd.0005300

Namvarpour, M., Tebianian, M., Mansouri, R., Ebrahimi, S. M., and Kashkooli, S. (2019). Comparison of different immunization routes on the immune responses induced by *Mycobacterium tuberculosis* ESAT-6/CFP-10 recombinant protein. *Biologicals* 59, 6–11. doi: 10.1016/j.biologicals.2019.04.002

Ning, H., Lu, Y., Kang, J., Xu, Y., Wang, L., Wang, Y., et al. (2017). Establishment of mouse models of persistent tuberculosis and characteristics of that infection. *J. Pathogen. Biol.* 12, 219–223. doi: 10.13350/j.cjpb.170306

Ning, H., Wang, L., Zhou, J., Lu, Y., Kang, J., Ding, T., et al. (2019). Recombinant BCG With Bacterial Signaling Molecule Cyclic di-AMP as Endogenous Adjuvant Induces Elevated Immune Responses After *Mycobacterium tuberculosis* Infection. *Front. Immunol.* 10:1519:1519. doi: 10.3389/fimmu.2019.01519

Paik, S., Kim, J. K., Chung, C., and Jo, E. K. (2019). Autophagy: A new strategy for host-directed therapy of tuberculosis. *Virulence* 10, 448–459. doi: 10.1080/21505594.2018.1536598

Paquin-Proulx, D., Costa, P. R., Terrassani Silveira, C. G., Marmorato, M. P., Cerqueira, N. B., Sutton, M. S., et al. (2018). Latent *Mycobacterium tuberculosis* Infection Is Associated With a Higher Frequency of Mucosal-Associated Invariant T and Invariant Natural Killer T Cells. *Front. Immunol.* 9:1394:1394. doi: 10.3389/fimmu.2018.01394

Patankar, Y. R., Sutiwisesak, R., Boyce, S., Lai, R., Lindestam Arlehamn, C. S., Sette, A., et al. (2020). Limited recognition of *Mycobacterium tuberculosis*-infected macrophages by polyclonal CD4 and CD8 T cells from the lungs of infected mice. *Mucosal Immunol.* 13, 140–148. doi: 10.1038/s41385-019-0217-6

Peng, X., and Sun, J. (2016). Mechanism of ESAT-6 membrane interaction and its roles in pathogenesis of *Mycobacterium tuberculosis*. *Toxicon.* 116, 29–34. doi: 10.1016/j.toxicon.2015.10.003

Peng, H., Wang, X., Barnes, P. F., Tang, H., Townsend, J. C., and Samten, B. (2011). The *Mycobacterium tuberculosis* early secreted antigenic target of 6 kDa inhibits T cell interferon-gamma production through the p38 mitogen-activated protein kinase pathway. *J. Biol. Chem.* 286, 24508–24518. doi: 10.1074/jbc.M111.234062

Racanelli, A. C., Kikkers, S. A., Choi, A. M. K., and Cloonan, S. M. (2018). Autophagy and inflammation in chronic respiratory disease. *Autophagy* 14, 221–232. doi: 10.1080/15548627.2017.1389823

Rueckert, C., Rand, U., Roy, U., Kasmapour, B., Strowig, T., and Guzman, C. A. (2017). Cyclic dinucleotides modulate induced type I IFN responses in innate immune cells by degradation of STING. *FASEB J. Off. Publ. Fed. Am. Soc. Exp. Biol.* 31, 3107–3115. doi: 10.1096/fj.201601093R

Sanchez, M. V., Ebensen, T., Schulze, K., Cargnelutti, D., Blazejewska, P., Scodeller, E. A., et al. (2014). Intranasal delivery of influenza rNP adjuvanted with c-di-AMP induces strong humoral and cellular immune responses and provides protection against virus challenge. *PloS One* 9, e104824. doi: 10.1371/journal.pone.0104824

Serbina, N. V., Lazarevic, V., and Flynn, J. L. (2001). CD4(+) T cells are required for the development of cytotoxic CD8(+) T cells during *Mycobacterium tuberculosis* infection. *J. Immunol.* 167, 6991–7000. doi: 10.4049/jimmunol.167.12.6991

Shaw, D. M., Merien, F., Braakhuis, A., and Dulson, D. (2018). T-cells and their cytokine production: The anti-inflammatory and immunosuppressive effects of strenuous exercise. *Cytokine* 104, 136–142. doi: 10.1016/j.cyto.2017.10.001

Singh, V., Kaur, C., Chaudhary, V. K., Rao, K. V., and Chatterjee, S. (2015). *M. tuberculosis* Secretory Protein ESAT-6 Induces Metabolic Flux Perturbations to Drive Foamy Macrophage Differentiation. *Sci. Rep.* 5:12906. doi: 10.1038/srep12906

Skrnjug, I., Guzman, C. A., and Rueckert, C. (2014). Cyclic GMP-AMP displays mucosal adjuvant activity in mice. *PloS One* 9, e110150. doi: 10.1371/journal.pone.0110150

Steigler, P., Daniels, N. J., McCulloch, T. R., Ryder, B. M., Sandford, S. K., and Kirman, J. R. (2018). BCG vaccination drives accumulation and effector function of innate lymphoid cells in murine lungs. *Immunol. Cell Biol.* 96, 379–389. doi: 10.1111/imcb.12007

Stylianou, E., Paul, M. J., Reljic, R., and McShane, H. (2019). Mucosal delivery of tuberculosis vaccines: a review of current approaches and challenges. *Expert Rev. Vaccines* 18, 1271–1284. doi: 10.1080/14760584.2019.1692657

Tang, J., Sun, M., Shi, G., Xu, Y., Han, Y., Li, X., et al. (2017). Toll-Like Receptor 8 Agonist Strengthens the Protective Efficacy of ESAT-6 Immunization to *Mycobacterium tuberculosis* Infection. *Front. Immunol.* 8:1972:1972. doi: 10.3389/fimmu.2017.01972

Unnikrishnan, M., Constantinidou, C., Palmer, T., and Pallen, M. J. (2017). The Enigmatic Esx Proteins: Looking Beyond Mycobacteria. *Trends Microbiol.* 25, 192–204. doi: 10.1016/j.tim.2016.11.004

Volckmar, J., Knop, L., Stegemann-Koniszewski, S., Schulze, K., Ebensen, T., Guzman, C. A., et al. (2019). The STING activator c-di-AMP exerts superior adjuvant properties than the formulation poly(I:C)/CpG after subcutaneous vaccination with soluble protein antigen or DEC-205-mediated antigen targeting to dendritic cells. *Vaccine* 37, 4963–4974. doi: 10.1016/j.vaccine.2019.07.019

Wang, X., Barnes, P. F., Dobos-Elder, K. M., Townsend, J. C., Chung, Y. T., Shams, H., et al. (2009). ESAT-6 inhibits production of IFN-gamma by *Mycobacterium tuberculosis*-responsive human T cells. *J. Immunol.* 182, 3668–3677. doi: 10.4049/jimmunol.0803579

Wang, X., Barnes, P. F., Huang, F., Alvarez, I. B., Neuenschwander, P. F., Sherman, D. R., et al. (2012). Early secreted antigenic target of 6-kDa protein of *Mycobacterium tuberculosis* primes dendritic cells to stimulate Th17 and inhibit Th1 immune responses. *J. Immunol.* 189, 3092–3103. doi: 10.4049/jimmunol.1200573

Wong, K.-W. (2017). The Role of ESX-1 in *Mycobacterium tuberculosis* Pathogenesis. *Microbiol. Spectrum.* 5. doi: 10.1128/microbiolspec.TBTB2-0001-2015

Woodward, J. J., Iavarone, A. T., and Portnoy, D. A. (2010). c-di-AMP secreted by intracellular *Listeria monocytogenes* activates a host type I interferon response. *Science* 328, 1703–1705. doi: 10.1126/science.1189801

World Health Organization (2020). *Global Tuberculosis Report*. Available at: https://www.who.int/tb/publications/global_report/esn/ (Accessed March 5, 2020).

Xu, C. (2014). *Preliminary evaluation of a subunit vaccine based on fusion proteins for its therapeutic efficacy in Mycobacterium tuberculosis infected guinea pig and mouse modle. [dissertation/master's thesis]* ([Xi'an (Shaanxi)]: Air Force Medical University).

Yang, J., Bai, Y., Zhang, Y., Gabrielle, V. D., Jin, L., and Bai, G. (2014). Deletion of the cyclic di-AMP phosphodiesterase gene (cnpB) in *Mycobacterium tuberculosis* leads to reduced virulence in a mouse model of infection. *Mol. Microbiol.* 93, 65–79. doi: 10.1111/mmi.12641

Yang, S. J., Chen, Y. Y., Hsu, C. H., Hsu, C. W., Chang, C. Y., Chang, J. R., et al. (2020). Activation of M1 Macrophages in Response to Recombinant TB Vaccines With Enhanced Antimycobacterial Activity. *Front. Immunol.* 11:1298:1298. doi: 10.3389/fimmu.2020.01298

Zarrella, T. M., and Bai, G. (2020). The many roles of the bacterial second messenger cyclic di-AMP in adapting to stress cues. *J. Bacteriol.* 203, e00348–20. doi: 10.1128/JB.00348-20

Zhu, B., Dockrell, H. M., Ottenhoff, T. H. M., Evans, T. G., and Zhang, Y. (2018). Tuberculosis vaccines: Opportunities and challenges. *Respirology* 23, 359–368. doi: 10.1111/resp.1324

Conflict of Interest: The authors declare that the research was conducted in the absence of any commercial or financial relationships that could be construed as a potential conflict of interest.

frontiers in Cellular and Infection Microbiology

ORIGINAL RESEARCH
published: 06 July 2021
doi: 10.3389/fcimb.2021.691823

Pre-Diabetes Increases Tuberculosis Disease Severity, While High Body Fat Without Impaired Glucose Tolerance Is Protective

Roma Sinha[1†], Minh Dao Ngo[1†], Stacey Bartlett[1], Helle Bielefeldt-Ohmann[2,3], Sahar Keshvari[1], Sumaira Z. Hasnain[1,3], Meg L. Donovan[4], Jessica C. Kling[4], Antje Blumenthal[3,4], Chen Chen[5], Kirsty R. Short[2,3] and Katharina Ronacher[1,3]*

[1] Translational Research Institute, Mater Research Institute, The University of Queensland, Brisbane, QLD, Australia, [2] School of Chemistry and Molecular Biosciences, The University of Queensland, Brisbane, QLD, Australia, [3] Australian Infectious Diseases Research Centre – The University of Queensland, Brisbane, QLD, Australia, [4] The University of Queensland Diamantina Institute, Brisbane, QLD, Australia, [5] School of Biomedical Sciences, The University of Queensland, Brisbane, QLD, Australia

Type 2 diabetes (T2D) is a well-known risk factor for tuberculosis (TB), but little is known about pre-diabetes and the relative contribution of impaired glucose tolerance *vs.* obesity towards susceptibility to TB. Here, we developed a preclinical model of pre-diabetes and TB. Mice fed a high fat diet (HFD) for 12 weeks presented with impaired glucose tolerance and hyperinsulinemia compared to mice fed normal chow diet (NCD). Infection with *M. tuberculosis* (Mtb) $H_{37}R_v$ after the onset of dysglycemia was associated with significantly increased lung pathology, lower concentrations of TNF-α, IFN-γ, IFN-β and IL-10 and a trend towards higher bacterial burden at 3 weeks post infection. To determine whether the increased susceptibility of pre-diabetic mice to TB is reversible and is associated with dysglycemia or increased body fat mass, we performed a diet reversal experiment. Pre-diabetic mice were fed a NCD for 10 additional weeks (HFD/NCD) at which point glucose tolerance was restored, but body fat mass remained higher compared to control mice that consumed NCD throughout the entire experiment (NCD/NCD). Upon Mtb infection HFD/NCD mice had significantly lower bacterial burden compared to NCD/NCD mice and this was accompanied by restored IFN-γ responses. Our findings demonstrate that pre-diabetes increases susceptibility to TB, but a high body mass index without dysglycemia is protective. This murine model offers the opportunity to further study the underlying immunological, metabolic and endocrine mechanisms of this association.

Keywords: impaired glucose tolerance, high fat diet, disease severity, pre-diabetes, diabetes, *Mycobacterium tuberculosis*, tuberculosis, interferon responses

OPEN ACCESS

Edited by:
Ozlem Yilmaz,
Medical University of South Carolina, United States

Reviewed by:
Brendan Podell,
Colorado State University, United States
Dhiraj Kumar Singh,
Southwest National Primate Research Center (SNPRC), United States

***Correspondence:**
Katharina Ronacher
katharina.ronacher@mater.uq.edu.au

†These authors have contributed equally to this work

Specialty section:
This article was submitted to Bacteria and Host, a section of the journal Frontiers in Cellular and Infection Microbiology

Received: *07 April 2021*
Accepted: *17 June 2021*
Published: *06 July 2021*

Citation:
Sinha R, Ngo MD, Bartlett S, Bielefeldt-Ohmann H, Keshvari S, Hasnain SZ, Donovan ML, Kling JC, Blumenthal A, Chen C, Short KR and Ronacher K (2021) Pre-Diabetes Increases Tuberculosis Disease Severity, While High Body Fat Without Impaired Glucose Tolerance Is Protective. Front. Cell. Infect. Microbiol. 11:691823. doi: 10.3389/fcimb.2021.691823

INTRODUCTION

Tuberculosis (TB) remains one of the top 10 causes of death worldwide killing more than 1.4 million people in 2019 (WHO, 2020). Type 2 diabetes (T2D) increases the risk of developing TB as well as the risk of adverse TB treatment outcomes (Critchley et al., 2017). People with TB and T2D co-morbidity have a 88% higher risk of death during treatment, a 64% higher risk of relapse and are twice as likely to develop drug-resistant TB (Huangfu et al., 2019). Paradoxically, obesity in absence of dysglycemia protects against TB (Lonnroth et al., 2010; Aibana et al., 2016; Lin et al., 2018) and individuals with high BMI are less likely to die during TB treatment (Yen et al., 2016).

Increased susceptibility of T2D patients to TB has been attributed to poor glycemic control (Critchley et al., 2018). However, immune dysfunction and altered immunity to TB has also been demonstrated in individuals with pre-diabetes (Kumar et al., 2014; Eckold et al., 2020). Strikingly, blood transcriptomic profiles of TB patients with pre-diabetes are more similar to TB patients with T2D than those without any form of dysglycemia (Eckold et al., 2020). Whether pre-diabetes increases susceptibility to TB and TB disease severity remains unknown and it is also not clear which immunological mechanisms underlie obesity associated resistance vs. diabetes associated susceptibility to TB.

Several different animal models of TB and type 1 or type 2 diabetes have been established to study the underlying immunological mechanisms of diabetes-induced increased susceptibility to TB (Yamashiro et al., 2005; Martens et al., 2007; Sugawara and Mizuno, 2008; Vallerskog et al., 2010; Podell et al., 2014; Martinez et al., 2016; Tripathi et al., 2019; Alim et al., 2020). Such animal models are particularly useful to study immune responses at the site of infection, the lung, which is difficult to achieve in patients. Despite differences in species and methods used for inducing diabetes, these studies demonstrate a clear association between diabetes and increased susceptibility to TB. Diabetic animals have higher bacterial loads, more severe tissue pathology and reduced survival. Therefore, these animal models mimic clinical observations from individuals with TB and diabetes co-morbidity. Whether pre-diabetes impacts susceptibility to TB has not been extensively investigated in animal models with only one study from guinea pigs (Podell et al., 2014). Most importantly, no published data exist relating to the relative contribution of dysglycemia and obesity in susceptibility or resistance to TB. Given the high global prevalence rates of pre-diabetes in TB household contacts from both low and high TB burden countries - with 23% and 25% in South Africa and South Texas, respectively (Restrepo et al., 2018) - it is imperative to expand TB and diabetes association studies to include obesity with and without dysglycemia.

Here, we developed a murine model of high fat-diet (HFD)-induced pre-diabetes and a diet reversal model to dissect the relative contribution of dysglycemia vs. obesity to susceptibility TB. Pre-diabetic mice had more severe TB and dysregulated cytokine production both at the site of infection and in the periphery, while obese animals with restored glucose tolerance were more resistant to TB.

MATERIALS AND METHODS

Ethics Statement

All experiments were carried out in accordance with protocols approved by the Health Sciences Animal Ethics Committee of The University of Queensland (MRI-UQ/413/17) and performed in accordance with the Australian Code of Practice for the Care and Use of Animals for Scientific Purposes.

Murine Pre-Diabetes and Diet-Reversal Models

Six-week-old male C57BL/6 mice were housed in a conventional pathogen free environment, on a 12-hour light/dark cycle at 22° C and fed *ad libitum*. Male mice were chosen for this study as they are more susceptible to developing HFD-induced hyperglycemia (Heydemann, 2016). Animals were either fed a lard based-HFD for 12 weeks (HFD), which contained 43% available energy as fat (total fat: 23.50%, SF04-001, Specialty Feeds, Western Australia) or normal chow diet (NCD) with 12% available energy from fat for the same period (total fat: 4.60%, Standard rodent diet, Specialty Feeds, Western Australia). For the diet reversal experiment 12-week HFD fed animals were fed NCD diet for a further 10 weeks (HFD/NCD) while the control group continued on a NCD for the same period of time (NCD/NCD). Body weights of all mice were recorded weekly throughout the experiment. The respective diets continued until conclusion of the experiment. Mice were infected with Mtb $H_{37}R_v$ at week 12 or 22 as described below.

Oral Glucose Tolerance Test, HbA1c and Insulin Measurement

At 12 or 22 weeks on the respective diets, oral glucose tolerance tests (OGTT), fasting insulin measurements and body composition analyses were performed. Mice were fasted for 5h with access to drinking water followed by oral gavage with a fixed dose of 50 mg glucose per mouse which has been proved sufficient to show glucose intolerance in mice irrespective of body weight (Andrikopoulos et al., 2008). Blood was collected from tail veins and glucose concentrations were determined using a glucometer (Sensocard Plus, Elektronika Kft., Budapest, Hungary) before (0 min) and at 15, 30, 60, and 120 min after gavage. HbA1c was measured from total blood using the DCA Vantage analyzer (Siemens Healthcare Diagnostics Inc., Germany). Fasting insulin levels were quantified in serum using Ultra-Sensitive Mouse Insulin ELISA Kit (Crystal Chem, IL, USA) as per manufacturer's instruction.

Body Composition Measurements and Physiological Monitoring

Whole body composition (fat and lean mass) was measured using a Bruker Minispec LF50H NMR instrument 7.5 MHz (Bruker Corporation, MA, USA) (Tinsley et al., 2004). A subset of five mice per group from the diet change experiment (at week

12 and week 22) were housed in single caging for 1 week for acclimatization followed by 3 days of metabolic profiling using the PhenoMaster System (TSE systems GmbH, Bad Homburg, Germany). Energy expenditures including CO_2 production (VCO_2) and O_2 consumption (VO_2) were monitored for 72h and respiratory exchange ratio (RER) was calculated VCO_2/VO_2. The mice were free to consume food and intake was measured. The resting energy expenditure (REE) was calculated using Weir equation (Weir, 1949).

Mtb Infection, Determination of Bacterial Burden and Immunopathology

Mtb $H_{37}R_v$ was grown on Middlebrook 7H9 medium containing 0.05% Tween-80 and supplemented with 10% Middlebrook Oleic Albumin Dextrose Catalase Growth Supplement (BD Biosciences, USA)/0.2% glycerol to mid-log phase (OD_{600} 0.4 to 0.6). On the day of infection, a single cell suspension was prepared (O.D. of 0.1, equivalent to 50 million cells/ml) and placed in a nebulizer of an inhalation exposure system (Glas-Col, LLC, IN, USA) for aerosol infection of mice. Approximately 100-150 colony forming units (CFU) were deposited in the lung. Lungs, livers, spleens and blood were collected for determination of bacterial counts, pathology, RNA extractions and cytokine analysis as described below. For bacterial load determination tissues were homogenized, serially diluted in PBS and plated on 7H10 agar plates supplemented with 10% OADC/0.5% glycerol and incubated at 37°C. Bacterial colonies were counted after 2-3 weeks. Formalin-fixed lung lobe sections were stained with hematoxylin and eosin (H&E). A qualified pathologist analyzed images of H&E-stained sections from lungs, without prior knowledge of the groupings, as previously described (Flores-Valdez et al., 2018). Briefly, the number of lesions apparent in a section was counted and the percentage of involved parenchyma estimated and assigned an extent score as follows: <10% = 1; 10-20% = 2; 21-30% = 3; 31-50% = 4; >50% = 5. The following features were assessed individually: peribronchiolitis, perivascular leukocyte infiltration, perivasculitis, alveolitis, "granuloma" formation (i.e., granulomatous inflammation), and necrosis on a scale of 0–5 [0 = within normal limits (no change); 1 = minimal changes; 2 = mild changes; 3 = moderate changes; 4 = marked changes; 5 = very severe changes]. In addition, the proportion of macrophages with foamy cytoplasm within the lesions was assessed on a scale of 0 to 5.

RNA Extraction and qRT-PCR

RNA was isolated from lung and blood using Isolate II RNA mini kit protocol (Bioline Reagents Ltd., London, UK) with slight modification. Briefly, blood cell pellet and lung lobes were homogenized in Trizol and vigorously mixed with chloroform (2.5:1) and centrifuged at 12,000 *x* g for 15 min at 4°C. The RNA in the aqueous phase was precipitated by mixing in cold 70% ethanol (1:2.5) followed by column-based RNA isolation using kit protocol including DNase treatment to remove genomic DNA contamination. Complementary DNA was synthesized using 2 µg of RNA and the Tetro cDNA synthesis kit (Bioline Reagents Ltd., London, UK) according to manufacturer's instructions. Gene expression analysis was performed by quantitative real time PCR (qRT-PCR) with SensiFAST™ SYBR® Lo-ROX Kit (Bioline Reagents Ltd., London, UK) run on the QuantStudio™ 7 Flex Real-Time PCR System (Applied Biosystems). All gene expression levels were normalized to *Hprt1* internal controls in each sample, and the fold changes were calculated using the $2^{-\Delta\Delta CT}$ method. The list of primers used is given in **Table S1**.

ELISA

Lung homogenate supernatants were collected by centrifugation at 2000 *x* g at 4°C and stored at -80°C with protease inhibitor cocktail (Sigma). Quantification of TNF-α, IL-1β, IFN-β, CCL2, IFN-γ, and IL-10 were performed by ELISA according to the manufacturer's instructions (R&D Systems).

Statistical Analysis

Data analyses were performed using GRAPHPAD PRISM Version 8 (GraphPad Software, Inc., La Jolla, CA). The results are expressed as the mean ± SEM. Comparisons between two groups were performed using non-parametric unpaired Mann-Whitney *U*-test. The relationship between two variables was ranked using Spearman's rank correlation coefficient. Statistically significant differences between two groups are indicated in the figures as follows *, $p < 0.05$; **, $p < 0.01$; ***, $p < 0.001$; ****, $p < 0.0001$.

RESULTS

Pre-Diabetes Increases TB Severity

We developed a murine model of pre-diabetes and Mtb infection. C57BL/6 mice were fed HFD or NCD for a period of 12 weeks (**Figure 1A**). HFD-fed mice had significantly higher body weight (**Figure 1B**) and body fat mass but similar lean mass (**Figure 1C**) compared to NCD-fed mice. HFD-fed mice developed hyperinsulinemia indicative of insulin resistance (**Figure 1D**). Blood glucose concentrations after glucose challenge were higher at 15, 30, 60 and 120 min in HFD-fed mice (**Figure 1E**) with significantly higher area under the curve (AUC) in OGTTs (**Figure 1F**), while fasting blood glucose and glycated hemoglobin (HbA1c) were similar between NCD and HFD-fed mice (**Figure S1**). This phenotype of obesity combined with dysglycemia therefore mimics human pre-diabetes, which is characterized by insulin resistance and impaired glucose tolerance, but HbA1c levels below those of diabetes patients.

We subsequently infected the mice with live Mtb $H_{37}R_v$. At 3 weeks post infection (p.i.), mice with pre-diabetes had higher lung Mtb burden, although this did not reach significance ($p = 0.07$, **Figure 2A**). Lung necrosis appeared at 3 weeks p.i. in HFD-fed mice while necrosis was not detectable at this early timepoint in

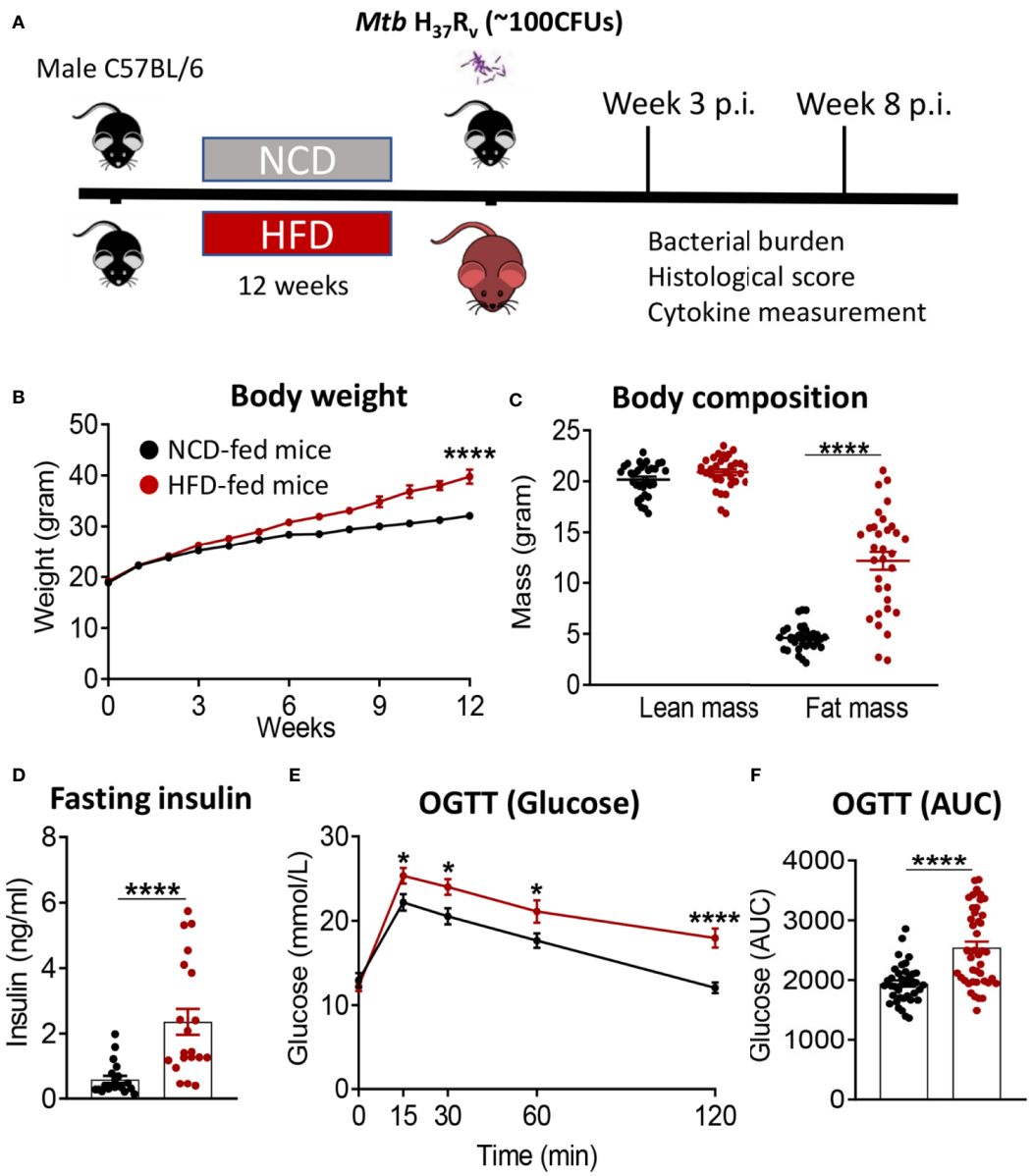

FIGURE 1 | Murine model of pre-diabetes. **(A)** Experimental design. **(B)** Body weight of mice fed NCD (black) or HFD (red) (n=30mice/group); **(C)** Body fat and lean mass at 12 weeks; **(D)** fasting insulin at 12 weeks (n=20 mice/group); **(E)** Blood glucose concentrations at baseline, 15, 30, 60, 120 minutes after oral glucose administration; **(F)** OGTT Area under curve (AUC) (n=30 mice/group). Data are means ± SEM. Data analysis was performed by Mann-Whitney *U* test. *p < 0.05 and ****p < 0.0001.

any NCD-fed mice. Necrosis scores were significantly higher in pre-diabetic mice by 8 weeks p.i. (**Figures 2B, C**) demonstrating increased lung immunopathology associated with pre-diabetes. Bacterial loads in spleens were comparable between pre-diabetic and control mice (**Figure 2D**). Interestingly, the Mtb burden in the fatty livers of HFD-fed mice was significantly lower than in NCD-fed mice at 3 weeks p.i, and this trend continued at 8 weeks p.i. (**Figure 2E**). Our data demonstrate that obesity with impaired glucose tolerance below the threshold of diabetes, i.e., pre-diabetes, increases susceptibility to pulmonary TB in a murine model.

Pre-Diabetes Alters the Immune Response to Mtb in the Lung

Next, we investigated whether immune responses to Mtb at the site of infection are modified by pre-diabetes. We determined relative cytokine and chemokine mRNA expression and protein concentrations in lung homogenates from obese mice with impaired glucose tolerance and healthy control animals at 3 and 8 weeks p.i. The mRNA expression of *Tnf, Ifng, Il1b, Ifnb1* and *Il10* was similar between animals (**Figures 3A–E**), however, mRNA expression of the chemokine *Ccl2* was significantly lower

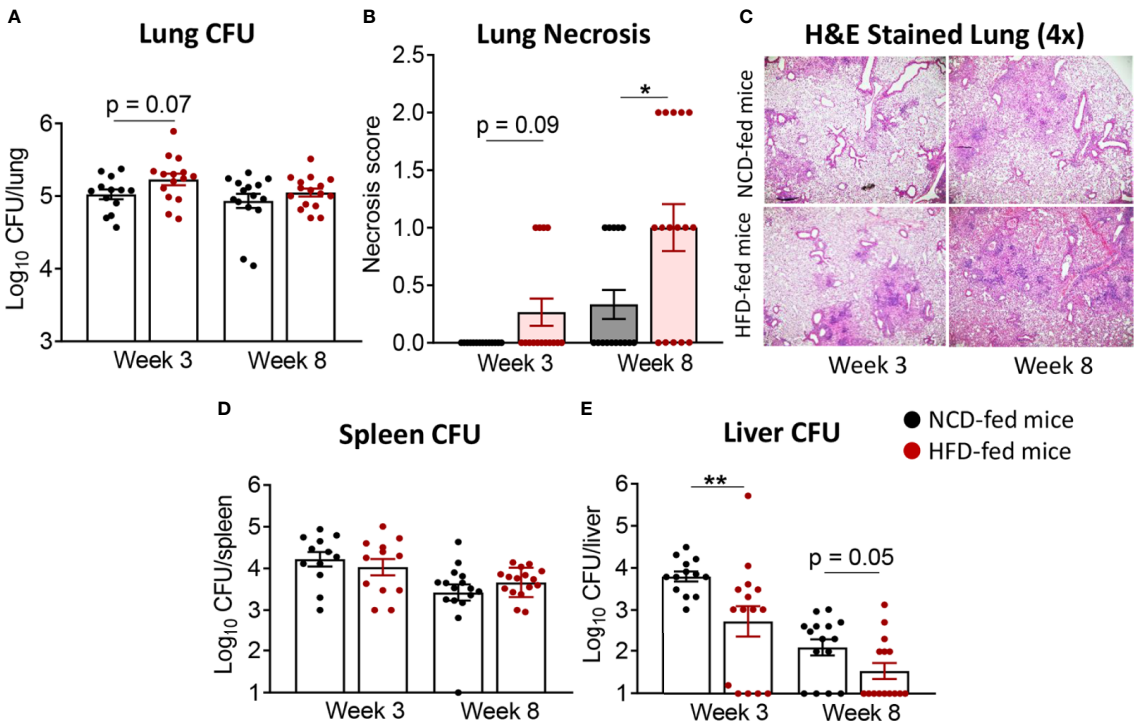

FIGURE 2 | Pre-diabetes increases lung pathology in Mtb-infected mice. **(A)** Lung Mtb burden in NCD- (black) and HFD-fed mice (red) at 3- and 8-weeks p.i.; **(B)** Lung Necrosis scores; **(C)** Representative lung histological images at 4x magnification; **(D)** Mtb burden in spleen and **(E)** in liver. Data are means ± SEM (n=13-16 mice/group) analyzed cumulatively in two independent experiments. Data analysis was performed by Mann-Whitney *U* test. ns = not significant *p < 0.05, and **p < 0.01.

in pre-diabetic mice compared to controls at 8 weeks p.i. (**Figure 3F**). At the protein level, TNF-α, IFN-γ and IL-10 were significantly lower at 3 weeks p.i. in pre-diabetic mice compared to control animals (**Figures 3A, B, D**) and concentrations of TNF-α and IFN-γ remained lower also at 8 weeks p.i. IFN-β was significantly lower in HFD-fed mice compared to NCD-fed mice at 8 weeks p.i. (**Figure 3E**), but IL-1β and CCL2 were not different between the groups (**Figures 3C, F**). TGF-β, IL-6 and IL-12 mRNA expression and protein concentrations were not impacted by HFD (data not shown). In uninfected animals, no significant differences in cytokine transcript levels between NCD- and HFD-fed mice were observed at both 3-and-8 weeks p.i. (**Figure S2**). A low IFN-γ/IL-10 ratio is a biomarker for increased TB disease severity in humans (Jamil et al., 2007) and this ratio was significantly lower in pre-diabetic mice compared to control animals at 8 weeks p.i. (**Figure 3G**). As expected, higher lung concentrations of TNF-α, IFN-γ, IL-1β, and CCL2 were associated with lower Mtb burden in NCD-fed mice, while this relationship was surprisingly inversed in pre-diabetic animals (**Figure S3**).

Pre-Diabetes Alters the Immune Response to Mtb in the Periphery

To determine whether changes in the immune response to Mtb infection in pre-diabetes are limited to the site of infection or also occur in the periphery, we assessed cytokine and chemokine expression in blood from HFD- and NCD-fed mice. We found that at 3 weeks p.i. *Tnf* was higher in HFD-fed mice, but this did not reach statistical significance (p = 0.06, **Figure 4A**). *Il1b* was significantly lower (**Figure 4C**), while *Il10* was significantly higher in pre-diabetic mice compared to control animals (**Figure 4D**). At 8 weeks p.i. *Ifng, Il1b* and *Ccl2* were significantly lower in HFD-fed mice (**Figures 4B, C, F**) and we did not observe any differences in *Ifnb1* expression in HFD- *vs.* NCD-fed animals (**Figure 4E**). At baseline, uninfected HFD-fed mice had reduced blood transcript levels of *Ifng*, *Il1b*, *Ccl2* but increased *Il10* compared to NCD-fed mice at both 3-and-8 weeks p.i. (**Figure S4**). These data demonstrate that pre-diabetes-induced changes in the immune response to Mtb are not confined to the lung and occur also in the periphery.

Restored Glucose Tolerance With Elevated Body Fat Mass Confers Mild Resistance to TB

In order to assess whether a change in diet can restore glucose tolerance and reverse susceptibility to TB, we established a diet reversal model. Mice fed HFD for 12 weeks (as described for the experiment above) were subsequently fed NCD for an additional 10 weeks, here referred to as HFD/NCD mice. Control mice

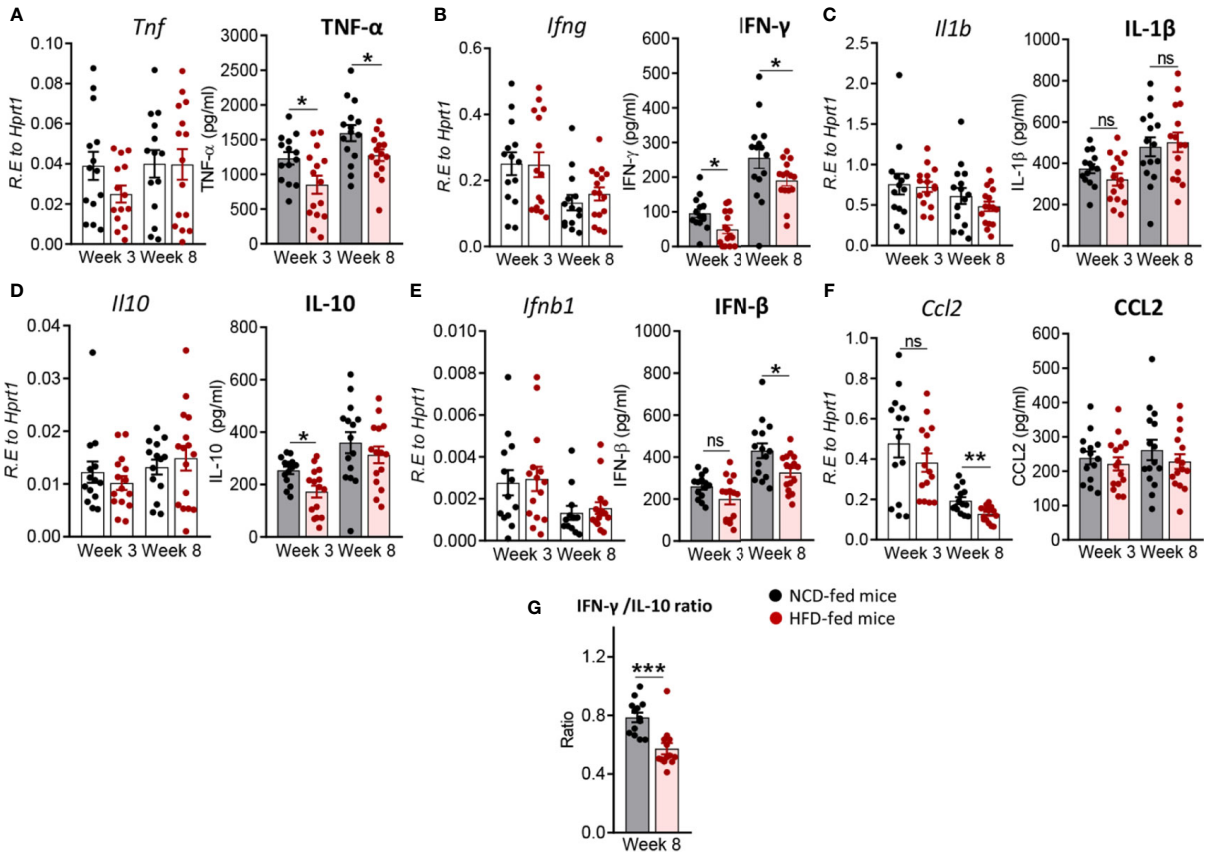

FIGURE 3 | Pre-diabetes alters cytokine production in Mtb-infected lungs. Cytokine mRNA and protein levels were determined in lung homogenates by qRT-PCR and ELISA. Lung mRNA expression and protein concentrations of **(A)** *Tnf*, TNF-α; **(B)** *Ifng*, IFN-γ; **(C)** *Il1b*, IL-1β; **(D)** *Il10*, IL-10; **(E)** *Ifnb1*, IFN-β and **(F)** *Ccl2*, CCL2 from NCD- and HFD fed-mice at 3-and-8 weeks p.i. **(G)** IFN-γ/IL-10 ratio was determined for each mouse at week 8. Data are means ± SEM of n=13-15 mice/group analyzed cumulatively across two independent experiments. Data analysis was performed by Mann-Whitney *U* test. ns = not significant, *p < 0.05, and ***p < 0.001.

(NCD/NCD) were fed NCD for the entire 22 weeks (**Figure 5A**). Diet reversal resulted in significant loss of total body weight (**Figure 5B**) and fat mass (**Figure 5C**) in HFD/NCD animals, while the lean mass increased over time (**Figure 5D**). However, HFD/NCD mice maintained significantly higher body weight (**Figure 5B**) and higher body fat mass (**Figure 5C**) compared to NCD/NCD mice. Diet reversal restored the average RER and decreased the REE across 24h of light/dark phases observed in NCD-fed mice (**Figure S5**). Most importantly, diet reversal resulted in complete restoration of glucose tolerance between HFD/NCD and NCD/NCD animals (**Figures 5E–G**). We next assessed the impact of this metabolic phenotype of restored glucose tolerance but elevated body fat mass on susceptibility to TB.

HFD/NCD and NCD/NCD mice were infected with Mtb $H_{37}R_v$ and Mtb burden was determined at 3 and 8 weeks p.i. Interestingly, the metabolic phenotype induced by the diet reversal, i.e., restored glucose tolerance with increased body fat mass compared to controls, conferred a mild but statistically significant resistance to TB. HFD/NCD mice had significantly lower lung Mtb burden at 8 weeks p.i. compared to control animals that only consumed NCD throughout the entire experiment (**Figure 6A**), while Mtb burden was similar at 3 weeks p.i. No significant differences were observed in lung necrosis scores or spleen and liver CFU (**Figures 6B–E**). Coinciding with significantly reduced Mtb burden in the lung at 8 weeks p.i., we observed more foamy macrophages in lung sections from normoglycemic, obese mice compared to control animals (**Figure 7**) which was not evident in dysglycemic obese mice (**Figure S7**).

Restoration of Glucose Tolerance Improves Immune Responses to Mtb in the Lung

We next assessed whether the change in diet and restoration of glucose tolerance while maintaining high body fat mass improves host protective immune responses to Mtb in the lung. While lung TNF-α and IFN-γ concentrations were significantly lower in pre-diabetic mice compared to control

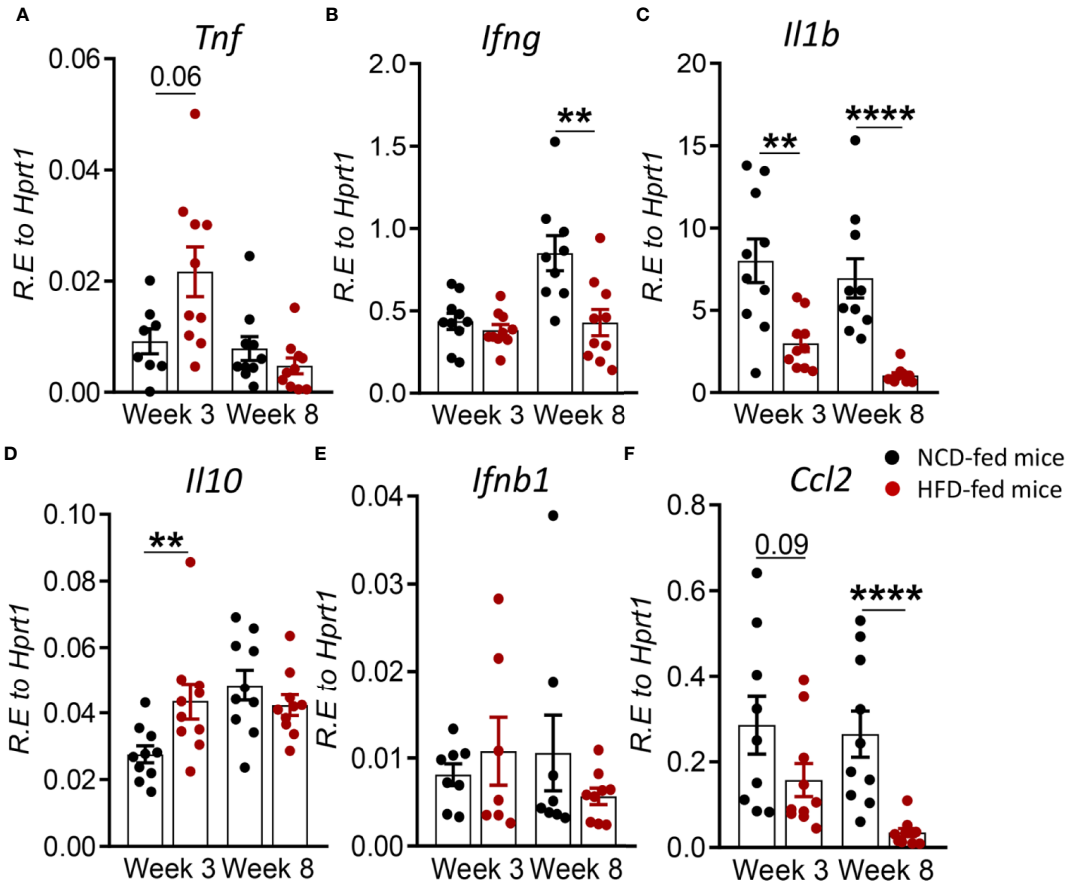

FIGURE 4 | Pre-diabetes alters cytokine responses to Mtb in the periphery. Cytokine mRNA expression was determined by qRT-PCR in blood from NCD- and HFD-fed mice at 3- and 8-weeks p.i. **(A)** *Tnf*, **(B)** *Ifng*, **(C)** *Il1b*, **(D)** *Il10*, **(E)** *Ifnb1*, and **(F)** *Ccl2*. Data are means ± SEM (n=7-10 mice/group analyzed in one independent experiment). Data analysis was performed by Mann-Whitney *U* test. ns = not significant **p < 0.01, and ****p < 0.0001.

mice at both 3 and 8 weeks p.i. (**Figures 3A, B**), concentrations of these cytokines were similar in mice with restored glucose tolerance (HFD/NCD) and their respective controls (NCD/NCD) at 8 weeks p.i., although TNF-α concentrations were still lower at 3 weeks p.i. (**Figures 8A, B**). At the mRNA level *Tnf*, *Ifng* and *Il1b* were lower in HFD/NCD *vs* NCD/NCD animals (**Figures 8A–C**). This demonstrates that production of these key cytokines for protective immune responses against Mtb was restored at the protein level by the change in diet. Similarly, IL-10 production was significantly lower in HFD-fed mice compared to NCD-fed mice at 3 weeks p.i. (**Figure 3D**), but after diet reversal IL-10 concentrations were comparable between HFD/NCD and NCD/NCD animals (**Figure 8D**). IL-1β and CCL2 concentrations, which were similar in pre-diabetic and control mice (**Figures 3C, F**), were significantly lower in HFD/NCD mice compared to NCD/NCD animals at 3 weeks p.i. (**Figures 8C, F**). While IFN-β concentrations were lower in pre-diabetic mice at 8 weeks p.i. (**Figure 3E**), they were lower in HFD/NCD fed mice compared to control animals at 3 weeks p.i. (**Figure 8E**). Correlation analysis of cytokine concentrations and lung Mtb burden are shown in **Figure S6**. Most importantly, the IFN-γ/IL-10 ratio, which was significantly lower in pre-diabetic *vs.* control mice (**Figure 3G**), was now similar in animals with restored glucose tolerance and their controls (**Figure 8G**).

These data demonstrate that diet reversal significantly improves this biomarker of TB disease severity.

Restoration of Glucose Tolerance Improves Immune Responses to Mtb in the Periphery

After diet reversal we found that cytokine mRNA expression in whole blood was restored or in the case of *tnfa* unchanged (**Figure 9A**) to those in control animals. For instance, mRNA expression of *Ifng, Il1b* and *Ccl2* which were lower in pre-diabetic mice *vs.* controls at week 8 (**Figures 4B, C, F**), but were similar in HFD/NCD vs. NCD/NCD animals (**Figures 9B, C, F**). *Il10* expression was higher in pre-diabetic animals at 3 weeks p.i. (**Figure 4D**) and was not significantly different in HFD/NCD *vs.*

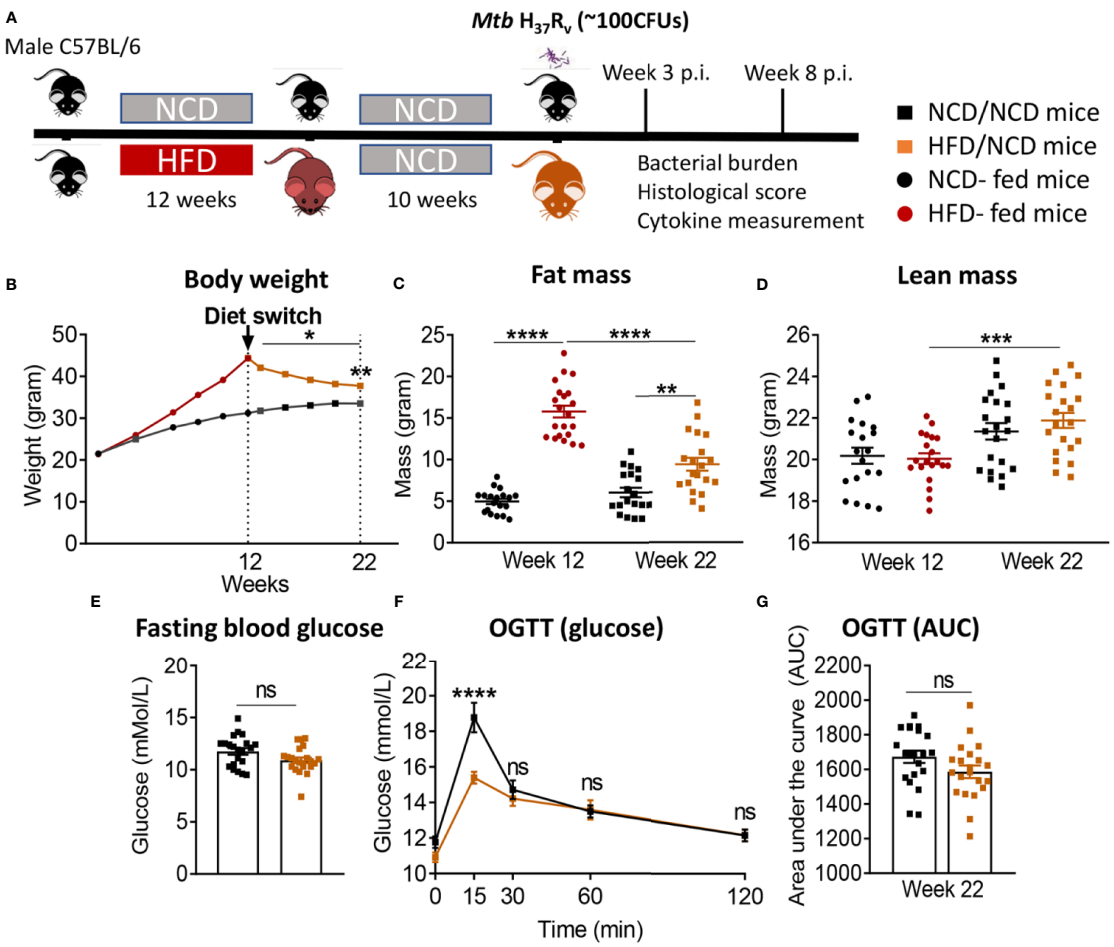

FIGURE 5 | Diet reversal restores glucose tolerance while maintaining higher fat mass. **(A)** Schematic showing experimental plan for diet reversal-TB model development. **(B)** Body weight of mice were monitored up to 22 weeks of diet; **(C)** Fat mass and **(D)** lean mass were measured. OGTT was performed on NCD/NCD and HFD/NCD mice; **(E)** Fasting blood glucose **(F)** Blood glucose concentrations at baseline, 15, 30, 60, 120 minutes after oral glucose administration and **(G)** Area under curve (AUC). Data represents mean ± SEM, (n=19-20 mice/group). Data analysis was performed by Mann-Whitney *U* test. ns=not significant, *p < 0.05, **p < 0.01, ***p < 0.001 and ****p < 0.0001.

NCD/NCD animals (**Figure 9D**). Interestingly, blood *Ifnb* mRNA expression was significantly higher in obese mice with restored glucose tolerance compared to controls at 8 weeks p.i. (**Figure 9E**). Together these data demonstrate that HFD significantly impacts immune responses to Mtb at the site of infection, the lung, as well as the periphery and thus can contribute to TB disease severity.

DISCUSSION

Increased susceptibility of T2D patients to TB is well established, however, whether pre-diabetes also predisposes to more severe manifestations of pulmonary TB remains elusive as large population-based studies on the association of pre-diabetes and TB have not been performed to date. Blood transcriptomic signatures from TB patients with pre-diabetes are more similar to those from TB patients with T2D compared to TB patients without any form of dysglycemia (Eckold et al., 2020). This suggests that impaired immune responses to Mtb occur already during the early stages of dysglycemia in pre-diabetes. Given the high prevalence rates of pre-diabetes in TB endemic countries, with 27% of TB contacts in India (Shivakumar et al., 2018) and 25% in South Africa (Restrepo et al., 2018) having impaired glucose tolerance, it is imperative to investigate any associations between pre-diabetes and susceptibility to TB. To address this current knowledge gap, we developed a pre-diabetes model of Mtb infection and demonstrated more severe TB disease and altered immune responses to Mtb in the lung and blood of mice with impaired glucose tolerance.

Several different animal models of diabetes and TB exist and generally show, similarly to our pre-diabetes murine

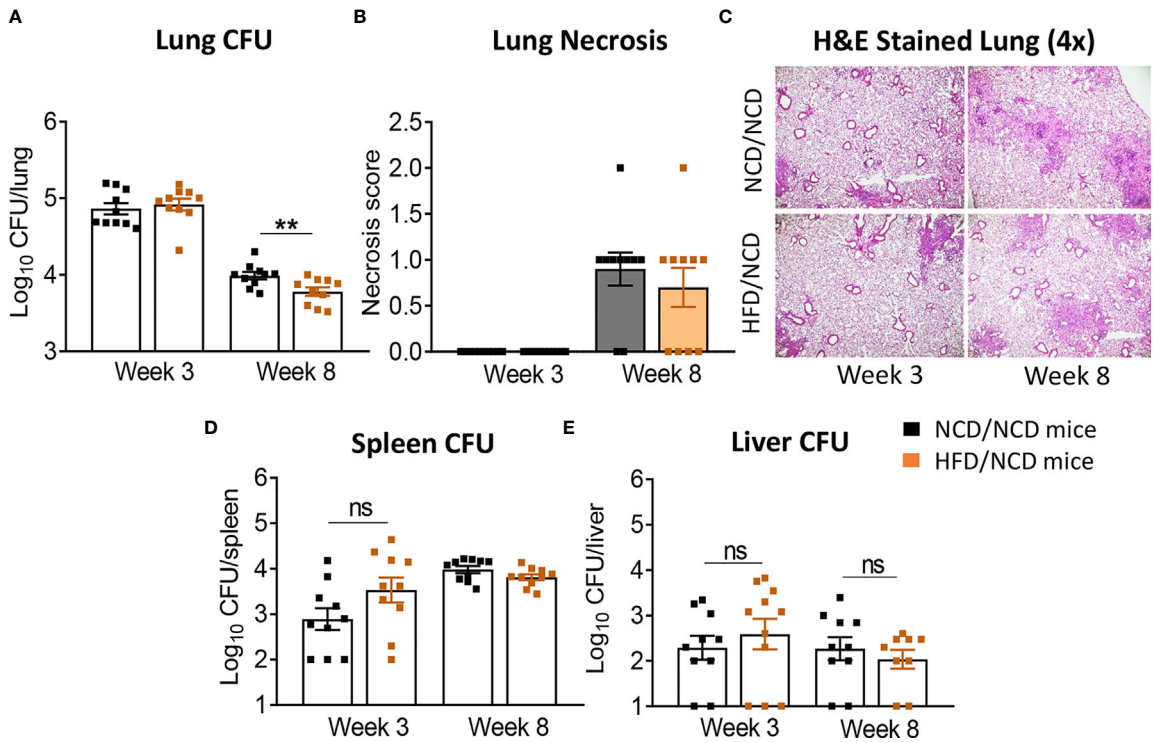

FIGURE 6 | Restoration of glucose tolerance with elevated fat mass confers mild resistance to TB. **(A)** Lung Mtb burden in NCD/NCD- (black) and HFD/NCD mice (orange) at 3- and 8-weeks p.i.; **(B)** Lung Necrosis scores; **(C)** Representative lung histological images; **(D)** Mtb burden in spleen and **(E)** in liver. Data are means ± SEM (n=10 mice/group analyzed in one independent experiment). Data analysis was performed by Mann-Whitney *U* test. ns = not significant. **p < 0.01.

model, more severe disease and impaired immune responses in hyperglycemic hosts upon Mtb infection (Yamashiro et al., 2005; Martens et al., 2007; Sugawara and Mizuno, 2008; Vallerskog et al., 2010; Podell et al., 2014; Martinez et al., 2016; Tripathi et al., 2019; Alim et al., 2020). Many of these models use Streptozotocin (STZ) to induce hyperglycemia, which does not accurately reflect the chronic inflammation and vascular complications associated with human T2D. Nevertheless, these models provide valuable insight into hyperglycemia associated immune impairment. STZ-induced chronic hyperglycemia resulted in increased Mtb lung burden, more inflammation and lower IFN-γ production in the lung (Martens et al., 2007). Similarly, we found lower IFN-γ and TNF-α production in the lungs of pre-diabetic mice combined with more severe immunopathology and significantly lower IFN-γ/IL-10 ratios, a biomarker for TB disease severity (Jamil et al., 2007). The increased susceptibility of STZ-treated mice was attributed to a delayed innate immune response due to impaired recognition of Mtb by alveolar macrophages from hyperglycemic animals, which subsequently results in delayed adaptive immune responses (Martinez et al., 2016). It is likely that pre-diabetic mice also have a delayed adaptive immune response given the lower IFN-production, however, whether this is due to impaired recognition of Mtb by pre-diabetic alveolar macrophages remains to be elucidated in future studies. Vallerskog *et al.* reported lower CCL2 expression in the lungs of STZ-induced hyperglycemic mice (Vallerskog et al., 2010). While pre-diabetic animals in our model showed lower *Ccl2* mRNA at 8- weeks p.i., protein concentrations of CCL2 were not significantly different. Eckhold *et al.* found reduced type I IFN responses in blood transcriptomic signatures from TB patients with pre-diabetes (Eckold et al., 2020). We did not observe reduced *Ifnb1* mRNA expression in blood, however, IFN-β concentrations were significantly reduced in lungs of pre-diabetic mice at 8 weeks p.i. A HFD-based model of T2D and TB recently demonstrated moderately higher Mtb burden in the early stages of infection at 2 weeks, but not during late infection, and reduced IFN-γ production in HFD-fed diabetic mice (Alim et al., 2020), which is consistent with our data in this pre-diabetes model. An interesting observation in our murine pre-diabetes model was the significantly reduced Mtb burden in the liver of HFD-fed animals. This finding is in line with human studies showing that diabetes does not increase the risk of developing extrapulmonary TB (Magee et al., 2016) despite a higher risk of pulmonary TB. Increased hepatic Mtb burden was however observed in the HFD-based murine model of diabetes (Alim et al., 2020), but in this study the

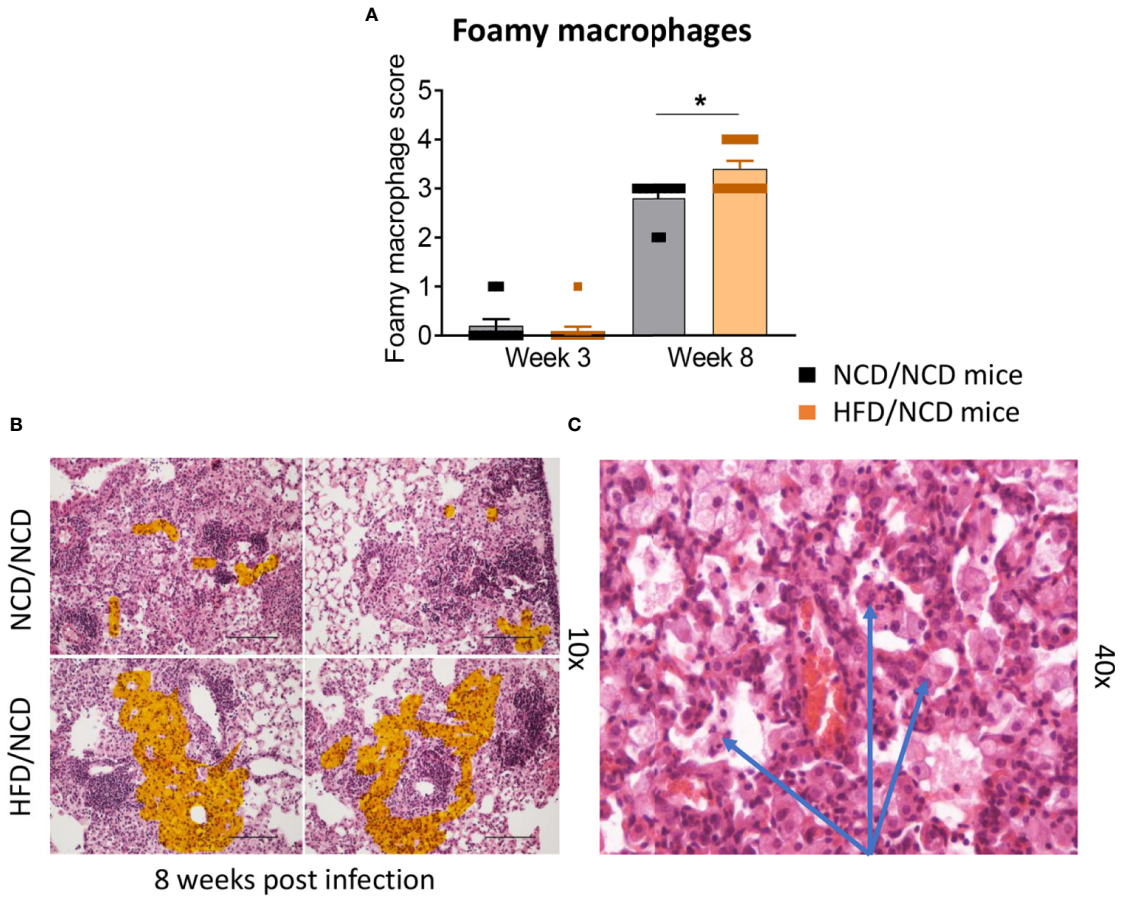

FIGURE 7 | Foamy macrophages were upregulated in the lung of HFD/NCD mice. **(A)** Histological scoring of foamy macrophages in lung sections of NCD/NCD mice and HFD/NCD mice at 3-and-8 weeks p.i. **(B)** Representative histological images with highlighted area (orange) of foamy macrophages; **(C)** Snapshot of foamy macrophages on H&E lung sections (arrows). Data represents mean ± SEM (n=10 mice/group analyzed in one independent experiment). Data analysis was performed by Mann-Whitney *U* test. *p < 0.05.

animals were infected *via* the intra-venous route and not *via* the natural aerosol route, which likely explain the increased hepatic Mtb burden. HFD-induced alterations in gut microflora leads to severe pulmonary damage and mortality in Toll-like receptor deficient mice (Ji et al., 2014) and it is possible that dysbiosis of the gut microbiota contributes in part to susceptibility of our pre-diabetic animals to TB. In contrast to our observation in HFD-fed mice and those by Alim et al. (2020), HFD-fed guinea pigs with impaired glucose tolerance do not show increased susceptibility to TB and had similar lung Mtb burden to control animals with exception of higher extrapulmonary Mtb burden in the liver 90 days p.i. (Podell et al., 2014). HFD-fed guinea pigs had also similar cytokine profiles in the lung compared to control animals through day 60 p.i., but elevated IL-1β concentrations at 90 days p.i. In the guinea pig model increased susceptibility to TB was only evident in diabetic animals that received a combination of HFD and STZ. These studies highlight distinct species-specific differences in the immune response in animals with dysglycemia.

To determine whether the increased susceptibility of pre-diabetic mice is due to impaired glucose tolerance or obesity, we performed a diet reversal experiment in which we could separate impaired glucose tolerance from obesity. Surprisingly, obese animals with restored glucose tolerance were able to better contain Mtb compared to their healthy-weight controls and had more lung macrophages with a foamy macrophage phenotype. Mtb persists predominantly in a dormant non-replicating state in foamy macrophages compared to infected non-foamy macrophages (Peyron et al., 2008; Russell et al., 2009; Rodriguez et al., 2014). This may explain the overall lower Mtb burden observed in animals with higher foamy macrophage scores. Adiposity and increased foam cell formation has also been suggested to promote latency in humans and contribute to lower TB progression rates in individuals with high BMI (Aibana et al., 2016). The restoration of glucose tolerance, while maintaining a high body fat mass, also resulted in restoration

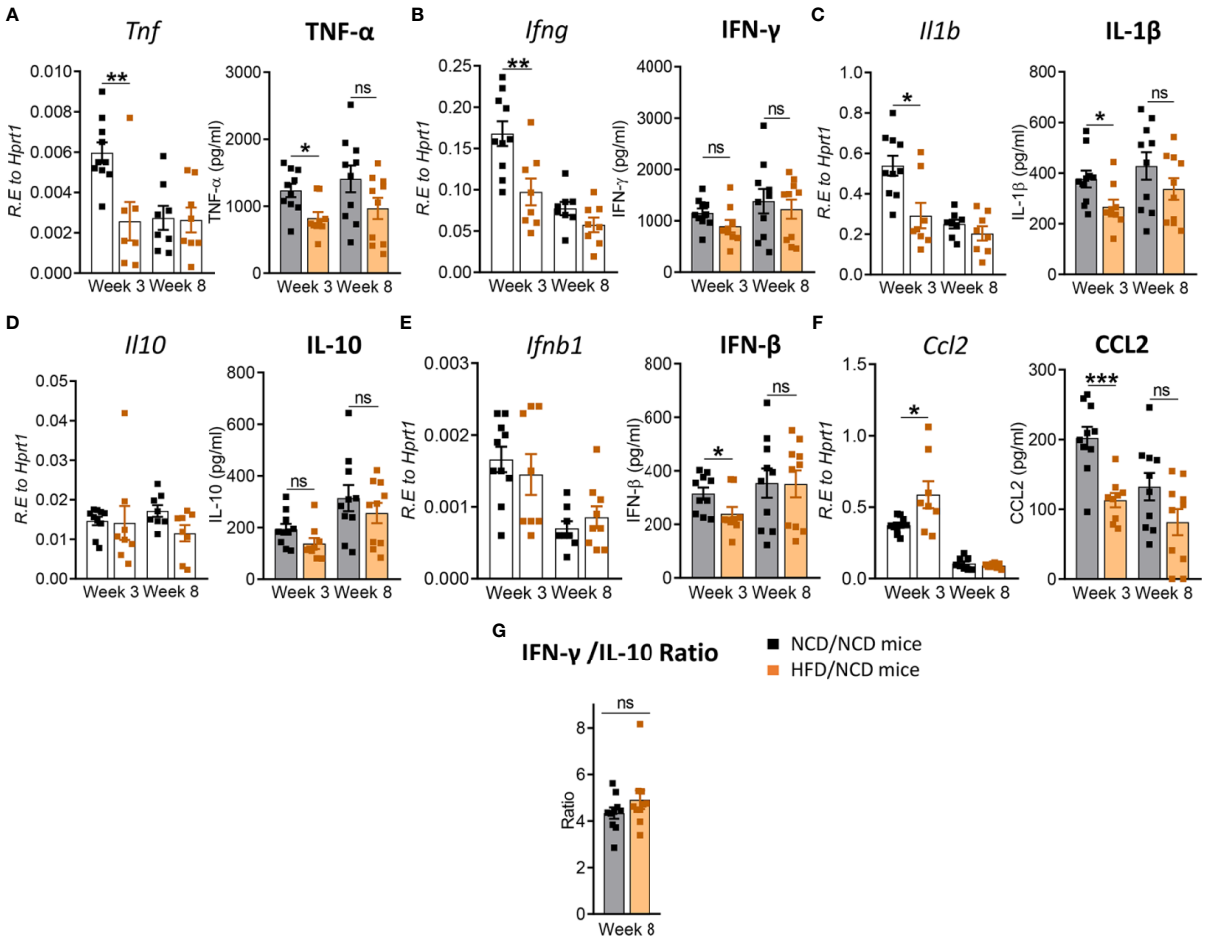

FIGURE 8 | Restoration of glucose tolerance improves lung cytokine profiles. Cytokine mRNA and protein levels were determined in lung homogenates by qPCR and ELISA. Lung mRNA expression and protein concentrations of **(A)** *Tnf*, TNF-α; **(B)** *Ifng*, IFN-γ; **(C)** *Il1b*, IL-1β; **(D)** *Il10*, IL-10; **(E)** *Ifnb1*, IFN-β; and **(F)** *Ccl2*, CCL2 from NCD- and HFD fed-mice at 3- and 8-weeks p.i. **(G)** IFN-γ/IL-10 ratio was determined for each mouse at week 8. Data are means ± SEM (n=8-10 mice/group analyzed in one independent experiment). Data analysis was performed by Mann-Whitney *U* test. ns = not significant *$p < 0.05$, ** $p<0.01$ and ***$p < 0.001$.

of IFN-γ responses. CCL2 concentrations on the other hand were significantly lower compared to NCD-fed mice. This may serve as a feedback mechanism to limit further recruitment of macrophages to the lung. The change in diet ultimately improved the IFN-γ/IL-10 ratio and necrosis scores were similar in obese animals with a history of glucose impairment compared to healthy chow-fed animals. Observations from our murine model are consistent with findings in humans where obesity in absence of dysglycemia protects against TB (Lonnroth et al., 2010; Lin et al., 2018). A potential limitation of our study is the absence of a control group that continue consumption of HFD for a total of 22 weeks. A published study in mice fed a HFD for 30 weeks showed a small but significant increase (approximately half a $\log_{10}$) in lung Mtb burden compared to NCD-fed animals at 14 days p.i., but no differences at later timepoints (Alim et al., 2020). This suggests that the HFD-induced susceptibility modestly increases with duration on HFD and mainly affects early infection with regards to lung Mtb burden.

Taken together, both our HFD-induced pre-diabetes model and the diet reversal model of Mtb infection mimic observations in humans. Our murine models offer the unique opportunity to elucidate the underlying immune-metabolic mechanisms of obesity-induced resistance *vs.* dysglycemia-associated susceptibility to TB. Importantly, our data provide clear evidence, that immune impairment to Mtb including decreased lung IFN-γ production indicative of delayed adaptive immune priming occurs already during pre-diabetes and likely contributes to more severe disease. Future experiments using this model should include investigations of diet-induced changes in immune cell recruitment to the site of infection and cellular immunophenotyping. We further posit that caloric restriction in patients with diabetes or pre-diabetes not only improves glucose tolerance but may also confer at least temporary resistance from TB progression. Thus, large population-based

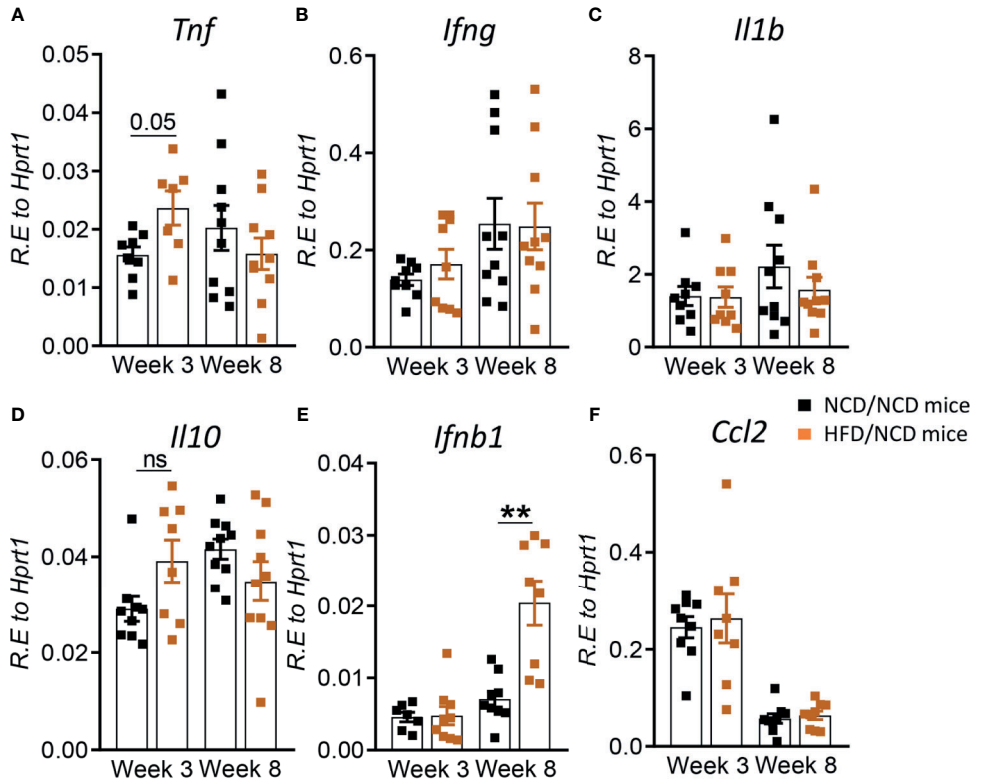

FIGURE 9 | Restoration of glucose tolerance improves blood cytokine profiles. Cytokine mRNA expression was determined by qRT-PCR in blood from NCD- and HFD-fed mice at 3- and 8-weeks p.i. **(A)** *Tnf*, **(B)** *Ifng*, **(C)** *Il1b*, **(D)** *Il10*, **(E)** *Ifnb1*, and **(F)** *Ccl2*. Data are means ± SEM (n=8-10 mice/group analyzed in one independent experiment). Data analysis was performed by Mann-Whitney *U* test. ns = not significant **p < 0.01.

studies are warranted to determine the impact of pre-diabetes and dietary interventions on susceptibility to TB.

DATA AVAILABILITY STATEMENT

The raw data supporting conclusions of this article will be made available by the authors, without undue reservation.

ETHICS STATEMENT

The animal study was reviewed and approved by The Health Sciences Animal Ethics Committee of The University of Queensland.

AUTHOR CONTRIBUTIONS

RS, MDN, and KR wrote the manuscript. RS, MDN, SK, MLD, JK, and AB carried out the experiments. RS, MDN, SB, and HB-O analyzed the data and compiled the figures. RS, MDN, SB, HB-O, SK, SH, AB, CC, KS, and KR interpreted the data and contributed intellectually. All authors contributed to the article and approved the submitted version.

FUNDING

This study was supported by grants to KR from the National Institutes of Health (NIH), National Institute of Allergy and Infectious Diseases (NIAID) grant number R01AI116039, the Mater Foundation, the Australian Respiratory Council and the Australian Infectious Diseases Research Centre. KRS received a Fellowship from the Australian Research Council (DE180100512). The Translational Research Institute is supported by a grant from the Australian Government.

ACKNOWLEDGMENTS

We thank Adrian T. Gemiarto for technical assistance and the staff of the biological resource facility at the Translational Research Institute for animal husbandry. This manuscript has been released as a pre-print at bioRxiv (BIORXIV/2021/438735).

SUPPLEMENTARY MATERIAL

The Supplementary Material for this article can be found online at: https://www.frontiersin.org/articles/10.3389/fcimb.2021.691823/full#supplementary-material

REFERENCES

Aibana, O., Acharya, X., Huang, C. C., Becerra, M. C., Galea, J. T., Chiang, S. S., et al. (2016). Nutritional Status and Tuberculosis Risk in Adult and Pediatric Household Contact. *PloS One* 11, e0166333. doi: 10.1371/journal.pone.0166333

Alim, M. A., Kupz, A., Sikder, S., Rush, C., Govan, B., and Ketheesan, N. (2020). Increased Susceptibility to Mycobacterium Tuberculosis Infection in a Diet-Induced Murine Model of Type 2 Diabetes. *Microbes Infect.* 22, 303–311. doi: 10.1016/j.micinf.2020.03.004

Andrikopoulos, S., Blair, A. R., Deluca, N., Fam, B. C., and Proietto, J. (2008). Evaluating the Glucose Tolerance Test in Mice. *Am. J. Physiol. Endocrinol. Metab.* 295, E1323–E1332. doi: 10.1152/ajpendo.90617.2008

Critchley, J. A., Carey, I. M., Harris, T., Dewilde, S., Hosking, F. J., and Cook, D. G. (2018). Glycemic Control and Risk of Infections Among People With Type 1 or Type 2 Diabetes in a Large Primary Care Cohort Study. *Diabetes Care* 41, 2127–2135. doi: 10.2337/dc18-0287

Critchley, J. A., Restrepo, B. I., Ronacher, K., Kapur, A., Bremer, A. A., Schlesinger, L. S., et al. (2017). Defining a Research Agenda to Address the Converging Epidemics of Tuberculosis and Diabetes: Part 1: Epidemiology and Clinical Management. *Chest* 152, 165–173. doi: 10.1016/j.chest.2017.04.155

Eckold, C., Kumar, V., Weiner Rd, J., Alisjahbana, B., Riza, A. L., Ronacher, K., et al. (2021). Impact of Intermediate Hyperglycaemia as Well as Diabetes on Immune Dysfunction in Tuberculosis. *Clin. Infect. Dis.* 72 (1), 69–78. doi: 10.1093/cid/ciaa751

Flores-Valdez, M. A., Pedroza-Roldan, C., Aceves-Sanchez, M. J., Peterson, E. J. R., Baliga, N. S., Hernandez-Pando, R., et al. (2018). The BCGDeltaBCG1419c Vaccine Candidate Reduces Lung Pathology, IL-6, TNF-Alpha, and IL-10 During Chronic TB Infection. *Front. Microbiol.* 9, 1281. doi: 10.3389/fmicb.2018.01281

Heydemann, A. (2016). An Overview of Murine High Fat Diet as a Model for Type 2 Diabetes Mellitus. *J. Diabetes Res.* 2016, 2902351. doi: 10.1155/2016/2902351

Huangfu, P., Ugarte-Gil, C., Golub, J., Pearson, F., and Critchley, J. (2019). The Effects of Diabetes on Tuberculosis Treatment Outcomes: An Updated Systematic Review and Meta-Analysis. *Int. J. Tuberc Lung Dis.* 23, 783–796. doi: 10.5588/ijtld.18.0433

Jamil, B., Shahid, F., Hasan, Z., Nasir, N., Razzaki, T., Dawood, G., et al. (2007). Interferon Gamma/IL10 Ratio Defines the Disease Severity in Pulmonary and Extra Pulmonary Tuberculosis. *Tuberculosis (Edinb)* 87, 279–287. doi: 10.1016/j.tube.2007.03.004

Ji, Y., Sun, S., Goodrich, J. K., Kim, H., Poole, A. C., Duhamel, G. E., et al. (2014). Diet-Induced Alterations in Gut Microflora Contribute to Lethal Pulmonary Damage in TLR2/TLR4-Deficient Mice. *Cell Rep.* 8, 137–149. doi: 10.1016/j.celrep.2014.05.040

Kumar, N. P., Banurekha, V. V., Nair, D., Sridhar, R., Kornfeld, H., Nutman, T. B., et al. (2014). Coincident Pre-Diabetes Is Associated With Dysregulated Cytokine Responses in Pulmonary Tuberculosis. *PloS One* 9, e112108. doi: 10.1371/journal.pone.0112108

Lin, H. H., Wu, C. Y., Wang, C. H., Fu, H., Lonnroth, K., Chang, Y. C., et al. (2018). Association of Obesity, Diabetes, and Risk of Tuberculosis: Two Population-Based Cohort. *Clin. Infect. Dis.* 66, 699–705. doi: 10.1093/cid/cix852

Lonnroth, K., Williams, B. G., Cegielski, P., and Dye, C. (2010). A Consistent Log-Linear Relationship Between Tuberculosis Incidence and Body Mass Index. *Int. J. Epidemiol.* 39, 149–155. doi: 10.1093/ije/dyp308

Magee, M. J., Foote, M., Ray, S. M., Gandhi, N. R., and Kempker, R. R. (2016). Diabetes Mellitus and Extrapulmonary Tuberculosis: Site Distribution and Risk of Mortality. *Epidemiol. Infect.* 144, 2209–2216. doi: 10.1017/S0950268816000364

Martens, G. W., Arikan, M. C., Lee, J., Ren, F., Greiner, D., and Kornfeld, H. (2007). Tuberculosis Susceptibility of Diabetic Mice. *Am. J. Respir. Cell Mol. Biol.* 37, 518–524. doi: 10.1165/rcmb.2006-0478OC

Martinez, N., Ketheesan, N., West, K., Vallerskog, T., and Kornfeld, H. (2016). Impaired Recognition of Mycobacterium Tuberculosis by Alveolar Macrophages From Diabetic Mice. *J. Infect. Dis.* 214, 1629–1637. doi: 10.1093/infdis/jiw436

Peyron, P., Vaubourgeix, J., Poquet, Y., Levillain, F., Botanch, C., Bardou, F., et al. (2008). Foamy Macrophages From Tuberculous Patients' Granulomas Constitute a Nutrient-Rich Reservoir for M. Tuberculosis Persistence. *PloS Pathog.* 4, e1000204. doi: 10.1371/journal.ppat.1000204

Podell, B. K., Ackart, D. F., Obregon-Henao, A., Eck, S. P., Henao-Tamayo, M., Richardson, M., et al. (2014). Increased Severity of Tuberculosis in Guinea Pigs With Type 2 Diabetes: A Model of Diabetes-Tuberculosis Comorbidity. *Am. J. Pathol.* 184, 1104–1118. doi: 10.1016/j.ajpath.2013.12.015

Restrepo, B. I., Kleynhans, L., Salinas, A. B., Abdelbary, B., Tshivhula, H., Aguillon-Duran, G. P., et al. (2018). Diabetes Screen During Tuberculosis Contact Investigations Highlights Opportunity for New Diabetes Diagnosis and Reveals Metabolic Differences Between Ethnic Groups. *Tuberculosis (Edinb)* 113, 10–18. doi: 10.1016/j.tube.2018.08.007

Rodriguez, J. G., Hernandez, A. C., Helguera-Repetto, C., Aguilar Ayala, D., Guadarrama-Medina, R., Anzola, J. M., et al. (2014). Global Adaptation to a Lipid Environment Triggers the Dormancy-Related Phenotype of Mycobacterium Tuberculosis. *mBio* 5, e01125–e01114. doi: 10.1128/mBio.01125-14

Russell, D. G., Cardona, P. J., Kim, M. J., Allain, S., and Altare, F. (2009). Foamy Macrophages and the Progression of the Human Tuberculosis Granuloma. *Nat. Immunol.* 10, 943–948. doi: 10.1038/ni.1781

Shivakumar, S., Chandrasekaran, P., Kumar, A. M. V., Paradkar, M., Dhanasekaran, K., Suryavarshini, N., et al. (2018). Diabetes and Pre-Diabetes Among Household Contacts of Tuberculosis Patients in India: Is it Time to Screen Them All? *Int. J. Tuberc Lung Dis.* 22, 686–694. doi: 10.5588/ijtld.17.0598

Sugawara, I., and Mizuno, S. (2008). Higher Susceptibility of Type 1 Diabetic Rats to Mycobacterium Tuberculosis Infection. *Tohoku J. Exp. Med.* 216, 363–370. doi: 10.1620/tjem.216.363

Tinsley, F. C., Taicher, G. Z., and Heiman, M. L. (2004). Evaluation of a Quantitative Magnetic Resonance Method for Mouse Whole Body Composition Analysis. *Obes. Res.* 12, 150–160. doi: 10.1038/oby.2004.20

Tripathi, D., Radhakrishnan, R. K., Sivangala Thandi, R., Paidipally, P., Devalraju, K. P., Neela, V. S. K., et al. (2019). IL-22 Produced by Type 3 Innate Lymphoid Cells (ILC3s) Reduces the Mortality of Type 2 Diabetes Mellitus (T2DM) Mice Infected With Mycobacterium Tuberculosis. *PloS Pathog.* 15, e1008140. doi: 10.1371/journal.ppat.1008140

Vallerskog, T., Martens, G. W., and Kornfeld, H. (2010). Diabetic Mice Display a Delayed Adaptive Immune Response to Mycobacterium Tuberculosis. *J.7 Immunol.* 184, 6275–6282. doi: 10.4049/jimmunol.1000304

Weir, J. B. (1949). New Methods for Calculating Metabolic Rate With Special Reference to Protein Metabolism. *J. Physiol.* 109, 1–9. doi: 10.1113/jphysiol.1949.sp004363

WHO (2020). *WHO Global Tuberculosis Report* (2020). Available at: https://apps.who.int/iris/bitstream/handle/10665/336069/9789240013131-eng.pdf?ua=1

Yamashiro, S., Kawakami, K., Uezu, K., Kinjo, T., Miyagi, K., Nakamura, K., et al. (2005). Lower Expression of Th1-Related Cytokines and Inducible Nitric Oxide Synthase in Mice With Streptozotocin-Induced Diabetes Mellitus Infected With Mycobacterium Tuberculosis. *Clin. Exp. Immunol.* 139, 57–64. doi: 10.1111/j.1365-2249.2005.02677.x

Yen, Y. F., Chuang, P. H., Yen, M. Y., Lin, S. Y., Chuang, P., Yuan, M. J., et al. (2016). Association of Body Mass Index With Tuberculosis Mortality: A Population-Based Follow-Up Study. *Med. (Baltimore)* 95, e2300. doi: 10.1097/MD.0000000000002300

Conflict of Interest: The authors declare that the research was conducted in the absence of any commercial or financial relationships that could be construed as a potential conflict of interest.

frontiers in Cellular and Infection Microbiology

ORIGINAL RESEARCH
published: 07 July 2021
doi: 10.3389/fcimb.2021.669168

Cumulative Signaling Through NOD-2 and TLR-4 Eliminates the *Mycobacterium Tuberculosis* Concealed Inside the Mesenchymal Stem Cells

Mohammad Aqdas[1†], *Sanpreet Singh*[1†], *Mohammed Amir*[1], *Sudeep Kumar Maurya*[1], *Susanta Pahari*[1] *and Javed Naim Agrewala*[1,2*]

[1] Division of Cell Biology and Immunology, CSIR-Institute of Microbial Technology, Chandigarh, India, [2] Immunology Laboratory, Center for Biomedical Engineering, Indian Institute of Technology, Ropar, India

OPEN ACCESS

Edited by:
Natarajaseenivasan Kalimuthusamy, Bharathidasan University, India

Reviewed by:
Oleh Andrukhov, University Dental Clinic Vienna, Austria
Shinsmon Jose, University of Cincinnati, United States

***Correspondence:**
Javed Naim Agrewala
jagrewala@iitrpr.ac.in

[†]These authors share first authorship

Specialty section:
This article was submitted to Bacteria and Host, a section of the journal Frontiers in Cellular and Infection Microbiology

Received: 18 February 2021
Accepted: 21 June 2021
Published: 07 July 2021

Citation:
Aqdas M, Singh S, Amir M, Maurya SK, Pahari S and Agrewala JN (2021) Cumulative Signaling Through NOD-2 and TLR-4 Eliminates the Mycobacterium Tuberculosis Concealed Inside the Mesenchymal Stem Cells. Front. Cell. Infect. Microbiol. 11:669168. doi: 10.3389/fcimb.2021.669168

For a long time, tuberculosis (TB) has been inflicting mankind with the highest morbidity and mortality. Although the current treatment is extremely potent, a few bacilli can still hide inside the host mesenchymal stem cells (MSC). The functional capabilities of MSCs are known to be modulated by TLRs, NOD-2, and RIG-1 signaling. Therefore, we hypothesize that modulating the MSC activity through TLR-4 and NOD-2 can be an attractive immunotherapeutic strategy to eliminate the *Mtb* hiding inside these cells. In our current study, we observed that MSC stimulated through TLR-4 and NOD-2 (N2.T4) i) activated MSC and augmented the secretion of pro-inflammatory cytokines; ii) co-localized *Mtb* in the lysosomes; iii) induced autophagy; iv) enhanced NF-κB activity *via* p38 MAPK signaling pathway; and v) significantly reduced the intracellular survival of *Mtb* in the MSC. Overall, the results suggest that the triggering through N2.T4 can be a future method of immunotherapy to eliminate the *Mtb* concealed inside the MSC.

Keywords: tuberculosis, mesenchymal stem cell, NOD-2, TLR-4, autophagy

INTRODUCTION

Tuberculosis (TB) is the cause of 2 million deaths each year and an estimated 1.8 billion people with latent disease worldwide (Mwaba et al., 2020). It is one of the top 10 diseases in terms of high morbidity and mortality worldwide (Herbert et al., 2014). Currently, drug-resistant TB is a major threat to mankind and quite common in TB endemic countries viz., India and China. Even though the available drugs remain the mainstay for the treatment of TB, certain limitations, such as their narrow therapeutic index and the associated toxicities, dilute their effectiveness (Forget and Menzies, 2006; Trauner et al., 2014). Due to its long duration, many patients fail to abide by the current regimen and quit before the completion of the course. This leads to the development of the very lethal drug-resistant TB (Munro et al., 2007). Innate and adaptive immune responses are responsible for protecting against invading pathogens. Early events include the engulfment of *Mtb* by the alveolar macrophages and dendritic cells, followed by their bactericidal mechanisms, such as the generation of reactive nitrogen intermediates (RNI) and reactive oxygen intermediates (ROI)

(Sia and Rengarajan, 2019). Cytokines (IFN-γ, TNF-α, IL-6, IL-12, IL-17, and IL-23) and chemokines (CCL2, CCL3, CCL5, CXCL8, and CXCL10) help in restricting the *Mtb* burden and recruiting other immune cells to the site (Peters and Ernst, 2003; Saunders and Britton, 2007). *Mtb* has successfully evolved specialized immune evasion strategies that permit it to establish, multiply, and extend its infection within the host. Macrophages are the primary cells for *Mtb* infection. The bug acquires various strategies to persist in a dormant state in the hostile environment of the macrophage by inhibiting phagosome-lysosome (PL) fusion and de-acidification of lysosomes; thus, it averts its degradation and killing (Russell, 2013). Another mechanism of circumvention is the neutralization of reactive oxygen radicals by secretion of powerful anti-oxidants (Kumar et al., 2011). Most importantly, the lipid-rich cell wall of *Mtb* shields it from various defensive mechanisms. Thus, it becomes difficult to eliminate the latent form of *Mtb* with the current regimen and demands an urgent need for novel remedies for treating TB (Gomez and McKinney, 2004).

Recently, many studies have illustrated that bone marrow mesenchymal stem cells (MSCs) may provide a niche for shielding latent *Mtb*. MSCs are multipotent cells with a prospect to differentiate into adipocytes, osteocytes, chondrocytes, and neuronal cells. In the murine model of TB, rapid dissemination of *Mtb* was noticed, after aerosol exposure from the primary infection sites to bone marrow; where it infected MSCs (Garhyan et al., 2015). The murine model of TB dormancy demonstrates long-term intracellular viability and maintenance of *Mtb* in the MSCs (Das et al., 2013). It has been demonstrated that MSCs have a high number of ATP-binding cassette (ABC) transporter efflux pumps, which expel anti-TB drugs from host cells. Interestingly, viable *Mtb* is seen in the MSCs of patients, who had undergone successful anti-TB chemotherapy (Beamer et al., 2014). Thus, it can be inferred from these findings that *Mtb* can successfully hide in the MSCs until it gets ambient conditions to reactivate itself.

Innate immunity is the first line of defense, which subsequently imparts a significant impact on adaptive immune responses (Hoebe et al., 2004). Toll-like receptors (TLRs), NOD-like receptors (NOD-2), and RIG-like receptors (RIG-1) serve as a frontline defense system to defend against pathogens. These potentiate the ability of innate cells to recognize and subsequently respond to microbial infections (Kawai and Akira, 2011). Our group has already shown the importance of various innate signaling molecules against *Mtb* (Khan et al., 2016b; Khan et al., 2016c; Pahari et al., 2016; Pahari et al., 2020). MSCs substantially express an array of innate receptors like TLRs, NOD-2, or RIG-1 (Kim et al., 2010; Lei et al., 2011; Yang et al., 2013). TLRs are well-defined molecules that play an important role in the differentiation and self-renewal of MSC (Hwa Cho et al., 2006; Pevsner-Fischer et al., 2007). Recently, the switch of pro-inflammatory from anti-inflammatory polarization was also accredited to the activation of MSCs by delivering signals through TLRs (Waterman et al., 2010). This shows that the MSCs can be stimulated by signaling through TLRs, NLRs, and RIGs.

Based on the above-mentioned findings, the current study was designed to exploit the immunomodulatory potential of TLR-4 and NOD-2 in eliminating *Mtb* concealed inside the MSCs. Interestingly, signaling MSCs through NOD-2 and TLR-4 exhibited augmented secretion of pro-inflammatory cytokines, improved co-localization of *Mtb* in lysosomes, and significantly cleared the intracellularly masked mycobacterium. Mechanistically, stimulation of MSCs through NOD-2 and TLR-4 activated NF-κB activity *via* the p38 MAPK pathway and induced autophagy. In future, this novel strategy of host-directed therapy may open new avenues to eradicate *Mtb* hidden within the MSC.

MATERIALS AND METHODS

Animals

Female BALB/c mice (6–8 weeks) were obtained from the Animal Facility, CSIR-Institute of Microbial Technology, Chandigarh, India. All the animal experiments were performed as approved by the 'Institutional Animal Ethics Committee' (IAEC) and accomplished according to the National Regulatory Guidelines issued by the 'Committee for the Purpose of Control and Supervision of Experiments on Animals' (No. 55/1999/CPCSEA), Ministry of Environment and Forest, Government of India.

Strains of Mycobacterium

The *Mycobacterium tuberculosis (Mtb)* strains (H37Rv, H37Ra) were obtained from Dr. V. M. Katoch (National JALMA Institute for Leprosy and Other Mycobacterial Diseases, Agra, India). Mycobacterium strains were grown and cultivated in Middlebrook 7H9 broth supplemented with glycerol (0.2%), tween-80 (0.05%), dextrose, albumin, and catalase. Bacterial viability was enumerated through colony-forming units (CFUs) by plating them on Middlebrook 7H11 medium, supplemented with dextrose, albumin, oleic acid, and catalase after 21d of plating.

Antibodies and Reagents

The standard reagents and chemicals were obtained from Sigma (St. Louis, MO). Recombinant cytokines and antibodies of IL-6, IL-12, TNF-α, and IL-10 were purchased from BD Biosciences (San Diego, CA). Fluorochrome-labelled antibodies (CD29 FITC, CD34 eFluor 660, CD44 PerCP-Cyanine5.5, CD45 APC, and Sca-1 PE) were purchased from eBiosciences (San Diego, CA) unless otherwise mentioned. Fetal bovine serum (FBS) was from GIBCO. LPS and N-glycolyl MDP used as ligands for TLR-4 and NOD-2 in the experiments were procured from InvivoGen (San Diego, CA). Oil Red-O stain was bought from Himedia (Mumbai, India). Alizarin Red S stain was acquired from Sigma (St. Louis, MO).

Isolation of Bone-Marrow-Derived Mesenchymal Stem Cells From Mice

Mouse MSCs were isolated according to a protocol reported previously (Huang et al., 2015). Briefly, the tibia and femur bones were taken from the hind limb of BALB/c and kept in sterile phosphate buffer saline (PBS) (1X), after the removal of all residual soft tissues. Then, with the help of a 23G needle and

syringe, bone cavities were flushed with Dulbecco's modified Eagle's medium (DMEM) having 10% heat-inactivated FBS, 1X penicillin-streptomycin, and 2 mM L-glutamine. Bone cavities were flushed repeatedly to obtain enough marrow cells. The cells were then cultured in cell culture dishes (100mm) for 5 days in 5% CO_2/37°C. Later, the cells were washed twice with PBS (1X) and digested with trypsin (0.25%) containing ethylenediaminetetraacetic acid (EDTA) (0.02%) at RT for 2 min followed by trypsin neutralization with DMEM + FBS (10%). The cells were then centrifuged at 2000 rpm for 3 min and replated at a split ratio of 1:3 in fresh complete media. The experiments were performed when the MSCs showed a homogeneous pattern after several set of passages. The MSCs were harvested, washed, and cultured for the experiments.

The activation of MSC was done by signaling through NOD-2 and TLR-4. The MSCs ($2x10^5$ cells/ml) were stimulated with a combination of N-glycolyl MDP (10 μg/ml) and ultra-purified LPS (5 ng/ml), the ligands of NOD-2 and TLR-4, respectively. The control cultures consist of unstimulated MSCs or cultured with either the ligand of NOD-2 or TLR-4. The cells were cultured in DMEM + FBS (10%) for 48h at 5% CO_2/37°C. The culture supernatants (SNs) were harvested after 48h for the estimation of cytokines by ELISA and cells for the isolation of total RNA at 6h to perform RT-PCR.

Estimation of Cytokine Secretion by ELISA

The cultures were set as mentioned above, and the cytokines (IL-12, IL-6, TNF-α, and IL-10) were estimated in the culture SNs of the MSCs by ELISA methods, according to the manufacturer's instructions. Briefly, ELISA plates were coated with antibodies to mouse IL-12 (2μg/ml), IL-6 (2μg/ml), TNF-alpha (2μg/ml) or IL-10 (4μg/ml) in phosphate buffer (0.01 M Na_2HPO_4, pH 9.2, and pH 6, respectively) at 4°C for overnight. Blocking was performed with 1% BSA at RT for 2h. Later, SNs (50μl/well) were added in the wells, or their respective recombinant cytokines as standards, and kept at 4°C overnight. Then, the respective biotinylated anti-mouse IL-12 (2μg/ml), IL-6 (2μg/ml), TNF-alpha (2μg/ml) or IL-10 (2μg/ml) antibodies were added into plates and incubated for 2h at RT. Afterward, avidin-HRP (1:10,000) was added and incubated at 37°C for 45 min. After each incubation, regular steps of washing were carried out. Subsequently, the color was developed using H_2O_2-OPD substrate-chromogen, and the reaction was stopped by the addition of 7% H_2SO_4 in the plates. The plates were then read at 492 nm in an ELISA reader. Serial dilutions of recombinant cytokines (rIL-6, rIL-12 and rIL-10) were used to plot standard curves for the estimation of cytokines in SNs. Results of ELISA were expressed in pg/ml.

RT-qPCR for the Quantification of *IL-12, IL-6, TNF-α, IL-10, iNOS*, and *TGF-β*

Isolation of total RNA was performed using TRIzol reagent from MSCs stimulated with N2.T4 ($MSC^{N2.T4}$) for 6h, according to the manufacturer's instruction (Invitrogen, Carlsbad, CA). Briefly, quantification of RNA was done using the NanoDrop spectrophotometer. The purity of all isolated RNA was in the range of 1.90 to 2.00 upon measured at A260/A280 (BioTek, Winooski, VT). The cDNA was synthesized using the Maxima first-strand cDNA synthesis kit for RT-qPCR (Thermo Fischer Scientific, K1642). Amplification-grade DNase1 (Sigma Aldrich, AMPD1-1KT) was used for removing DNA contamination from RNA samples. RNA samples (1μg) were treated with DNase1 (1U) in the reaction buffer for 15 min. DNase activity was stopped with the addition of a stop solution followed by incubating samples at 70°C for 10 min. Analysis was performed by the comparative Ct method, whereas normalization of the Ct values was done against a housekeeping control β-actin. Relative gene expression was determined using the comparative Ct method as $2(^{-\Delta\Delta}Ct)$, where ΔCt = Ct (gene of interest) - Ct (normalizer = β-actin) and the ΔΔCt = ΔCt (sample) - ΔCt (calibrator). RT-qPCR, along with the analysis of data, was carried out using the ABI 7500 Fast Real-time PCR system (Applied Biosystems, Chromas, Singapore). Results were presented as a relative expression (fold change). The primer sequences for RT-qPCR are mentioned below.

TNF-α
Fwd 5'-CCTGTAGCCCACGTCGTAG -3'
Rev 5'-GGGAGTAGACAAGGTACAACCC -3'
TGF-β
Fwd 5'- TGACGTCACTGGAGTTGTACGG-3'
Rev 5'-GGTTCATGTCATGGATGGTGC-3'
β-actin
Fwd 5'-AGAGGGAAATCGTGCGTGAC-3'
Rev 5'-CAATAGTGATGACCTGGCCGT-3'
IL-6
Fwd 5'-GAGGATACCACTCCCAACAGACC-3'
Rev 5'-AAGTGCATCATCATCGTTGTTCATACA-3'
IL-12
Fwd 5'-GGAAGCACGGCAGCAGCAGAATA-3'
Rev 5'-AACTTGAGGGAGAAGTAGGAATGG-3'
iNOS
Fwd 5'-AACGGAGAACGTTGGATTTG-3'
Rev 5'-CAGCACAAGGGGTTTTCTT-3'

The Characterization of Phenotypic Markers of MSCs

For the immunophenotype assay, flow cytometry analysis was carried out. MSCs ($2X10^5$ cells) were washed and harvested from the plates after they attained the confluency. Cells were then incubated with Fc receptor blocking antibody (anti-CD16/32) for 20 min at 4°C. Subsequently, cells were stained with fluorochrome-conjugated Abs specific for CD34, CD44 (osteopontin and hyaluronate marker), Sca-1 (stem cell antigen-1), CD29 (Integrin β-1), and CD45 (pan-leukocyte marker) Abs at 4°C for 30 min. Washing was done at each step. Later, cells were fixed using paraformaldehyde (1X) and acquired on the FACS ARIA flowcytometer. The data were analyzed using BD DIVA software (BD Biosciences, San Jose, CA).

Evaluation of the Differentiation of MSCs

For adipogenesis differentiation assay, MSCs ($2 X 10^5$/well) were seeded in a 6-well plate in DMEM+10% FBS complete media. The next day, a fresh medium was poured along with a pre-warmed complete adipogenesis differentiation medium

(StemPro® Adipogenesis Differentiation Kit; A10070-01) and kept at 37°C in a 5% CO_2 incubator. Cultures were fed every 3–4 days with adipogenesis differentiation media. After 21 days, cells were washed twice with PBS (1X) followed by fixation with 10% formalin. Cells were then stained with Oil red O (Himedia: TC256) stain. The pictures were taken under a phase-contrast microscope (10X) (Olympus IX71, Tokyo, Japan).

For osteogenesis differentiation assay, MSCs (2 X 10^5/well) were seeded in a 6-well plate in DMEM+10% FBS complete media. After 24h, fresh media (DMEM+10% FBS) was added along with a pre-warmed osteogenesis differentiation medium (StemPro® Osteogenesis Differentiation Kit; A10072-01). Cultures were replenished every 3–4 days with osteogenesis differentiation media. After 3 weeks, fixation of cells was done using formalin (10%) and stained for calcium deposition with Alizarin Red S (Sigma Aldrich, St. Louis, MO).

In Vitro Infection of MSCs With *Mtb* and Determination of CFUs

Mtb (H37Rv) was grown till the mid-log phase and stored in a glycerol stock at -80°C. Later, the bacterium was thawed, and MSCs (2 X 10^5/well) were infected with *Mtb* at multiplicity of infection (MOI) 1:5 for 4h. The extracellular bacteria were eliminated by treatment with gentamicin (10 μg/ml) for 1h and then washed with PBS (1X). *Mtb*-infected MSCs were then stimulated with ligands of NOD-2 and TLR-4 (N2.T4) for 48h and plates were kept in a CO_2 (5%) incubator at 37°C. Later, the SNs were collected for the cytokine ELISA and cells were lysed with saponin (0.1%). 100X serial dilutions of cell lysate were plated on 7H11 agar plates. Plates were kept in an incubator at 37°C. Bacterial colonies were enumerated for CFUs after 3 weeks.

Tracking of *Mtb* Into Autolysosomes by LysoTracker Red Staining

MSC (2 X 10^5 cells/well) were infected with GFP-*Mtb* (H37Ra) for 4h at MOI of 1:5. The extensive washing was done with PBS (1X) to get rid of extracellular *Mtb* followed by gentamicin (10 μg/ml) treatment for 1h. The cells were stimulated with N2.T4 for 12 h. The cells were stained with 200 nM of LysoTracker Red (prepared in media) for 20 min at 37°C/5% CO_2. The cells were then washed twice with PBS (1X) followed by fixing with PFA (4%). After fixation, the nucleus was stained with DAPI (1 μg/ml) for 10 min, followed by washing three times with PBS (1X). The coverslips were mounted onto the slide with help of a mounting reagent and observed under a confocal microscope (Nikon A1R, Nikon, Yokohama, Japan), using the lasers 488 nm (GFP-*Mtb*H37Rv), 561 nm (LysoTracker Red), and 405 nm (DAPI) with the same power set for controls. In total, 10 random fields were imaged, and the percentage of *Mtb* containing autophagosomes colocalized with lysosomes was counted.

Evaluation of Signaling in $MSC^{N2.T4}$ by Western Blotting

MSC (2 X 10^6 cells/well) were stimulated with N2.T4 ($MSC^{N2.T4}$) for 24h. Cells were then harvested, washed, and lysed in a lysis buffer (RIPA buffer, protease and phosphatase inhibitor cocktail). Proteins in the lysate were then estimated and equal concentrations of lysates were subjected to SDS-PAGE electrophoresis. After transfer to the nitrocellulose membrane, followed by blocking with BSA (2%), the membranes were then immunoblotted with Abs specific for LC3-I/LC3II, beclin-1, phospho-p38/p38, and NF-κB-p65. Actin was used as a loading control. The blots were developed using a chemiluminescence kit (Amersham Pharmacia Biotech, Buckinghamshire, UK). Blots were then scanned with ImageQuant LAS 4000 (GE Healthcare, Pittsburgh, PA). The image analysis was performed with ImageJ software.

Statistical Analysis

All data were analyzed using student "t-test" and one-way analysis of variance (ANOVA) with post-Tukey-Kramer multiple comparisons test by Graph Pad Prism 6 software (GraphPad Software, La Jolla, CA). Data were expressed as mean ± SD. The *$p<0.05$ was considered significant.

RESULTS

Characterization of MSCs Isolated From the Bone Marrow

Bone-marrow-derived MSCs were isolated and cultured, as described elsewhere (Huang et al., 2015). The cellular morphology of MSCs was spindle shaped (fibroblast like), as observed under a microscope (**Figures 1A, B**). Further, isolated MSCs were stained with rhodamine phalloidin (selectively binds to F-actin) and DAPI to study their morphological features. MSCs have the potential to differentiate into various lineages (Robert et al., 2020). Subsequently, the MSC were checked for their adipogenic and osteogenic differentiation characteristics. We observed red-colored intracellular lipid vacuoles after Oil Red O staining (**Figure 1C**). Further, Alizarin Red S stained the calcium nodules deposition, which confirmed the osteoblasts formation in MSC (**Figure 1D**). It has been reported that the MSCs can be phenotypically characterized by the expression of several positive and negative markers on their surface (Soleimani and Nadri, 2009). Flow cytometric analysis confirmed the expression of Sca-1, CD44, and CD29 markers and the absence of CD45 molecules (**Supplementary Figure 1**). Thus, the cells isolated from bone marrow were phenotypically and functionally characterized as MSCs and all the subsequent experiments were performed using these cells.

Signaling Delivered Through NOD-2 and TLR-4 Stimulates MSCs

MSC expresses innate receptors, such as TLRs, NOD-2, and RIG-1 (Kim et al., 2010; Lei et al., 2011; Yang et al., 2013). Hence, we thought whether ligation of NOD-2 and TLR-4 can stimulate MSCs. Unfortunately, we could not observe any statistical change in the activation of MSCs, as depicted by the release of IL-6 and IL-12 (**Figure 2A**). Intriguingly, when we activated MSCs by combinatorial signaling through NOD-2 and TLR-4 ($MSC^{N2.T4}$), a substantial ($p<0.001$) increase in the release of IL-6 and IL-12

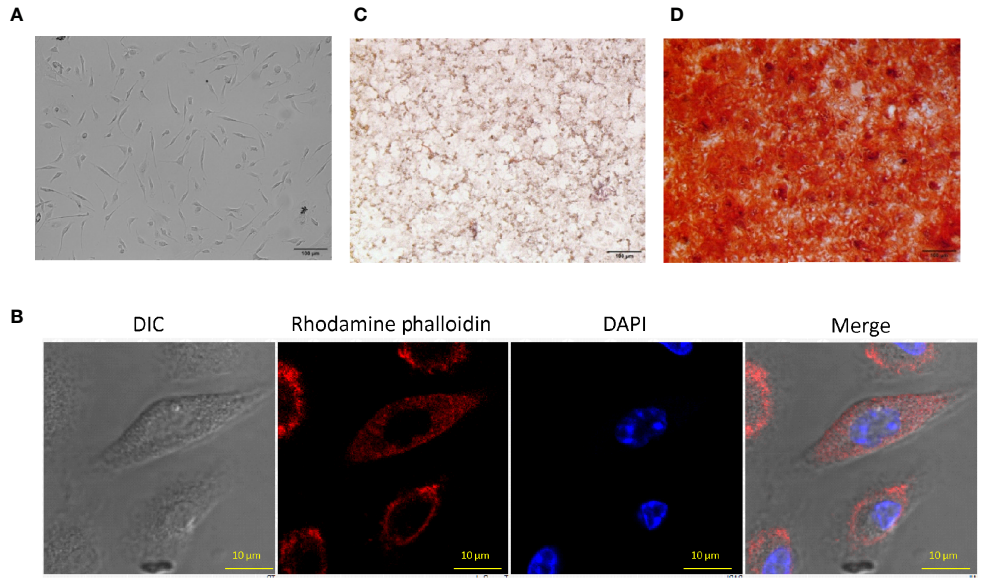

FIGURE 1 | Characteristics of mouse bone marrow-derived mesenchymal stem cells (MSC). **(A)** MSCs were isolated from mouse bone marrow and expanded to several passages that showed fibroblast-like morphology and arranged in the swirl. The photographs were taken using an Olympus IX71phase contrast microscope (10X). **(B)** MSCs were stained with rhodamine phalloidin (red) and DAPI (blue) and observed under a confocal microscope (60X). **(C)** Intercellular lipid vacuoles were stained with Oil Red O to determine the adipogenic differentiation potential of MSC. The pictures were taken using an Olympus phase contrast microscope (10X). **(D)** The MSC were stained with the Alizarin Red S to assess the osteogenic differentiation by the formation of calcium nodules. The pictures were clicked using a phase contrast microscope (10X). The photographs shown are the representative of three experiments.

was noted, as compared to the control MSCs stimulated with the ligand of either NOD-2 or TLR-4 (**Figures 2A, B**). Therefore, the combination of ligands of NOD-2 and TLR-4 (N2.T4) were used in all the subsequent experiments to stimulate MSCs ($MSC^{N2.T4}$). It has been reported that TNF-α, IL-12, IL-6, and iNOS play a crucial role in curbing the intracellular growth of pathogens like *Mtb*, leishmania, salmonella, HIV, etc. (Black et al., 1990; Jankovic et al., 2002; Chakravortty and Hensel, 2003). Further, this observation was corroborated through gene expression in MSCs by RT-qPCR. Besides *IL-12* ($p<0.001$) and *IL-6* ($p<0.001$), *iNOS* ($p<0.001$) along with *TNF-α* ($p<0.001$) also showed elevation in their expressions upon stimulation with N2.T4 (**Figures 2C–F**). Contrary to this, there was a substantial ($p<0.001$) reduction in the anti-inflammatory cytokine TGF-β (**Figure 2G**). Hence, we observed a shift from anti-inflammatory to pro-inflammatory phenotype after triggering MSCs through N2.T4.

Signaling *Mtb*-Infected MSCs Through N2.T4 Augments the Release of Pro-Inflammatory Cytokines and Constrains the Intracellular Growth of the *Mtb*

Recent studies have shown that *Mtb* can successfully infect and hide inside the MSCs (Das et al., 2013). Hence, we were curious to monitor the influence of N2.T4 signaling of MSCs ($MSC^{N2.T4}$) on the intracellular survival of the bacterium. Interestingly, MSCs infected with *Mtb* (H37Rv) upon N2.T4 stimulation significantly ($p<0.01$) restricted the bacterial burden compared to unstimulated (US) MSCs (**Figure 3A**). Furthermore, remarkable elevation was noticed in the secretion of pro-inflammatory cytokines TNF-α ($p<0.01$) and IL-6 ($p<0.001$) by $MSC^{N2.T4}$ (**Figures 3B, C**). The non-significant decrease was observed in the level of anti-inflammatory cytokine IL-10 (**Figure 3D**). These results suggest that combinatorial stimulation of MSCs through NOD-2 and TLR-4 can successfully restrict the intracellular growth of *Mtb* masked inside these cells.

Signaling of $MSC^{N2.T4}$ Augments the Co-Localization of *Mtb* in Lysosomes

One of the potent mechanisms responsible for the killing of various intracellular pathogens is the lysosomal degradation pathway (Jo, 2010). Scavenger receptors like MARCO and SR-B1 present on MSCs play an important role in internalizing *Mtb* (Khan et al., 2017). Phagosome lysosome fusion is decisive for the eradication of the intracellularly hidden *Mtb* (Khan et al., 2017). However, *Mtb* has a unique tendency to evade the immune system by inhibiting the phagosome lysosome fusion; thereby can successfully survive in the hostile environment of macrophages and MSC (Jamwal et al., 2016). Consequently, we next studied the signaling of MSCs through N2.T4 and its influence on the intracellular trafficking of *Mtb*. MSCs were infected with *Mtb* overexpressing GFP. Further, MSCs were stained with LysoTracker Red dye to monitor the acidification of the lysosome. Later, the signaling was delivered in MSCs through N2.T4. We observed that *Mtb* inhibited the phagosome lysosome fusion of the infected MSC (**Figure 4A**). It was interesting to note that $MSC^{N2.T4}$ could efficiently overcome

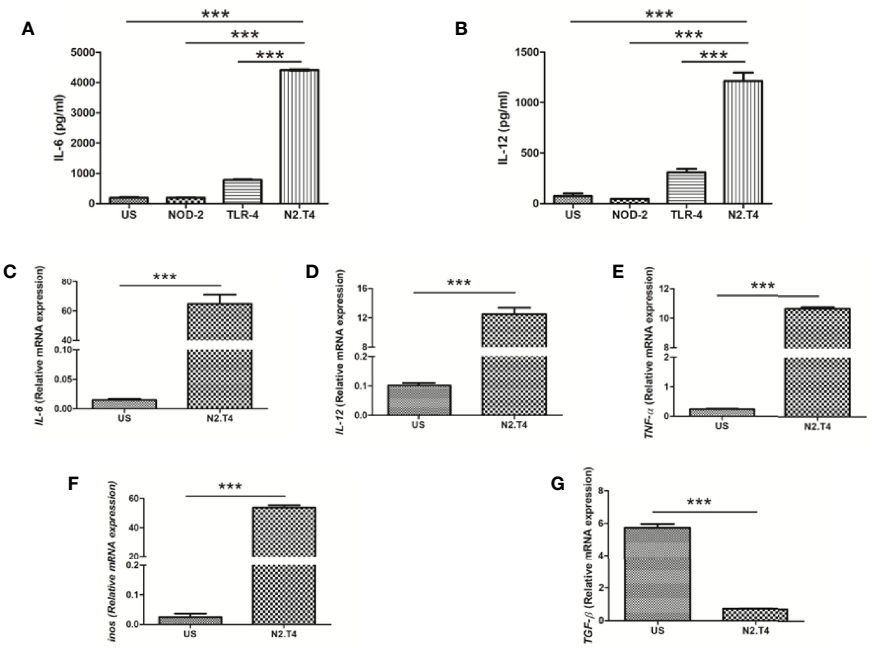

FIGURE 2 | Cumulative signaling through NOD-2 and TLR-4 stimulates MSC to release IL-6 and IL-12. **(A, B)** MSCs were cultured with the ligands of NOD-2 and TLR-2 (N2.T4). The controls were set using unstimulated MSCs (US) or stimulated with either the ligand of NOD-2 (NOD-2L) or TLR-4 (TLR-4L). The culture SNs were collected after 48h and estimated for the production of **(A)** IL-6 and **(B)** IL-12 cytokines by ELISA. **(C–G)** The MSCs were stimulated as indicated above **(A, B)** and the mRNA expression of *Il6* **(C)**, *Il12* **(D)**, *Tnfa* **(E)**, *Inos* **(F)** and *Tgfb* **(G)** was performed by RT-PCR. Graphs depict the 'mRNA expression relative to unstimulated (US) control'. Data expressed as mean ± SD are representative of two independent experiments. Statistical analysis was done using one way ANOVA for ELISA and unpaired t-test for RT-PCR. ***$p < 0.001$.

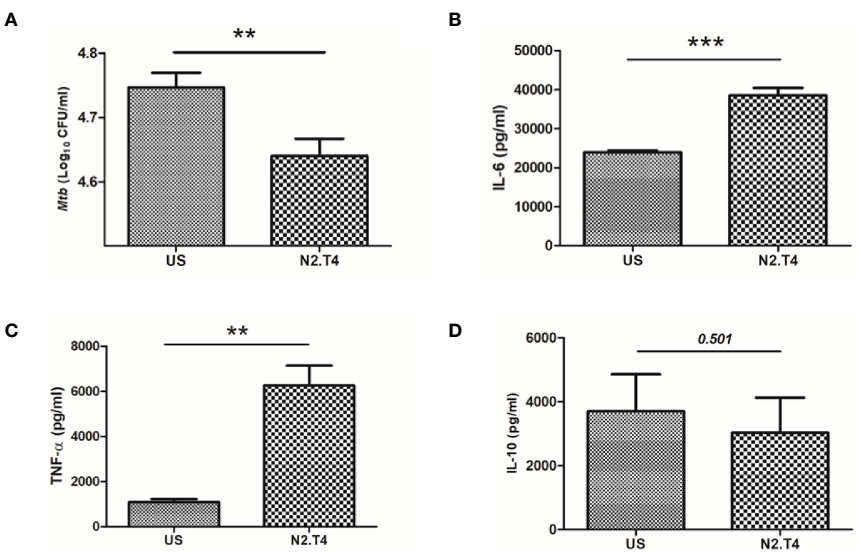

FIGURE 3 | Signaling MSCs through N2.T4 restricted the intracellular growth of *Mtb* and elicited the secretion of pro-inflammatory cytokines. **(A)** MSCs were infected with *Mtb* (GFP-H37Ra) for 4h and then stimulated with N2.T4 for 48h. Later, cells were lysed and CFUs were enumerated on 21d by CFU assay. The Bar diagram represents the mean ± SEM and is indicative of three independent experiments. Statistical analysis was done using one-way ANOVA. The culture SNs were collected after 48h for determining the yield of cytokines **(B)** IL-6, **(C)** TNF-α and **(D)** IL-10 by ELISA. Statistical analysis was done using an unpaired t-test. The inset represents p value. **$p < 0.01$ and ***$p < 0.001$.

the *Mtb* induced inhibition of phagosome lysosome fusion, as demonstrated by a significant ($p<0.01$) increase in the co-localization of *Mtb* and LysoTracker Red dye (**Figures 4A, B**). These results signify that the mechanism responsible for the killing of *Mtb* by $MSC^{N2.T4}$ may be operating through the enhanced fusion of phagolysosomes (**Figures 3A** and **4A, B**). Hence, N2.T4 may have an important immunotherapeutic role in eliminating *Mtb* concealed in the MSCs.

Signaling Through N2.T4 Induces Autophagy in MSC

The intrinsic autophagy mechanism is known to inhibit the growth of *Mtb* inside MSCs (Khan et al., 2017). The transition of LC3-I to LC3-II is evidence of autophagy. Consequently, we next checked the induction of autophagy in $MSCs^{N2.T4}$. Interestingly, we observed conversion of LC3-I to LC3-II (**Figures 5A, B**). These results suggest a novel role of signaling of MSC through N2.T4 in inducing autophagy. Beclin-1 is a well-known initiator and master regulator of autophagy. Thus, the levels of beclin-1 in $MSC^{N2.T4}$ were monitored. We observed an increased level of beclin-1 in $MSC^{N2.T4}$ (**Figures 5C, D**). The modulation of the expression of markers LC3 and beclin-1, suggests the role of autophagy as a possible mechanism operating in curtailing the intracellular growth of *Mtb* in $MSC^{N2.T4}$.

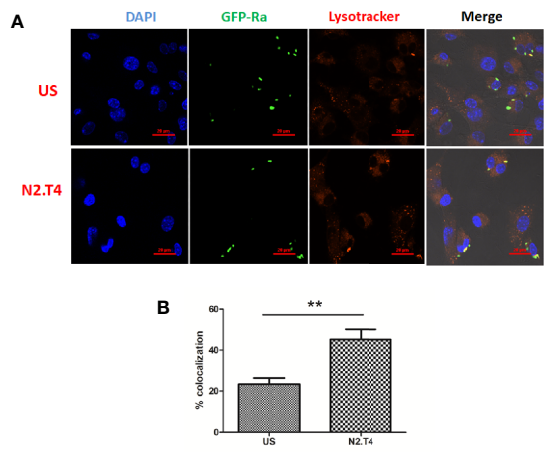

FIGURE 4 | Triggering MSCs through N2.T4 induced trafficking of *Mtb* to autolysosomes. **(A)** MSCs (2 X 10^5 cells/well)were infected with GFP-*Mtb* (H37Ra) for 4h followed by signaling through N2.T4 for 12h. Later, the lysosomes were stained with LysoTracker Red for 20 min. The cells were fixed with PFA (4%) and slides were prepared for confocal microscopy. The panel shows the representative image of *Mtb* (green channel, 488 nm) colocalization with LysoTracker Red (red channel, 561 nm) (60X). **(B)** The data from **(A)** are also illustrated as a graph depicting the percentage of colocalization of *Mtb* with the lysosome. The data shown as mean ± SEM are representative of three independent experiments. Statistical significance was determined using the unpaired t-test. $^{**}p < 0.01$.

N2.T4 Signaling of MSC Induces NF-κB Activity *via* p38 MAPK Pathway

The TLR signaling is known to initiate MAPK pathways through MyD88 molecules (Kim et al., 2010). Further, NF-κB is activated after degradation of IκB and translocates into the nucleus to affect the target genes, denoting the activation status of the cell. We noticed a substantial induction of p38 in $MSC^{N2.T4}$, as compared to unstimulated cells (**Figures 6A, B**). Furthermore, we noticed increased levels of NF-κB-p65 (**Figures 6C, D**). These results suggest the importance of combinatorial signaling of NOD-2 and TLR-4 in enhancing the activation and functionality of the $MSC^{N2.T4}$ to kill covert *Mtb*.

DISCUSSION

Mycobacterium tuberculosis (Mtb) is one of the most astute pathogens that the human race has ever encountered. This is evident by the fact that it understands the mechanism of i) living in a dormant state in a hostile environment of the host; ii) impairing the functioning of BCG vaccine; iii) developing resistance against the drugs designed to kill it; iv) developing coalition with HIV; and v) attacking malnourished individuals. Further, the problem has been compounded with a recent discovery of enduring residency of *Mtb* in the multipotent cells i.e. MSC (Das et al., 2013; Beamer et al., 2014). Consequently, *Mtb* continues to make its elimination a daunting task for the scientific community.

Only 5–15% of people infected with *Mtb* develop TB. This indicates 85–95% of infected individuals develop a remarkably strong immunity to remain protected throughout their lives. This indicates that host immunity plays a primary role in protecting against TB. Therefore, boosting host immunity can play a cardinal role in protecting against *Mtb*. Recently, host-directed therapy (HDT) has gained considerable momentum following the observation that it not only controls the infection and devastating inflammatory responses inflicted by *Mtb* to the host but also the emergence of drug-resistant strains of the bacterium (Zumla et al., 2016; Young et al., 2020). Exploration and exploitation of the molecules of innate immunity may be an estimable idea for bolstering host immunity since innate immunity plays an imperative role against *Mtb* (Fremond et al., 2004). The NOD-2 is an important receptor of innate immunity because its role has been reported in effectively modulating the cell's immunity (Divangahi et al., 2008; Jo, 2008). Likewise, TLR-4 plays a crucial function in boosting immunity against many pathogens (Kleinnijenhuis et al., 2011; Mortaz et al., 2015). Recently, we have demonstrated a combinatorial role of NOD-2 and TLR-4 in substantially augmenting the functionality of dendritic cells in priming T cells and killing *Mtb* (Khan et al., 2016a). Mesenchymal stem cells express various innate receptors on their surface, including NOD-2 and TLR-4. These receptors assist in the recognition and delivering signals on encounters with the pathogens (Kim et al., 2010; Lei et al., 2011; Yang et al., 2013). Signaling through innate

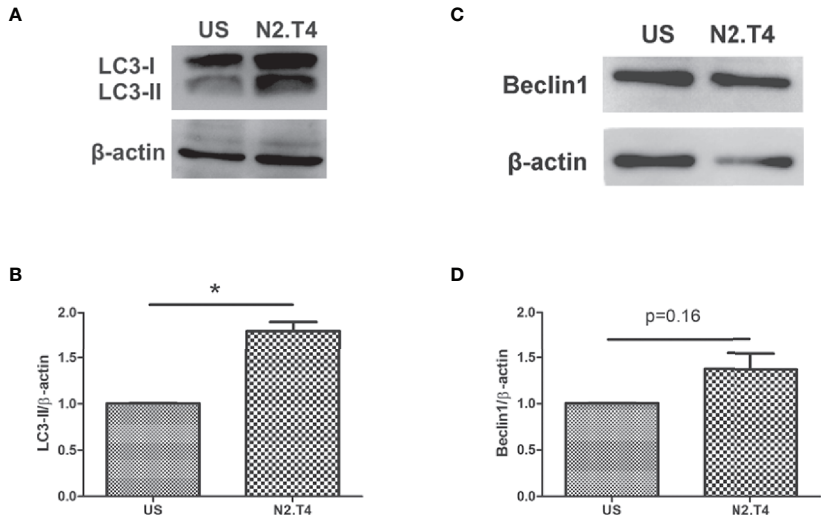

FIGURE 5 | N2.T4 signaling induced autophagy in MSC. MSC (2 X 10^6 cells/well) were stimulated with either N2.T4 or left untreated for 24h. The cells were lysed with a RIPA buffer containing a protease inhibitor cocktail. The samples were subjected to SDS-PAGE and Western blotting. The blots were probed with antibodies against autophagy markers LC3 and beclin-1 **(A, C)**. The densitometric analysis of LC3 and beclin-1, normalized with β-actin is represented in graphs **(B, D)**, respectively. The data shown are representative of three independent experiments. The inset represents p value. *p < 0.05.

receptors can polarize MSCs from anti-inflammatory to pro-inflammatory phenotype (Waterman et al., 2010).

Based on the above-mentioned studies, we thought to examine the influence of signaling through NOD-2 and TLR-4 in modulating the activity of MSCs against *Mtb*. MSCs were infected with *Mtb*, and signaling was delivered using the ligands of NOD-2 and TLR-4. Following major findings emerged out of this study. $MSC^{N2.T4}$ exhibited i) activation phenotype, as illustrated by the enhanced release of IL-6, IL-12, TNF-alpha, iNOS and decrease in TGF-β; ii) increased co-localization of *Mtb* in lysosomes; iii) induction of NF-κB activity *via* the p38 MAPK pathway; iv) augmented autophagy; and v) a decline in the survival of *Mtb* inside the MSCs.

NODs and TLRs are innately expressed on MSCs (Delarosa et al., 2012). NOD-2 and TLR-4 coordinate with each other in imparting protection against pathogens like *Mtb* (Khan et al., 2016c).

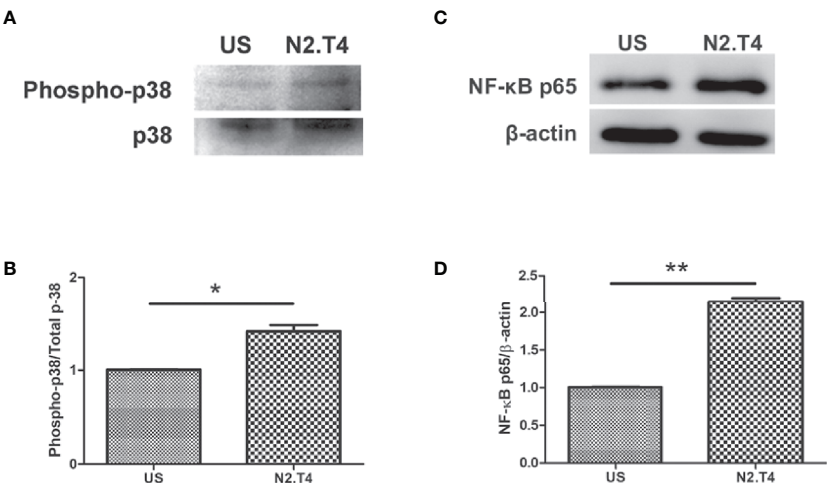

FIGURE 6 | Stimulation of MSCs through N2.T4 induced NF-κB activity *via the* p38 MAPK pathway. MSCs were stimulated with the ligands of N2.T4 for 24 hours and control cells were left unstimulated (US). The cells were lysed with a RIPA buffer containing protease inhibitor cocktail. Total cell lysates were subjected to SDS-PAGE and Western blotting. The blots were probed with antibodies against **(A)** phosphor-p38/p38 and **(C)** NF-κB-p65 with densitometric analysis normalized with β-actin, represented in graphs **(B, D)**, respectively. The data shown are representative of two independent experiments. *p < 0.05, **p < 0.01.

Likewise, our study demonstrated that combinatorial signaling of TLR-4 and NOD-2 can activate MSCs and thereby can restrict the intracellular growth of *Mtb*. N-glycolyl MDP was selected as a NOD-2 agonist because it is 10–100 fold more effective, as compared to N-acetylated MDP (Coulombe et al., 2009). Ultrapure LPS was used for triggering TLR-4, which has remarkable adjuvant properties. Further, the Food and Drug Administration (FDA) has approved the immunotherapeutic use of the ligand of TLR-4 (Bohannon et al., 2013; Needham et al., 2013).

It was intriguing to note that the signaling of MSCs through NOD-2 and TLR-4 ($MSC^{N2.T4}$) exhibited anti-*Mtb* immunity, as evidenced by a significant increase in the pro-inflammatory molecules IL-12, IL-6, TNF-α, and iNOS and reduction in anti-inflammatory cytokine TGF-β. This was further reflected by a substantial decline in the survival of *Mtb* in the MSCs. Mesenchymal stem cells express TLR-4 as a type I transmembrane glycoprotein (Takeda and Akira, 2005). The activation of TLR-4 requires adaptors and co-receptors (MD2, LMP, and CD14) for dimerization that facilitates MyD88/TRIF-dependent activation of the transcription factors (Zhu et al., 2006; Najar et al., 2017). It has been shown that the effect of LPS is compromised in MSCs derived from $MyD88^{-/-}$ mice (Chu et al., 2019). Moreover, LPS has been shown to convert MSCs from anti-inflammatory to pro-inflammatory phenotype (Waterman et al., 2010). Further, TLR-4 activation enhanced the proliferation of MSCs (Pevsner-Fischer et al., 2007). Thus, indicating the potential role of TLR-4 in the signaling of MSCs.

In general, TLR stimulation activates MyD88-dependent and independent signaling pathways. MyD88 recruitment to TLRs triggers numerous signaling pathways *via* IRAKs, which subsequently initiate MAPK pathways. Therefore, to decipher the mechanism operating in restricting the survival of *Mtb* in MSC, we checked the level of the p38 MAPK signaling pathway. We observed elevated expression of p38 molecule in $MSC^{N2.T4}$. It is already reported that the p38 phosphorylation activates NF-κB followed by subsequent translocation to the nucleus (Olson et al., 2007; Karunakaran and Ravindranath, 2009). Increased levels of NF-κB p65 in $MSC^{N2.T4}$ were observed, as compared to unstimulated cells. Furthermore, it was observed that the decline in the survival of *Mtb* was through autophagy, as revealed by the modulation in the expression LC3 and beclin-1. Autophagy is an inherent quality of many stem cell types and is considered to be vital for their pluripotency, differentiation, and self-renewal (Phadwal et al., 2013). Autophagy has been described to exhibit a dual role in *Mtb* protection. Firstly, it targets the antigen for lysosomal degradation, and, secondly, it prevents the inflammatory reaction; thus protecting from tissue necrosis along with the associated pathology (Castillo et al., 2012).

CONCLUSION

Overall, our results suggest that host-directed therapy through N2.T4 may be a good option for priming MSC to kill non-replicating quiescent intracellular *Mtb*. Further, the results suggest that this strategy may have enough potential in inhibiting the intracellular growth of drug-resistant *Mtb*. Finally, in future, this novel immunotherapeutic strategy may sufficiently contribute in successfully treating TB patients.

DATA AVAILABILITY STATEMENT

The original contributions presented in the study are included in the article/**Supplementary Material**. Further inquiries can be directed to the corresponding author.

ETHICS STATEMENT

The animal study was reviewed and approved by Institutional Animal Ethics Committees (IAEC) of IMTECH, Chandigarh.

AUTHOR CONTRIBUTIONS

The concept, experiment designing, and data analysis were done by JA and MAq. The experiments were conducted by MAq, SS, SP, MA, and SM. The manuscript was written by JA, MAq, and SS. All authors contributed to the article and approved the submitted version.

FUNDING

The work was carried out under funding support from the Council of Scientific and Industrial Research (CSIR), India. MAq received a fellowship from the Department of Science and Technology (DST), SS from the Indian Council of Medical Research (ICMR), MA from University Grant Commission, and SM and SP were the recipients of fellowships from CSIR.

SUPPLEMENTARY MATERIAL

The Supplementary Material for this article can be found online at: https://www.frontiersin.org/articles/10.3389/fcimb.2021.669168/full#supplementary-material

Supplementary Figure 1 | The MSC were stained with the fluorochrome-labeled respective Abs and analyzed by flowcytometry for the expression of phenotypic markers viz CD44, CD29, Sca-1, and CD45. The black and red histograms represent unstained and stained MSCs, respectively.

REFERENCES

Beamer, G., Major, S., Das, B., and Campos-Neto, A. (2014). Bone Marrow Mesenchymal Stem Cells Provide an Antibiotic-Protective Niche for Persistent Viable *Mycobacterium Tuberculosis* That Survive Antibiotic Treatment. *Am. J. Pathol.* 184 (12), 3170–3175. doi: 10.1016/j.ajpath.2014.08.024

Black, C. M., Bermudez, L. E., Young, L. S., and Remington, J. S. (1990). Co-Infection of Macrophages Modulates Interferon Gamma and Tumor Necrosis Factor-Induced Activation Against Intracellular Pathogens. *J. Exp. Med.* 172 (3), 977–980. doi: 10.1084/jem.172.3.977

Bohannon, J. K., Hernandez, A., Enkhbaatar, P., Adams, W. L., and Sherwood, E. R. (2013). The Immunobiology of Toll-Like Receptor 4 Agonists: From

Endotoxin Tolerance to Immunoadjuvants. *Shock* 40 (6), 451–462. doi: 10.1097/SHK.0000000000000042

Castillo, E. F., Dekonenko, A., Arko-Mensah, J., Mandell, M. A., Dupont, N., Jiang, S., et al. (2012). Autophagy Protects Against Active Tuberculosis by Suppressing Bacterial Burden and Inflammation. *Proc. Natl. Acad. Sci. U. S. A.* 109 (46), E3168–E3176. doi: 10.1073/pnas.1210500109

Chakravortty, D., and Hensel, M. (2003). Inducible Nitric Oxide Synthase and Control of Intracellular Bacterial Pathogens. *Microbes Infect.* 5 (7), 621–627. doi: 10.1016/s1286-4579(03)00096-0

Chu, X., Xu, B., Gao, H., Li, B. Y., Liu, Y., Reiter, J. L., et al. (2019). Lipopolysaccharides Improve Mesenchymal Stem Cell-Mediated Cardioprotection by MyD88 and Stat3 Signaling in a Mouse Model of Cardiac Ischemia/Reperfusion Injury. *Stem Cells Dev.* 28 (9), 620–631. doi: 10.1089/scd.2018.0213

Coulombe, F., Divangahi, M., Veyrier, F., de Leseleuc, L., Gleason, J. L., Yang, Y., et al. (2009). Increased NOD2-Mediated Recognition of N-Glycolyl Muramyl Dipeptide. *J. Exp. Med.* 206 (8), 1709–1716. doi: 10.1084/jem.20081779

Das, B., Kashino, S. S., Pulu, I., Kalita, D., Swami, V., Yeger, H., et al. (2013). CD271(+) Bone Marrow Mesenchymal Stem Cells may Provide a Niche for Dormant *Mycobacterium Tuberculosis*. *Sci. Trans. Med.* 5 (170), 170ra113. doi: 10.1126/scitranslmed.3004912

Delarosa, O., Dalemans, W., and Lombardo, E. (2012). Toll-Like Receptors as Modulators of Mesenchymal Stem Cells. *Front. Immunol.* 3, 182. doi: 10.3389/fimmu.2012.00182

Divangahi, M., Mostowy, S., Coulombe, F., Kozak, R., Guillot, L., Veyrier, F., et al. (2008). NOD2-Deficient Mice Have Impaired Resistance to *Mycobacterium Tuberculosis* Infection Through Defective Innate and Adaptive Immunity. *J. Immunol.* 181 (10), 7157–7165. doi: 10.4049/jimmunol.181.10.7157

Forget, E. J., and Menzies, D. (2006). Adverse Reactions to First-Line Antituberculosis Drugs. *Expert Opin. Drug Saf.* 5 (2), 231–249. doi: 10.1517/14740338.5.2.231

Fremond, C. M., Yeremeev, V., Nicolle, D. M., Jacobs, M., Quesniaux, V. F., and Ryffel, B. (2004). Fatal *Mycobacterium Tuberculosis* Infection Despite Adaptive Immune Response in the Absence of Myd88. *J. Clin. Invest.* 114 (12), 1790–1799. doi: 10.1172/JCI21027

Garhyan, J., Bhuyan, S., Pulu, I., Kalita, D., Das, B., and Bhatnagar, R. (2015). Preclinical and Clinical Evidence of *Mycobacterium Tuberculosis* Persistence in the Hypoxic Niche of Bone Marrow Mesenchymal Stem Cells After Therapy. *Am. J. Pathol.* 185 (7), 1924–1934. doi: 10.1016/j.ajpath.2015.03.028

Gomez, J. E., and McKinney, J. D. (2004). M. Tuberculosis Persistence, Latency, and Drug Tolerance. *Tuberculosis* 84 (1–2), 29–44. doi: 10.1016/j.tube.2003.08.003

Herbert, N., George, A., Baroness Masham of, I., Sharma, V., Oliver, M., Oxley, A., et al. (2014). World TB Day 2014: Finding the Missing 3 Million. *Lancet* 383 (9922), 1016–1018. doi: 10.1016/S0140-6736(14)60422-0

Hoebe, K., Janssen, E., and Beutler, B. (2004). The Interface Between Innate and Adaptive Immunity. *Nat. Immunol.* 5 (10), 971–974. doi: 10.1038/ni1004-971

Huang, S., Xu, L., Sun, Y., Wu, T., Wang, K., and Li, G. (2015). An improved protocol for isolation and culture of mesenchymal stem cells from mouse bone marrow. *J. Orthop. Translat.* 3 (1), 26–33. doi: 10.1016/j.jot.2014.07.005

Hwa Cho, H., Bae, Y. C., and Jung, J. S. (2006). Role of Toll-Like Receptors on Human Adipose-Derived Stromal Cells. *Stem Cells* 24 (12), 2744–2752. doi: 10.1634/stemcells.2006-0189

Jamwal, S. V., Mehrotra, P., Singh, A., Siddiqui, Z., Basu, A., and Rao, K. V. (2016). Mycobacterial Escape From Macrophage Phagosomes to the Cytoplasm Represents an Alternate Adaptation Mechanism. *Sci. Rep.* 6, 23089. doi: 10.1038/srep23089

Jankovic, D., Kullberg, M. C., Hieny, S., Caspar, P., Collazo, C. M., and Sher, A. (2002). In the Absence of IL-12, CD4(+) T Cell Responses to Intracellular Pathogens Fail to Default to a Th2 Pattern and are Host Protective in an IL-10 (-/-) Setting. *Immunity* 16 (3), 429–439. doi: 10.1016/s1074-7613(02)00278-9

Jo, E. K. (2008). Mycobacterial Interaction With Innate Receptors: TLRs, C-Type Lectins, and NLRs. *Curr. Opin. Infect. Dis.* 21 (3), 279–286. doi: 10.1097/QCO.0b013e3282f88b5d

Jo, E. K. (2010). Innate Immunity to Mycobacteria: Vitamin D and Autophagy. *Cell Microbiol.* 12 (8), 1026–1035. doi: 10.1111/j.1462-5822.2010.01491.x

Karunakaran, S., and Ravindranath, V. (2009). Activation of P38 MAPK in the Substantia Nigra Leads to Nuclear Translocation of NF-kappaB in MPTP-Treated Mice: Implication in Parkinson's Disease. *J. Neurochem* 109 (6), 1791–1799. doi: 10.1111/j.1471-4159.2009.06112.x

Kawai, T., and Akira, S. (2011). Toll-Like Receptors and Their Crosstalk With Other Innate Receptors in Infection and Immunity. *Immunity* 34 (5), 637–650. doi: 10.1016/j.immuni.2011.05.006

Khan, N., Aqdas, M., Vidyarthi, A., Negi, S., Pahari, S., Agnihotri, T., et al. (2016a). Triggering Through NOD-2 Differentiates Bone Marrow Precursors to Dendritic Cells With Potent Bactericidal Activity. *Sci. Rep.* 6, 27263. doi: 10.1038/srep27263

Khan, A., Mann, L., Papanna, R., Lyu, M. A., Singh, C. R., Olson, S., et al. (2017). Mesenchymal Stem Cells Internalize *Mycobacterium Tuberculosis* Through Scavenger Receptors and Restrict Bacterial Growth Through Autophagy. *Sci. Rep.* 7 (1), 15010. doi: 10.1038/s41598-017-15290-z

Khan, N., Pahari, S., Vidyarthi, A., Aqdas, M., and Agrewala, J. N. (2016b). NOD-2 and TLR-4 Signaling Reinforces the Efficacy of Dendritic Cells and Reduces the Dose of TB Drugs Against *Mycobacterium Tuberculosis*. *J. Innate Immun.* 8 (3), 228–242. doi: 10.1159/000439591

Khan, N., Vidyarthi, A., Pahari, S., Negi, S., Aqdas, M., Nadeem, S., et al. (2016c). Signaling Through NOD-2 and TLR-4 Bolsters the T Cell Priming Capability of Dendritic Cells by Inducing Autophagy. *Sci. Rep.* 6, 19084. doi: 10.1038/srep19084

Kim, H. S., Shin, T. H., Yang, S. R., Seo, M. S., Kim, D. J., Kang, S. K., et al. (2010). Implication of NOD1 and NOD2 for the Differentiation of Multipotent Mesenchymal Stem Cells Derived From Human Umbilical Cord Blood. *PloS One* 5 (10), e15369. doi: 10.1371/journal.pone.0015369

Kleinnijenhuis, J., Oosting, M., Joosten, L. A., Netea, M. G., and Van Crevel, R. (2011). Innate Immune Recognition of *Mycobacterium Tuberculosis*. *Clin. Dev. Immunol.* 2011, 405310. doi: 10.1155/2011/405310

Kumar, A., Farhana, A., Guidry, L., Saini, V., Hondalus, M., and Steyn, A. J. (2011). Redox Homeostasis in Mycobacteria: The Key to Tuberculosis Control? *Expert Rev. Mol. Med.* 13, e39. doi: 10.1017/S1462399411002079

Lei, J., Wang, Z., Hui, D., Yu, W., Zhou, D., Xia, W., et al. (2011). Ligation of TLR2 and TLR4 on Murine Bone Marrow-Derived Mesenchymal Stem Cells Triggers Differential Effects on Their Immunosuppressive Activity. *Cell. Immunol.* 271 (1), 147–156. doi: 10.1016/j.cellimm.2011.06.014

Mortaz, E., Adcock, I. M., Tabarsi, P., Masjedi, M. R., Mansouri, D., Velayati, A. A., et al. (2015). Interaction of Pattern Recognition Receptors With *Mycobacterium Tuberculosis*. *J. Clin. Immunol.* 35 (1), 1–10. doi: 10.1007/s10875-014-0103-7

Munro, S. A., Lewin, S. A., Smith, H. J., Engel, M. E., Fretheim, A., and Volmink, J. (2007). Patient Adherence to Tuberculosis Treatment: A Systematic Review of Qualitative Research. *PloS Med.* 4 (7), e238. doi: 10.1371/journal.pmed.0040238

Mwaba, P., Chakaya, J. M., Petersen, E., Wejse, C., Zumla, A., and Kapata, N. (2020). Advancing New Diagnostic Tests for Latent Tuberculosis Infection Due to Multidrug-Resistant Strains of *Mycobacterium Tuberculosis* - End of the Road? *Int. J. Infect. Dis.* 92S, S69–S71. doi: 10.1016/j.ijid.2020.02.011

Najar, M., Krayem, M., Meuleman, N., Bron, D., and Lagneaux, L. (2017). Mesenchymal Stromal Cells and Toll-Like Receptor Priming: A Critical Review. *Immune Netw.* 17 (2), 89–102. doi: 10.4110/in.2017.17.2.89

Needham, B. D., Carroll, S. M., Giles, D. K., Georgiou, G., Whiteley, M., and Trent, M. S. (2013). Modulating the Innate Immune Response by Combinatorial Engineering of Endotoxin. *Proc. Natl. Acad. Sci. U. S. A.* 110 (4), 1464–1469. doi: 10.1073/pnas.1218080110

Olson, C. M., Hedrick, M. N., Izadi, H., Bates, T. C., Olivera, E. R., and Anguita, J. (2007). P38 Mitogen-Activated Protein Kinase Controls NF-kappaB Transcriptional Activation and Tumor Necrosis Factor Alpha Production Through RelA Phosphorylation Mediated by Mitogen- and Stress-Activated Protein Kinase 1 in Response to Borrelia Burgdorferi Antigens. *Infect Immun.* 75 (1), 270–277. doi: 10.1128/IAI.01412-06

Pahari, S., Khan, N., Aqdas, M., Negi, S., Kaur, J., and Agrewala, J. N. (2016). Infergen Stimulated Macrophages Restrict *Mycobacterium Tuberculosis* Growth by Autophagy and Release of Nitric Oxide. *Sci. Rep.* 6, 39492. doi: 10.1038/srep39492

Pahari, S., Negi, S., Aqdas, M., Arnett, E., Schlesinger, L. S., and Agrewala, J. N. (2020). Induction of Autophagy Through CLEC4E in Combination With TLR4: An Innovative Strategy to Restrict the Survival of *Mycobacterium Tuberculosis*. *Autophagy* 16 (6), 1021–1043. doi: 10.1080/15548627.2019.1658436

Peters, W., and Ernst, J. D. (2003). Mechanisms of Cell Recruitment in the Immune Response to *Mycobacterium Tuberculosis*. *Microbes Infect.* 5 (2), 151–158. doi: 10.1016/s1286-4579(02)00082-5

Pevsner-Fischer, M., Morad, V., Cohen-Sfady, M., Rousso-Noori, L., Zanin-Zhorov, A., Cohen, S., et al. (2007). Toll-Like Receptors and Their Ligands

Control Mesenchymal Stem Cell Functions. *Blood* 109 (4), 1422–1432. doi: 10.1182/blood-2006-06-028704

Phadwal, K., Watson, A. S., and Simon, A. K. (2013). Tightrope Act: Autophagy in Stem Cell Renewal, Differentiation, Proliferation, and Aging. *Cell. Mol. Life Sci: CMLS* 70 (1), 89–103. doi: 10.1007/s00018-012-1032-3

Robert, A. W., Marcon, B. H., Dallagiovanna, B., and Shigunov, P. (2020). Adipogenesis, Osteogenesis, and Chondrogenesis of Human Mesenchymal Stem/Stromal Cells: A Comparative Transcriptome Approach. *Front. Cell Dev. Biol.* 8, 561. doi: 10.3389/fcell.2020.00561

Russell, D. G. (2013). The Evolutionary Pressures That Have Molded *Mycobacterium Tuberculosis* Into an Infectious Adjuvant. *Curr. Opin. Microbiol.* 16 (1), 78–84. doi: 10.1016/j.mib.2012.11.007

Saunders, B. M., and Britton, W. J. (2007). Life and Death in the Granuloma: Immunopathology of Tuberculosis. *Immunol. Cell Biol.* 85 (2), 103–111. doi: 10.1038/sj.icb.7100027

Sia, J. K., and Rengarajan, J. (2019). Immunology of *Mycobacterium Tuberculosis* Infections. *Microbiol. Spectr.* 7 (4), 10.1128/microbiolspec.GPP3-0022-2018. doi: 10.1128/microbiolspec.GPP3-0022-2018

Soleimani, M., and Nadri, S. (2009). A Protocol for Isolation and Culture of Mesenchymal Stem Cells From Mouse Bone Marrow. *Nat. Protoc.* 4 (1), 102–106. doi: 10.1038/nprot.2008.221

Takeda, K., and Akira, S. (2005). Toll-Like Receptors in Innate Immunity. *Int. Immunol.* 17 (1), 1–14. doi: 10.1093/intimm/dxh186

Trauner, A., Borrell, S., Reither, K., and Gagneux, S. (2014). Evolution of Drug Resistance in Tuberculosis: Recent Progress and Implications for Diagnosis and Therapy. *Drugs* 74 (10), 1063–1072. doi: 10.1007/s40265-014-0248-y

Waterman, R. S., Tomchuck, S. L., Henkle, S. L., and Betancourt, A. M. (2010). A New Mesenchymal Stem Cell (MSC) Paradigm: Polarization Into a Pro-Inflammatory MSC1 or an Immunosuppressive MSC2 Phenotype. *PloS One* 5 (4), e10088. doi: 10.1371/journal.pone.0010088

Yang, K., Wang, J., Xiang, A. P., Zhan, X., Wang, Y., Wu, M., et al. (2013). Functional RIG-I-Like Receptors Control the Survival of Mesenchymal Stem Cells. *Cell Death Dis.* 4, e967. doi: 10.1038/cddis.2013.504

Young, C., Walzl, G., and Du Plessis, N. (2020). Therapeutic Host-Directed Strategies to Improve Outcome in Tuberculosis. *Mucosal Immunol.* 13 (2), 190–204. doi: 10.1038/s41385-019-0226-5

Zhu, X., Zhao, H., Graveline, A. R., Buys, E. S., Schmidt, U., Bloch, K. D., et al. (2006). MyD88 and NOS2 Are Essential for Toll-Like Receptor 4-Mediated Survival Effect in Cardiomyocytes. *Am. J. Physiol. Heart Circ. Physiol.* 291 (4), H1900–H1909. doi: 10.1152/ajpheart.00112.2006

Zumla, A., Rao, M., Wallis, R. S., Kaufmann, S. H., Rustomjee, R., Mwaba, P., et al. (2016). Host-Directed Therapies for Infectious Diseases: Current Status, Recent Progress, and Future Prospects. *Lancet Infect. Dis.* 16 (4), e47–e63. doi: 10.1016/S1473-3099(16)00078-5

Conflict of Interest: The authors declare that the research was conducted in the absence of any commercial or financial relationships that could be construed as a potential conflict of interest.

frontiers in Cellular and Infection Microbiology

ORIGINAL RESEARCH
published: 07 July 2021
doi: 10.3389/fcimb.2021.669394

Genetics and Functional Mechanisms of STAT3 Polymorphisms in Human Tuberculosis

Feifei Wang[1,2†], Guixian Huang[1†], Ling Shen[3], Ying Peng[1], Wei Sha[1], Zheng W. Chen[3] and Hongbo Shen[1*]*

[1] Clinic and Research Center of Tuberculosis, Shanghai Key Laboratory of Tuberculosis, Shanghai Pulmonary Hospital, Institute for Advanced Study, Tongji University School of Medicine, Shanghai, China, [2] Key Laboratory of Medical Molecular Virology (MOE/NHC/CAMS), Department of Medical Microbiology and Parasitology, School of Basic Medical Sciences, Shanghai Medical College, Fudan University, Shanghai, China, [3] Department of Microbiology & Immunology and Center for Primate Biomedical Research, University of Illinois College of Medicine, Chicago, IL, United States

OPEN ACCESS

Edited by:
Natarajaseenivasan Kalimuthusamy, Bharathidasan University, India

Reviewed by:
Jianping Xie, Southwest University, China
Yu-Fan Liu, Chung Shan Medical University, Taiwan

***Correspondence:**
Hongbo Shen
hbshen@tongji.edu.cn
Wei Sha
shfksw@126.com

†These authors have contributed equally to this work

Specialty section:
This article was submitted to Bacteria and Host, a section of the journal Frontiers in Cellular and Infection Microbiology

Received: *18 February 2021*
Accepted: *14 June 2021*
Published: *07 July 2021*

Citation:
Wang F, Huang G, Shen L, Peng Y, Sha W, Chen ZW and Shen H (2021) Genetics and Functional Mechanisms of STAT3 Polymorphisms in Human Tuberculosis. Front. Cell. Infect. Microbiol. 11:669394. doi: 10.3389/fcimb.2021.669394

Signal transducer and activator of transcription-3 (STAT3) plays an important role in biological balance. Our and others previous studies implied that STAT3 had a great effect on fast-acting innate immunity against tuberculosis (TB). We hypothesized that *stat3* SNP down-regulation of STAT3 leads to a change in susceptibility to TB in humans. To test this hypothesis, we investigated STAT3 SNPs using SNP scan™ technique in a case-control study of TB patients (n = 470) and HC subjects (n = 356), and then conducted functional studies of them using cellular models. We found that SNPs in STAT3 3`-UTR of rs1053004 TT and rs1053005 AA genotypes or T-A haplotype were associated with susceptibility to TB or TB severity. While the TT/AA genotype correlated with the low constitutive expression of *stat3* and *IL-17A* in PBMC, the variant *stat3* of rs1053004-rs1053005 T-A haplotype indeed reduced *stat3* expression in reporter assays. Interestingly, host PBMC expressing the rs1053005 AA genotype and low constitutive *stat3* exhibited the reduced ability to mount fast-acting innate immunity against mycobacterial infection in cellular models. Finally, mechanistic experiments showed that the STAT3 down-regulation broadly depressed STAT3 downstream anti-mycobacterial activities involving VDR-related CAMP pathway as well as IL-32, iNOS and autophagy mechanisms, leading to an enhanced mycobacterial infection. The findings of this study suggest that low constitutive stat3 derived from the TT/AA genotype/T-A haplotype acts to down-regulate STAT3, depressing multiple anti-mycobacterial pathways/mechanisms downstream, which leads to an enhanced mycobacterial infection or TB in high-risk individuals.

Keywords: tuberculosis severity, STAT3, polymorphisms, anti-mycobacterial pathways, VDR-related pathway

INTRODUCTION

Tuberculosis (TB), caused by *Mycobacterium tuberculosis* (Mtb), is one of the top 10 causes of death worldwide and a leading killer among infectious diseases. Around 10 million people fell ill with TB, and 1.2 million died from the disease in 2018. After exposure to TB pathogen aerosol, host immune factors are decisive for a potential clinical outcome of resulting active TB, latent TB infection (LTBI) or resisters with early clearance of TB bacillus without immune signature of infection (Simmons et al., 2018).

Signal transducers and activators of transcription-3 (STAT3) are widely expressed in host cells and have been shown to play multiple and distinct biological roles in regulating immune balance (Hillmer et al., 2016). STAT3, as acute-phase response factor, displays single nucleotide polymorphisms (SNP) or aberrant expression in some selected human populations. It has been reported that STAT3 SNP were significantly associated with cancers, immunodeficiency, autoimmunity and viral hepatitis (Hong et al., 2016). SNP rs1053004 in 3'-UTR of STAT3 was associated with a reduced risk of pancreatic cancer (Zhu et al., 2016). STAT3 rs1905341 was associated with better response to IFN-α in patients with metastatic renal cell carcinoma, serving as a potential predictive marker for treatment with IFN-α (Eto et al., 2013). STAT3 SNP (rs744166) was associated with multiple sclerosis (MS), whereas the protective haplotype for MS in STAT3 is a risk allele for Crohn's disease, implying that STAT3 represents a shared risk locus for at least two autoimmune diseases (Jakkula et al., 2010). Furthermore, aberrantly expressed STAT3 was also associated with viral hepatitis. SNP rs1053004 genotype CC and the rs1053005 genotype GG were more frequent in patients with chronic hepatitis B virus (HBV) infection than in healthy controls. The rs1053004-rs1053005 haplotype T-G was less frequent in patients with chronic HBV infection than in healthy controls (Li et al., 2018). Nevertheless, the reported STAT3 SNPs have not been characterized for an altered susceptibility or immunity *via* in-depth mechanistic studies of human diseases.

Correlation between STAT3 SNP and susceptibility to TB has not been demonstrated, although STAT3 has been reported to regulate the development and function of T helper 17 (Th17) cells for anti-TB cellular immune responses (Ernst, 2018). In fact, STAT3 plays essential roles in differentiating both the adaptive CD4+ Th17 subset and the unconventional T subset such as γδ T cells (Wilson et al., 2015; Shen et al., 2017). Th17 and microbe-specific γδ T subsets appear to be required for host defense against Mtb infection (Khader et al., 2007; Shen et al., 2019). Despite the role of STAT3 in T-cell functions, STAT3 and its downstream innate pathways have not been well-defined in fast immunity and protective mechanisms in human TB and other infections. Given the broad biological roles of STAT3 (Hillmer et al., 2016), we hypothesized that STAT3 and relevant downstream pathways play an important role in fast-acting innate immunity against TB, and that *stat3* SNP down-regulation of STAT3 and downstream pathways leads to a change in susceptibility to TB in humans.

To test our hypothesis, we performed the STAT3 SNP analysis in humans and then conducted in-depth mechanistic experiments using cellular models. Our experimental studies in humans and cellular models support the hypothesis and provides previously unreported findings and potential mechanisms regarding molecular genetics and functions of STAT3 SNP in human TB.

MATERIALS AND METHODS

Human Subjects and SNP Genotypes Analysis

The study was approved by the institutional review boards for human subjects' research and institutional biosafety committees at the Shanghai Pulmonary Hospital (SPH) of Tongji University. All subjects are adults, and signed written informed consent.

TB patients were recruited at the Shanghai Pulmonary Hospital (Shanghai, China). The severe TB and mild TB patients were classified according to our previous study (Fan et al., 2017). Briefly, all active TB patients were confirmed by bacteriology or pathology. According to the chest computed tomography (CT) scan results, severe TB patients were classified with at least one large cavity of ≥3 cm in diameter or at least three cavities regardless of the diameter of cavities, mild TB patients had mild lesions in ≤2 lung fields or non-cavitary lesions in lungs. Age- and sex-matched uninfected volunteers without clinical and immunological evidence of TB or latent TB were recruited as healthy control (HC). All participants were tested for human immunodeficiency virus (HIV), hepatitis C virus (HCV) and HBV. Individuals with HIV, HCV, HBV infection and other infectious diseases or cancers were excluded.

Whole blood samples were collected from enrolled subjects and used to isolate genomic DNA using the QIAamp DNA Blood Mini kit (Qiagen, Hilden, Germany). SNP sites were selected from previous reports, by functional relevance and haplotype-tagging capacity as indicated on the hapmap website (www.hapmap.org). SNP genotypes were determined by SNP scan TM kits (Genesky Biotechnologies Inc., Shanghai, China). The collaborative genetic studies of most subjects at SPH and others were completed.

Peripheral Blood Mononuclear Cell (PBMC) Isolation and Real-Time Quantitative Polymerase Chain Reaction (q-PCR) Analysis for Gene Expression

PBMCs were isolated from ethylenediaminetetraacetic acid (EDTA)-treated blood of human subjects using Ficoll–Paque plus density gradient centrifugation and then cultured with RPMI1640 media supplemented with 2 mM glutamine, 50 U/ml of penicillin and 50 μg/ml of streptomycin, and containing 10% FBS (Invitrogen) according to our previous publications (Chen et al., 2012; Shen et al., 2017).

Total RNA was extracted from human PBMCs using RNA column enrichment procedures (Zymo Research, CA). CD14+ and Vδ2+ T cells were isolated and enriched from fresh PBMC using MACS methods (Miltenyi Biotec, German), respectively. RNA was reverse-transcribed into complementary DNA

(cDNA). The cDNA was used to amplify target gene fragment in triplicate reactions for each gene. Sequences of q-PCR primers were listed in **Table 1**. The β-actin was used as internal control gene for normalization.

Dual-Luciferase Reporter Assay

A wild-type or 3'-UTR of STAT3 fragments with haplotypes of T-A, T-G and C-G of SNP rs1053004-rs1053005 were constructed and inserted downstream of the luciferase reporter gene of the miR-RB-Report vector (Ribobio, Guangzhou, China), respectively. Lipofectamine 3000 were used to transfect the reporter plasmids into 293T cells. Dual luciferase reporter system kit (Promega, USA) was used to detect firefly and renilla luciferase activity.

Mycobacteria Strains and Culture

The *Mycobacteria bovis* Bacillus Calmette–Guerin (BCG) Danish strain (ATCC 35733) and *M. tuberculosis* H37Rv were grown at 37°C in Difco Middlebrook 7H9 broth (Becton Dickinson) or on Middlebrook 7H10 agar supplemented with 10% oleic acid-albumin-dextrose-catalase-enriched Middlebrook (OADC, BD), 0.2% glycerol and 0.05% Tween-80 for 3–4 weeks. Mycobacteria were cultured in the ABSL-II level lab of the Shanghai Pulmonary Hospital of Tongji University.

Mycobacteria Infection of Host Cells

The human alveolar epithelial cell line A549, human macrophage THP-1 and mice macrophage RAW264.7 were grown in RPMI 1640 supplemented with L-glutamine (2 mM), sodium pyruvate (1 mM) and 10% heat-inactivated fetal bovine serum (FBS).

THP-1 cells were treated with 50 ng/ml Phorbol 12-myristate 13-actate (PMA, Sigma-Aldrich) for 48 h to differentiate into macrophages, then washed with PBS and maintained for infection.

In brief, cells were infected with BCG at a multiplicity-of-infection (MOI) of 10 for ~4 h. Cells were infected with H37Rv at a MOI of 4 for 4 h. After infection, extracellular bacilli were removed by washing with PBS four times. Then, mycobacteria-infected cells were co-cultured with naive PBMC containing monocytes/macrophages, innate-like γδ T cells and other innate lymphocytes in media without antibiotics for 3 days. Then, co-cultured PBMC with the infected monocytes/macrophages and lung cells were lysed in sterile PBS with SDS. Serials dilutions were performed for quantitative culturing. Mycobacteria viability were quantified *via* counting CFU (Yang et al., 2018).

Western Blotting

Cells were transferred by lentivirus vector carrying STAT3 shRNA or empty lentivirus vector, and stimulated by Vitamin D (VD), BCG and medium overnight, respectively. Then, cells were lysed by incubation in RIPA lysis buffer on ice for 5 min. Next, lysates were separated by SDS-PAGE and transferred to a polyvinylidene difluoride membrane (Merck/Millipore). After blocking with 5% BSA, the membrane was incubated with Abs against STAT3 (Sangon Biotech), LC3 (Abcam), or GAPDH (Sangon Biotech) overnight at 4°C, followed by incubation with the respective secondary Abs.

Statistical Analysis

The allele and genotype frequencies were determined by direct counting. The demographic characteristics of the different groups were compared by chi-squared test using Statistical Package for Social Sciences (SPSS) version 21.0 software (SPSS Inc., IBM, Chicago, USA). A chi-squared test was performed to investigate the associations between allele frequencies and TB, and unconditional logistic regression analysis was used to investigate the associations between genotypes and TB assuming various genetic models (dominant, recessive and additive), respectively, in case and control groups using Plink software (http://pngu.mgh.harvard.edu/~purcell/plink/) in accordance with the Hardy–Weinberg equilibrium in the controls. False discovery rate (FDR) correction of multiple hypothesis testing was performed.

Statistical analysis was done by using GraphPad Prism software (GraphPad Software, CA). Data were analyzed by the Student *t* test (parametric method) or by the Mann–Whitney test (nonparametric method).

RESULTS

STAT3 SNP rs1053004 and rs1053005 Loci Exhibited Linkage Disequilibrium in TB Patients; rs1053004 TT and rs1053005 AA Genotypes or the T-A Haplotype Were Associated With an Increased Susceptibility to TB

It remains unknown whether genetic variations of STAT3 could influence the susceptibility or resistance to TB in humans. Some publications demonstrated that STAT3 SNPs appeared to be associated with cancers, autoimmunity or selected infections.

TABLE 1 | Primers used for qPCR.

Gene	Forward primer	Reverse primer
STAT3	5′-TTTGAGACCGAGGTGTATCACC-3′	5′-GGTCAGCATGTTGTACCACAGG-3′
SOCS3	5′-TTCTGATCCGCGACAGCTC-3′	5′-TGCAGAGAGAAGCTGCCCC-3′
IL-32	5′-ATGCACCAGGCCATAGAAAG-3′	5′-CGGCACCGTAATCCATCTC-3′
VDR	5′-CTGACCCTGGAGACTTTGAC-3′	5′-TTCCTCTGCACTTCCTCATC-3′
CAMP	5′-AGGATTGTGACTTCAAGAAGGACG-3′	5′-GTTTATTTCTCAGAGCCCAGAAGC-3′
CYP27B1	5′-ACC CGA CAC GGA GAC CTT C-3′	5′-CACAGGTGCGACAACTGGTA-3′
DEFB4A	5′-GGT GTT TTT GGT GGT ATA GGC G-3′	5′-AGG GCA AAA GAC TGG ATG ACA-3′
β-actin	5′-GCCCTGAGGCACTCTTCCA-3′	5′-TGTTGGCGTACAGGTCTTTGC-3′

However, STAT3 SNP association with TB has not been reported in humans. Here, we analyzed genetic polymorphisms of rs1053005, rs1053004, rs2293152, rs744166 using SNP scan™ technique in a case-control study of TB patients (n = 470) and HC subjects (n = 356). The genetic frequencies of four SNPs in this study were accorded with Hardy–Weinberg Equilibrium (**Table 2**), using the method previously reported (Györffy et al., 2004). Logistic regression analysis was also performed for four SNPs (**Table 3**), using the analysis models of Codominant, Dominant, Recessive and Additive superposition, as previously reported (Eto et al., 2013).

Some STAT3-SNP genotypes appeared to be more frequent in HC than in TB. Virtually, the frequency of rs2293152 genotype GG in HC subjects was significantly higher than that in TB patients compared to genotype CC/CG (**Table 3**, OR (95% CI) = 0.6586 (0.4657–0.9314), P = 0.01819), as analyzed by the Recessive model. Such statistical significance for GG versus CC/CG comparison between HC and TB was also revealed by Chi-squared distribution analysis (X2 = 5.619, P = 0.01776). In addition, the frequency of rs1053005 genotype AG/GG in HC subjects was higher than that in TB patients compared to genotype TT using both the Dominant model (**Table 3**, OR (95% CI) = 0.7426 (0.5622–0.9808), P = 0.03603) and the Chi-squared distribution (X2 = 4.404, P = 0.03585), respectively. The frequency of rs1053004 genotype TC in HC subjects was also significantly higher than that in TB patients compared to genotype TT and CC (**Table 3**, OR (95%CI) = 0.6995 (0.5113–0.957), P = 0.02542), as analyzed by the Codominant model. Furthermore, the frequency of allele CC of rs1053004 in HC control was significantly higher than that in TB patients using both the Additive model (**Table 3**, OR(95%CI) = 0.7781 (0.6286–0.9632), P = 0.0211) and the Chi-squared distribution (X2 = 5.319, P = 0.0211), respectively. Thus, the above SNP genotypes were more frequent in HC than in TB, suggesting that they were associated with healthy status, but not TB.

Interestingly, we found that two selected genotypes in the 2 STAT3-SNP loci rs1053004 and rs1053005 were associated with TB status. In fact, we found that the frequency of rs1053004 genotype TT in TB patients was significantly higher than that in HC subjects compared to genotype TC/CC, as analyzed by both the Dominant model (**Table 3**, OR (95% CI) = 0.694 (0.5175–0.9307), P = 0.01469) and the Chi-squared distribution analysis

TABLE 2 | Hardy–Weinberg equilibrium analysis.

SNPs	HWpval
rs1053005	0.3181
rs1053004	0.2529
rs2293152	0.3979
rs744166	0.8234

TABLE 3 | Logistic regression analysis results.

SNPs	Model	Genotype	Cases (n)	n%	Controls (n)	n%	OR (95%CI)	P-value
s2293152	Codominant	C/C	108	23.0%	76	21.3%	-	-
		C/G	260	55.3%	185	52.0%	0.989 (0.6978-1.402)	0.9504
		G/G	78	16.6%	84	23.6%	0.6534 (0.427-1)	0.05003
	Dominant	C/C	108	23.0%	76	21.3%	0.8842 (0.6329-1.235)	0.4706
		C/G-G/G	338	71.9%	269	75.6%		
	Recessive	C/C-C/G	368	78.3%	261	73.3%	0.6586 (0.4657-0.9314)	0.01819
		G/G	78	16.6%	84	23.6%		
	Additive	–	–		–		0.8123 (0.656-1.006)	0.05668
rs1053005	Codominant	A/A	231	49.1%	149	41.9%	-	-
		A/G	185	39.4%	160	44.9%	0.7458 (0.5551-1.002)	0.05156
		G/G	51	10.9%	45	12.6%	0.731 (0.4658-1.147)	0.173
	Dominant	A/A	231	49.1%	149	41.9%	0.7426 (0.5622-0.9808)	0.03603
		A/G-G/G	236	50.2%	205	57.6%		
	Recessive	A/A-A/G	416	88.5%	309	86.8%	0.8418 (0.5492-1.29)	0.4294
		G/G	51	10.9%	45	12.6%		
	Additive	–	–		–		0.8197 (0.6687-1.005)	0.05561
rs1053004	Codominant	T/T	194	41.3%	129	36.2%	-	-
		T/C	162	34.5%	154	43.3%	0.6995 (0.5113-0.957)	0.02542
		C/C	53	11.3%	52	14.6%	0.6777 (0.4353-1.055)	0.08499
	Dominant	T/T	194	41.3%	129	36.2%	0.694 (0.5175-0.9307)	0.01469
		T/C-C/C	215	45.7%	206	57.9%		
	Recessive	T/T-T/C	356	75.7%	283	79.5%	0.8102 (0.536-1.225)	0.3182
		C/C	53	11.3%	52	14.6%		
	Additive	–	–		–		0.7906 (0.6427-0.9725)	0.02619
rs744166	Codominant	T/T	182	38.7%	120	33.7%	-	-
		T/C	206	43.8%	181	50.8%	0.7504 (0.5532-1.018)	0.06496
		C/C	61	13.0%	47	13.2%	0.8557 (0.5485-1.335)	0.4924
	Dominant	T/T	182	38.7%	120	33.7%	0.7721 (0.5775-1.032)	0.08095
		T/C-C/C	267	56.8%	228	64.0%		
	Recessive	T/T-T/C	388	82.6%	301	84.6%	1.007 (0.6688-1.516)	0.9739
		C/C	61	13.0%	47	13.2%		
	Additive	–	–		–		0.8771 (0.7127-1.079)	0.2155

(X2 = 5.972, P = 0.01454), respectively. Moreover, rs1053005 genotype AA was significantly more frequent in TB than in HC compared to genotype AG/GG, as analyzed by the Dominant model (**Table 3**, OR (95%CI = 0.7426 (0.5622–0.9808), P = 0.03603). In contrast, none of the genotypes in the other two loci rs2293152 and rs744166 were significantly higher in TB patients than in HC, suggesting that these two STAT3-SNP loci were not associated with TB status.

To assess STAT3 SNP haplotypes for correlation with TB, we analyzed the linkage disequilibrium (**Table 4**) using the method as previously reported (Boulling et al., 2015). We found that the frequency of rs1053004–rs1053005 T-A haplotype in TB patients was significantly higher than that in HC (**Table 4**, OR 1.2989, 95%CI 1.0489–1.6086, P = 0.0165). The T-G haplotype was less frequent in TB patients compared with healthy controls (**Table 4**, OR 0.7855, 95% CI 0.6306–0.9784, P = 0.0312). Notably, the SNP rs1053004 locus is located in chromosome 17:42314074 and is close to the rs1053005 locus mapped to chromosome 17: 42313892.

Our results therefore suggest that while STAT3-SNP rs1053004 and rs1053005 loci exhibited linkage disequilibrium, rs1053004 TT and rs1053005 AA genotypes or the T-A haplotype were associated with increased susceptibility to TB.

STAT3 SNP rs1053004 TT and rs1053005 AA Genotypes Each Correlated With Severity of TB

We then examined whether the rs1053004 or rs1053005 genotype correlated with severe TB. To this end, we compared frequencies of rs1053004 and rs1053005 genotypes between patients with a mild form of TB and those with a severe form of TB. We focused on the rs1053004 TT genotype and the rs1053005 AA genotype, as these two STAT3-SNP loci each were associated with TB. Consistently, the rs1053004 TT genotype was significantly more frequent in severe TB than that in mild TB patients (**Figure 1A**). Similarly, the rs1053005 AA genotype was more frequent in severe TB than mild TB (**Figure 1B**). In contrast, the rs1053004 CT genotype and rs1053005 GG genotype were each more frequent in mild TB than in severe TB (**Figures 1A, B**). These results suggest that the rs1053004 TT and the rs1053005 AA genotypes not only were associated with susceptibility to TB but also correlated with TB severity.

The rs1053005 AA Genotype Coincided With Low Constitutive Expression of *stat3* and *IL-17A* in PBMC, and the Variant *stat3* of rs1053004–rs1053005 T-A Haplotype Indeed Reduced *stat3* Expression in Reporter Assays

Because the SNP rs1053004 and rs1053005 loci both locate in 3'-UTR of the *stat3* gene, these *stat3* variants were anticipated to influence the STAT3 gene expression. From a gene-regulation standpoint, the *stat3* RNA structure of rs1053004 TT or rs1053005 AA genotype may directly impact the *in vivo* STAT3 expression in those TB patients. To address this, we comparatively measured *stat3* expression in PBMC between the HC subjects who exhibited rs1053005 AA genotype and those who displayed AG or GG genotype. Interestingly, we found that *stat3* expression in PBMC of HC subjects carrying the AA genotype was significantly lower than that in PBMC of subjects displaying AG or GG (AG/GG) genotype ($p < 0.05$) (**Figure 2A**).

TABLE 4 | The association of haplotypes with the risk of tuberculosis.

Hap	CHR	SNPS	HAPLOTYPE	case_F	control_F	OR	95%CI	P-value
STAT3	17	rs1053004;rs1053005	TG	27 (0.033)	25 (0.038)	0.8819	0.5068-1.5345	0.6565
STAT3	17	rs1053004;rs1053005	CG	239 (0.294)	231 (0.347)	0.7855	0.6306-0.9784	0.0312
STAT3	17	rs1053004;rs1053005	TA	545 (0.671)	407 (0.611)	1.2989	1.0489-1.6086	0.0165

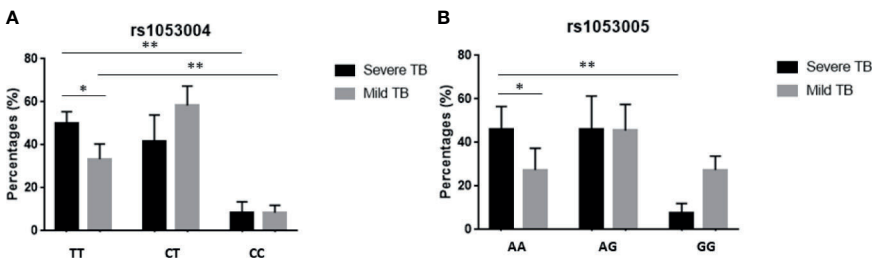

FIGURE 1 | The percentages of subjects with different genotypes in TB patients. The bars showed the percentages of subjects with genotypes TT, CT and CC of rs1053004 **(A)**, and with AA, AG and GG of rs1053005 **(B)** in mild TB and severe TB, respectively. Data from 110 mild TB patients and 130 severe TB patients. *P < 0.05 and **P < 0.01.

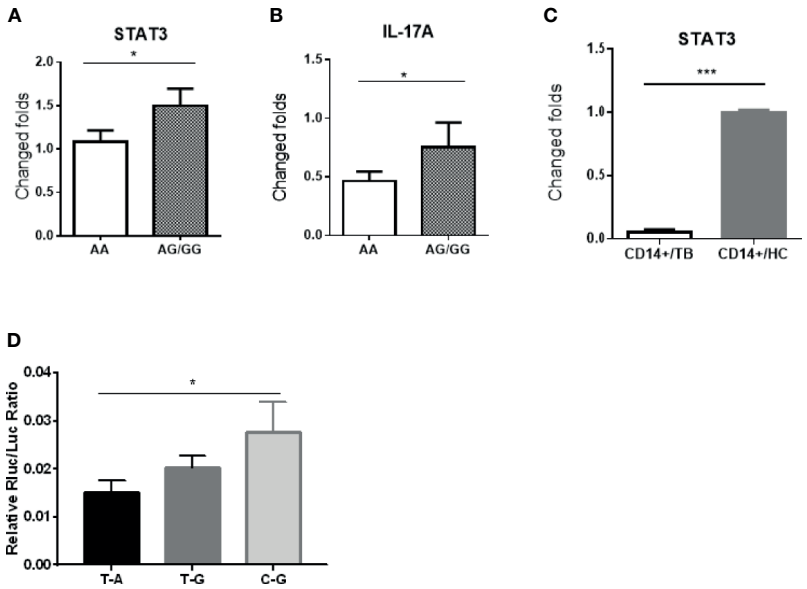

FIGURE 2 | The *stat3* rs1053005 AA genotype coincided with the reduced constitutive expression of *stat3* and *IL-17A* in PBMC, and the variant *stat3* of rs1053004–rs1053005 T-A haplotype indeed resulted in a reduced *stat3* expression in reporter assays. Shown in **(A, B)** were expression levels of *stat3* and IL-17A RNA, respectively, in PBMC of uninfected healthy control (HC) subjects expressing genotype AA (84 subjects) and AG or GG (AG/GG, 72 subjects). *Stat3* and IL-17A RNA expressions were measured by qRT-PCR using PBMC freshly isolated from HC donors, and plotted as fold changes based on *stat3* expression in genotype AA subjects. **(C)** shows comparative expression of *stat3* RNA in CD14+ cells isolated from 30 HC subjects and 40 TB patients who were associated with the AA genotype or T-A haplotype. The *stat3* expressions were measured by qRT-PCR and plotted as relative expression as described above. **(D)** shows that the variant *stat3* of rs1053004–rs1053005 T-A haplotype indeed resulted in a reduced *stat3* expression in reporter assays. A luciferase encoding gene expression system was used to determine if the variant *stat3* RNA of rs1053004–rs1053005 T-A haplotype of *stat3* 3'UTR could influence the expression of *stat3* itself. 293T cells were transformed with plasmids containing SNP rs1053004–rs1053005 haplotypes T-A, T-G and C-G, respectively, and were tested for luciferase activity. Data are means ± standard errors. *P < 0.05 and ***P < 0.001.

Surprisingly, the constitutive *IL-17A* expression in PBMC of HC subjects carrying the AA genotype was also significantly lower than that of those subjects displaying AG or GG genotype ($p < 0.05$) (**Figure 2B**). This *in vivo* finding appeared to be consistent with the scenario that STAT3 regulates IL-17A expression (Khader et al., 2007; Shen and Chen, 2018). We and others previously reported lower *stat3* expression in protective CD4+ T cells and γδ T cells in PBMC of TB patients (Shen et al., 2002; Bandaru et al., 2014). In the current study, we established that TB patients correlated with STAT3 SNP rs1053005 AA/rs1053004 TT genotypes. Thus, the correlation between low *stat3* in PBMC of HC and the rs1053005 AA genotype appeared to be in line with reduced *stat3* expression in CD4+ T and γδ T cells in PBMC of TB patients, as we and others previously published (Bandaru et al., 2014; Shen et al., 2017). To extend these findings, we examined whether TB also coincided with altered *stat3* expression in Mtb-targeted cells, CD14+ monocytes/macrophages in PBMC. We found that CD14+ monocytes/macrophages isolated from TB patients, who were associated with the AA/TT genotypes, expressed only ~10% of the *stat3* level as seen in HC (**Figure 2C**). The findings suggest that TB-associated STAT3 SNP AA genotype correlated with a reduced *stat3* expression in PBMC containing CD14+ monocytes/macrophages, CD4+ T and γδ T cells.

We then sought to test the hypothesis that *stat3* RNA structure derived from SNP genotype/haplotype at 3'-UTR ultimately leads to a reduced *stat3* expression. We already showed that the SNP rs1053004 TT and rs1053005 AA genotypes were in linkage disequilibrium, and that rs1053004/rs1053005 TT/AA genotypes and/or T-A haplotype were associated with TB. We therefore took advantage of these findings to examine whether variant *stat3* RNA structure derived from rs1053004–rs1053005 T-A haplotype led to a decreased expression of *stat3* itself. To this end, we exploited the double-luciferase reporter STAT3 expression system, as recently described (Wang et al., 2019). We constructed the STAT3 expression system by transfecting cells with expression plasmids recombined with the *stat3* 3'-UTR variants of rs1053004–rs1053005 T-A, T-G and C-G haplotypes, respectively. We then measured the luciferase activities of these transfected cells. The results showed that 293T cells transfected with the reporter plasmid carrying the T-A haplotype exhibited significantly lower relative luciferase activities than those with the C-G haplotype (**Figure 2D**), suggesting that *stat3* rs1053004–rs1053005 T-A haplotype in 3'-UTR could reduce the *stat3* gene expression.

Together, our results suggest that the TB-associated rs1053005 AA genotype coincided with the reduced expression

of *stat3* and *IL-17A* in PBMC, and the rs1053004–rs1053005 T-A haplotype at 3'-UTR indeed resulted in a reduced *stat3* expression due to the variant *stat3* RNA structure in the reporter expression system.

Host PBMC Expressing rs1053005 AA Genotype and Low Constitutive *stat3* Exhibited the Reduced Ability to Mount Fast-Acting Innate Immunity Against Mycobacterial Infection in Cellular Model

We already established that HC subjects carrying SNP rs1053005 AA genotype coincided with the reduced constitutive *stat3/IL-17A* expression and that the rs1053004–rs1053005 T-A haplotype indeed resulted in a reduced *stat3* expression due to the variant *stat3* RNA structure. To facilitate explanation of *stat3* SNP-associated susceptibility to TB/TB severity, we determined whether humans carrying rs1053005 AA genotype and reduced *stat3* expression exhibited a reduced ability to mount fast-acting innate immunity against TB infection. For proof-of-concept, we transiently co-cultured both the isolated PBMC and the BCG-infected A549 cells as a fast-acting innate immunity model and tested the ability of innate PBMC to limit/control intracellular mycobacterial infection from infected A549 lung cells. Use of BCG-infected cells, instead of direct Mtb exposure to PBMC, would optimize better control of individual variations of BCG uptake. Thus, PBMC containing monocytes/macrophages and γδ T cells (representative of innate-like cell populations) were isolated from uninfected HC who expressed the *stat3* rs1053005 AA, AG and GG genotypes, respectively. The isolated PBMC were then co-cultured for 3 days with BCG-infected A549 lung-epithelial cells, and then assessed for CFU counts in lysate of co-cultured cells. The use of BCG, not Mtb, for transient intracellular infection of lung cells/monocytes was justified, because published studies demonstrated that BCG was similar to Mtb in transient short-term (3-day) infection or replication in monocytes/macrophages (Worku and Hoft, 2000; Yang et al., 2019). Such 3-day infection of A549 and monocytes/macrophages (acquired from A549) in co-culture allowed us to evaluate fast-acting innate immunity components including macrophage antimicrobial activities and γδ T-mediated anti-mycobacterial immunity in the cellular model.

Surprisingly, BCG CFU counts in co-cultures from PBMC of uninfected HC expressing the *stat3* SNP AA genotype and low *stat3* were significantly higher than those displaying the AG or GG (AG/GG) genotype (**Figure 3**). Given the innate PBMC inhibition of mycobacteria in A549 cells and in monocytes/macrophages spread from infected A549 cells, we interpreted growth inhibition as fast-acting innate anti-mycobacterial immunity in cellular models. The results in our innate immunity model implied that the AA genotype/low STAT3 reduced the ability of innate populations in PBMC to mount fast-acting cellular immunity against intracellular mycobacterial infection.

Results from these in-depth mechanistic experiments support our hypothesis that *stat3* SNP AA genotypes and the low constitutive *stat3* expression reduce the ability of host innate cell populations to mount fast-acting immune defense against mycobacterial infection.

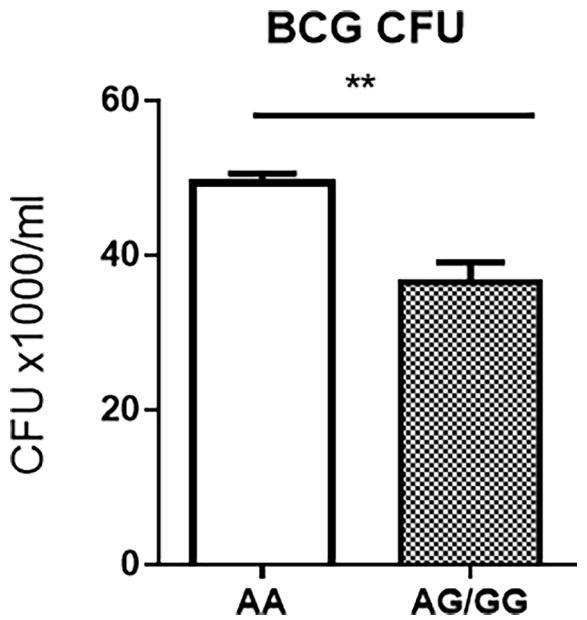

FIGURE 3 | Host PBMC expressing the rs1053005 AA genotype and low constitutive *stat3* exhibited the reduced ability to mount fast-acting innate immunity against mycobacterial infection in cellular models. The graph shows that mean BCG CFU counts in co-cultures of BCG-infected A549 cells and PBMC isolated from uninfected HC expressing the *stat3* SNP AA genotype and low *stat3* were significantly higher than those displaying the AG (25 subjects) or GG (AG/GG, 42 subjects) genotype. The isolated PBMC were co-cultured for 3 days with BCG-infected A549 cells (6 h of MOI = 10) at the 10:1 ratio of PBMC: A549, and then the lysates of the co-cultures were assessed for BCG CFU counts. The co-culture system allowed us to minimize BCG-uptake/infection variations among tested individuals and to assess fast-acting innate immunity against mycobacterial infection in cellular models (see *Results/Discussion*). Data are means ± standard errors. **$P < 0.01$.

STAT3 Down-Regulation Depressed Diverse Antimicrobial Activities Involving VDR-Related CYP27B1, DEFB4A and CAMP Pathways as Well as IL-32, iNOS and Autophagy Mechanisms, and Led to an Enhanced Mycobacterial Infection

Finally, we conducted additional in-depth mechanistic experiments to examine mechanisms whereby variant *stat3* RNA structure derived from SNP AA genotype at 3'-UTR, low constitutive *stat3* expression can depress STAT3-downstream pathways of fast-acting innate immunity against mycobacterial infection. Our above experiments already demonstrated that *stat3* SNP AA genotypes and the low constitutive *stat3* expression reduce the ability of host innate cell populations to mount fast-acting immune defense against mycobacterial infection.

Based on these results, we determined if down-regulation of STAT3 perturbed potential STAT3 downstream pathways of

antimicrobial responses in target cells, promoting mycobacterial infection. It has been well known that one STAT3 downstream pathway activates Th17/Th22 differentiation in anti-TB immune responses of T cells (Wang et al., 2013). However, it remains unknown what other undefined STAT3 downstream pathways can also involve antimicrobial activity or fast-acting innate-like immunity against mycobacterial infection (Queval et al., 2016; Arcos et al., 2017). Given the possibility that Vitamin D receptor (VDR)-related CYP27B1, DEFB4A and CAMP pathways involve not only macrophages but also innate-like γδ T cells or others, we tested the hypothesis that low STAT3 broadly inhibit CYP27B1, DEFB4A and CAMP pathways, leading to an enhanced mycobacterial infection.

To knock-down or silence STAT3 expression, we transduced cells with lentivirus expressing shRNA of *stat3* gene (shSTAT3). This would provide an alternative approach to circumvent the unavailability of *stat3* knockout mice due to the crucial role of STAT3 in embryogenesis (Takeda et al., 1997a). Our shSTAT3 approach reproducibly silenced or knocked-down *stat3* expression by ~80% compared to the control (**Figure 4A**), and consistently decreased STAT3 protein production in shSTAT3-transduced cells as shown in western blot assay (**Figure 4D**). These results demonstrated that shSTAT3 could successfully knock down or silence STAT3 expression.

Using this shSTAT3 approach, we first demonstrated that silencing STAT3 reduced the vitamin D (VD)-mediated inhibition of intracellular BCG growth in the transduced cells compared to the control (**Figure 4B**). Then, we sought to determine if silencing STAT3 by shSTAT3 could reduce IL-32 expression altering innate antimicrobial response. To date, it remains unknown whether STAT3 can activate the IL-32 pathway (Pham et al., 2019), although IL-32 was reported to mediate IFN-γ- and VD-driven antimicrobial activity (Montoya et al., 2014) and induce expression of iNOS for NO inhibition of intracellular mycobacteria (Zhou and Zhu, 2015). We found that silencing STAT3 by shSTAT3 led to ~75% reduction of IL-32 expression compared to the control (**Figure 4C**), suggesting that STAT3 signaling can indeed activate IL-32 expression. Because IL-32 signaling can activate VD and NO antimicrobial pathways, we determined whether silencing STAT3 caused changes in key genes involving these two pathways. We found that silencing STAT3 by shSTAT3 significantly decreased the expressions of VDR, CAMP, and iNOs compared to the control during BCG infection (**Figure 4C**). These results indicate that reduction in

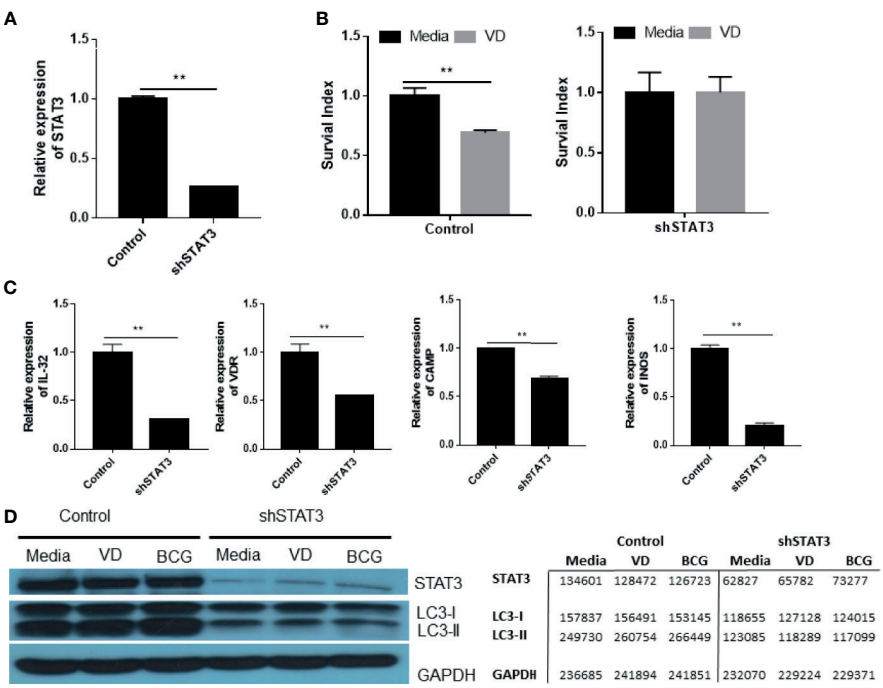

	Control			shSTAT3		
	Media	VD	BCG	Media	VD	BCG
STAT3	134601	128472	126723	62827	65782	73277
LC3-I	157837	156491	153145	118655	127128	124015
LC3-II	249730	260754	266449	123085	118289	117099
GAPDH	236685	241894	241851	232070	229224	229371

FIGURE 4 | STAT3 down-regulation depressed diverse antimicrobial activities involving VDR-related CYP27B1, DEFB4A and CAMP pathways as well as IL-32, iNOS and autophagy mechanisms, and led to an enhanced mycobacterial infection. **(A)** shows STAT3 down-regulation in A549 cells after transfection with the plasmid encoding STAT3 shRNA. **(B)** shows that the Vitamin D (VD) treatment of BCG-infected A549 cells transfected with plasmid control mediated inhibition of BCG growth (left panel), whereas STAT3 down-regulation in A549 cells transfected with the shRNA reduced the VD-mediated inhibition of BCG infection (right panel). Shown was the percentage growth index representing intracellular bacteria survival calculated as follows: Growth Index = 100 × CFU of treatment/CFU of media. **(C)** shows that STAT3 down-regulation by the shRNA transfection into A549 decreased expressions of gene encoding IL-32, VDR, CAMP, and iNOS during BCG infection, compared with controls. **(D)** shows representative results in Western blot (WB) indicating that STAT3 down-regulation by the shRNA indeed reduced protein expressions of STAT3, IC3 I and II in the settings of media control, VD treatment and BCG infection, respectively. The values of band densities in WB figure were measured by ImageJ software and shown in right. Data are means ± standard errors. **P < 0.001.

STAT3 expression could depress IL-32-driven VD and NO antimicrobial pathways.

Furthermore, we determined whether silencing STAT3 could impact autophagy pathway. The ability of STAT3 to regulate autophagy has not been reported (Upadhyay et al., 2018), although autophagy acts as an important part to eliminate intracellular microorganisms by lysosomal degradation (You et al., 2015). Here we examined whether the shSTAT3-induced silencing of STAT3 could decrease the expression of LC-3II, an essential processed form of autophagy response against microbes. We found that silencing STAT3 by shRNA remarkably decreased the production of LC-3II protein even in the VD stimulation or BCG infection (**Figure 4D**). In fact, the LC-3II protein was less abundant than LC-3I (**Figure 4D**), suggesting that reduced expression of STAT3 indeed suppresses autophagy response in the presence of VD or BCG stimulation.

Thus, our results and in-depth mechanistic studies demonstrated that STAT3 down-regulation depressed diverse antimicrobial activities involving VDR-related CYP27B1, DEFB4A and CAMP pathways as well as IL-32, iNOS and autophagy mechanisms, leading to an enhanced mycobacterial infection.

DISCUSSION

STAT3 is an important transcriptional factor involved in a broad spectrum of biological functions (Li et al., 2014). Since germline deletion of STAT3 in mice results in an early embryonic lethality (Takeda et al., 1997), Cre-loxP recombination system to ablate the mouse STAT3 gene in later life emerged as a complex/unpractical tool to assess STAT3 for biological roles. However, in the setting of human diseases, STAT3 SNP analysis appears to be important and practical for studies of cancers and virus infections/diseases (Eto et al., 2013; Xie et al., 2013; Moazeni-Roodi and Hashemi, 2018; Lai et al., 2019). In the current study, we employed a combination of STAT3 SNP analysis and mechanistic experiments in humans and cellular models, because the identified STAT3 SNP and relevant functions can be evaluated and characterized in cellular models with gene-targeted manipulations including short-term STAT3 knock-down (Shen et al., 2017; Shen and Chen, 2018).

STAT3 SNP TT/AA genotypes and T-A haplotype appear to be a genetic risk factor predisposing humans to TB and TB severity. Our large-scale case-control studies of STAT3 SNP demonstrated that rs1053004 TT and rs1053005 AA genotypes or T-A haplotype were associated with an increased susceptibility to TB and severe TB. Similarly, other studies have shown that rs1053004–rs1053005 T-A haplotype were also associated with higher HBV DNA levels (Li et al., 2018). Given the diverse biological functions of STAT3 (Bharadwaj et al., 2020), further STAT3 SNP studies in other human infections may uncover that rs1053004 TT and rs1053005 AA genotypes or T-A haplotype could be a broad risk factor susceptible to diseases after infection.

Our data in humans and cellular models implicated that the STAT3 SNP AA genotype and T-A haplotype in 3'-UTR indeed reduced *stat3* RNA expression. In fact, rs1053005 AA genotype correlated with the reduced constitutive expression of STAT3 in PBMC of HC. And the AA genotype/T-A haplotype coincided with a reduced STAT3 expression in CD14+ monocytes/macrophages in PBMC from TB patients who significantly associated with the AA allele and T-A haplotype. These results were consistent with the reduced STAT3 expression in CD4+ T cells and γδ T cells of TB patients, as published by us and another group. Notably, our mechanistic experiments confirmed that the variant *stat3* RNA derived from rs1053004–rs1053005 T-A haplotype indeed reduced *stat3* expression perhaps due to the variant structure itself in the reporter gene-expression system. Our extensive findings are in line of the other report demonstrating that cancer patients with STAT3 SNP rs1053004 TT genotype expressed lower STAT3 protein as detected by Western blotting when compared to those with CC genotype (Lai et al., 2019).

Our in-depth mechanistic experiments also demonstrated for the first time that TB-associated STAT3 SNP AA genotype and low constitutive STAT3 led to a reduced ability of innate PBMC to control mycobacterial infection spread from BCG-infected lung cells in the cellular model. In general, the mycobacterial growth inhibition that we detected here in naïve PBMC from uninfected subjects mainly involved anti-mycobacterial activities of monocytes/macrophages and innate-like γδ T cells or other innate lymphocytes, because adaptive CD4+/CD8+ T cells in PBMC usually require *in vivo* priming or prior *in vitro* stimulation by antibodies or others in the purification process in the mycobacterial growth inhibition assay (Shen et al., 2017; Yang et al., 2019). Notably, because of huge labors for mycobacterial inhibition assays, we were unable to purify macrophages, γδ T cells and others, respectively, in our large-scale studies. We therefore used naïve PBMC isolated from subjects to detect anti-mycobacterial function of monocytes or representative innate-like γδ T cells. Based on the innate PBMC inhibition of mycobacterium BCG in A549 cells and in monocytes/macrophages spread from infected A549 cells, we interpreted the growth inhibition as fast-acting innate anti-mycobacterial immunity in cellular models. Recently, PBMC or whole blood has been widely employed in mycobacterial inhibition assays for human TB studies (Cheon et al., 2002; Lee et al., 2019). In fact, we found that the assay of PBMC co-culturing with BCG-infected A549 cells was practically achievable and reproducible.

To date, in-depth human studies have not been done to determine whether *stat3* SNP and STAT3 down-regulation can influence downstream innate immunity pathways or reduce host immunity against human TB. Our findings in the current study implicate that *stat3* SNP TT/AA genotypes or T-A haplotype to reduce STAT3 expression or signaling. We also demonstrated for the first time that such STAT3 down-regulation can depress downstream multiple anti-mycobacterial pathways of VDR-related CAMP pathway as well as IL-32, iNOS and autophagy mechanisms. It is likely that the *stat3* SNP and STAT3 down-regulation reduce both the ability of macrophages to exert the antimicrobial phagosome/NO killing and the capability of

innate-like T cells/lymphocytes to mount the anti-mycobacterial immunity. Consequently, such reduced innate/innate-like immunity would compromise the development of adaptive immune response, leading to an enhanced mycobacterial infection or progression to TB. Thus, these complex interactions postulate consequences as follows: STAT3 SNP–STAT3 downregulation–downstream multiple anti-mycobacterial pathways–an enhanced mycobacterial infection (Verway et al., 2013; Kim et al., 2018).

In summary, our experimental studies in humans and cellular models provided previously unreported findings and functional mechanisms as follows: (i) *stat3* SNP rs1053004 TT and rs1053005 AA genotypes or T-A haplotype were associated with susceptibility to TB or TB severity; (ii) the rs1053005 AA genotype coincided with the reduced constitutive expression of *stat3* and *IL-17A* in PBMC, and the variant *stat3* of rs1053004–rs1053005 T-A haplotype indeed resulted in a reduced *stat3* expression in reporter assays; (iii) host PBMC expressing the rs1053005 AA genotype and low constitutive *stat3* exhibited the reduced ability to mount fast-acting innate immunity against mycobacterial infection in cellular models; (iv) the STAT3 down-regulation broadly depressed STAT3 downstream anti-mycobacterial activities involving VDR-related CAMP pathway as well as IL-32, iNOS and autophagy mechanisms, leading to an enhanced mycobacterial infection. Thus, the current study helps to establish the hypothetical regulatory axis of STAT3 SNP–STAT3 downregulation–downstream multiple anti-mycobacterial pathways in enhanced mycobacterial infection. Together, our findings suggest that low constitutive *stat3* derived from the AA genotype or T-A haplotype to down-regulate STAT3, then depress downstream multiple anti-mycobacterial pathways/mechanisms, and then lead to an enhanced mycobacterial infection or TB.

DATA AVAILABILITY STATEMENT

The original contributions presented in the study are included in the article/supplementary material. Further inquiries can be directed to the corresponding authors.

ETHICS STATEMENT

The studies involving human participants were reviewed and approved by the Shanghai Pulmonary Hospital. The patients/participants provided their written informed consent to participate in this study.

AUTHOR CONTRIBUTIONS

FW, ZC, and HS conceptualized the study and conceived the project. FW, GH, and WS contributed with study design, sample processing and data analysis. LS contributed with data analysis. YP helped with sample processing. WS contributed with the recruitment of the participants and sample collection. ZC and HS wrote the paper with input from all other authors. All authors contributed to the article and approved the submitted version.

FUNDING

This work was supported by the Chinese National Major Projects Grants [2018ZX10731301-006-001 to HS], National Natural Science Foundation of China Grants [81401711 to FW, 31970876 and 32070943 to HS], Shanghai National Natural Science Foundation of Grant [20ZR1406200 to FW], Medical Research Plan of Fudan University [DGF501022/028/002 to FW], and Clinical Research Plan of SHDC [16CR1028B to WS].

REFERENCES

Arcos, J., Sasindran, S. J., Moliva, J. I., Scordo, J. M., Sidiki, S., Guo, H., et al. (2017). Mycobacterium Tuberculosis Cell Wall Released Fragments by the Action of the Human Lung Mucosa Modulate Macrophages to Control Infection in an IL-10-Dependent Manner. *Mucosal Immunol.* 10, 1248–1258. doi: 10.1038/mi.2016.115

Bandaru, A., Devalraju, K. P., Paidipally, P., Dhiman, R., Venkatasubramanian, S., Barnes, P. F., et al. (2014). Phosphorylated STAT3 and PD-1 Regulate IL-17 Production and IL-23 Receptor Expression in Mycobacterium Tuberculosis Infection. *Eur. J. Immunol.* 44, 2013–24. doi: 10.1002/eji.201343680

Bharadwaj, U., Kasembeli, M. M., Robinson, P., and Tweardy, D. J. (2020). Targeting Janus Kinases and Signal Transducer and Activator of Transcription 3 to Treat Inflammation, Fibrosis, and Cancer: Rationale, Progress, and Caution. *Pharmacol. Rev.* 72, 486–526. doi: 10.1124/pr.119.018440

Boulling, A., Sato, M., Masson, E., Génin, E., Chen, J.-M., and Férec, C. (2015). Identification of a Functional PRSS1 Promoter Variant in Linkage Disequilibrium With the Chronic Pancreatitis-Protecting Rs10273639. *Gut* 64, 1837–1838. doi: 10.1136/gutjnl-2015-310254

Chen, C. Y., Huang, D., Yao, S., Halliday, L., Zeng, G., Wang, R. C., et al. (2012). IL-2 Simultaneously Expands Foxp3+ T Regulatory and T Effector Cells and Confers Resistance to Severe Tuberculosis (TB): Implicative Treg-T Effevtor Cooperation in Immunity to TB. *J. Immunol.* 199, 4278–4288. doi: 10.4049/jimmunol.1101291

Cheon, S.-H., Kampmann, B., Hise, A. G., Phillips, M., Song, H.-Y., Landen, K., et al. (2002). Bactericidal Activity in Whole Blood as a Potential Surrogate Marker of Immunity After Vaccination Against Tuberculosis. *Clin. Diagn. Lab. Immunol.* 9, 901–907. doi: 10.1128/CDLI.9.4.901-907.2002

Ernst, J. D. (2018). Mechanisms of M. Tuberculosis Immune Evasion as Challenges to TB Vaccine Design. *Cell Host Microbe* 24, 34–42. doi: 10.1016/j.chom.2018.06.004

Eto, M., Kamba, T., Miyake, H., Fujisawa, M., Kamai, T., Uemura, H., et al. (2013). STAT3 Polymorphism can Predict the Response to Interferon-α Therapy in Patients With Metastatic Renal Cell Carcinoma. *Eur. Urol* 63, 745–752. doi: 10.1016/j.eururo.2012.09.052

Fan, L., Shen, H., Huang, H., Yang, R., and Yao, L. (2017). Impairment of Wnt/β-Catenin Signaling in Blood Cells of Patients With Severe Cavitary Pulmonary Tuberculosis. *PloS One* 12, e0172549. doi: 10.1371/journal.pone.0172549

Györffy, B., Kocsis, I., and Vásárhelyi, B. (2004). Biallelic Genotype Distributions in Papers Published in Gut Between 1998 and 2003: Altered Conclusions After Recalculating the Hardy-Weinberg Equilibrium. *Gut* 53, 614–615. doi: 10.1136/gut.2003.31856

Hillmer, E. J., Zhang, H., Li, H. S., and Watowich, S. S. (2016). STAT3 Signaling in Immunity. *Cytokine Growth Factor Rev.* 31, 1–15. doi: 10.1016/j.cytogfr.2016.05.001

Hong, S. N., Park, C., Park, S. J., Lee, C. K., Ye, B. D., Kim, Y. S., et al. (2016). Deep Resequencing of 131 Crohn's Disease Associated Genes in Pooled DNA Confirmed Three Reported Variants and Identified Eight Novel Variants. *Gut* 65, 788–796. doi: 10.1136/gutjnl-2014-308617

Jakkula, E., Leppä, V., Sulonen, A.-M., Varilo, T., Kallio, S., Kemppinen, A., et al. (2010). Genome-Wide Association Study in a High-Risk Isolate for Multiple Sclerosis Reveals Associated Variants in STAT3 Gene. *Am. J. Hum. Genet.* 86, 285–291. doi: 10.1016/j.ajhg.2010.01.017

Khader, S. A., Bell, G. K., Pearl, J. E., Fountain, J. J., Rangel-Moreno, J., Cilley, G. E., et al. (2007). IL-23 and IL-17 in the Establishment of Protective Pulmonary CD4+ T Cell Responses After Vaccination and During Mycobacterium Tuberculosis Challenge. *Nat. Immunol.* 8, 369–377. doi: 10.1038/ni1449

Kim, E. W., Teles, R. M. B., Haile, S., Liu, P. T., and Modlin, R. L. (2018). Vitamin D Status Contributes to the Antimicrobial Activity of Macrophages Against Mycobacterium Leprae. *PloS Negl. Trop. Dis.* 12, e0006608. doi: 10.1371/journal.pntd.0006608

Lai, H., Xu, G., Meng, H., and Zhu, H. (2019). Association of SP1 Rs1353058818 and STAT3 Rs1053004 Gene Polymorphisms With Human Tongue Squamous Cell Carcinoma. *Biosci. Rep.* 39, BSR20190955. doi: 10.1042/BSR20190955

Lee, H., Kim, J., Kang, Y. A., Kim, D. R., Sim, B., Zelmer, A., et al. (2019). In Vitro Mycobacterial Growth Inhibition in South Korean Adults With Latent TB Infection. *Front. Immunol.* 10, 896. doi: 10.3389/fimmu.2019.00896

Li, M., Li, F., Li, N., Sang, J., Fan, X., Deng, H., et al. (2018). Association of Polymorphism Rs1053005 in STAT3 With Chronic Hepatitis B Virus Infection in Han Chinese Population. *BMC Med. Genet.* 19, 1–8. doi: 10.1186/s12881-018-0569-x

Li, P., Spolski, R., Liao, W., and Leonard, W. J. (2014). Complex Interactions of Transcription Factors in Mediating Cytokine Biology in T Cells. *Immunol. Rev.* 261, 141–156. doi: 10.1111/imr.12199

Moazeni-Roodi, A., and Hashemi, M. (2018). Association Between STAT3 Rs1053004 Polymorphism and Cancer Risk: A Meta-Analysis. *Mol. Biol. Res. Commun.* 7, 119–124. doi: 10.22099/mbrc.2018.29688.1323

Montoya, D., Inkeles, M. S., Liu, P. T., Realegeno, S., Teles, R. M. B., Vaidya, P., et al. (2014). IL-32 is a Molecular Marker of a Host Defense Network in Human Tuberculosis. *Sci. Transl. Med.* 6, 250ra114. doi: 10.1126/scitranslmed.3009546

Pham, T.-H., Bak, Y., Oh, J.-W., Hong, J., Lee, S., Hong, J. T., et al. (2019). Inhibition of IL-13 and IL-13Rα2 Expression by IL-32θ in Human Monocytic Cells Requires PKCδ and STAT3 Association. *Int. J. Mol. Sci.* 20, E1949. doi: 10.3390/ijms20081949

Queval, C. J., Song, O.-R., Deboosère, N., Delorme, V., Debrie, A.-S., Iantomasi, R., et al. (2016). STAT3 Represses Nitric Oxide Synthesis in Human Macrophages Upon Mycobacterium Tuberculosis Infection. *Sci. Rep.* 6, 29297. doi: 10.1038/srep29297

Shen, H., and Chen, Z. W. (2018). The Crucial Roles of Th17-Related Cytokines/Signal Pathways in M. Tuberculosis Infection. *Cell Mol. Immunol.* 15, 216–225. doi: 10.1038/cmi.2017.128

Shen, L., Frencher, J., Huang, D., Wang, W., Yang, E., Chen, C. Y., et al. (2019). Immunization of Vγ2Vδ2 T Cells Programs Sustained Effector Memory Responses That Control Tuberculosis in Nonhuman Primates. *Proc. Natl. Acad. Sci. U. S. A.* 116, 6371–6378. doi: 10.1073/pnas.1811380116

Shen, H., Gu, J., Xiao, H., Liang, S., Yang, E., Yang, R., et al. (2017). Selective Destruction of Interleukin 23-Induced Expansion of a Major Antigen-Specific γδ T-Cell Subset in Patients With Tuberculosis. *J. Infect. Dis.* 215, 420–430. doi: 10.1093/infdis/jiw511

Shen, Y., Zhou, D., Qiu, L., Lai, X., Simon, M., Shen, L., et al. (2002). Adaptive Immune Response of Vγ2vδ2+ T Cells During Mycobacterial Infections. *Science* 295, 2255–2258. doi: 10.1126/science.1068819

Simmons, J. D., Stein, C. M., Seshadri, C., Campo, M., Alter, G., Fortune, S., et al. (2018). Immunological Mechanisms of Human Resistance to Persistent Mycobacterium Tuberculosis Infection. *Nat. Rev. Immunol.* 18, 575–589. doi: 10.1038/s41577-018-0025-3

Takeda, K., Noguchi, K., Shi, W., Tanaka, T., Matsumoto, M., Yoshida, N., et al. (1997). Targeted Disruption of the Mouse Stat3 Gene Leads to Early Embryonic Lethality. *Proc. Natl. Acad. Sci. U. S. A.* 94, 3801–3804. doi: 10.1073/pnas.94.8.3801

Upadhyay, R., Sanchez-Hidalgo, A., Wilusz, C. J., Lenaerts, A. J., Arab, J., Yeh, J., et al. (2018). Host Directed Therapy for Chronic Tuberculosis *via* Intrapulmonary Delivery of Aerosolized Peptide Inhibitors Targeting the IL-10-STAT3 Pathway. *Sci. Rep.* 8, 16610. doi: 10.1038/s41598-018-35023-0

Verway, M., Bouttier, M., Wang, T.-T., Carrier, M., Calderon, M., An, B.-S., et al. (2013). Vitamin D Induces Interleukin-1β Expression: Paracrine Macrophage Epithelial Signaling Controls M. Tuberculosis Infection. *PloS Pathog.* 9, e1003407. doi: 10.1371/journal.ppat.1003407

Wang, K., Grivennikov, S. I., and Karin, M. (2013). Implications of Anti-Cytokine Therapy in Colorectal Cancer and Autoimmune Diseases. *Ann. Rheum Dis.* 72, ii100–ii103. doi: 10.1136/annrheumdis-2012-202201

Wang, S., Zhang, Y., Cai, Q., Ma, M., Jin, L. Y., Weng, M., et al. (2019). Circular RNA FOXP1 Promotes Tumor Progression and Warburg Effect in Gallbladder Cancer by Regulating PKLR Expression. *Mol. Cancer* 18, 145. doi: 10.1186/s12943-019-1078-z

Wilson, R. P., Ives, M. L., Rao, G., Lau, A., Payne, K., Kobayashi, M., et al. (2015). STAT3 is a Critical Cell-Intrinsic Regulator of Human Unconventional T Cell Numbers and Function. *J. Exp. Med.* 212, 855–864. doi: 10.1084/jem.20141992

Worku, S., and Hoft, D. F. (2000). *In Vitro* Measurement of Protective Mycobacterial Immunity: Antigen-Specific Expansion of T Cells Capable of Inhibiting Intracellular Growth of Bacille Calmette-Guérin. *Clin. Infect. Dis.* 30, S257–S261. doi: 10.1086/313887

Xie, J., Zhang, Y., Zhang, Q., Han, Y., Yin, J., Pu, R., et al. (2013). Interaction of Signal Transducer and Activator of Transcription 3 Polymorphisms With Hepatitis B Virus Mutations in Hepatocellular Carcinoma. *Hepatology* 57, 2369–2377. doi: 10.1002/hep.26303

Yang, R., Yang, E., Shen, L., Modlin, R. L., Shen, H., and Chen, Z. W. (2018). IL-12+ IL-18 Cosignaling in Human Macrophages and Lung Epithelial Cells Activates Cathelicidin and Autophagy, Inhibiting Intracellular Mycobacterial Growth. *J. Immunol.* 200, 2405–2417. doi: 10.4049/jimmunol.1701073

Yang, R., Yao, L., Shen, L., Sha, W., Modlin, R. L., Shen, H., et al. (2019). IL-12 Expands and Differentiates Human Vγ2vδ2 T Effector Cells Producing Antimicrobial Cytokines and Inhibiting Intracellular Mycobacterial Growth. *Front. Immunol.* 10, 913. doi: 10.3389/fimmu.2019.00913

You, L., Wang, Z., Li, H., Shou, J., Jing, Z., Xie, J., et al. (2015). The Role of STAT3 in Autophagy. *Autophagy* 11, 729–739. doi: 10.1080/15548627.2015.1017192

Zhou, Y., and Zhu, Y. (2015). Important Role of the IL-32 Inflammatory Network in the Host Response Against Viral Infection. *Viruses* 7, 3116–3129. doi: 10.3390/v7062762

Zhu, B., Zhu, Y., Lou, J., Ke, J., Zhang, Y., Li, J., et al. (2016). A Single Nucleotide Polymorphism in the 3'-UTR of STAT3 Regulates its Expression and Reduces Risk of Pancreatic Cancer in a Chinese Population. *Oncotarget* 7, 62305–62311. doi: 10.18632/oncotarget.11607

Conflict of Interest: The authors declare that the research was conducted in the absence of any commercial or financial relationships that could be construed as a potential conflict of interest.

frontiers in Cellular and Infection Microbiology

ORIGINAL RESEARCH
published: 09 July 2021
doi: 10.3389/fcimb.2021.669623

Plasma LOX-Products and Monocyte Signaling Is Reduced by Adjunctive Cyclooxygenase-2 Inhibitor in a Phase I Clinical Trial of Tuberculosis Patients

Marthe Jøntvedt Jørgensen[1,2†], Kristin G. Nore[1†], Hans Christian D. Aass[3†], Emilie Layre[4†], Jérôme Nigou[4†], Rasmus Mortensen[5†], Kjetil Tasken[1,6], Dag Kvale[1], Synne Jenum[2†], Kristian Tonby[1,2†] and Anne Ma Dyrhol-Riise[1,2†]*

[1] Institute of Clinical Medicine, University of Oslo, Oslo, Norway, [2] Department of Infectious Diseases, Oslo University Hospital, Oslo, Norway, [3] Department of Medical Biochemistry, Oslo University Hospital, Oslo, Norway, [4] Institut de Pharmacologie et de Biologie Structurale, Université de Toulouse, CNRS, Université Paul Sabatier, Toulouse, France, [5] Department of Infectious Disease Immunology, Statens Serum Institut, Copenhagen, Denmark, [6] Deparment of Cancer Immunology, Institute for Cancer Research, Oslo University Hospital, Oslo, Norway

Introduction: Eicosanoids and intracellular signaling pathways are potential targets for host-directed therapy (HDT) in tuberculosis (TB). We have explored the effect of cyclooxygenase 2 inhibitor (COX-2i) treatment on eicosanoid levels and signaling pathways in monocytes.

Methods: Peripheral blood mononuclear cells isolated from TB patients included in a randomized phase I clinical trial of standard TB treatment with (n=21) or without (n=18) adjunctive COX-2i (etoricoxib) were analyzed at baseline, day 14 and day 56. Plasma eicosanoids were analyzed by ELISA and liquid chromatography-mass spectrometry (LC-MS), plasma cytokines by multiplex, and monocyte signaling by phospho-flow with a defined set of phospho-specific antibodies.

Results: Lipoxygenase (LOX)-derived products (LXA4 and 12-HETE) and pro-inflammatory cytokines were associated with TB disease severity and were reduced during TB therapy, possibly accelerated by adjunctive COX-2i. Phosphorylation of p38 MAPK, NFkB, Erk1/2, and Akt in monocytes as well as plasma levels of MIG/CXCL9 and procalcitonin were reduced in the COX-2i group compared to controls.

Conclusion: COX-2i may reduce excess inflammation in TB *via* the LOX-pathway in addition to modulation of phosphorylation patterns in monocytes. Immunomodulatory effects of adjunctive COX-2i in TB should be further investigated before recommended for use as a HDT strategy.

Keywords: host-directed therapy (HDT), eicosanoids, cyclooxygenase-2 inhibitor, tuberculosis, monocytes, cytokines, innate immunity, lipooxygenase

OPEN ACCESS

Edited by:
Natarajaseenivasan Kalimuthusamy, Bharathidasan University, India

Reviewed by:
Md. Areeful Haque, International Islamic University Chittagong, Bangladesh
Ramalingam Bethunaickan, National Institute of Research in Tuberculosis (ICMR), India

****Correspondence:***
Anne Ma Dyrhol-Riise
a.m.d.riise@medisin.uio.no

†ORCID:
Marthe Jøntvedt Jørgensen
orcid.org/0000-0003-0791-2507
Kristin G. Nore
orcid.org/0000-0002-1592-7613
Hans Christian D. Aass
orcid.org/0000-0002-0395-047X
Emilie Layre
orcid.org/0000-0003-3044-1299
Jérôme Nigou
orcid.org/0000-0002-6233-2487
Rasmus Mortensen
orcid.org/0000-0003-0177-3032
Synne Jenum
orcid.org/0000-0001-8187-775X
Kristian Tonby
orcid.org/0000-0002-8465-1315
Anne Ma Dyrhol-Riise
orcid.org/0000-0003-4009-4032

Specialty section:
This article was submitted to Bacteria and Host, a section of the journal Frontiers in Cellular and Infection Microbiology

Received: *19 February 2021*
Accepted: *21 June 2021*
Published: *09 July 2021*

INTRODUCTION

Tuberculosis (TB), caused by *Mycobacterium tuberculosis* (*Mtb*) is responsible for an estimated 1.5 million deaths annually (WHO, 2020). Although a curable disease, effective TB treatment is challenged by increasing incidence of multi-drug resistant TB (MDR-TB). Host-directed therapy (HDT) has emerged as an alternative treatment strategy, aiming to increase treatment efficacy and shorten treatment duration by modulation of host immunity (Kolloli and Subbian, 2017).

The eicosanoid system, encompassing several biologically active lipid mediators, have been proposed to play an important role in the pathophysiology of *Mtb* infection (Peres et al., 2007; Dennis and Norris, 2015; Sorgi et al., 2020). Their synthesis is predominantly regulated by two families of intracellular enzymes, Cyclooxygenase (COX) and Lipoxygenase (LOX), of which there are several different subclasses. COX-2 is upregulated by inflammation and generates prostanoids including prostaglandin E2 (PGE2) while 5-LOX, 12-LOX, 15-LOX and 8-LOX produce lipoxins, leukotrienes and intermediate metabolites such as hydroxyeicosatetraenoic acids (HETEs) (**Figure 1**) (Dennis and Norris, 2015). Recent reports highlight a dysregulation of the eicosanoid network, with a skewed balance toward LOX products, promoting tissue damage and mycobacterial survival (Chen et al., 2008; O'connor et al., 2016; Pedruzzi et al., 2016). Lipoxin A4 (LXA4) seems to induce macrophage death while 12/15-HETE drive neutrophilic inflammation with subsequent tissue damage (Chen et al., 2008; Mishra et al., 2017), but effects of other products of the LOX pathway in TB pathogenesis are unclear.

Approved drugs that augment PGE2 levels have been suggested as a possible HDT-strategy in TB as PGE2 has been reported to limit detrimental type I interferon (IFN)-production in *Mtb* infected mice (Mayer-Barber et al., 2014) and induce macrophage apoptosis rather than necrosis (Divangahi et al., 2013). However, excess levels of PGE2 may also contribute to disease progression by inhibiting cell-mediated immunity (Rangel Moreno et al., 2002). COX-2 inhibitors (COX-2i) that inhibit PGE2 production reduce bacterial burden and increase survival in some animal models (Vilaplana et al., 2013; Sorgi et al., 2020), although the effect of COX-2i seems to be dependent on route of infection (Mortensen et al., 2019). Thus, COX-2i is of interest as potential HDT.

Monocytes and macrophages are key cellular players in TB pathogenesis and major producers of inflammatory mediators and eicosanoids (Rangel Moreno et al., 2002; Chen et al., 2008; Dennis and Norris, 2015). Toll like receptors (TLRs) and other bacterial pattern recognition receptors on the cell surface recognize foreign pathogens and initiate downstream signaling, resulting in the initiation of the early immune responses. Upon binding to the receptor, protein phosphorylation induces a set of transcription factors leading to production of pro-inflammatory cytokines such as PGE2, TNF- α, IL-12, IL-1 and IL-6 (Guha and Mackman, 2001; Basu et al., 2012).

The signaling pathways of p38 mitogen-activating protein kinase (MAPK), inhibitory κB kinase (IkK) and nuclear factor-κB (NFκB), interferon regulatory factors (IRF) and extracellular signal-regulated kinase (ERK) seem to be involved in monocyte/macrophage-derived cytokine signaling in response to mycobacterial antigens (Barnes and Karin, 1997;

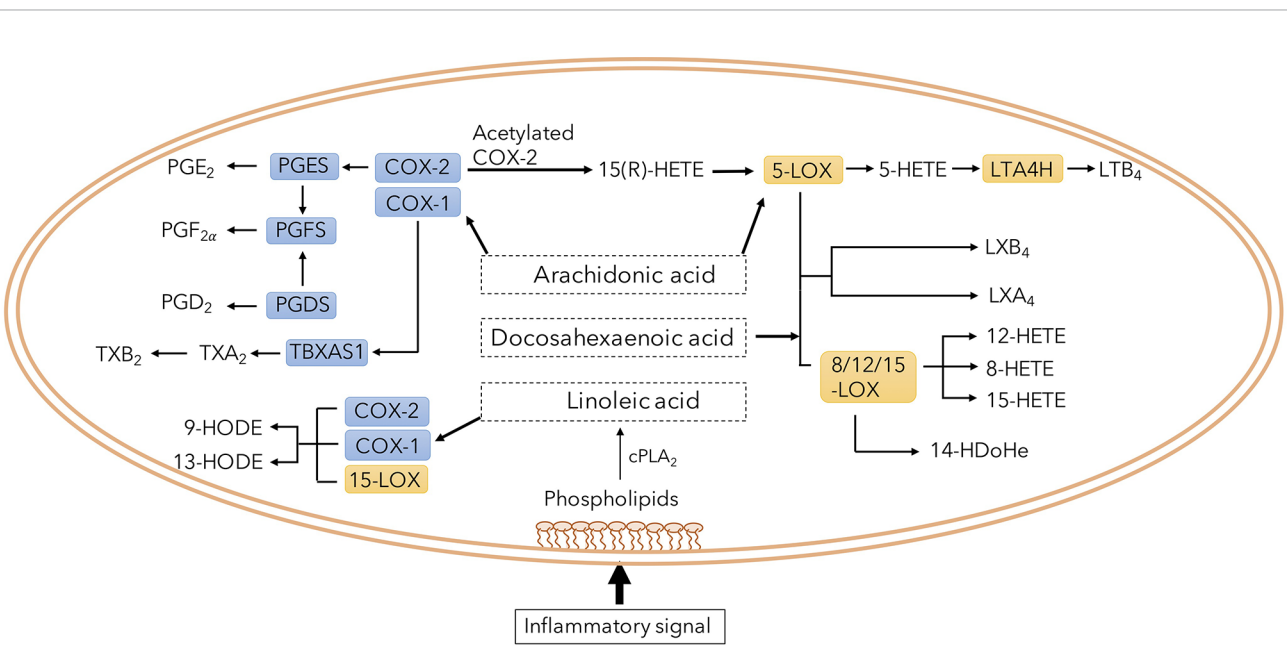

FIGURE 1 | Overview of eicosanoid pathway and its metabolites. Phospholipids in the plasma membrane is converted to several specific fatty acids. Among them, arachidonic acid is a common substrate for both COX and LOX enzymes generating immune modulatory prostaglandins, lipoxins and leukotrienes.

Zingarelli et al., 2003; Jo et al., 2007). *Mtb* infected macrophages produce high levels of PGE_2, partly mediated through TLR2/p38 MAPK signaling, thereby inducing apoptosis of *Mtb* infected macrophages (Nishimura et al., 2013). Translocation of NFκB to the nucleus and transcription of pro-inflammatory genes plays a key role in TB control, and NFκB has been suggested as a possible therapeutic target (Zingarelli et al., 2003; Tay et al., 2010; Fallahi-Sichani et al., 2012; Bai et al., 2013). During TB infection, eicosanoids seem to exert immunomodulatory functions by affecting the production of cytokines such as IL-1, IFN-γ and TNF-α (Tobin et al., 2010; Braverman et al., 2016; Cadena et al., 2016) through altered intracellular signaling, hereby representing a potential HDT target (Almeida et al., 2014). However, the effects of COX-2i treatment on eicosanoid production and monocyte signaling during TB disease remain unknown.

To obtain more insight into eicosanoid biology in TB we first studied the association between different eicosanoid mediators and severity of TB disease. To further evaluate the potential of COX-2i as HDT we investigated the effects of COX-2i on eicosanoid and cytokine levels in plasma from TB patient recruited into a phase I/II clinical trial assessing the safety and immunogenicity of adjunctive COX-2i in TB disease (TBCOX2 study). Finally, to explore novel HDT targets related to innate immunity we analyzed various signaling pathways in monocytes and the *in vitro* and *ex vivo* effects of COX-2i on signal transduction.

MATERIALS AND METHODS

Study Participants

Samples were collected from a total of 39 patients with culture confirmed drug sensitive TB recruited from a phase I/II/clinical trial at Oslo University Hospital, Norway in the period 2015-2019 (TBCOX2, *NCT02503839*). 18 patients received adjunctive COX-2i treatment (etoricoxib) for 140 days in addition to standard TB treatment and 21 patients received only standard TB treatment (**Table 1**). All participants experienced clinical improvement and culture conversion after 2 months of treatment. In addition, five patients (age 18-70) with pulmonary TB were included in a pilot study with blood sampling before TB treatment initiation. All participants were HIV negative. Clinical examination, symptoms, analyses of erythrocyte sedimentation rates (ESR), monocytes and lymphocytes (ML) ratio in peripheral blood, and chest X-ray performed at baseline were recorded. For an overview of the patients included in the different assays see **Supplementary Figure S1**.

Sample Collection and Preparation

Peripheral blood was drawn at baseline, day 14 and day 56. Blood samples were collected in CPT™ Cell Preparation tube (BD Biosciences), using Sodium-Heparin as anti-coagulant, and immediately centrifuged 15 minutes at 1700 g. Plasma was snap-frozen and stored at -80°C until analysis. Peripheral

TABLE 1 | Patient characteristics.

	Total (n = 39)	COX-2i (n = 18)	Control (n = 21)
Age (median)	27 (18-52)	29 (19-49)	26 (18-52)
Male (%)	21 (54)	9 (50)	12 (57)
Origin			
Black	20 (51)	8 (44)	12 (57)
Asian	11 (28)	5 (28)	6 (29)
Caucasian	6 (15)	3 (17)	3 (14)
Other	2 (5)	2 (11)	0
Clinical presentation			
Pulmonary	28[a]	14[b]	16[c]
Cavity	9	5	4
Extrapulmonary	7	4	3
Symptoms			
Cough (%)	20 (51)	10 (56)	10 (48)
Night-Sweat (%)	18 (46)	7 (39)	11 (52)
Weight loss (%)	15 (39)	9 (50)	6 (29)
Fever (%)	9 (23)	5 (28)	4 (19)
Chest pain (%)	11 (28)	4 (22)	7 (33)
Low:high symptom score[d]	17:22	8:10	9:12
Findings			
BMI[e] (min-max)	21 (16-30)	21 (16-30)	21 (17-27)
ML ratio[f] (min-max)	0.33 (0.13-1.36)	0.36 (0.13-1.36)	0.33 (0.17-1.14)
ESR[g] (mm/hour, min-max)	20 (1-116)	26 (2-105)	20 (1-116)
TTP[h] (min-max)	12.2 (2.7-42.1)	12.8 (2.71-24.9)	12.2 (4.7-42.1)
Ct values[i] (min-max)	36 (31-46)	34 (31-46)	41 (31-46)

[a]*4/28,* [b]*2/14 and* [c]*2/16 with both PTB and EPTB.*
[d]*High =≥2 of the following symptoms: Cough, night-sweat, weightloss and fever (>38°C). Low = 1 symptom or asymptomatic/detected by screening.*
[e]*Body mass index (n= 34).*
[f]*Myeloid:lymphocyte ratio (n = 34).*
[g]*Erythrocyte Sedimentation Rate (n=34).*
[h]*Time to Mtb positive culture, days (n=30).*
[i]*Cycle threshold values.*

blood mononuclear cells (PBMC) were isolated and frozen containing freezing media with 10% DMSO. Sputum or relevant tissue specimens were incubated at 37°C for minimum 42 days in Mycobacteria Growth Indicator Tube (MGIT, BD biosciences, New Jersey, USA) and the number of days to detection of bacteria can be measured as time to positive sample (TTP). Cycle threshold (Ct) values were obtained from analysis with quantitative PCR assay (Xpert MTB/RIF) for rapid detection of *Mtb*-specific nucleic acids.

Chemicals and Reagents

Commercially available EIA kits were used to measure PGE2 (cat.no. 514010, Cayman chemical, Ann Harbour, Michigan, USA) and LXA4 (cat.no. EA45 Oxford Biomedical Research, Oxford, Michigan, USA). Samples underwent extraction protocols using C18-SPE Cartridges (Cat.no WAT023501, Waters Inc, Massachusetts, USA) prior to EIA analysis. Cytokines were analyzed using Magnetic Luminex assay (cat.no. LXSAHM-24, RnD systems, Minneapolis, Canada and SAA Human ProCartaPlex™ Simplex Kit (cat.no. EPX01A-12136-901, Thermo Fisher Scientific, Massachusetts, USA)

Directly conjugated monoclonal antibodies for staining monocyte surface markers were directed to HLA-DR FITC (cat.no. 307604, Biolegend, San Diego, USA) and anti-CD14 PE antibodies (cat.no. 345785, BD Bioscience), antibodies for intracellular phosphoflow staining were anti – p38 mitogen activated protein kinase (MAPK) (pS180/S182) (cat.no. 612595), extracellular signal-regulated kinase (ERK) 1/2 (pT202/pY204) (cat.no. 6125939), Protein kinase B (Akt) (pS473) (cat.no. 560343), Nuclear factor κB (NFκB) p65 (pS529) (cat.no. 5584229, interferon regulatory factor (IRF)-7 (pS477) (cat.no. 558630), Cyclic AMP- response element binding protein (CREB) (pS133) ATF-1 (pS63) (cat.no. 558434), protein kinase A (PKA) RIIb (pS114) (cat.no. 560205) all from BD, Biosciences, San Jose, CA, USA. Fluorescent cell barcoding reagents were Pacific Blue Succinimidyl Ester (cat.no. P10163, Thermo Fisher Scientific, Massachusetts, USA) and Pacific Orange Succinimidyl Ester (cat.no. P30253, Thermo Fisher Scientific). Cells were fixed and permeabilized using BD Phosphoflow™ Fix Buffer I (BD Bioscience, cat.no. 557870) and BD Perm/Wash (BD Bioscience, cat.no. 554723).

COX-1/2 inhibitor used in the *in vitro* signaling assay were Indomethacin (20uM, cat.no. I7378-100G, Sigma Aldrich, Saint Louis, Missouri, USA). Cells were counted using Trypan Blue Solution 0.4% (cat.no. 15250061, Gibco™, Thermo Fisher Scientific) and stimulated with either 10ug/mL PPD (SSI, Denmark), 10ng/mL lipopolysaccharide (LPS) or 10mM Prostaglandin E2 (cat.no. HY101952, MedChemExpress, New Jersey, USA).

Enzyme-Linked Immunosorbent Assay

Using a competitive parameter immunoassay, human plasma concentrations of PGE2 and LXA4 from TB patients treated with or without adjunctive COX-2i, at diagnosis and day 14 was quantified using commercial EIA. All assays were performed according to manufacturer's instructions. Briefly, samples underwent extraction protocols using C18-SPE Cartridges. Samples were run in duplicates and optical density was determined at 450 nm or 650 nm using a Spectramax Abs plus microplate reader (Molecular devices Corporation).

Liquid Chromatography – Mass Spectrometry

Eicosanoid concentrations in plasma from patients treated with or without adjunctive COX-2i were analyzed at baseline, day 14 and day 56. Quantification of 5 – hydroxyeicosatetraenoic acid (HETE), 8-, 12 and 15 – HETE, 9-hydroxyoctadecadienoic acid (HODE), 13 – HODE, 14 Hydroxydocosahexaenoic acid (HDoHe) using liquid chromatography – mass spectrometry (LC-MS) was performed as previously described (Le Faouder et al., 2013) at the MetaToul Lipidomic Core Facility (I2MC, Inserm 1048, Toulouse, France, MetaboHUBANR-11-INSB-0010). In the panel, 19 metabolites were not detectable in plasma [resolvin (RV) E1, D1, D2, D3, D5, thromboxane B2, 11B-prostaglandin (PG) F2a, PGE3, PGF2a, PGE2, PGD2, PGA1, 8-iso-PGA2, 6-keto PGF1a, 15-deoxy-delta PGJ2, LXB4, LXA4, LTB5, 7-Maresin 1, 18-hyrdoxyeicosapentanoic acid (HEPE), 5,6 DiHETE, 17-HDoHe, 14,15-epoxy eicosatrienoic acid (EET), 5-oxo-EET, 11,12-EET, 8,9-EET, 5,6-EET]. Briefly, methanol and internal standard (Deuterium labeled compounds) was added before centrifugation (2000 g for 15 min at 4°C). Supernatants were transferred into 96-well deep plates and diluted in H2O. Samples were then submitted to solid phase extraction (SPE) using OASIS HLB 96-well plate (30 mg/well, Waters) and reconstituted in MeOH. Lipid mediators were separated on a ZorBAX SB-C18 column (Agilent Technologies) using Agilent 1290 Infinity HPLC system (Technologies) coupled to an ESI-triple quadruple G6460 mass spectrometer (Agilent Technologies). Data were acquired in Multiple Reaction Monitoring (MRM) mode with optimized conditions (ion optics and collision energy). Peak detection, integration and quantitative analysis were done using Mass Hunter Quantitative analysis software (Agilent Technologies) based on calibration lines built with commercially available eicosanoids standards (Cayman Chemicals). Metabolites that were not detectable in more than 30% of the samples were excluded for further analysis.

Cytokine Analysis

Measurements of cytokines in plasma collected from the COX-2i and control groups at baseline, day 14 and day 56 were performed using a Magnetic Luminex assay with a Luminex IS200 instrument (Bio-Rad). Measurements of chemokine (C-C motif) ligand 1 (CCL1), macrophage inflammatory protein-1α (MIP-1α/CCL3), MIP-1β/CCL4, interferon (IFN) IFN-α, IFN-β, IFN-γ, macrophage-derived chemokine (MDC/CCL22), Monokine induced by gamma (MIG/CXCL9), granulocyte colony stimulating factor (G-CSF), monocyte chemoattractant protein-1 (MCP-1/CCL2), interleukin (IL)-1β /IL-1F2, IL-2, IL-12p70, IL-1rα, IL-4rα, IL-8/CXCL8, IL-18/IL-1F4, CD25/IL-2rα, pentraxin 3, S100 calcium-binding protein A9 (S100A9), IFN-γ inducible protein (IP-10/CXCL10), matrix metalloproteinase-1 (MMP-1), procalcitonin and tumor necrosis factor (TNF)-α were analyzed using 24-plex kit while serum amyloid A(SAA) were analyzed using ProCartaPlex.

Analyses were performed in duplicates and analyzed with the Bio-Plex manager Software version 6.2 (build 175). Out of range values (OOR)> were set to the highest measurable concentration and OOR< were set to zero. Values that were out of the standard range but stipulated from the standard curve were included. Levels of IFN-α, IFN-β, IFN-γ, MIP-1β/CCL4, IL-12p70 were not detectable in more than 30% of the samples and were therefore excluded for further analysis

Cell Culture

Cryopreserved PBMCs were thawed and rested for 1h in a 37°C w/5% CO_2 incubator. Thawed cells were manually counted by microscope, and viability was measured by using Trypan Blue Solution. All samples included had a viability above 80% and the majority of the samples had a viability above 90%. Next, cells were subjected to various stimulation conditions ranging from 0 to 60 min. In a pilot study, PBMCs from confirmed pulmonary TB patients were collected before initiation of TB treatment. Cells were either unstimulated or stimulated with 10ng/mL LPS, 10ug/mL PPD or PPD in combination with 20uM Indomethacin and immediately fixed at 0 min, 10, 30 and 60 min after stimulation. Indomethacin was added to cells 30 min prior to PPD stimulation. PBMCs from the TBCOX2 clinical trial (COX-2i group, n= 8, controls, n=6) were subjected to the same procedures as the pilot study and stimulated with either 10ng/mL LPS, 10ug/mL PPD or 10uM PGE2 for the same period of time, but with no addition of Indomethacin to cultures.

Flow Cytometry

Phosphoflow were performed as previously described (Hermansen et al., 2018; Skanland, 2018). Briefly, prior to permeabilization, the different stimuli conditions were barcoded with different combinations of Pacific Blue and Pacific Orange in room temperature for 20 min. After barcoding, cells were washed with PBS containing 2%FBS, pooled, permeabilized and stained with anti-HLA-DR FITC and anti-CD14 PE antibodies (BD Bioscience) and 6 different phospho – specific antibodies namely anti – p38 mitogen activated protein kinase (MAPK) (pS180/S182), extracellular signal-regulated kinase (ERK) 1/2 (pT202/pY204), Protein kinase B (Akt) (pS473), Nuclear factor κB (NFκB) p65 (pS529), interferon regulatory factor (IRF)-7 (pS477), Cyclic AMP-response element binding protein (CREB) (pS133) ATF-1 (pS63) and in samples from TB patients treated with or without adjunctive COX-2i: Protein kinase A (PKA) RIIb (pS114) was included. **Supplementary Table S1** display antibodies included in the experiments. After 30 min incubation, cells were subjected to flow cytometry analysis with BD FACS Canto II. Monocytes were defined as HLA-DR^+ and $CD14^+$, the gating strategy can be found in **Supplementary Figure S2**. Cell acquisition (<300,000 events) was performed on a FACS Canto II (BD Biosciences). Instrument calibration was performed according to manufacturer's instructions and compensation settings adjusted using antibody-capture beads (CompBeads, BD Biosciences).

Statistical Analysis

For plasma analytes, all data are expressed as median and interquartile range (IQR). Non-parametrical statistical methods were applied, Mann-Whitney U test was used for unpaired data and Wilcoxon for matched pairs, Spearman for correlation analysis. Due to the exploratory nature of the data, it was not corrected for multiple comparisons, but cation was taken when interpreting the results. For flow cytometry analysis, the pooled stimulated samples could be deconvoluted with the different barcoding signatures and analyzed individually. Samples were analyzed using Cytobank (https://cellmass.cytobank.org) and Graphpad Prism (LCC, San Diego, US) and phosphorylation intensities are displayed as arcsinh ratio of medians. Mann U Whitney test was used to compare two unrelated groups. Multiple comparison with Holm Sidak's correction was used to compare phosphorylation time courses between the control and COX-2i group.

RESULTS

Lipoxygenase (LOX)-Derived Metabolites Are Elevated in Cavitary TB Disease

To investigate the role of eicosanoid metabolites in TB pathology, we stratified our cohort based on clinical criteria for disease severity at diagnosis (**Table 1**). In our cohort of 39 TB patients, 23% (n=9) displayed pulmonary TB with cavitary disease and 18% (n=7) were defined as extrapulmonary TB. A total of 22 patients had a high symptom score while 17 patients had low symptom score. Clinical parameters such as erythrocyte sedimentation rate (ESR), monocyte-lymphocyte (ML) ratio, time-to-positive *Mtb* culture (TTP) and cycle threshold (Ct) values were comparable in both groups at diagnosis.

While there was no difference in the levels of PGE2 between the clinical groups at baseline, mediators of the LOX pathway were elevated (LXA4, p=0.006 and 12-HETE, p=0.042) in cavitary disease compared to non-cavitary disease (**Figure 2**). No difference in eicosanoid concentrations were found when patients were stratified by symptom score (**Supplementary Figure S3**). PGE2 levels did not correlate with any laboratory markers of disease severity (ESR, ML ratio, TTP and Ct values), whereas LXA4 (r = -0.413, p=0.052) and 12-HETE (r = -0.522, p = 0.018) correlated inversely with time to positive *Mtb* culture (TTP) (**Figure 2C**).

Lipoxygenase (LOX)-Derived Products Decline With Adjunctive COX-2i Treatment

To explore possible effects of adjunctive COX-2i treatment we analyzed eicosanoid metabolites in plasma after 14 days of treatment when etoricoxib was expected to reach a steady state. Etoricoxib concentrations were detectable in plasma in all patients (data not shown). We observed no significant decline in PGE2 levels (COX-2 derived) in the COX-2i-group nor in controls (**Figure 3A**). By contrast, LXA4 levels (5-LOX-derived) declined significantly (p = 0.024) in the COX-2i-group but not in controls. Although the median PGE2/LXA4 ratio was higher in the COX-2i group at baseline, no significant changes were observed for any of the groups after 14 days of treatment (**Figure 3A**).

We then analyzed longitudinal effects of adjunctive COX-2i on eicosanoid plasma profiles after 14 and 56 days in more detail

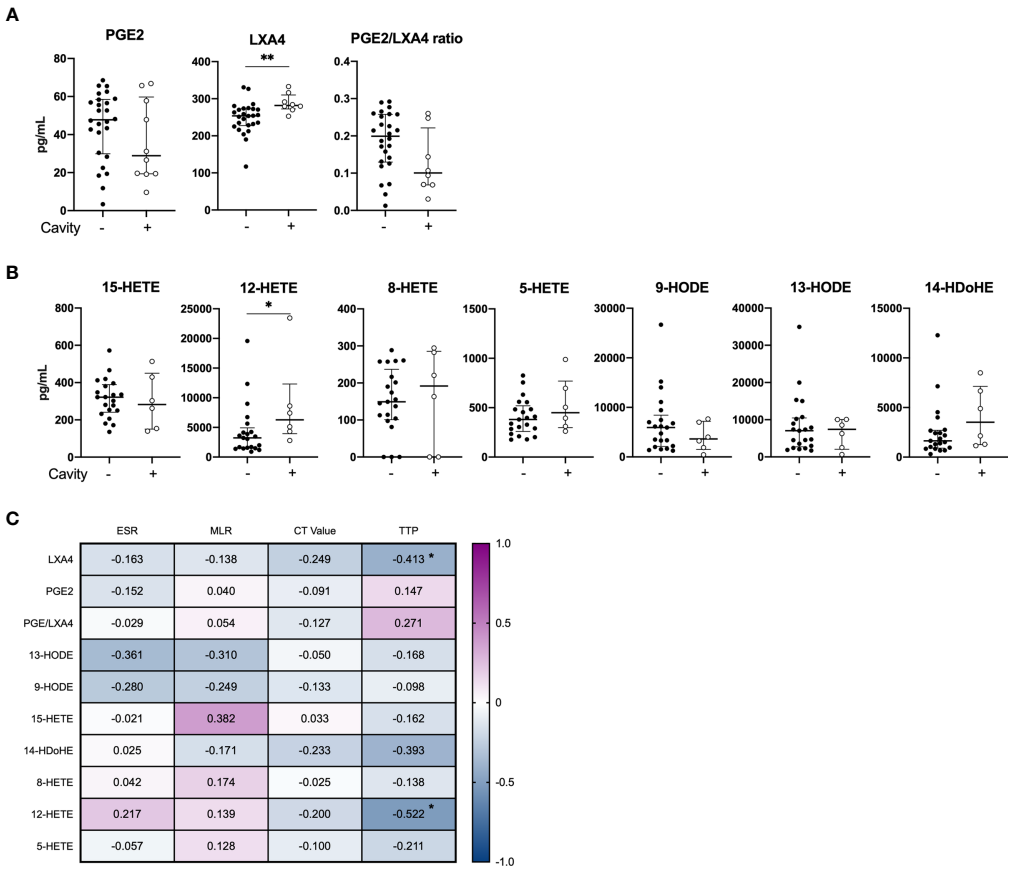

FIGURE 2 | Baseline plasma eicosanoid profiles in cavitary vs. non-cavitary TB disease and correlations to clinical markers. Plasma levels of **(A)** PGE2, LXA4 and PGE2/LXA4 ratio displaying cavitary (n = 8) and non-cavitary disease (n = 26) in TB patients at diagnosis measured by ELISA (included 16 patients in the control group and 18 patients in the COX-2i group) and **(B)** Eicosanoid metabolites comparing cavitary (n=6) and non-cavitary disease (n = 21) in TB patients at diagnosis measured by LC-MS (included 10 patients in control group and 18 patients in COX-2i group). One baseline sample was excluded due to limited plasma. **(C)** Eicosanoid correlations to clinical parameters erythrocyte sedimentation rate (ESR), monocyte lymphocyte (ML) ratio, Cycle threshold (CT) values and time to positive *Mtb* culture (TTP) collected at diagnosis. Significance calculated with Mann Whitney T test, *p < 0.05, **p < 0.01, Lines indicate median with interquartile range (IQR). Rho calculated with spearman correlation.

by LC-MS (**Figure 3B**). From diagnosis up to day 56, LOX metabolites such as 15-HETE (day 14, p = 0.034, day 56, p = 0.048), 8-HETE (day 14, p = 0.045), 12-HETE (day 56, p = 0.054) and 14-HDoHE (day 56, p = 0.01) were significantly reduced in the COX-2i-group. In controls, the only metabolite that was decreased at day 56 was 14-HDoHE (day 56, p = 0.01). Still, there were no significant differences at day 14 nor 56 when comparing the levels of metabolites between the COX-2i-group and controls at the respective time points (**Supplementary Figure S4**).

The Adjunctive Effects of COX-2i on Plasma Cytokines During TB Treatment

A broad specter of plasma cytokines was screened using a 24-plex kit and a single-plex Luminex Kit. The pro-inflammatory cytokines CCL1, Pentraxin3, CD25/IL-2ra, IP-10, S100A9 and MMP-1 correlated with markers of disease severity (**Supplementary Figure S5**). As COX-2i has anti-inflammatory properties (Kroesen et al., 2017) we investigated if COX-2i treatment influenced on plasma cytokines levels. In general, the inflammatory mediators declined during TB therapy in both the COX-2i group and in controls. Still, CXCL9/MIG and procalcitonin levels were significantly reduced after 56 days only in the COX-2i-group (**Figure 4A**). In contrast, CCL22/MDC, S100A9, IL-4Ra, CD25/IL-2ra, MMP-1, IP-10 and SAA were significantly reduced while CCL2/MCP-1 increased in both groups after 56 days.

Next, we investigated the association between eicosanoid and cytokine levels in plasma (**Figure 4B**). Interestingly, CXCL9/MIG showed a diverse relationship with products of the two eicosanoid pathways, with a weak positive correlation with PGE2 (r = 0.373, p = 0.050) and a moderate negative correlation with LXA4 (r = -0.497, p = 0.007), 13-HODE (r = -0.417, p = 0.031), 14-HDoHE (r = -0.630 p = 0.0001), 12-HETE (r = -0.552, p = 0.003) and 5-HETE (r = -0.372, p = 0.056). Further, LXA4 correlated positively with Pentraxin 3 (r = 0.369, p = 0.053) and IL-18 (r = 0.0389, p = 0.040). The LOX-products 15-HETE,

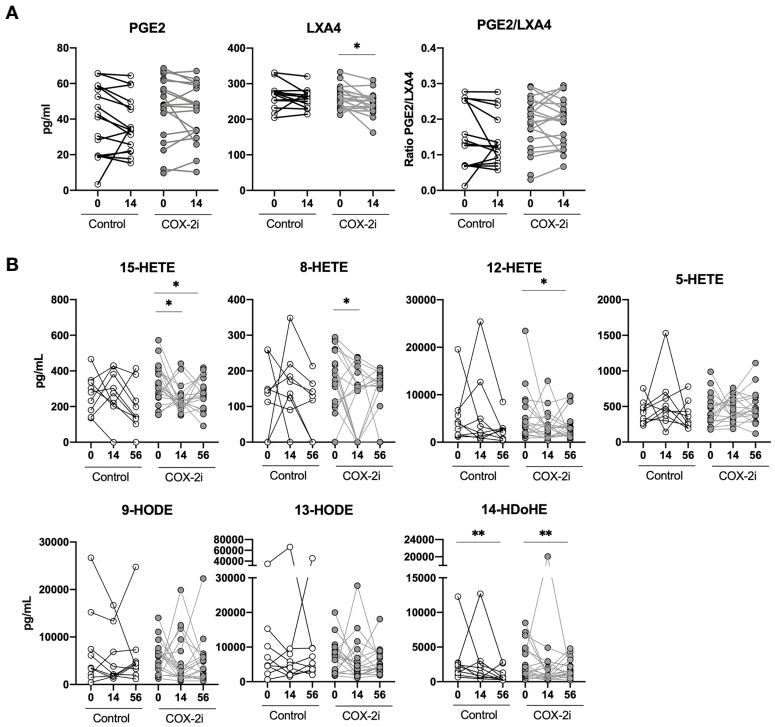

FIGURE 3 | Plasma eicosanoids levels during standard TB therapy alone and with adjunctive COX-2i. **(A)** Plasma levels of PGE2, LXA4 and PGE2/LXA4 ratio measured by ELISA comparing 14 days of treatment without (n = 16) and with (n = 18) COX-2i therapy. **(B)** eicosanoid metabolites measured by LC-MS at diagnosis, 14 and 56 days after treatment without (open circles, n = 10) and with (grey circles, n = 18) COX-2i. Significance calculated with Wilcoxon test comparing baseline and day 14 and baseline and day 56. *p < 0.05, **p < 0.01. Lines indicate median with interquartile range (IQR).

12-HETE and 5-HETE all showed positive correlations with CCL1, Pentraxin3, CD25/IL-2ra and IP-10, respectively.

Signaling Pathways in Peripheral Monocytes Induced by Lipopolysaccharide and Mycobacterial Antigens

Lipopolysaccharide and mycobacterial antigens bind TLRs in monocytes and induce signaling cascades with immune-modulatory effects. Thus, to further explore targets for HDT in a pilot study, we analyzed by phospho-flow cytometry the phosphorylation patterns in peripheral blood monocytes from another prospective cohort of TB patients before start of TB therapy (**Supplementary Figure S6**). We detected several phospho-epitopes following *in vitro* stimulation with endotoxin lipopolysaccharide (LPS) and mycobacterial antigens (purified protein derivative, PPD), but no effects on phosphorylation was observed by adding COX-2i to the cell cultures (**Supplementary Figure S6**). We then investigated the same phospho-epitopes during stimulation with either PGE2, LPS or PPD in samples collected from the TBCOX2 study after 14 days of standard TB treatment (**Figure 5**). *In vitro* stimulation by LPS induced phosphorylation of p38 MAPK (pS180/S182), Erk1/2 (pT202/Y204), Akt (pS473) with significantly higher intensities compared to PPD and PGE2 stimulation. In contrast, PGE2 induced higher intensity of PKA RIIb (pS114) phosphorylation than LPS and PPD as expected (**Figure 5**), indicating that LPS and PPD induce similar signaling cascades while PGE2 induce distinct pathways involving PKA. A schematic overview of the signaling pathways and the potential targets is illustrated in **Supplementary Figure S7**.

Adjunctive COX-2i Influences Phosphorylation in Peripheral Monocytes

The phosphorylation signaling pathways are upstream of the transcription of pro-inflammatory cytokines. Therefore, we investigated if adjunctive COX-2i for 14 days influenced monocyte signaling and responsiveness to *Mtb* antigens in TB patients from the TBCOX2 trial. The phosphorylation kinetics of p38 MAPK (pS180/S182), NFκB (pS529), Erk1/2 (pT202/Y204), Akt (pS473), CREB (pS133)/ATF-1 (pS63) and IRF-7 (pS477/479) showed a similar pattern in these patients as that seen in the pilot study (**Supplementary Figure S6**). Overall, we observed lower levels of phosphorylation in the COX-2i group compared to controls, especially pronounced for LPS induced phosphorylation of p38 MAPK (pS180/S182) ($p<0.001$), NFκB (pS529) ($p<0.01$), Erk1/2 (pT202/Y204) ($p<0.05$) and Akt (pS473) ($p<0.05$) (**Figure 6A**). The intensity of PPD-induced phosphorylation of p38 MAPK (**Figures 6A, B**) was significantly lower in the COX-2i group compared to controls. Interestingly, the phospho-sites that were induced by PGE2 (IRF-7 (pS477/479), CREB (pS133)/ATF-1 (pS63) and PKA RIIb (pS114) displayed more pronounced

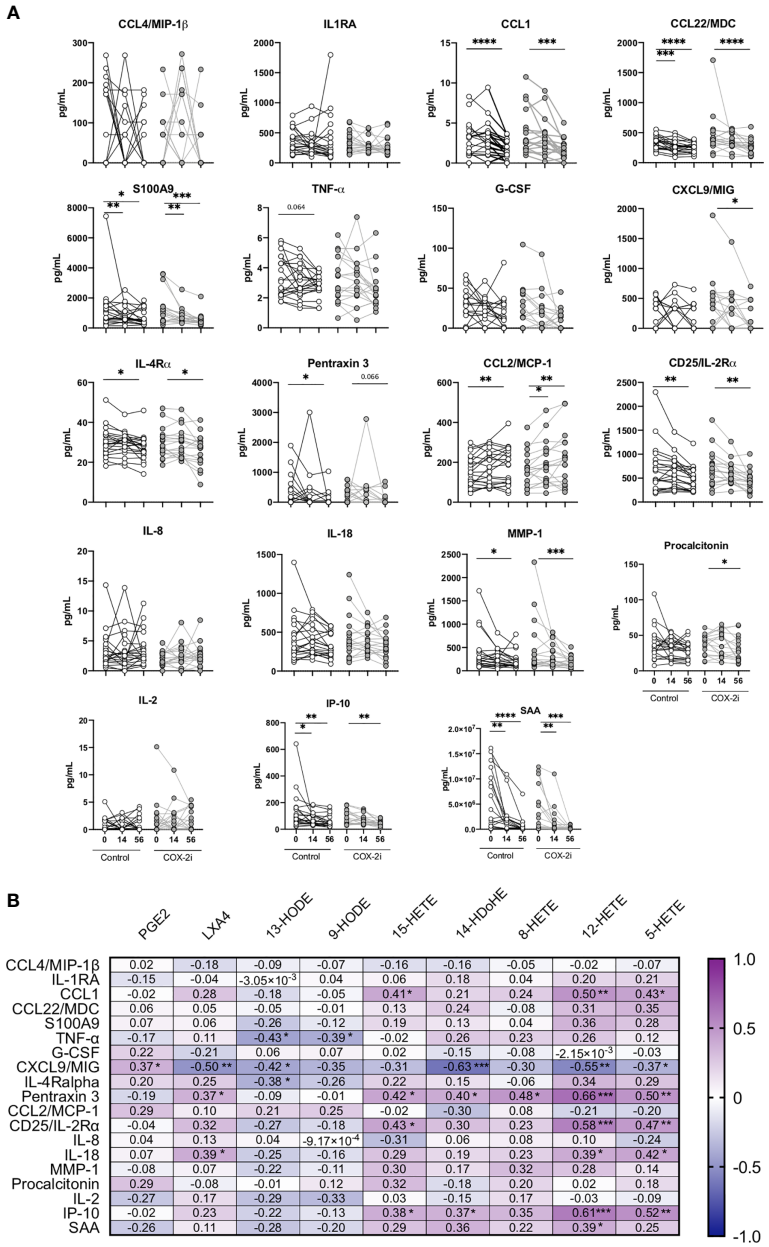

FIGURE 4 | Plasma cytokine levels during standard TB therapy alone and with adjunctive COX-2i. **(A)** Levels of cytokines in plasma in TB patients without (n = 21) and with (n = 18) COX-2i therapy. Significance calculated with Wilcoxon test comparing baseline and day 14 and baseline and day 56. *p < 0.05, **p < 0.01, ***p < 0.001, ****p < 0.0001, Lines indicate median with interquartile range (IQR). **(B)** Relationship between eicosanoids and cytokines levels in plasma from TB patients at diagnosis. Correlations are displayed using the Rho-value calculated with spearman correlation.

phosphorylation in the COX-2i-group compared to controls, although differences were not significant.

DISCUSSION

Targeted immunomodulating therapy may improve TB treatment strategies. COX-2i could possibly reduce excess inflammation and tissue damage in chronic stages of TB infection with clinical benefits for patients. Still, for some patients this might come at a cost of reduced bacterial clearance due to reduced pro-inflammatory responses (Kroesen et al., 2017). In the context of a phase I/II clinical trial assessing the safety of COX-2i given adjunctive to standard TB treatment we observed that the LOX-derived products LXA4 and 12-HETE were associated with disease severity at diagnosis. Several

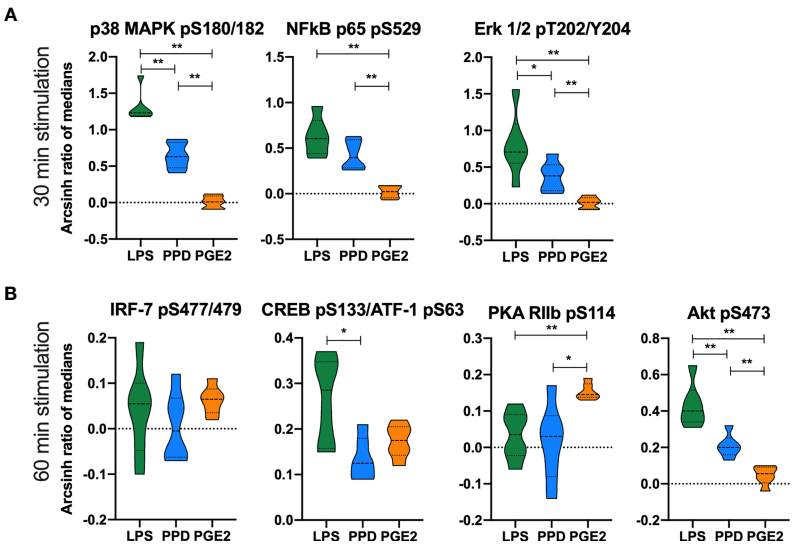

FIGURE 5 | Differential phosphorylation responses in monocytes to *in vitro* stimulation with LPS, PPD and PGE2. Phosphorylation intensities measured as arcsinh ratio of medians from patients receiving standard TB treatment for 14 days (n=6) after stimulation with LPS (green), PPD (blue) and PGE2 (orange) for **(A)** 30 min and **(B)** 60 min. Significance calculated with Mann Whitney test *p < 0.05, **p < 0.01. Violin plot displaying line at median and quartiles.

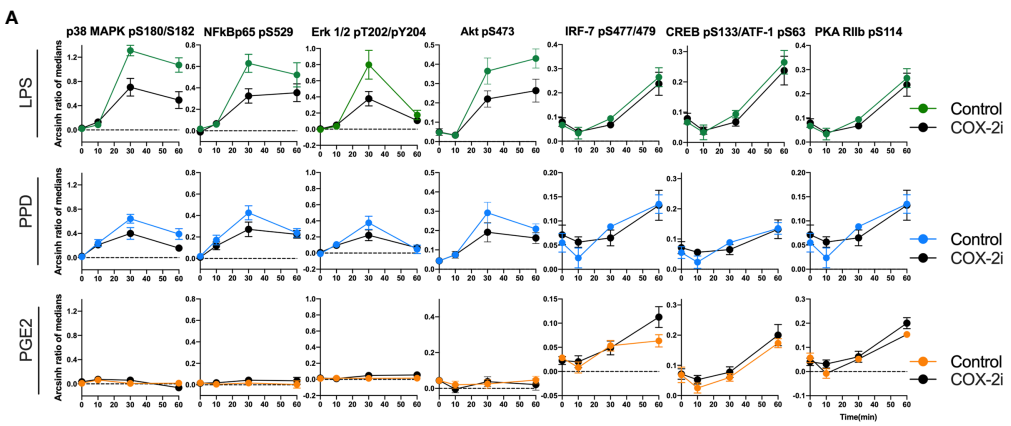

B

Phosphosite	LPS	PPD	PGE2
p38 MAPK pS180/182	***	**	ns
NFkB p65 pS529	**	ns	ns
Erk 1/2 pT202/204	*	ns	ns
Akt pS473	*	ns	ns
IRF-7 pS477/479	ns	ns	ns
CREB pS133/ATF-1 pS63	ns	ns	ns
PKA RIIb pS114	ns	ns	ns

FIGURE 6 | Distinct signal intensities in TB patients receiving COX-2i as adjunctive treatment. **(A)** Phosphorylation intensity induced by LPS (green), PPD (blue) and PGE2 (orange) in comparing COX-2i group (n = 8, black circles) and controls (n = 6, colored circles) after 0, 10, 30 and 60 min of stimulation. Phosphorylation intensity is measured as archsin ratio of medians. **(B)** Table of statistically significant differences between phosphorylation of the various sites in the control and COX-2i group after LPS, PPD and PGE2 stimulation. Significance calculated with multiple comparison with Holm Sidak's correction, asterix indicate significance p-value (*p < 0.05, **p < 0.01, ***p < 0.001, ns: not significant). Error bars indicate Mean±SEM.

eicosanoid metabolites were significantly reduced after 56 days of standard TB treatment, some already after 14 days, with a possible accelerated effect of COX-2i. Independent of COX-2i, pro-inflammatory plasma cytokines were reduced during the first two months of standard TB treatment, many already after 14 days while experiencing clinical improvement. Of interest, CXCL9/MIG and procalcitonin were significantly reduced only in the COX-2i-group indicating a possible adjunctive effect of COX-2i. In our *in vitro* monocyte signaling assay, LPS and mycobacterial antigens induced phosphorylation of the same phospho-epitopes. However, our findings suggest that IRF-7 is not activated by mycobacterial antigens, but rather by eicosanoids such as PGE2. We show novel data that TB patients treated with adjunctive COX-2i displayed an overall lowered signaling potential by LPS and PPD induced phosphorylation compared to controls suggesting reduced transcription of inflammatory cytokines in monocytes.

Clinical markers of TB disease severity and bacterial burden such as cavitary disease and number of days to *Mtb* positive culture (TTP) were both associated with levels of the LOX-derived metabolites LXA4, 12-HETE and 8-HETE in plasma. A detrimental role of 5/12-LOX derived metabolites in TB have been suggested due to LXA4-mediated necrosis of macrophages (Chen et al., 2008; Behar et al., 2010). Further, 12/15-LOX-derived products found in cavitary lesions may facilitate mycobacterial spread by driving neutrophilic inflammation, granuloma disintegration and tissue damage contributing to bacterial dissemination (Chen et al., 2008; Divangahi et al., 2010; Divangahi et al., 2013; Lau et al., 2015; Mishra et al., 2017). Our data are in accordance with a previous study reporting no association between PGE2 and TB disease severity, but rather an increase of LXA4, 15-epi LXA4 and LTB4 in cavitary TB disease correlating to bacterial burden (Pavan Kumar et al., 2019).

We further evaluated the effect of adjunctive COX-2i in TB patients by measuring plasma eicosanoids levels. We show that selective COX-2 inhibition influences the LOX arm of the eicosanoid system as several LOX-metabolites (LXA4, 15-HETE, 12-HETE, 8-HETE and 14-HDoHE) were reduced in the COX-2i-group, but not in controls. Our findings suggest possible beneficial effects of reduced levels of unfavorable LOX-metabolites, although it has previous been shown that COX-2 inhibition may also increase the activity of LOX-enzymes and its products (Dennis and Norris, 2015). Surprisingly, we observed no effect of COX-2i on PGE2 levels in plasma. This might be due to a suboptimal inhibitor dose or that 14 days are too early to detect possible effects. Further, we observed no association with disease severity, indicating a limited role of PGE2 than initially hypothesized in this stage of TB disease (Rangel Moreno et al., 2002). Therefore, selectively targeting the LOX-products by LOX inhibitors such as Zileuton or MK886 might be a better approach to avoid inhibiting potentially beneficial effects of the COX-2/PGE2 axis (Kaul et al., 2012; Sorgi et al., 2020).

A balanced and timely coordinated cytokine response is paramount in host immune defenses. Elucidating the systemic inflammatory milieu could expose novel HDT targets (Cicchese et al., 2018) as well as biomarkers for disease severity and treatment efficacy (Walzl et al., 2014; Kumar et al., 2019). We and others have previously reported that CCL1 and IP-10 could serve such a purpose (Tonby et al., 2015; Wergeland et al., 2015; Xiong et al., 2016; Kumar et al., 2019). Intriguingly, the cytokines pentraxin 3, IL-18, CD25 (IL-2R) and IP-10 associated with TB disease severity, were positively correlated with LOX-derived metabolites. The levels of several of these pro-inflammatory cytokines were reduced after 56 days of TB treatment, independent on COX-2i intervention, indicating that standard TB treatment is the main contributor to reduced bacterial load and inflammation. Still, there was reduced CXCL9/MIG and procalcitonin after 56 days of COX-2i treatment, not found in controls. The LOX-pathway produces both pro- and anti-inflammatory mediators (Dennis and Norris, 2015) often induced simultaneously. COX-2 induction by NFκB leads to conversion of 15-HETE and induction of 5-LOX, ultimately promoting lipoxin production. Thus, prolonged and excess inflammation facilitate *Mtb* survival and result in increased TB pathology (Stek et al., 2018; Vinhaes et al., 2019).

We further explored the relationship between monocytes and COX-2i by investigating monocytes signaling induced by the endotoxin LPS, that engages TLR4, and by mycobacterial antigens (PPD) that engage both TLR4 and TLR2 (Jo et al., 2007). Several of the investigated proteins, such as p38 MAPK (Balboa et al., 2013), NFκB (Bai et al., 2013), and Akt (Singh and Subbian, 2018) have been suggested as therapeutic targets in TB as they confer regulatory roles of infection and inflammation (Blumenthal et al., 2002; Yadav et al., 2004; Basu et al., 2012). TNFα-induced NFκB phosphorylation is crucial in conferring mycobacterial control and granuloma formation (Fallahi-Sichani et al., 2012). We observed increased NFκB p65 (pS529) phosphorylation after 30 min stimulation with LPS and PPD. PGE2 stimulation was also investigated to study potential indirect effects of COX-2i, such as altered PGE2 responsiveness. PGE2 induced phosphorylation of PKA RIIb (pS114), IRF-7 (pS477/479) and CREB (pS133)/ATF-1 (pS63) but not NFκB p65 (pS529), p38 MAPK (pS180/182) and Erk1/2 (pT202/Y204), indicating that PGE2 induces distinct pathways compared to LPS and/or PPD stimulation. Bound to transmembrane EP receptors, PGE2 induce accumulation of cAMP and thus activation of the PKA signaling pathway (Diaz-Munoz et al., 2012) while IRF-7 has a multifaceted role in *Mtb* infection as it can either promote or impair pathogen control (Manca et al., 2005; Mayer-Barber et al., 2011). Our findings suggest that PGE2 rather than LPS and PPD activate IRF-7 and PKA.

To the best of our knowledge, we present for the first time novel data on the effects of COX-2i on phosphorylation patterns in peripheral blood monocytes from TB patients harvested 14 days following initiation of adjunctive COX-2i. In line with already known anti-inflammatory properties of COX-2i (Williams et al., 1999), we observed reduced LPS-induced phosphorylation of p38 MAPK (pS180/182), NFκB p65 (pS529), Erk1/2 (pT202/Y204) and Akt (pS473) in the COX-2i-group possibly indicating reduced responsiveness of monocytes in patients treated with COX-2i. As several of these signaling pathways regulate transcription of pro-inflammatory cytokines (Jo et al., 2007), adjunctive COX-2i

potentially reduces pro-inflammatory responses in monocytes. However, whether this reduction is beneficial or detrimental for the patients with chronic TB must be further explored. A trend of higher PGE2-induced phosphorylation was observed in the COX-2i-group compared to controls, indicating COX-2i-driven susceptibly for PGE2 in monocytes. A possible explanation is a rescue mechanism to maintain PGE2 effects in the cells possibly by upregulation of EP receptors on the cell surface (Nishimura et al., 2013). This could also explain why we observed no effect of adjunctive COX-2i on plasma PGE2 levels. The mechanism could be upregulation of EP receptors with a simultaneous lowered ability to phosphorylate components of LPS and/or PPD induced pathways.

The major limitation of our study is the small sample size due to the phase I clinical trial design. Thus, our study is exploratory and the results hypothesis generating concerning possible effects of COX-2i on the eicosanoid pathways and monocytes in TB. Also, different tissue compartments must be studied to increase the understanding of eicosanoid metabolites and cellular interplay in TB pathogenesis. Future investigations on the effects of LOX-inhibitors on cell signaling and eicosanoid pathways are needed, to illuminate their potential role as HDT-targets. In addition, the potential efficacy of both COX-2 and LOX inhibitors as adjunctive HDT in TB should be investigated in larger patient cohorts with various clinical presentations where modest differences in cell behavior can be detected.

In conclusion, we show that LOX-derived products are associated with disease severity in untreated TB, while PGE2 seem to play a less important role during the first 14 days of TB treatment. While COX-2i primarily targets the prostaglandin pathways we observed an early reduction in potentially harmful effects of LOX-derived products. COX-2i seemed to reduce pro-inflammatory responses reflected in reduced phosphorylation potential and signal transduction in monocytes. These data provide knowledge on the possible benefits and disadvantages of using adjunctive COX-2i as an HDT strategy in TB disease.

DATA AVAILABILITY STATEMENT

The datasets presented in this article are not readily available because of the privacy of the research participants included in the study. Requests to access the datasets should be directed to Professor AM-DR, email: a.m.d.riise@medisin.uio.no.

ETHICS STATEMENT

The studies involving human participants were reviewed and approved by The Regional Committees for Medical and Health Research Ethics (REK SØ 2015/692, EudraCT nr: 2014-004986-26). The patients/participants provided their written informed consent to participate in this study.

AUTHOR CONTRIBUTIONS

Study concept and design, AM-DR, KTa, and MJ. Funding, AM-DR. Recruitment of participants, KTo, SJ, and AM-DR. Laboratory analyses and acquisition of data, multiplex (HCDA), flow cytometry (MJ and KN), LC-MS (EL and JN). Statistical analyses MJ and KN. Interpretation of data, MJ, KN, KTo, SJ, RM, KTa, DK, and AM-DR. Drafting of the manuscript, MJ and KN. Critical revision of the manuscript and intellectual content: KTo, SJ, AM-DR, RM, KTa, DK, HA, EL, and JN. All authors contributed to the article and approved the submitted version.

FUNDING

This work was funded and supported by The Research Council of Norway (GlobVac no 234493), South Eastern Norway Regional Health Authority, Oslo University Hospital and University of Oslo.

ACKNOWLEDGMENTS

We would like to thank all participants of the study and the collaborators in the clinical trial at Statens Serum Institute, Denmark and Oslo University Hospital, Norway. We would also acknowledge European Union's Horizon 2020 research and innovation program under grant agreement No 847762.

SUPPLEMENTARY MATERIAL

The Supplementary Material for this article can be found online at: https://www.frontiersin.org/articles/10.3389/fcimb.2021.669623/full#supplementary-material

REFERENCES

Almeida, P. E., Roque, N. R., Magalhães, K. G., Mattos, K. A., Teixeira, L., Maya-Monteiro, C., et al. (2014). Differential TLR2 Downstream Signaling Regulates Lipid Metabolism and Cytokine Production Triggered by Mycobacterium Bovis BCG Infection. *Biochim. Biophys. Acta (BBA) - Mol. Cell Biol. Lipids* 1841, 97–107. doi: 10.1016/j.bbalip.2013.10.008

Bai, X., Feldman, N. E., Chmura, K., Ovrutsky, A. R., Su, W. L., Griffin, L., et al. (2013). Inhibition of Nuclear Factor-Kappa B Activation Decreases Survival of Mycobacterium Tuberculosis in Human Macrophages. *PloS One* 8, e61925. doi: 10.1371/journal.pone.0061925

Balboa, L., Romero, M. M., Laborde, E., Sabio, Y. G. C. A., Basile, J. I., Schierloh, P., et al. (2013). Impaired Dendritic Cell Differentiation of CD16-Positive Monocytes in Tuberculosis: Role of P38 MAPK. *Eur. J. Immunol.* 43, 335–347. doi: 10.1002/eji.201242557

Barnes, P. J., and Karin, M. (1997). Nuclear Factor-Kappab: A Pivotal Transcription Factor in Chronic Inflammatory Diseases. *N. Engl. J. Med.* 336, 1066–1071. doi: 10.1056/NEJM199704103361506

Basu, J., Shin, D.-M., and Jo, E.-K. (2012). Mycobacterial Signaling Through Toll-Like Receptors. *Front. Cell. Infect. Microbiol.* 2, 145. doi: 10.3389/fcimb.2012.00145

Behar, S. M., Divangahi, M., and Remold, H. G. (2010). Evasion of Innate Immunity by Mycobacterium Tuberculosis: Is Death an Exit Strategy? *Nat. Rev. Microbiol.* 8, 668–674. doi: 10.1038/nrmicro2387

Blumenthal, A., Ehlers, S., Ernst, M., Flad, H. D., and Reiling, N. (2002). Control of Mycobacterial Replication in Human Macrophages: Roles of Extracellular Signal-Regulated Kinases 1 and 2 and P38 Mitogen-Activated Protein Kinase

Pathways. *Infect. Immun.* 70, 4961–4967. doi: 10.1128/IAI.70.9.4961-4967.2002

Braverman, J., Sogi, K. M., Benjamin, D., Nomura, D. K., and Stanley, S. A. (2016). HIF-1α Is an Essential Mediator of IFN-γ-Dependent Immunity to Mycobacterium Tuberculosis. *J. Immunol.* 197, 1287–1297. doi: 10.4049/jimmunol.1600266

Cadena, A. M., Flynn, J. L., and Fortune, S. M. (2016). The Importance of First Impressions: Early Events in Mycobacterium Tuberculosis Infection Influence Outcome. *mBio* 7, e00342–e00316. doi: 10.1128/mBio.00342-16

Chen, M., Divangahi, M., Gan, H., Shin, D. S., Hong, S., Lee, D. M., et al. (2008). Lipid Mediators in Innate Immunity Against Tuberculosis: Opposing Roles of PGE2 and LXA4 in the Induction of Macrophage Death. *J. Exp. Med.* 205, 2791–2801. doi: 10.1084/jem.20080767

Cicchese, J. M., Evans, S., Hult, C., Joslyn, L. R., Wessler, T., Millar, J. A., et al. (2018). Dynamic Balance of Pro- and Anti-Inflammatory Signals Controls Disease and Limits Pathology. *Immunol. Rev.* 285, 147–167. doi: 10.1111/imr.12671

Dennis, E. A., and Norris, P. C. (2015). Eicosanoid Storm in Infection and Inflammation. *Nat. Rev. Immunol.* 15, 511–523. doi: 10.1038/nri3859

Diaz-Munoz, M. D., Osma-Garcia, I. C., Fresno, M., and Iniguez, M. A. (2012). Involvement of PGE2 and the cAMP Signalling Pathway in the Up-Regulation of COX-2 and mPGES-1 Expression in LPS-Activated Macrophages. *Biochem. J.* 443, 451–461. doi: 10.1042/BJ20111052

Divangahi, M., Behar, S. M., and Remold, H. (2013). Dying to Live: How the Death Modality of the Infected Macrophage Affects Immunity to Tuberculosis. *Adv. Exp. Med. Biol.* 783, 103–120. doi: 10.1007/978-1-4614-6111-1_6

Divangahi, M., Desjardins, D., Nunes-Alves, C., Remold, H. G., and Behar, S. M. (2010). Eicosanoid Pathways Regulate Adaptive Immunity to Mycobacterium Tuberculosis. *Nat. Immunol.* 11, 751–758. doi: 10.1038/ni.1904

Fallahi-Sichani, M., Kirschner, D. E., and Linderman, J. J. (2012). NF-KappaB Signaling Dynamics Play a Key Role in Infection Control in Tuberculosis. *Front. Physiol.* 3, 170. doi: 10.3389/fphys.2012.00170

Guha, M., and Mackman, N. (2001). LPS Induction of Gene Expression in Human Monocytes. *Cell Signal.* 13, 85–94. doi: 10.1016/S0898-6568(00)00149-2

Hermansen, J. U., Tjønnfjord, G. E., Munthe, L. A., Taskén, K., and Skånland, S. S. (2018). Cryopreservation of Primary B Cells Minimally Influences Their Signaling Responses. *Sci. Rep.* 8, 17651. doi: 10.1038/s41598-018-36121-9

Jo, E. K., Yang, C. S., Choi, C. H., and Harding, C. V. (2007). Intracellular Signalling Cascades Regulating Innate Immune Responses to Mycobacteria: Branching Out From Toll-Like Receptors. *Cell Microbiol.* 9, 1087–1098. doi: 10.1111/j.1462-5822.2007.00914.x

Kaul, V., Bhattacharya, D., Singh, Y., Van Kaer, L., Peters-Golden, M., Bishai, W. R., et al. (2012). An Important Role of Prostanoid Receptor EP2 in Host Resistance to Mycobacterium Tuberculosis Infection in Mice. *J. Infect. Dis.* 206, 1816–1825. doi: 10.1093/infdis/jis609

Kolloli, A., and Subbian, S. (2017). Host-Directed Therapeutic Strategies for Tuberculosis. *Front. Med.* 4, 171. doi: 10.3389/fmed.2017.00171

Kroesen, V. M., Gröschel, M. I., Martinson, N., Zumla, A., Maeurer, M., van der Werf, T. S., et al. (2017). Non-Steroidal Anti-Inflammatory Drugs As Host-Directed Therapy for Tuberculosis: A Systematic Review. *Front. Immunol.* 8, 772. doi: 10.3389/fimmu.2017.00772

Kumar, N. P., Moideen, K., Nancy, A., Viswanathan, V., Shruthi, B. S., Sivakumar, S., et al. (2019). Plasma Chemokines Are Biomarkers of Disease Severity, Higher Bacterial Burden and Delayed Sputum Culture Conversion in Pulmonary Tuberculosis. *Sci. Rep.* 9, 18217. doi: 10.1038/s41598-019-54803-w

Lau, S. K. P., Lee, K. C., Curreem, S. O. T., Chow, W. N., To, K. K. W., Hung, I. F. N., et al. (2015). Metabolomic Profiling of Plasma From Patients With Tuberculosis by Use of Untargeted Mass Spectrometry Reveals Novel Biomarkers for Diagnosis. *J. Clin. Microbiol.* 53, 3750–3759. doi: 10.1128/JCM.01568-15

Le Faouder, P., Baillif, V., Spreadbury, I., Motta, J. P., Rousset, P., Chêne, G., et al. (2013). LC-MS/MS Method for Rapid and Concomitant Quantification of Pro-Inflammatory and Pro-Resolving Polyunsaturated Fatty Acid Metabolites. *J. Chromatogr. B Anal. Technol. BioMed. Life Sci.* 932, 123–133. doi: 10.1016/j.jchromb.2013.06.014

Manca, C., Tsenova, L., Freeman, S., Barczak, A. K., Tovey, M., Murray, P. J., et al. (2005). Hypervirulent M. Tuberculosis W/Beijing Strains Upregulate Type I IFNs and Increase Expression of Negative Regulators of the Jak-Stat Pathway. *J. Interferon Cytokine Res.* 25, 694–701. doi: 10.1089/jir.2005.25.694

Mayer-Barber, K. D., Andrade, B. B., Barber, D. L., Hieny, S., Feng, C. G., Caspar, P., et al. (2011). Innate and Adaptive Interferons Suppress IL-1alpha and IL-1beta Production by Distinct Pulmonary Myeloid Subsets During Mycobacterium Tuberculosis Infection. *Immunity* 35, 1023–1034. doi: 10.1016/j.immuni.2011.12.002

Mayer-Barber, K. D., Andrade, B. B., Oland, S. D., Amaral, E. P., Barber, D. L., Gonzales, J., et al. (2014). Host-Directed Therapy of Tuberculosis Based on Interleukin-1 and Type I Interferon Crosstalk. *Nature* 511, 99–103. doi: 10.1038/nature13489

Mishra, B. B., Lovewell, R. R., Olive, A. J., Zhang, G., Wang, W., Eugenin, E., et al. (2017). Nitric Oxide Prevents a Pathogen-Permissive Granulocytic Inflammation During Tuberculosis. *Nat. Microbiol.* 2, 17072. doi: 10.1038/nmicrobiol.2017.72

Mortensen, R., Clemmensen, H. S., Woodworth, J. S., Therkelsen, M. L., Mustafa, T., Tonby, K., et al. (2019). Cyclooxygenase Inhibitors Impair CD4 T Cell Immunity and Exacerbate Mycobacterium Tuberculosis Infection in Aerosol-Challenged Mice. *Commun. Biol.* 2, 288. doi: 10.1038/s42003-019-0530-3

Nishimura, T., Zhao, X., Gan, H., Koyasu, S., and Remold, H. G. (2013). The Prostaglandin E2 Receptor EP4 Is Integral to a Positive Feedback Loop for Prostaglandin E2 Production in Human Macrophages Infected With Mycobacterium Tuberculosis. *FASEB J.* 27, 3827–3836. doi: 10.1096/fj.13-228858

O'connor, G., Gleeson, L. E., Fagan-Murphy, A., Cryan, S. A., O'sullivan, M. P., and Keane, J. (2016). Sharpening Nature's Tools for Efficient Tuberculosis Control: A Review of the Potential Role and Development of Host-Directed Therapies and Strategies for Targeted Respiratory Delivery. *Adv. Drug Deliv. Rev.* 102, 33–54. doi: 10.1016/j.addr.2016.04.024

Pavan Kumar, N., Moideen, K., Nancy, A., Viswanathan, V., Shruthi, B. S., Shanmugam, S., et al. (2019). Plasma Eicosanoid Levels in Tuberculosis and Tuberculosis-Diabetes Co-Morbidity Are Associated With Lung Pathology and Bacterial Burden. *Front. Cell Infect. Microbiol.* 9, 335. doi: 10.3389/fcimb.2019.00335

Pedruzzi, G., Das, P. N., Rao, K. V. S., and Chatterjee, S. (2016). Understanding PGE2, LXA4 and LTB4 Balance During Mycobacterium Tuberculosis Infection Through Mathematical Model. *J. Theor. Biol.* 389, 159–170. doi: 10.1016/j.jtbi.2015.10.025

Peres, C. M., De Paula, L., Medeiros, A. I., Sorgi, C. A., Soares, E. G., Carlos, D., et al. (2007). Inhibition of Leukotriene Biosynthesis Abrogates the Host Control of Mycobacterium Tuberculosis. *Microbes Infect.* 9, 483–489. doi: 10.1016/j.micinf.2007.01.006

Rangel Moreno, J., Estrada Garcia, I., de la Luz Garcia Hernandez, M., Aguilar Leon, D., Marquez, R., and Hernandez Pando, R. (2002). The Role of Prostaglandin E2 in the Immunopathogenesis of Experimental Pulmonary Tuberculosis. *Immunology* 106, 257–266. doi: 10.1046/j.1365-2567.2002.01403.x

Singh, P., and Subbian, S. (2018). Harnessing the mTOR Pathway for Tuberculosis Treatment. *Front. Microbiol.* 9, 70. doi: 10.3389/fmicb.2018.00070

Skanland, S. S. (2018). Phospho Flow Cytometry With Fluorescent Cell Barcoding for Single Cell Signaling Analysis and Biomarker Discovery. *J. Vis. Exp.* 140, e58386. doi: 10.3791/58386

Sorgi, C. A., Soares, E. M., Rosada, R. S., Bitencourt, C. S., Zoccal, K. F., Pereira, P., et al. (2020). Eicosanoid Pathway on Host Resistance and Inflammation During Mycobacterium Tuberculosis Infection Is Comprised by LTB4 Reduction But Not PGE2 Increment. *Biochim. Biophys. Acta Mol. Basis Dis.* 1866, 165574. doi: 10.1016/j.bbadis.2019.165574

Stek, C., Allwood, B., Walker, N. F., Wilkinson, R. J., Lynen, L., and Meintjes, G. (2018). The Immune Mechanisms of Lung Parenchymal Damage in Tuberculosis and the Role of Host-Directed Therapy. *Front. Microbiol.* 9, 2603–2603. doi: 10.3389/fmicb.2018.02603

Tay, S., Hughey, J. J., Lee, T. K., Lipniacki, T., Quake, S. R., and Covert, M. W. (2010). Single-Cell NF-kappaB Dynamics Reveal Digital Activation and Analogue Information Processing. *Nature* 466, 267–271. doi: 10.1038/nature09145

Tobin, D. M., Vary, J. C.Jr., Ray, J. P., Walsh, G. S., Dunstan, S. J., Bang, N. D., et al. (2010). The Lta4h Locus Modulates Susceptibility to Mycobacterial Infection in Zebrafish and Humans. *Cell* 140, 717–730. doi: 10.1016/j.cell.2010.02.013

Tonby, K., Ruhwald, M., Kvale, D., and Dyrhol-Riise, A. M. (2015). IP-10 Measured by Dry Plasma Spots as Biomarker for Therapy Responses in Mycobacterium Tuberculosis Infection. *Sci. Rep.* 5, 9223. doi: 10.1038/srep09223

Vilaplana, C., Marzo, E., Tapia, G., Diaz, J., Garcia, V., and Cardona, P. J. (2013). Ibuprofen Therapy Resulted in Significantly Decreased Tissue Bacillary Loads

and Increased Survival in a New Murine Experimental Model of Active Tuberculosis. *J. Infect. Dis.* 208, 199–202. doi: 10.1093/infdis/jit152

Vinhaes, C. L., Oliveira-De-Souza, D., Silveira-Mattos, P. S., Nogueira, B., Shi, R., Wei, W., et al. (2019). Changes in Inflammatory Protein and Lipid Mediator Profiles Persist After Antitubercular Treatment of Pulmonary and Extrapulmonary Tuberculosis: A Prospective Cohort Study. *Cytokine* 123, 154759. doi: 10.1016/j.cyto.2019.154759

Walzl, G., Haks, M. C., Joosten, S. A., Kleynhans, L., Ronacher, K., and Ottenhoff, T. H. M. (2014). Clinical Immunology and Multiplex Biomarkers of Human Tuberculosis. *Cold Spring Harbor Perspect. Med.* 5, a018515. doi: 10.1101/cshperspect.a018515

Wergeland, I., Pullar, N., Assmus, J., Ueland, T., Tonby, K., Feruglio, S., et al. (2015). IP-10 Differentiates Between Active and Latent Tuberculosis Irrespective of HIV Status and Declines During Therapy. *J. Infect.* 70, 381–391. doi: 10.1016/j.jinf.2014.12.019

WHO (2020). *"Global Tuberculosis Report 2020"* (World Health Organization). Available at: https://www.who.int/tb/publications/global_report/en/.

Williams, C. S., Mann, M., and Dubois, R. N. (1999). The Role of Cyclooxygenases in Inflammation, Cancer, and Development. *Oncogene* 18, 7908. doi: 10.1038/sj.onc.1203286

Xiong, W., Dong, H., Wang, J., Zou, X., Wen, Q., Luo, W., et al. (2016). Analysis of Plasma Cytokine and Chemokine Profiles in Patients With and Without Tuberculosis by Liquid Array-Based Multiplexed Immunoassays. *PloS One* 11, e0148885. doi: 10.1371/journal.pone.0148885

Yadav, M., Roach, S. K., and Schorey, J. S. (2004). Increased Mitogen-Activated Protein Kinase Activity and TNF-Alpha Production Associated With Mycobacterium Smegmatis- But Not Mycobacterium Avium-Infected Macrophages Requires Prolonged Stimulation of the Calmodulin/Calmodulin Kinase and Cyclic AMP/Protein Kinase A Pathways. *J. Immunol.* 172, 5588–5597. doi: 10.4049/jimmunol.172.9.5588

Zingarelli, B., Sheehan, M., and Wong, H. R. (2003). Nuclear Factor-kappaB as a Therapeutic Target in Critical Care Medicine. *Crit. Care Med.* 31, S105–S111. doi: 10.1097/00003246-200301001-00015

Conflict of Interest: The authors declare that the research was conducted in the absence of any commercial or financial relationships that could be construed as a potential conflict of interest.

Citation: *Jøntvedt Jørgensen M, Nore KG, Aass HCD, Layre E, Nigou J, Mortensen R, Tasken K, Kvale D, Jenum S, Tonby K and Dyrhol-Riise AM (2021) Plasma LOX-Products and Monocyte Signaling Is Reduced by Adjunctive Cyclooxygenase-2 Inhibitor in a Phase I Clinical Trial of Tuberculosis Patients. Front. Cell. Infect. Microbiol. 11:669623. doi: 10.3389/fcimb.2021.669623*

frontiers in Cellular and Infection Microbiology

ORIGINAL RESEARCH
published: 26 July 2021
doi: 10.3389/fcimb.2021.676456

Mycobacterium tuberculosis Phosphoribosyltransferase Promotes Bacterial Survival in Macrophages by Inducing Histone Hypermethylation in Autophagy-Related Genes

Srabasti Sengupta[1], *Barsa Nayak*[2], *Michael Meuli*[3], *Peter Sander*[3,4], *Snehasish Mishra*[1] *and Avinash Sonawane*[2*]

[1] School of Biotechnology, KIIT Deemed to be University, Bhubaneswar, India, [2] Department of Biosciences and Biomedical Engineering, Indian Institute of Technology Indore, Indore, India, [3] Institut für Medizinische Mikrobiologie, Universität Zürich, Zurich, Switzerland, [4] Nationales Zentrum für Mykobakterien, Zürich, Switzerland

OPEN ACCESS

Edited by:
Daniel E. Voth,
University of Arkansas for Medical Sciences, United States

Reviewed by:
Lu Huang,
University of Arkansas for Medical Sciences, United States
Chinnaswamy Jagannath,
Weill Cornell Medical College of Cornell University, United States

***Correspondence:**
Avinash Sonawane
asonawane@iiti.ac.in

Specialty section:
This article was submitted to Bacteria and Host, a section of the journal Frontiers in Cellular and Infection Microbiology

Received: 05 March 2021
Accepted: 29 June 2021
Published: 26 July 2021

Citation:
Sengupta S, Nayak B, Meuli M, Sander P, Mishra S and Sonawane A (2021) Mycobacterium tuberculosis Phosphoribosyltransferase Promotes Bacterial Survival in Macrophages by Inducing Histone Hypermethylation in Autophagy-Related Genes. Front. Cell. Infect. Microbiol. 11:676456. doi: 10.3389/fcimb.2021.676456

Mycobacterium tuberculosis (Mtb) inhibits autophagy to promote its survival in host cells. However, the molecular mechanisms by which *Mtb* inhibits autophagy are poorly understood. Here, we report a previously unknown mechanism in which *Mtb* phosphoribosyltransferase (*Mtb*PRT) inhibits autophagy in an mTOR, negative regulator of autophagy, independent manner by inducing histone hypermethylation (H3K9me2/3) at the *Atg5* and *Atg7* promoters by activating p38-MAPK- and EHMT2 methyltransferase-dependent signaling pathways. Additionally, we find that *Mtb*PRT induces EZH2 methyltransferase-dependent H3K27me3 hypermethylation and reduces histone acetylation modifications (H3K9ac and H3K27ac) by upregulating histone deacetylase 3 to inhibit autophagy. In summary, this is the first demonstration that *Mtb* inhibits autophagy by inducing histone hypermethylation in autophagy-related genes to promote intracellular bacterial survival.

Keywords: Tuberculosis, *Mycobacterium tuberculosis*, Autophagy, Histone hypermethylation, MAPK pathway, epigenetic modification

INTRODUCTION

Pathogens are equipped with various strategies to dampen the host immune responses. Upon infection, a battle between the host and the pathogen occurs, wherein the pathogen strives to command the host defence, and the host endeavours to eliminate the pathogen. This orchestrated tussle involves alterations in cell-signalling cascades and genome regulatory mechanisms.

Abbreviations: *Mtb*, *Mycobacterium tuberculosis*; *Msm*, *Mycobacterium smegmatis*; PRT, phosphoribosyltransferase; ATG, Autophagy-related proteins; LC3, Microtubule-associated proteins 1A/1B light chain 3B; MAPK, The mitogen activated protein (MAP) kinases; EHMT2, Euchromatic histone-lysine N-methyltransferase 2 also known as G9a; HDAC, Histone deacetylases; $Msm_{pSMT3,}$ *Msm* harbouring pSMT3 plasmid; Mtb_{Prt}, recombinant *Msm* expressing *MtbPrt (Rv3242c)*; *MtbΔPrt*, *Mtb*Prt deletion mutant in *Mtb* H37Rv; BMDM, Bone marrow derived macrophages; CFU, Colony forming units.

Accumulating evidence demonstrates that pathogens can reprogram host gene expression to facilitate their survival by inducing various histone modifications such as methylation, acetylation, and phosphorylation that control the accessibility of activation or repression transcription factors to target genes (Hamon and Cossart, 2008; Allis and Jenuwein, 2016). For example, *Anapalsma phagocytophilum* transcriptionally silences host defence genes by inducing histone deacetylation (Cabezas-Cruz et al., 2016), *Chlamydia trachomatis* promotes histone methylation (Pennini et al., 2010), *Escherischia coli* induces DNA methylation to down-regulate the tumor suppressor CDKN (Tolg et al., 2011), and *Shigella flexneri* infection inhibits MAPK-dependent histone H3 serine 10 (H3S10) phosphorylation to impair the recruitment of nuclear factor-kappa B (NF-κB) at the interleukin-8 (IL-8) promoter (Philpott et al., 2000). Moreover, some bacterial proteins interact with host chromatins to modulate transcription of genes involved in host defence mechanisms (Rolando et al., 2013; Yaseen et al., 2015). Examples include *Listeria monocytogens* listeriolysin O which dephosphorylates H3 and deacetylates H4 to suppress host immunity factors (Hamon et al., 2007) and *Mycobacterium tuberculosis* (*Mtb*) ESAT-6 and LpqH proteins induce histone modifications into the MHC class II transactivator promoter to inhibit MHC-II expression and antigen presentation (Pennini et al., 2006; Kumar et al., 2012). Similarly, *Mtb* Rv1988 hyper-methylates histone H3 to repress host genes involved in the defence against mycobacteria (Yaseen et al., 2015). Another report showed histone methyl transferase SET8 induces H4K20me1 to regulate apoptosis and inflammation to assist *Mtb* survival (Singh et al., 2017). Then, (Chandran et al., 2015) showed that *Mtb* suppresses IL-12B expression *via* HDAC1. Thus, there is considerable evidence that epigenetic modifications are critical determinants of bacterial virulence.

Mtb, which causes human tuberculosis (TB), is one of the most successful and devastating pathogens (Glickman and Jacobs, 2001). This is because *Mtb* is profoundly evolved with plethora of strategies to weaken host immunity. Such strategies include inhibition of phago-lysosome fusion, oxidative stress, antigen presentation, and T-cell immunity (Forrellad et al., 2013). Inhibition of the host's autophagy machinery is another predominant mechanism by which *Mtb* increases intracellular persistence (Deretic et al., 2006; Mohanty et al., 2015). Autophagy involves the synthesis of a double-membrane structure known as the autophagosome, which sequesters cytoplasmic proteins and organelles. These matured autophagosomes then subsequently fuse with acidified lysosomes to degrade their contents (Ohsumi, 2014). This process involves a series of dynamic membrane rearrangements by a set of autophagy-related (ATG) proteins (Mizushima et al., 2011; Nishimura and Tooze, 2020). ATG5 and ATG7 are crucial autophagy-inducing molecules and LC3 is an autophagy indicator (Arakawa et al., 2017). *Mtb* has developed extraordinary attributes to evade autophagy-dependent immune surveillance mechanisms. Induction of autophagy in infected macrophages targeted *Mtb* to lysosomal degradation, thus reducing its intracellular survival (Gutierrez et al., 2004). A genome-wide screen identified 44 autophagy-related genes responsible for the *Mtb* clearance (Kumar et al., 2010). Studies in autophagy-deficient mice also confirmed that autophagy protects against active TB by decreasing bacterial burden and inflammation (Castillo et al., 2012).

Emerging data suggest that p38 mitogen activated protein (p38-MAP) kinase, which links signal transduction molecules during biological processes (Zarubin and Han, 2005), is involved in the inhibition of autophagy. Blockade of p38 MAPK increases autophagy by facilitating the interaction between p38 interacting protein (p38IP) and autophagy protein 9 (ATG9) (Henson et al., 2014). Another report showed that p38 MAPK phosphorylates the autophagy inducer ULK1 protein to inhibit autophagy (He et al., 2018). Despite increasing awareness of the importance of the transcriptional regulation of autophagy during stress conditions, epigenetic control of bacterial infections is a largely unexplored phenomenon. Few reports have demonstrated that histone modifications regulate autophagy to determine cellular fate (Füllgrabe et al., 2014; Lapierre et al., 2015; Byun et al., 2020).

Several studies have clearly demonstrated that *Mtb* inhibits autophagy to promote its intracellular persistence; however, the underlying molecular mechanisms of autophagy inhibition during *Mtb* infection are poorly understood. Our previous study showed that the *Mtb* phosphoribosyltransferase (*Mtb* PRT) enzyme, found in the cell wall of *Mtb*, inhibits autophagy to facilitate *Mtb* persistence inside macrophages and zebrafish (Mohanty et al., 2015). Here, we report for the first time that *Mtb* inhibits autophagy by two concurrent mechanisms; inducing histone methylation enrichment that causes transcriptional repression, and down-regulating histone acetylations that cause transcriptional activation in autophagy-related genes. We report that *Mtb* PRT inhibits autophagy in an mTOR-independent manner by inducing histone H3 lysine 9 (H3K9me2/3) and lysine 27(H3K27me3) hypermethylation at the promoter regions of *Atg5* and *Atg7* genes involved in p38 MAPK-, EHMT2- and EZH2 methyltransferase-dependent signalling pathways. We further show that *Mtb* PRT reduces transcriptional activation H3K9ac and H3K27ac histone modifications by upregulating of HDAC3 (histone deacetylase 3) expression to inhibit autophagy. To the best of our knowledge, this is the first report to demonstrate that *Mtb* introduces both transcriptional activation and repression of epigenetic modifications to inhibit autophagy and aids its cellular persistence.

MATERIALS AND METHODS

Ethical Statement

All experiments were approved by the Institutional Biosafety committee of KIIT University (vide DBT memorandum No-BT/BS/17/493/2012-PID). All the bacterial mutants were handled in adherence to experimental guidelines and procedures approved by the Institutional Biosafety Committee (IBSC) of School of Biotechnology, KIIT University (KIIT/3-12). All studies involving virulent mycobacterial strains were carried out at the BSL-3 facility at Universität Zürich, Zurich (Switzerland).

Animal care and use protocol adhered were approved by national guidelines of the Committee for the Purpose of Control and Supervision of Experiments on Animals (CPCSEA), Government of India.

Chemicals, Reagents and Cell Culture Conditions

Mycobacterium smegmatis mc^2155 was grown in Middlebrook's 7H9 broth medium (Difco, New Jersey, USA) containing 0.05% Tween 80, 0.5% glucose and 0.5% albumin at 37°C on a shaker at 120 rpm. Murine RAW264.7 macrophage cell line was cultured in Dulbecco's Modified Eagle's medium (DMEM; HiMedia, Mumbai, India) supplemented with 10% fetal bovine serum, 1% penicillin-streptomycin solution, and 1% L-glutamine. The cells were seeded onto 24-well and 6-well culture dishes at a density of $2x10^5$ cells/ml and $1x10^7$ cells/ml, respectively and proceeded for experiments. Anti- ATG5, anti-ATG7, anti-Beclin1, anti- H3K9me3, anti- H3K27me3, anti- H3K9ac, anti- H3K27ac, anti-HDAC1, anti-HDAC2, anti-HDAC3, anti-phospho–p38, anti-p62/SQSTM1, anti-GAPDH, anti-β-actin, and secondary goat anti-rabbit and goat anti-mouse antibodies were purchased from Cell Signaling Technologies (Massachusetts, USA). Anti-LC3I/II antibody was purchased from Sigma (Missouri, USA). All the pharmacological inhibitors were purchased from Sigma (Missouri, USA) and Calbiochem (Massachusetts, USA) and reconstituted in DMSO (Himedia, Mumbai, India) or sterile H_2O at the following concentrations: U0126 (10 μM), SB203580 (10 μM), UNC0638 hydrate (5μM), rapamycin (50nM) and 3MA (10mM).

Construction of *M. tuberculosis* Phosphoribosyltransferase Deletion Mutant

A 1.5 kb fragment comprised of the upstream region of *Rv3242c* and 129 bp of the 5' part of *Rv3242c* was amplified with primers (CA'TATGGGTAGTCGTTGACGGTGACG; forward) and (GTT'AACGAGTCGGTCCGGGTCTTG; reverse) containing *NdeI* and *HpaI* restriction sites using *Mtb* H37Rv genomic DNA as a template. Likewise, a 1.4 kbp fragment comprisingof 69 bp of the 3' part of *Rv3242c* and its downstream region was amplified with primers (GTT'AACGTCAACACGAGGACTCACCA, forward and A'CATGTCCAGTTCGCCC TGACCTA, reverse) containing *Hpa* and *PscI* restriction sites. The fragments were initially cloned into pGEM-T Easy vector (Promega, Madison, USA) and transformed into *E. coli* XL1-blue. Recombinant *E. coli* strains were propagated and fragments were isolated from plasmids by restriction enzyme digestion and gel purification and were stepwise cloned into the suicide vector pMCS5-rpsL-hyg, containing a hygromycin resistance cassette for positive selection and an $rpsL^+$ allele for counter-selection in a mycobacteria strain with a*rpsL* mutation conferring streptomycin resistance (Brülle et al., 2013) to result in pMCS5-rpsL-hyg-ΔRv3242c. The plasmid was transformed into electrocompetent *Mtb* SMR strain (Davis et al., 2002). The transformants were selected on 7H10 agar plates containing hygromycin (25 mg/L). Single crossover transformants resulting from intermolecular homologous recombination between the suicide vector and the *Rv3242c* genomic locus were identified by Southern blot analysis and subsequently subjected to counter selection on 7H10 plates containing streptomycin (100 mg/L). Deletion mutant (*MtbΔPrt*) with a 444 bp in-frame deletion in *Rv3242c* were identified by Southern blot analysis of a genomic DNA digested with *AgeI* and hybridized to a 128 bp *Rv3242c* 5' probe amplified with primers (CGTGCGGTTCACCGGC, forward) and (TGACCGCGACACTTGGTGTG, reverse) using genomic DNA as a template.

Western Blot Analysis

RAW264.7 cells were infected with mycobacterial strains. After 24 h of infection, protein samples were prepared by cell lysis using RIPA buffer (HiMedia, Mumbai, India) containing 5mM EDTA, 5mM EGTA, 1 mM PMSF, protease inhibitor cocktail, 50 mM NaF, 1mM DTT and 1mM Sodium orthovanadate. Proteins were electrophoresed in 12% SDS-PAGE and transferred to polyvinylidene difluoride membrane (PVDF) (GE Healthcare Life sciences) overnight at 28 volts. Blots were blocked with 5% BSA or skimmed milk in TBST (20 mM Tris-HCl, pH 7.4, 137 mM NaCl and 0.1% Tween 20) for 60 min. Then the blots were incubated with primary rabbit IgG antibodies (1:1000) overnight at 4°C and then with HRP-conjugated anti-rabbit or anti-mouse IgG secondary antibodies in 5% BSA or skimmed milk (1:1000) for 2 h. The membrane was washed using 1X TBST and X-ray film was developed using standard chemiluminescent solvent. β-actin and GAPDH were used as loading controls. Each desired protein band densities were quantified by ImageJ software with respect to their corresponding loading controls. For LC3, ratio of LC3 I to II (LC3II/LC3I) with respect to corresponding loading control were calculated and plotted onto graphs for representation.

Similarly, mice bone marrow derived macrophages (BMDMs) ($8x10^5$ cells) were infected with mycobacterial strains followed by UNCO638 inhibition for western blot analysis.

Confocal Microscopy

RAW 264.7 macrophages ($5X10^4$) were seeded on coverslips. After infection, the cells were treated with UNCO638, washed with 1XPBS and fixed with 4% PFA followed by incubation for 30 min at 37°C. Then the cells were permeabilized with blocking agent (5% BSA and 0.1% saponin). The cells were then incubated overnight with anti-LC3 antibody (1:250, Sigma, Missouri, USA) at 4°C and then stained with secondary antibodies for 2 h at room temperature. Finally, the cells were mounted in mounting solution with DAPI and the images were analysed using LEICA laser scanning confocal microscope.

RNA Isolation and Quantitative Real-Time RT-PCR

Total RNA was isolated from the infected or uninfected macrophages using TRIzol reagent (Invitrogen, California, USA) as per the manufacturer's protocol. cDNA synthesis kit (Thermofisher Scientific, Massachusetts, USA) was used for reverse transcription according to the manufacturer's protocol. Quantitative real time RT-PCR amplification was performed for quantification of target gene expression using SYBR Green PCR mixture (KAPA Biosystems) in Realplex master cycler

(Eppendorf, Hamburg, Germany) with initial denaturation at 95°C for 10 min, final denaturation at 95°C for 30 s, annealing at 52°C for 30 s and extension at 72°C for 30 s to generate 200-bp amplicons. All reactions were repeated at least thrice independently to ensure reproducibility of the result. The mRNA levels were normalized to the transcript levels of *gapdh* and the relative fold changes were calculated.

Chromatin Immunoprecipitation (ChIP) Assay

For ChIP assay, RAW 264.7 ($1X10^7$) cells were seeded onto 100 mm tissue culture disks and infected with mycobacterial strains. After 24 h of infection, cells were washed twice with 1X PBS and then crosslinked with 11% formaldehyde solution for 15 min followed by 2.5 M glycine treatment for quenching formaldehyde solution. The cells were washed with ice cold 1X PBS twice. The cells were then harvested by scrapping using ice cold 1X PBS and centrifuged at 2500 rpm for 5 min at 4°C followed by washing with 1X PBS. The pellets were resuspended in ice-cold 1ml Farnham buffer and centrifuged at 2000 rpm for 5 min at 4°C. The pellet was resuspended with 300 µl of RIPA buffer and kept on ice for 10 min followed by sonication in Bioruptor at high setting for a total time of 40 min (30 seconds ON and 30 seconds OFF) at 4°C. The chromatin length was verified and proceeded for further steps. The sonicated mixture was centrifuged at 14000 rpm for 15 min at 4°C. The supernatant was collected, quantified and adjusted to volume with RIPA buffer so that each reaction contains 150 µg/ml of chromatin. The suspension was incubated with previously prepared Protein-A sepharose beads for 1h at 4°C in a rotator. After centrifugation at 1500 rpm for 2 min at 4°C, the supernatant was taken and incubated overnight with 6 µg of antibodies against H3K9me2/3 and H3K27me3 per IP in rotator at 4°C. Next day, the suspensions were again incubated with Protein-A sepharose beads for 2 h in rotator at 4°C and centrifuged at 2000 rpm for 1 min. The pellets were washed using LiCl wash buffer (7-8times) and TE buffer (once). The pellet was dissolved in IP elution buffer for 30 min at RT and the supernatants were left at 65°C overnight for reverse cross-linking. Next day, RNA and protein were digested with RNase and Proteinase K to obtain purified DNA. Isolated DNA was further processed for qPCR using specific primers for *Atg5, Atg7* and *gapdh*promoters. The qPCR data were normalized to input DNA. Primers for *gapdh* promoter were used as a negative control.

Macrophage Infection Assay

Msm harbouring pSMT3 plasmid *(Msm_{pSMT3})* and recombinant *Msm* expressing *Mtb PRT (Rv3242c)* (*Mtb_{Prt}*) strains were grown to mid-exponential phase. Bacterial cultures were pelleted, washed in 1X PBS and re-suspended in DMEM medium to a final OD_{600} 0.1. Bacterial clumps were broken by ultrasonication for 5 min followed by a low-speed centrifugation for 2 min. RAW264.7 macrophages ($2x10^5$ cells/well) were seeded on 24-well tissue culture plates with media containing no antibiotic solution and grown for 18-20 h. The cells were infected at a multiplicity of infection (MOI) 10, treated with UNCO638 (5µm) and intracellular bacterial survival was determined by lysis of infected macrophages with 0.5% Triton-X 100 at different time points and plating the serially diluted samples onto 7H9 plates. The equal input and time zero (T_0) count of infecting bacilli were determined to calculate the percentage survival (% survival= CFU at specific time/CFU of bacteria added for infection X 100).

To determine the intracellular survival of *Mtb* and *MtbΔPrt*, RAW 264.7 ($2.5 X 10^5$) cells were seeded onto 48-well plate and infected at a MOI of 1. After 0, 3 and 5 days of infection, the adherent cells were covered with ice cold dH_2O for 10 min at RT followed by further incubation with 7H9 media and 0.17% SDS. The pellets were resuspended, plated onto 7H10 plates and incubated at 37°C followed for CFU enumeration.

Isolation of BMDM

Six to eight weeks old Balb/C mice were sacrificed by cervical dislocation. The femur and tibia bones were flushed with RPMI by inserting a 26-gauge needle. The marrow was dispersed by passing through a 19-gauge needle twice. The isolated cells were passed through a 70 µm cell strainer (Himedia, Mumbai, India). The strained cells were centrifuged at 1500 rpm for 5 min at 4°C and the cell pellet was washed with 1X RBC lysis buffer (Sigma, Missouri, USA) to remove the contaminating RBCs. The cells were briefly centrifuged, washed and counted after staining with trypan blue (Sigma, Missouri, USA) counterstain. Appropriate number of cells were seeded onto 6 well plate in presence of 20 ng/ml recombinant macrophage colony stimulating factor (M-CSF) for 7 days and then used for infection assays.

Statistical Analysis

All experiments were performed at least three times (n=3). Statistical analyses were performed using the Mann-Whitney U-test (two-tailed, equal variances). Significance was referred as: *** for $P<0.001$, ** for $P \leq 0.01$ and * for $P \leq 0.05$.

RESULTS

M. tuberculosis Phosphoribosyltransferase Inhibits Autophagy Through an mTOR-Independent Mechanism

Mtb inhibits autophagy to increase its intracellular persistence (Deretic et al., 2006; Chandra et al., 2015). Our recent study showed that *Mtb* PRT, encoded by *Rv3242c*, promotes mycobacterial survival in macrophages and zebrafish by inhibiting autophagy (Mohanty et al., 2015). Based on these observations, we first determined the expression of various autophagy markers such as LC3I/II, Atg5, Atg7, Beclin-1 and sequestosome 1 p62/SQSTM1 in uninfected and *Mtb* PRT-exposed macrophages. For this, we used two models. First, wild-type *Mtb* PRT was episomally expressed in *Mycobacterium smegmatis* (*Mtb_{Prt}*), and we also constructed *Mtb* PRT deletion mutant (*MtbΔPrt*). *Mycobacterium smegmatis* (*Msm)* is an established surrogate model organism for the study of *Mtb* virulence proteins (Mohanty et al., 2015; Yaseen et al., 2015; Mohanty et al., 2016; Padhi et al., 2016; Sethi et al., 2016; Padhi

et al., 2019). Mtb_{Prt} -exposed macrophages had lower expression of autophagic markers such as Atg-5 and Atg-7 (**Figure 1A**), which are recruited to the phagosomal compartments during autophagic vesicle formation. Moreover, the conversion of LC3-I to the characteristic autophagic induction marker LC3-II (**Figure 1B**) was lower than Msm_{pSMT3}-infected (vector control) and uninfected macrophages. Autophagy is also characterized by the distribution of LC3 protein as puncta in the cytoplasm. Confocal microscopy showed LC3 puncta were less-widely distributed in Mtb_{Prt}-infected macrophages (**Figure 1C**). We also examined the expression of the autophagic flux marker p62 (SQSTM1). During autophagy induction, p62/SQSTM1 binds to LC3 and is subsequently degraded, however when autophagy is inhibited, p62 accumulates (Pankiv et al., 2007). As shown in **Figure 1D**, p62/SQSTM1 accumulated in Mtb_{Prt}-infected macrophages but not in Msm_{pSMT3}-infected cells. In accordance with our previous report (Mohanty et al., 2015), Mtb_{Prt} did not significantly alter the expression of Beclin1 (**Figure 1E**). As anticipated, treatment with an autophagy inducer (rapamycin, 50 nM) or inhibitor (3-methyladenine, 10mM) significantly induced or inhibited Atg-5, Atg-7, LC3-II and p62 proteins, respectively. We did not observe any measurable differences in the level of in phospho-mTOR (p-mTOR), an autophagy regulator, in Mtb_{Prt}-exposed and control macrophages (**Figure 1E**). These results indicate that *Mtb* PRT inhibits autophagy through an mTOR-independent mechanism.

To confirm the role of *Mtb* PRT in autophagy inhibition, we compared the expression of Atg-5 and LC3-II in *Mtb* H37Rv-(wild-type) and *MtbΔPrt* mutant-infected macrophages. Macrophages infected with *Mtb ΔPrt* (**Figure S1**) had higher expression of Atg-5 and LC3-II (**Figure 1F**) than *Mtb* H37Rv-infected macrophages.

Comparative genomic analysis showed that the *Msm* genome contains MSMEG_1877, an orthologue of *Mtb* PRT. To preclude an effect of MSMEG_1877 in autophagy inhibition, we checked the expression of LC3-I/II, Atg-5 and Atg-7 in macrophages infected with an *Msm* strain that over-expressed *MSMEG_1877*. Autophagy was not inhibited in these macrophages (**Figure 1G**), indicating that only *Mtb* PRT, and not MSMEG_1877, is involved in autophagy inhibition. Here, and in our previous studies, we found that the *Mtb* PRT deletion mutant (*MtbΔPrt*) did not inhibit autophagy, whereas *Mtb* PRT inhibit autophagy,

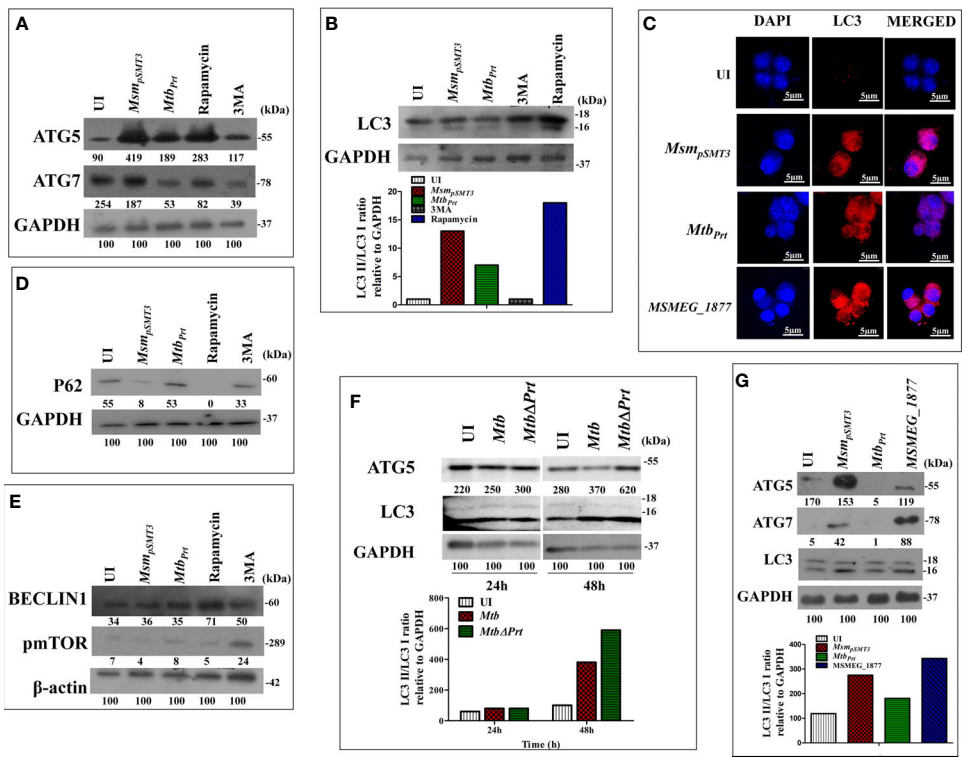

FIGURE 1 | Expression of Autophagy related genes in Msm_{pSMT3}, Mtb_{Prt}, *Mtb*H37Rv, *MtbΔPrt* and *MSMEG_1877* infected macrophages. RAW264.7 cells were infected with Msm_{pSMT3} and Mtb_{Prt} for 24 h. The level of **(A)** ATG5 and ATG7 expression at protein level was checked by western blotting. The conversion of LC3I to II was estimated using **(B)** western blotting (Densitometry is representative to the particular western blot data) and **(C)** confocal microscopy using LC3I/II specific antibodies. The level of **(D)** P62**, (E)** Beclin1 and phospho- mTOR expression at protein level was checked by western blotting in RAW264.7 infected with Msm_{pSMT3} and Mtb_{Prt}. **(F)** The level of ATG5 and conversion of LC3-I to II was checked in *Mtb* H37Rv and *Mtb ΔPrt* infected RAW264.7 cells by western blotting after 48 h of infection. **(G)** The conversion of LC3I to II, ATG5 and ATG7 expression in RAW264.7 infected with Msm_{pSMT3}, Mtb_{Prt} and *MSMEG_1877* was checked by western blotting. The experiments were performed in triplicate (n=3). Msm_{pSMT3}- *Msm* harbouring pSMT3 plasmid; Mtb_{Prt}- recombinant *Msm* expressing *MtbPrt (Rv3242c)*; *MtbΔPrt –Mtb* Prt deletion mutant in *Mtb* H37Rv.

and so we selected the Mtb_{Prt} strain (unless otherwise mentioned) for further experiments.

M. tuberculosis Phosphoribosyltransferase Induces Histone Hypermethylation in Macrophages

Several pathogenic bacteria such as *S. flexneri, L. monocytogenes, Helicobacter pylori* and *Mtb* induce histone modifications to alter host immune responses in favour of a pathogen (Hamon et al., 2007; Hamon and Cossart, 2008; Ohsumi, 2014). Few epigenetic modifications regulate autophagy under non-infectious disease conditions (Artal-Martinez de Narvajas et al., 2013; Füllgrabe et al., 2014; Baek and Kim, 2017). H3K9me2/3 and H3K27me3 are histone modifications that predominantly repress transcription (Bannister et al., 2001; Ngollo et al., 2017). Therefore, we hypothesised that *Mtb* PRT may inhibit autophagy by introducing histone modifications that repress transcription of autophagy-related genes. Indeed, our western blot analysis showed that the levels of H3K9me2/3 (**Figure 2A**) and H3K27me3 (**Figure 2B**) were significantly higher in Mtb_{Prt} (*M. smegmatis* harbouring *Mtb PRT*) infected macrophages than in Msm_{pSMT3} (*M. smegmatis* harbouring only pSMT3 vector)-infected cells, suggesting that these modifications play a role in regulating autophagy. Rapamycin treatment down-regulated H3K9me2/3 and H3K27me3 levels, whereas 3MA treatment increased these histone modifications (**Figures 2A, B**).

Few bacterial proteins are able to concomitantly induce different histone modifications to change the dynamics of host gene expression to favour pathogen survival (Pennini et al., 2006; Hamon et al., 2007; Kumar et al., 2012; Yaseen et al., 2015). As detailed above, transcription was repressed in *Mtb* PRT-infected macrophages. Next, we examined the effect of *Mtb* PRT on the activation of transcription, *i.e.*, H3K9 and H3K27 acetylation modifications. We observed that the levels of H3K9ac (**Figure 2C**) and H3K27ac (**Figure 2D**) were significantly lower in Mtb_{Prt}-infected cells than in Msm_{pSMT3}-infected macrophages, suggesting that *Mtb* PRT can induce dual histone modifications, *i.e.*, histone hypermethylation and histone deacetylation. Further, the levels of H3K9me2/3 and H3K27me3 did not change in *Mtb ΔPrt*-infected macrophages (**Figure 2E**). We confirmed that the *Mtb* PRT orthologue MSMEG_1877 does not affect these histone modifications.

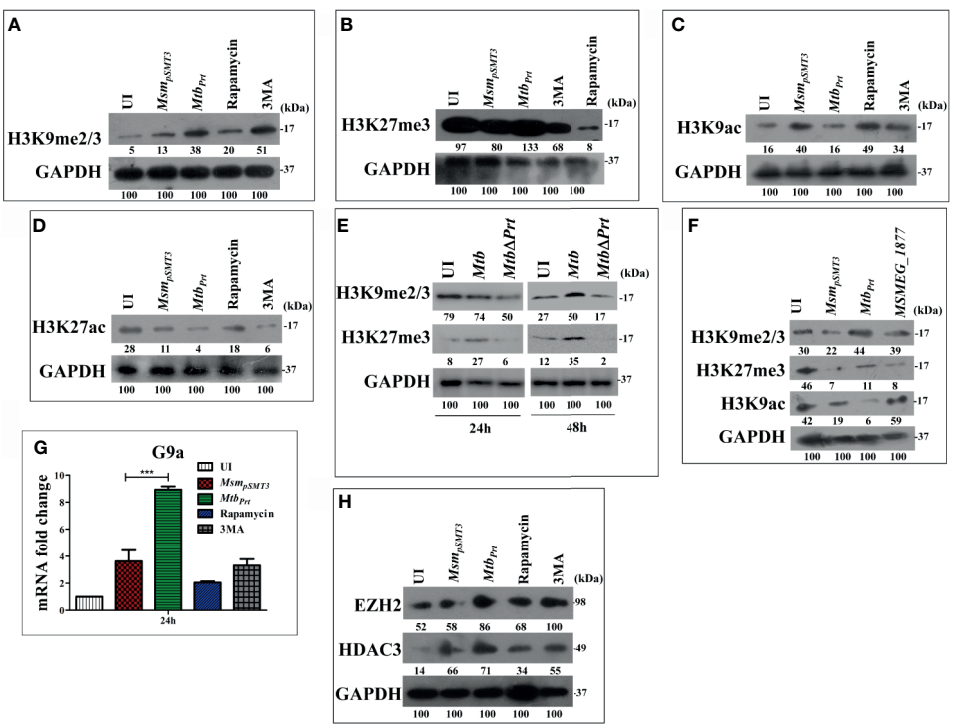

FIGURE 2 | Expression of Histone hypermethylation and acetylation in RAW macrophages infected with Msm_{pSMT3}, Mtb_{Prt}, *Mtb* H37Rv, *Mtb ΔPrt* and *MSMEG_1877*. RAW264.7 cells were infected with Msm_{pSMT3} and Mtb_{Prt} for 24 h. Additionally, RAW 264.7 cells were treated with rapamycin and 3MA for 2 h. The expression of **(A)** H3K9me2/3, **(B)** H3K27me3, **(C)** H3K9ac and **(D)** H3K27ac was checked at protein level by western blotting using specific antibodies. **(E)** The level of H3K9me2/3 and H3K27me3 was checked in *Mtb* H37Rv and *Mtb ΔPrt* infected RAW264.7 cells by western blotting after 24 and 48 h of infection. **(F)** The expression of H3K9me2/3, H3K27me3 and H3K9ac in RAW264.7 infected with Msm_{pSMT3}, Mtb_{Prt} and *MSMEG_1877* was checked by western blotting. **(G)** The expression of G9a was checked at transcription level by qRT-PCR in macrophages infected with Msm_{pSMT3} and Mtb_{Prt} for 24 h. **(H)** The level of EZH2 and HDAC3 was checked by western blotting in macrophages infected with Msm_{pSMT3} and Mtb_{Prt} for 24 h. For qRT-PCR, *GAPDH was* taken as an internal control. The experiments were performed in triplicate (n=3). Results are shown as mean ± S.D. (error bars); ***$p \leq 0.001$. Msm_{pSMT3}- *Msm* harbouring pSMT3 plasmid; Mtb_{Prt}-recombinant *Msm* expressing *Mtb Prt (Rv3242c)*; *MtbΔPrt –Mtb* Prt deletion mutant in *Mtb* H37Rv.

The expression levels of H3K9me2/3, H3K27me3 and H3K9ac (**Figure 2F**) were significantly lower in Msm_{pSMT3}- and *MSMEG_1877*-infected macrophages than in Mtb_{Prt}-infected cells. These results suggest that *Mtb* PRT, but not MSMEG_1877, induces histone modifications that repress transcription.

Induction of Histone Hypermethylation and Histone Deacetylation Is Mediated Through EHMT2/G9a Methyltransferase and Histone Deacetylase 3

Several histone methyltransferases such as Eset, KMT1E, G9a/EHMT2, Suv38H1 and EZH2 are responsible for histone hypermethylation. G9a (also known as euchromatin histone-lysine N-methyltransferase2, EHMT2) is a key histone methyltransferase that methylates H3K9. EZH2, a catalytic subunit of polycomb repressive complex 2 (PRC2), is another highly conserved histone methyltransferase that hypermethylates H3K27 (Fritsch et al., 2010). Next, we aimed to identify the specific methyltransferases responsible for *Mtb* PRT-induced histone hypermethylation. The expression of G9a (**Figure 2G**; $P \leq 0.001$) and EZH2 (**Figure 2H**) methyltransferases were significantly higher in Mtb_{Prt}-infected macrophages.

Next, we attempted to identify the histone deacetylase enzyme that reduces H3K9 and H3K27 acetylation in Mtb_{Prt}-infected cells. Histone deacetylation is catalysed by various histone deacetylases (HDAC) such as HDAC1, HDAC2 and HDAC3 (Seto and Yoshida, 2014). Specifically, H3K9 and H3K27 deacetylation is induced by HDAC1, HDAC2 and HDAC3 (Večeřa et al., 2018; Præstholm et al., 2020; Gandhi et al., 2021).We observed that the level of HDAC3 was higher in Mtb_{Prt}-infected macrophages than in control cells (**Figure 2H**), whereas HDAC1 and HDAC2 expression levels did not change (**Figure S2**). These data show that *Mtb* PRT-induced HDAC3 expression mediates H3K9 and H3K27 deacetylation.

H3K9 Hypermethylation at the Atg5 and Atg7 Promoters *via* G9a Methyltransferase Activity Mediates Autophagy Inhibition

Since we observed autophagy inhibition and increase in the levels of H3K9me2/3 and H3K27me3 modifications in Mtb_{Prt}-infected macrophages, we performed ChIP-qPCR assay to enumerate the enrichment of these two histone hypermethylation modifications at the promoter region of autophagy-related genes. H3K9me2/3 was significantly enriched at the promoter regions of both *Atg5* (**Figure 3A**; $P \leq 0.01$) and *Atg7* (**Figure 3B**;$P \leq 0.001$) in response to Mtb_{Prt} bacterial infection, while no such enrichment was observed in uninfected and Msm_{pSMT3}-infected cells. However, H3K27me3 was not enriched at either *Atg5* (**Figure 3C**) or *Atg7* (**Figure 3D**) promoters under similar infection conditions. These results suggest that *Mtb* PRT inhibits autophagy by promoting H3K9me2/3 at the *Atg5* and*Atg7* promoters. As *Mtb* PRT did not alter Beclin1 expression, we did not investigate H3K9me2/3 enrichment at the Beclin1 promoter.

To investigate if the H3K9me2/3 enrichment at the *Atg5* and *Atg7*promoters is dependent on G9a, we used the G9a inhibitor UNCO638 (5μM). Results of ChIP-qPCR analysis showed that inhibition of G9a significantly reduced the enrichment of H3K9me2/3 at the *Atg5* and *Atg7* promoters in Mtb_{Prt}-infected cells (**Figure 3E**; $P \leq 0.01$, $P \leq 0.05$), thus strongly supporting the role of G9a in H3K9me2/3 enrichment at the *Atg5* and *Atg7* promoters. We did not perform a ChIP-qPCR assay with an EZH2 inhibitor due to absence of H3K27me3 enrichment at either the *Atg5* or *Atg7* promoters.

Inhibition of G9a Methyltransferase Abrogates H3K9me2/3- Mediated Autophagy Inhibition

Because our above results established that *Mtb* PRT induces H3K9me2/3 at the *Atg5* and *Atg7* promoters, we further investigated the role of G9a mediated-H3K9me2/3 in autophagy inhibition. Immunoblot analysis showed that G9a inhibitor (UNCO638) treatment abrogated the induction of H3K9me2/3 after Mtb_{Prt}-infection (**Figure 3F**). Next, we investigated the effect of UNCO638 on the expression of autophagy-related proteins. We found that G9a inhibition reversed the down-regulation of ATG5 and ATG7 (**Figure 3G**) and LC3 (**Figure 3H**) by *Mtb* PRT. Confocal microscopy analysis showed that UNCO638 significantly increased in the number of LC3 puncta in Mtb_{Prt}-infected cells (**Figure 3I**). These results clearly indicate that the inhibition of autophagy by *Mtb*Prt was due to G9a-dependent H3K9me2/3 hypermethylation.

Down-Regulation of H3K9me2/3 Augments Clearance of Mtb_{Prt}

Our previous results indicated that the presence of *Mtb* PRT inside macrophages inhibits autophagy to promote mycobacterial survival (Mohanty et al., 2015). In contrast, deletion of *Mycobacterium marinum mimG* (*MmΔmimG*), an orthologue of *Mtb* PRT, decreases bacterial survival and TB pathology in zebrafish (Mohanty et al., 2015). In the present study we also found that the deletion of *Mtb* PRT reduced the survival of the *MtbΔPrt* mutant in macrophages (at day 5) compared with wild-type *Mtb* (**Figure 3J**; $P \leq 0.001$). Next, we assessed the impact of H3K9 hypermethylation and autophagy inhibition on the intracellular survival of *Mtb*. We observed that, in contrast to the untreated cells, inhibition of G9a decreased the survival of intracellular Mtb_{Prt} 24 h after infection (**Figure 3K**; $P \leq 0.001$); inhibition of autophagy further increased the survival of Mtb_{prt} (**Figure S3**). Altogether these findings strongly suggest that *Mtb* PRT promotes bacterial survival by inhibiting autophagy through histone hypermethylation.

M. tuberculosis Phosphoribosyltransferase Induces H3K9 Hypermethylation Followed by Autophagy Inhibition Is Dependent on the p38-MAPK Signalling Pathway

MAPK pathways regulate eukaryotic gene expression by inducing epigenetic modifications (Vermeulen et al., 2009). Previously, we showed that *Mtb* PRT activates p-ERK and p38-

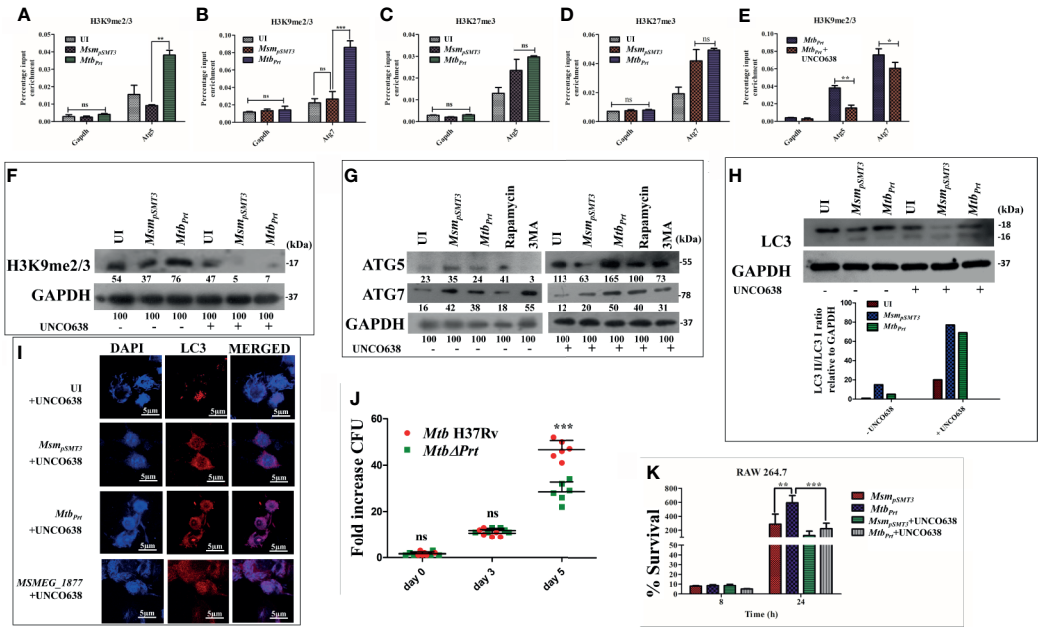

FIGURE 3 | Role of H3K9 and H3K27 hypermethylation in inhibition of autophagy by Mtb_{Prt}.. ChIP assay was performed to check the H3K9me2/3 enrichment at **(A)** *Atg5* and **(B)** *Atg7* promoter after infecting RAW264.7 with Msm_{pSMT3} and Mtb_{Prt}. To check the H3K27me3 enrichment at **(C)** *Atg5* and **(D)** *Atg7*, ChIP assay was performed after infecting RAW macrophages with Msm_{pSMT3} and Mtb_{Prt}. **(E)** ChIP assay was performed to check the H3K9me2/3 enrichment after treatment with G9a inhibitor. Quantification of the data was done by qRT-PCR using gene specific ChIP primers. RAW264.7 cells were infected with Msm_{pSMT3} and Mtb_{Prt} followed by treatment with UNC0638 (G9a inhibitor) for 24 h. Expressions of **(F)** H3K9me2/3, **(G)** ATG5 and ATG7, and **(H)** LC3-I to II conversion were checked by western blotting after 24 h of infection (Densitometry is representative to the particular western blot data). **(I)** LC3 puncta formation was confirmed by performing confocal microscopy in cells infected with Msm_{pSMT3}, Mtb_{Prt} and *MSMEG_1877* followed by treatment with UNCO638 treatment for 24 h. **(J)** RAW264.7 were infected with *Mtb* H37Rv and *Mtb ΔPrt* strains. Cells were lysed and intracellular survival was determined 0, 3- and 5-days post-infection by a CFU assay. **(K)** RAW 264.7 were infected with Msm_{pSMT3} and Mtb_{Prt} strains followed by UNCO638 treatment. Cells were lysed and intracellular bacterial survival was determined 8 and 24 h post-infection by a CFU assay. Experiments were performed in triplicate (n = 3). Results are shown as mean ± S.D. ***p ≤ 0.001; **p ≤ 0.01; *p ≤ 0.05.; ns, not significant. Msm_{pSMT3}- *Msm* harbouring pSMT3 plasmid; Mtb_{Prt}- recombinant *Msm* expressing *Mtb Prt (Rv3242c)*; *MtbΔPrt –Mtb* Prt deletion mutant in *Mtb* H37Rv.

MAPK signalling pathways (Mohanty et al., 2015). In this context, we investigated if MAPK signalling cascades regulate H3K9me2/3 and autophagy. First, we evaluated the level of G9a transcripts in the presence and absence of ERK (U0126, 10μM) and p38 (SB203580, 10μM) inhibitors. The p38 inhibitor decreased G9a expression in Mtb_{Prt}-infected cells (**Figure 4A**; $P \leq 0.001$) but the ERK inhibitor did not decrease G9a expression (**Figure 4B**). This result suggests that p38-MAPK plays a role in H3K9me2/3 modification and autophagy inhibition. We confirmed that treatment with SB203580 inhibitor abated the induction of p38 by Mtb_{Prt} (**Figure 4C**). Next, we assessed the expression of ATG5, ATG7 and LC3I/II in the presence and absence of the p38 inhibitor. SB203580 significantly inhibited expression levels of ATG5 (**Figure 4D**), ATG7 (**Figure 4D**) and LC3I/II (**Figure 4E**) in Mtb_{Prt}-infected cells. These results confirm that the inhibition of autophagy by *Mtb* PRT induced H3K9 hypermethylation is dependent on the p38-MAPK signalling pathway. Finally, we investigated the effect of SB203580 on the expression of H3K9me2/3, H3K9ac and HDAC3. The immunoblot analysis demonstrated that p38 inhibition decreased the expression of H3K9me2/3 (**Figure 4F**) and increased the level of H3K9ac (**Figure 4G**) in Mtb_{Prt}-infected macrophages. An increase in H3K9ac could be attributed to reduced expression of HDAC3 due to inhibition of p38 expression (**Figure 4G**). These results suggest that *Mtb* PRT-mediated H3K9 hypermethylation followed by autophagy inhibition is facilitated by activation of the p38-MAPK signalling pathway.

M. tuberculosis Phosphoribosyltransferase Induces Histone Hypermethylation and Inhibits Autophagy in Murine Bone Marrow-Derived Macrophages

To confirm our key findings from a murine cell line (RAW264.7 macrophages), we performed representative experiments in primary bone marrow-derived macrophages (BMDM) isolated from Balb/C mice. The expression of LC3-II (**Figure 5A**), ATG5 and ATG7 (**Figure 5B**) was lower in Mtb_{Prt}-infected BMDM than in uninfected cells, and inhibition of G9a increased the expression of these autophagic proteins. Similarly, H3K9me2/3 (**Figure 5C**) was higher in Mtb_{Prt}-infected BMDM than in uninfected cells, and this effect was reversed by inhibition of G9a methyltransferase. Thus, similar data obtained in BMDM and RAW264.7 macrophages confirmed that *Mtb* PRT induces epigenetic modifications to inhibit autophagy and augment *Mtb* persistence in macrophages.

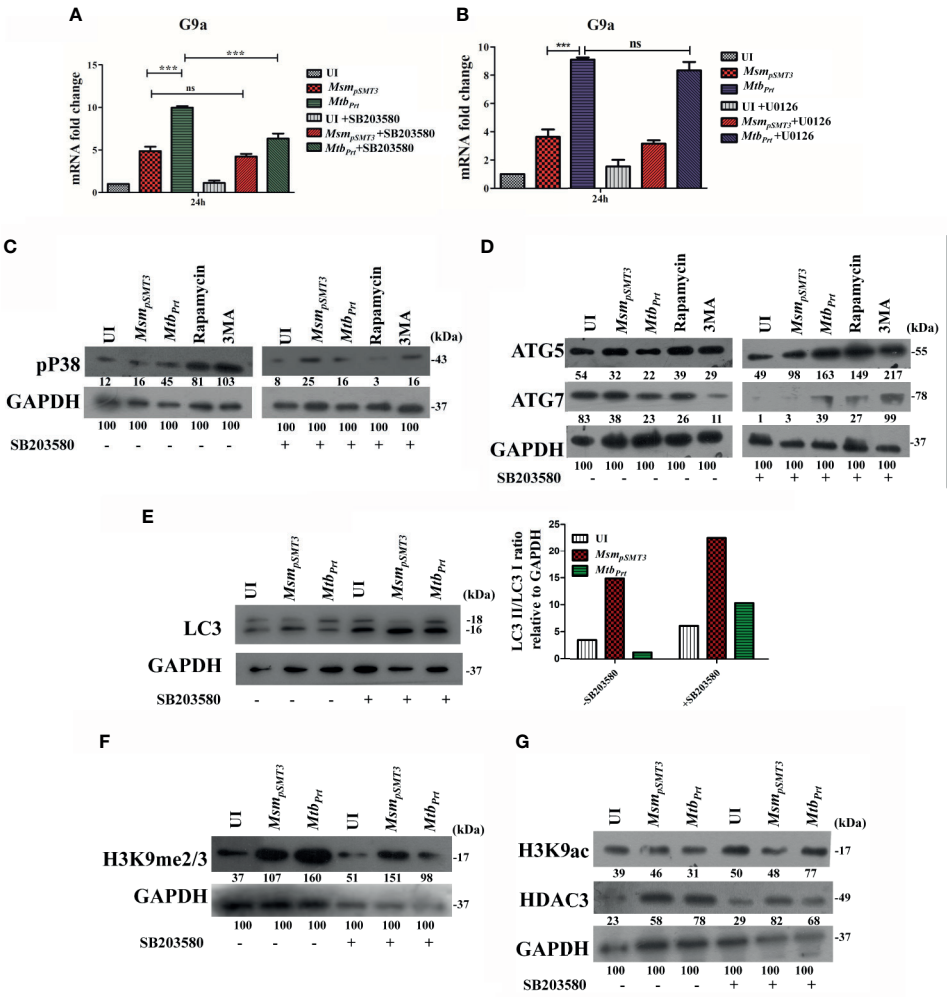

FIGURE 4 | Role of MAPK in H3K9 hypermethylation and autophagy inhibition. Expression of G9a transcripts was checked in RAW264.7 cells infected with Msm_{pSMT3} and Mtb_{Prt} followed by treatment with **(A)** SB203580 and **(B)** U0126 for 24 h. Expression of **(C)** p-P38, **(D)** ATG5 and ATG7, **(E)** LC3-I to II conversion (Densitometry is representative to the particular western blot data), **(F)** H3K9me2/3, **(G)** H3K9ac and HDAC3 were checked in RAW cells infected with Msm_{pSMT3} and Mtb_{Prt} in presence and absence of SB203580 (P38 inhibitor) for 24 h. The experiments were performed in triplicate (n=3). Msm_{pSMT3}- *Msm* harbouring pSMT3 plasmid; Mtb_{Prt}- recombinant *Msm* expressing *MtbPrt (Rv3242c)*. Results are shown as mean ± S.D. ***p < 0.001; ns, not significant.

DISCUSSION

Mtb employs various strategies to evade host immune responses. One mechanism involves reprogramming of host genes to modulate autophagy, thereby avoiding killing by host cells (Deretic, 2014). However, the molecular mechanisms that underlie autophagy inhibition by *Mtb* are poorly understood. Here, we report that *Mtb* PRT inhibits autophagy through an mTOR independent mechanism to promote mycobacterial persistence inside the macrophages (**Figure 6**).

Atg5 is an autophagy-related gene that is crucially involved in *Mtb*-mediated autophagy inhibition. We found that the presence of *Mtb* PRT in macrophages significantly down-regulated the expression of LC3-II, ATG5 and ATG7. These molecules are involved in the formation of the ATG5–ATG12 complex, which is responsible for the elongation and closure of autophagosomes, generation of lipidated forms of LC3 and their localisation to the autophagosome membrane (Mizushima et al., 2011; Ohsumi, 2014; Arakawa et al., 2017; Nishimura and Tooze, 2020). In agreement with our previous report, we observed that *Mtb* PRT did not alter the expression of Beclin1, which after dissociation from the apoptosis regulator Bcl2 forms a complex with hVps34. This complex is important for the crosstalk between autophagy and apoptosis (Liang et al., 2006). Thus, the absence of any effect of *Mtb* PRT on beclin1 suggests that *Mtb* PRT is involved in autophagy but not apoptosis. To understand the underlying molecular mechanism(s) of *Mtb* infection, we investigated how epigenetic modifications contribute to *Mtb* PRT-mediated inhibition of autophagy. We found that *Mtb* infection increased H3K9, H3K27 hypermethylation (involved in

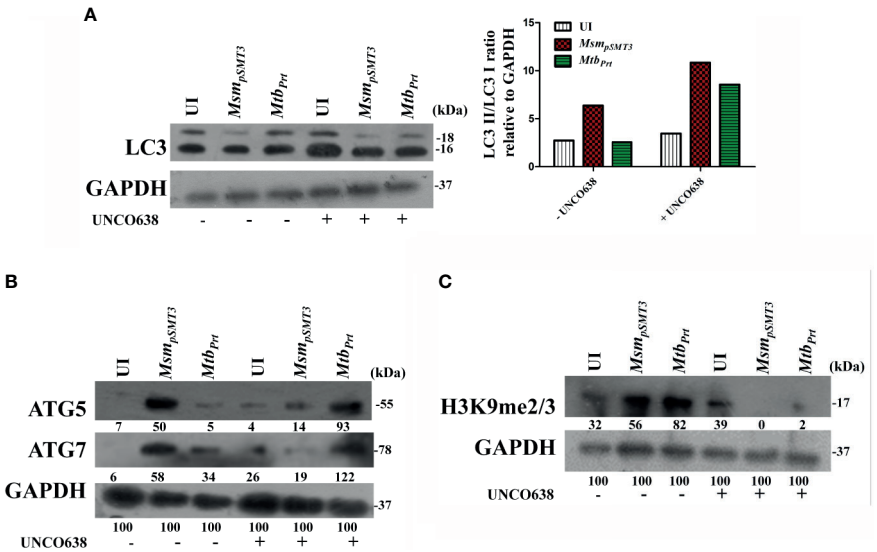

FIGURE 5 | Expression of histone hypermethylation and autophagy in bone marrow derived macrophages infected with Msm_{pSMT3} and Mtb_{Prt}. Bone marrow derived macrophages were infected with Msm_{pSMT3} and Mtb_{Prt} strains followed by treatment with UNCO638 (G9a inhibitor) for 24 h. Western blot analysis was performed to check the **(A)** conversion of LC3I to II (Densitometry is representative to the particular western blot data), and expression of **(B)** ATG5 and ATG7, and **(C)** H3K9me2/3. The experiments were performed in triplicate (n=3). Msm_{pSMT3}- *Msm* harbouring pSMT3 plasmid; Mtb_{Prt}- recombinant *Msm* expressing *MtbPrt (Rv3242c)*.

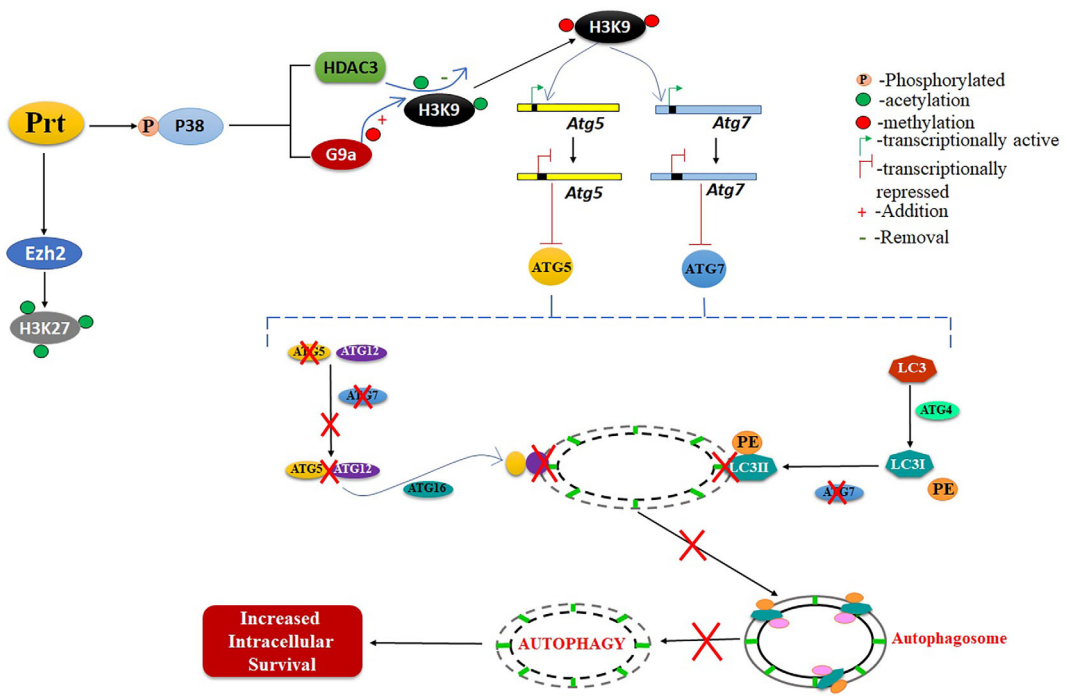

FIGURE 6 | Schematic representation of role of *Mtb*PRT in induction of histone hypermethylation, which down regulates the autophagy. This downregulation of autophagy leads to increased intracellular survival.

transcription repression), and reduced H3K9 and H3K27 acetylation (involved in transcription activation). These results suggest that *Mtb* PRT performs dual histone modifications to favour *Mtb* survival. Histone hypermethylation is catalysed by histone methyltransferases such as G9a, Suv39h1/h2 (which catalyses H3K9 hypermethylation) and Ezh2 (which catalyses H3K27 hypermethylation) (Mozzetta et al., 2015). Our results indicate that G9a and EZH2 are involved in the induction of H3K9 and H3K27 hypermethylation in infected macrophages. On the other hand, *Mtb* PRT caused a significant decrease in H3K9ac and H3K27ac in exposed macrophages. Histone deacetylation is catalysed by histone deacetylases (HDACs) such as HDAC1, HDAC2, HDAC3 and sirtuans (Seto and Yoshida, 2014). We found that HDAC3 is predominantly responsible for deacetylation during Mtb_{Prt} infection. Together, these results suggested that *Mtb* PRT induced histone hypermethylation and deacetylation events are responsible for the alteration of autophagy. The concurrent induction of histone hypermethylation and deacetylation has been shown in previous reports during chromosome condensation and cell cycle progression (Park et al., 2011). The levels of H3K9 and H2K27 hypermethylation and H3K9 and H3K27 deacetylation did not change inmacrophages treated with rapamycin (an autophagy inducer) or 3MA (an autophagy inhibitor), indicating that both hypermethylation and deacetylation are upstream of autophagy and are specific to *Mtb* PRT.

Hypermethylation of lysine residues on histone proteins leads to the formation of condensed chromatin which represses the transcription by preventing the binding of transcription factors (Park et al., 2011; Mozzetta et al., 2015). Thus, H3K9me2/3 or H3K27me3 enrichment at the promoter regions of target genes will inactivate transcription. Our ChIP-qPCR assay showed that H3K9me2/3, but not H3K27me3, increased at the promoters of *Atg5* and *Atg7*genes in macrophages expressing *Mtb* PRT. This finding indicates that H3K9me2/3 predominantly mediates repression of *Atg5* and *Atg7* genes, while H3K27me3 may be involved in the repression of genes other than *Atg5* and *Atg7*. Overall, our results demonstrate that *Mtb* PRT inhibits autophagy by specifically recruiting H3K9me3 at the *Atg5* and *Atg7* promoters.

We showed that *Mtb* PRT induces H3K9me2/3 by up-regulating G9a methyltransferase. Chemical inhibition of G9a decreased H3K9me2/3 expression and at the same time increased in the expression of LC3-II, ATG5 and ATG7, thus confirming that G9a methyltransferase-induced H3K9 hypermethylation is responsible for autophagy inhibition. Non-pathogenic mycobacteria such as *Msm* are readily killed by macrophages, whereas pathogenic *Mtb* survive inside macrophages (Rahman et al., 2014). Our previous report showed that episomal expression of *Mtb* PRT in non-pathogenic *Msm* increased bacterial survival in macrophages (Mohanty et al., 2015). Here, we demonstrated that deletion of *MtbPrt* (*MtbδPrt)* reduced the survival of bacteria in macrophages. These results suggest that *Mtb* PRT is a virulence factor important for *Mtb* survival. Inhibition of G9a, which demethylates H3K9, decreased the intracellular survival of *Mtb* PRT. Conversely, infection with the *MtbδPrt* mutant reduced H3K9 hypermethylation and increased H3K9ac and autophagy. Thus, our previous and present results indicate that *Mtb* PRT induces H3K9 hypermethylation by upregulating G9a methyltransferase, which inhibits autophagy, and inhibition of autophagy subsequently promotes intracellular bacterial survival.

The MAPK signaling pathway plays a crucial role in mycobacterial infection (Pasquinelli et al., 2013; Mohanty et al., 2016), yet only a limited number of mycobacterial proteins are known to induce epigenetic modifications in p38-MAPK-dependent pathways (Pennini et al., 2006; Vermeulen et al., 2009). We found that although *Mtb* PRT activates both p38-MAPK and ERK signalling pathways, histone hypermethylation followed by autophagy inhibition was specifically dependent on the p38-MAPK pathway. Inhibition of p38 decreased histone hypermethylation, which subsequently up-regulated ATG5, ATG7 and LC3-II expression. However, it is important to demonstrate these findings in *MtbδPrt* mutant. Moreover, the underlying mechanism responsible for P38 mediated histone methylation is poorly studied. There are couple of reports which show the involvement of NF-κB in p38 mediated histone modifications in *Shigella flexnari* and *Listeria monocytogenes* (Hamon and Cossart, 2008). *Mtb* PRT is also reported to increase NF-κB expression in our previously published report (Mohanty et al., 2015). Additionally, involvement of NF-κB in autophagy inhibition and intracellular survival is also well known (Djavaheri-Mergny et al., 2007; Bai et al., 2013; Espert et al., 2015). So, involvement of NF-κB in p38 mediated histone methylation in *Mtb* can be a possible mechanism which needs to be studied. Further, it remains to be investigated if inhibition of H3K9me2/3 has any impact on the survival of *Mtb* in tuberculosis mice model. In summary, to the best of our knowledge, this is the first report that shows *Mtb* induces H3K27me3 in the promoter region of autophagy-related genes to inhibit autophagy. Thus, *Mtb* PRT could be a potential drug target to improve TB therapy.

DATA AVAILABILITY STATEMENT

The raw data supporting the conclusions of this article will be made available by the authors, without undue reservation.

AUTHOR CONTRIBUTIONS

SS planned the experimental setup, performed the experiments, analysed the data and wrote the manuscript. BN analysed the experiments and provided technical assistance. MM performed experiments with Mtb and analysed the data. PS planned experimental setup with Mtb strain and provided resources. AS planned the experimental setup, data analysis, wrote the manuscript and provided all the necessary resources and support for the completion of the study. SM contributed in the

design of the study and analysed data. All authors contributed to the article and approved the submitted version.

FUNDING

This work was supported by grant (BT/PR23317/MED/29/1186/2017) from the Department of Biotechnology, Government of India to AS. SS is grateful to the Department of Science and Technology, Government of India for awarding DST-INSPIRE fellowship (IF150081). This study was supported by the University of Zurich, Institute of Medical Microbiology and Swiss National Science Foundation (IZK0Z3_154138/1 and 310030_197699).

ACKNOWLEDGMENTS

We would like to thank Dr. Sunil Raghav and his students Abdul Ahad and Suchismita, Institute of Life Sciences, Bhubaneswar, India for their help in performing ChIP assay. We would like to thank Sonawane lab members for fruitful discussions and critical reading of the manuscript.

SUPPLEMENTARY MATERIAL

The Supplementary Material for this article can be found online at: https://www.frontiersin.org/articles/10.3389/fcimb.2021.676456/full#supplementary-material

Supplementary Figure 1 | Expression of HDAC1 and HDAC2. RAW264.7 cells were infected with Msm_{pSMT3} and Mtb_{Prt} for 24 h. The level of HDAC1 and HDAC2 expression at protein level was checked by western blotting.The experiments were performed in triplicate (n=3).

Supplementary Figure 2 | Intracellular survival of *Mtb* PRT after autophagy inhibition by 3MA. RAW 264.7 were infected with Msm_{pSMT3} and Mtb_{Prt} strains followed by 3MA treatment. Cells were lysed and intracellular bacterial survival was determined 8 and 24 h post-infection by a CFU assay. Experiments were performed in triplicate (n=3). Results are shown as mean ± S.D. ***, $p \leq 0.001$; **, $p \leq 0.01$; *, $p \leq 0.05$.; ns, not significant.

Supplementary Figure 3 | Southern blot analysis of *M. tuberculosis prt* locus. *M. tuberculosis* (1, wt) was transformed with *prt* targeting vector pMCS5-rpsL-hyg-Δ3242c, transformants were selected on 7H10 agar containing hygromycin. Putative single cross-over transformant (2, sco) was colony purified and subjected to streptomycin counter selection to obtain putative *Δprt* deletion mutant (3, Δ). Genomic DNA of the indicated strains was isolated, digested with *AgeI*, separated on an agarose gel, blotted and probed with a 128bp probe located upstream of the target gene. The band patterns confirm the predicted genotypes.

REFERENCES

Allis, C. D., and Jenuwein, T. (2016). The Molecular Hallmarks of Epigenetic Control. *Nat. Rev. Genet.* 17, 487–500. doi: 10.1038/nrg.2016.59

Arakawa, S., Honda, S., Yamaguchi, H., and Shimizu, S. (2017). Molecular Mechanisms and Physiological Roles of Atg5/Atg7-Independent Alternative Autophagy. *Proc. Japan Acad. Ser. B Phys. Biol. Sci.* 93, 378–385. doi: 10.2183/pjab.93.023

Artal-Martinez de Narvajas, A., Gomez, T. S., Zhang, J.-S., Mann, A. O., Taoda, Y., Gorman, J. A., et al. (2013). Epigenetic Regulation of Autophagy by the Methyltransferase G9a. *Mol. Cell. Biol.* 33, 3983–3993. doi: 10.1128/mcb.00813-13

Baek, S. H., and Kim, K. Il (2017). Epigenetic Control of Autophagy: Nuclear Events Gain More Attention. *Mol. Cell.* 65, 781–785. doi: 10.1016/j.molcel.2016.12.027

Bai, X., Feldman, N. E., Chmura, K., Ovrutsky, A. R., Su, W.-L., Griffin, L., et al. (2013). Inhibition of Nuclear Factor-Kappa B Activation Decreases Survival of Mycobacterium Tuberculosis in Human Macrophages. *PloS One* 8, e61925. doi: 10.1371/journal.pone.0061925

Bannister, A. J., Zegerman, P., Partridge, J. F., Miska, E. A., Thomas, J. O., Allshire, R. C., et al. (2001). Selective Recognition of Methylated Lysine 9 on Histone H3 by the HP1 Chromo Domain. *Nature.* 410, 120–124. doi: 10.1038/35065138

Brülle, J. K., Tschumi, A., and Sander, P. (2013). Lipoproteins of Slow-Growing Mycobacteria Carry Three Fatty Acids and are N-Acylated by Apolipoprotein N-Acyltransferase BCG-2070c. *BMC Microbiol.* 13, 223. doi: 10.1186/1471-2180-13-223

Byun, S., Seok, S., Kim, Y. C., Zhang, Y., Yau, P., Iwamori, N., et al. (2020). Fasting-Induced FGF21 Signaling Activates Hepatic Autophagy and Lipid Degradation *via* JMJD3 Histone Demethylase. *Nat. Commun.* 11, 807. doi: 10.1038/s41467-020-14384-z

Cabezas-Cruz, A., Alberdi, P., Ayllón, N., Valdés, J. J., Pierce, R., Villar, M., et al. (2016). Anaplasma Phagocytophilum Increases the Levels of Histone Modifying Enzymes to Inhibit Cell Apoptosis and Facilitate Pathogen Infection in the Tick Vector Ixodes Scapularis. *Epigenetics.* 11, 303–319. doi: 10.1080/15592294.2016.1163460

Castillo, E. F., Dekonenko, A., Arko-Mensah, J., Mandell, M. A., Dupont, N., Jiang, S., et al. (2012). Autophagy Protects Against Active Tuberculosis by Suppressing Bacterial Burden and Inflammation. *Proc. Natl. Acad. Sci. U. S. A.* 109, E3168–76. doi: 10.1073/pnas.1210500109

Chandra, V., Bhagyaraj, E., Nanduri, R., Ahuja, N., and Gupta, P. (2015). NR1D1 Ameliorates Mycobacterium Tuberculosis Clearance Through Regulation of Autophagy. *Autophagy* 11, 1987–1997. doi: 10.1080/15548627.2015.1091140

Chandran, A., Antony, C., Jose, L., Mundayoor, S., Natarajan, K., and Kumar, R. A. (2015). Mycobacterium Tuberculosis Infection Induces HDAC1-Mediated Suppression of IL-12b Gene Expression in Macrophages. *Front. Cell. Infect. Microbiol.* 5:90. doi: 10.3389/fcimb.2015.00090

Davis, E. O., Springer, B., Gopaul, K. K., Papavinasasundaram, K. G., Sander, P., and Böttger, E. C. (2002). DNA Damage Induction of recA in Mycobacterium Tuberculosis Independently of RecA and LexA. *Mol. Microbiol.* 46, 791–800. doi: 10.1046/j.1365-2958.2002.03199.x

Deretic, V. (2014). Autophagy in Tuberculosis. *Cold Spring Harb. Perspect. Med.* 4, doi: 10.1101/cshperspect.a018481

Deretic, V., Singh, S., Master, S., Harris, J., Roberts, E., Kyei, G., et al. (2006). Mycobacterium Tuberculosis Inhibition of Phagolysosome Biogenesis and Autophagy as a Host Defence Mechanism. *Cell. Microbiol.* 8, 719–727. doi: 10.1111/j.1462-5822.2006.00705.x

Djavaheri-Mergny, M., Amelotti, M., Mathieu, J., Besançon, F., Bauvy, C., and Codogno, P. (2007). Regulation of Autophagy by NF-kappaB Transcription Factor and Reactives Oxygen Species. *Autophagy* 3, 390–392. doi: 10.4161/auto.4248

Espert, L., Beaumelle, B., and Vergne, I. (2015). Autophagy in Mycobacterium Tuberculosis and HIV Infections. *Front. Cell. Infect. Microbiol.* 5:49. doi: 10.3389/fcimb.2015.00049

Forrellad, M. A., Klepp, L. I., Gioffré, A., García, J. S., Morbidoni, H. R., de la Paz Santangelo, M., et al. (2013). Virulence Factors of the Mycobacterium Tuberculosis Complex. *Virulence* 4, 33–66. doi: 10.4161/viru.22329

Fritsch, L., Robin, P., Mathieu, J. R. R., Souidi, M., Hinaux, H., Rougeulle, C., et al. (2010). A Subset of the Histone H3 Lysine 9 Methyltransferases Suv39h1, G9a, GLP, and SETDB1 Participate in a Multimeric Complex. *Mol. Cell* 37, 46–56. doi: 10.1016/j.molcel.2009.12.017

Füllgrabe, J., Klionsky, D. J., and Joseph, B. (2014). The Return of the Nucleus: Transcriptional and Epigenetic Control of Autophagy. *Nat. Rev. Mol. Cell Biol.* 15, 65–74. doi: 10.1038/nrm3716

Gandhi, S., Mitterhoff, R., Rapoport, R., Eden, S., Goran, A., and Simon, I. (2021). Mitotic H3K9ac is Controlled by Phase-Specific Activity of HDAC2, HDAC3 and SIRT1. *bioRxiv* 2021.03.08.434337. doi: 10.1101/2021.03.08.434337

Glickman, M. S., and Jacobs, W. R. (2001). Microbial Pathogenesis of Mycobacterium Tuberculosis: Dawn of a Discipline. *Cell.* 104, 477–485. doi: 10.1016/S0092-8674(01)00236-7

Gutierrez, M. G., Master, S. S., Singh, S. B., Taylor, G. A., Colombo, M. I., and Deretic, V. (2004). Autophagy is a Defense Mechanism Inhibiting BCG and Mycobacterium Tuberculosis Survival in Infected Macrophages. *Cell.* 119, 753–766. doi: 10.1016/j.cell.2004.11.038

Hamon, M. A., Batsché, E., Régnault, B., To, N. T., Seveau, S., Muchardt, C., et al. (2007). Histone Modifications Induced by a Family of Bacterial Toxins. *Proc. Natl. Acad. Sci. U. S. A.* 104, 13467–13472. doi: 10.1073/pnas.0702729104

Hamon, M. A., and Cossart, P. (2008). Histone Modifications and Chromatin Remodeling During Bacterial Infections. *Cell Host Microbe* 4, 100–109. doi: 10.1016/j.chom.2008.07.009

Henson, S. M., Lanna, A., Riddel, N. E., Franzese, O., Macaulay, R., Griffiths, S. J., et al. (2014). P38 Signaling Inhibits Mtorc1-Independent Autophagy in Senescent Human CD8+ T Cells. *J. Clin. Invest.* 124, 4004–4016. doi: 10.1172/JCI75051

He, Y., She, H., Zhang, T., Xu, H., Cheng, L., Yepes, M., et al. (2018). P38 MAPK Inhibits Autophagy and Promotes Microglial Inflammatory Responses by Phosphorylating ULK1. *J. Cell Biol.* 217, 315–328. doi: 10.1083/jcb.201701049

Kumar, P., Agarwal, R., Siddiqui, I., Vora, H., Das, G., and Sharma, P. (2012). ESAT6 Differentially Inhibits IFN-γ-Inducible Class II Transactivator Isoforms in Both a TLR2-Dependent and -Independent Manner. *Immunol. Cell Biol.* 90, 411–420. doi: 10.1038/icb.2011.54

Kumar, D., Nath, L., Kamal, M. A., Varshney, A., Jain, A., Singh, S., et al. (2010). Genome-Wide Analysis of the Host Intracellular Network That Regulates Survival of Mycobacterium Tuberculosis. *Cell.* 140, 731–743. doi: 10.1016/j.cell.2010.02.012

Lapierre, L. R., Kumsta, C., Sandri, M., Ballabio, A., and Hansen, M. (2015). Transcriptional and Epigenetic Regulation of Autophagy in Aging. *Autophagy.* 11, 867–880. doi: 10.1080/15548627.2015.1034410

Liang, C., Feng, P., Ku, B., Dotan, I., Canaani, D., Oh, B. H., et al. (2006). Autophagic and Tumour Suppressor Activity of a Novel Beclin1-Binding Protein UVRAG. *Nat. Cell Biol.* 8, 688–698. doi: 10.1038/ncb1426

Mizushima, N., Yoshimori, T., and Ohsumi, Y. (2011). The Role of Atg Proteins in Autophagosome Formation. *Annu. Rev. Cell Dev. Biol.* 27, 107–132. doi: 10.1146/annurev-cellbio-092910-154005

Mohanty, S., Dal Molin, M., Ganguli, G., Padhi, A., Jena, P., Selchow, P., et al. (2016). Mycobacterium Tuberculosis EsxO (Rv2346c) Promotes Bacillary Survival by Inducing Oxidative Stress Mediated Genomic Instability in Macrophages. *Tuberculosis* 96, 44–57. doi: 10.1016/j.tube.2015.11.006

Mohanty, S., Jagannathan, L., Ganguli, G., Padhi, A., Roy, D., Alaridah, N., et al. (2015). A Mycobacterial Phosphoribosyltransferase Promotes Bacillary Survival by Inhibiting Oxidative Stress and Autophagy Pathways in Macrophages and Zebrafish. *J. Biol. Chem.* 290, 13321–13343. doi: 10.1074/jbc.M114.598482

Mozzetta, C., Boyarchuk, E., Pontis, J., and Ait-Si-Ali, S. (2015). Sound of Silence: The Properties and Functions of Repressive Lys Methyltransferases. *Nat. Rev. Mol. Cell Biol.* 16, 499–513. doi: 10.1038/nrm4029

Ngollo, M., Lebert, A., Daures, M., Judes, G., Rifai, K., Dubois, L., et al. (2017). Global Analysis of H3K27me3 as an Epigenetic Marker in Prostate Cancer Progression. *BMC Cancer.* 17, 261. doi: 10.1186/s12885-017-3256-y

Nishimura, T., and Tooze, S. A. (2020). Emerging Roles of ATG Proteins and Membrane Lipids in Autophagosome Formation. *Cell Discovery.* 6, 32. doi: 10.1038/s41421-020-0161-3

Ohsumi, Y. (2014). Historical Landmarks of Autophagy Research. *Cell Res.* 24, 9–23. doi: 10.1038/cr.2013.169

Padhi, A., Naik, S. K., Sengupta, S., Ganguli, G., and Sonawane, A. (2016). Expression of Mycobacterium Tuberculosis NLPC/p60 Family Protein Rv0024 Induce Biofilm Formation and Resistance Against Cell Wall Acting Anti-Tuberculosis Drugs in Mycobacterium Smegmatis. *Microbes Infect.* 18, 224–236. doi: 10.1016/j.micinf.2015.11.007

Padhi, A., Pattnaik, K., Biswas, M., Jagadeb, M., Behera, A., and Sonawane, A. (2019). Mycobacterium Tuberculosis LprE Suppresses TLR2-Dependent Cathelicidin and Autophagy Expression to Enhance Bacterial Survival in Macrophages. *J. Immunol.* 203, 2665–2678. doi: 10.4049/jimmunol.1801301

Pankiv, S., Clausen, T. H., Lamark, T., Brech, A., Bruun, J. A., Outzen, H., et al. (2007). P62/SQSTM1 Binds Directly to Atg8/LC3 to Facilitate Degradation of Ubiquitinated Protein Aggregates by Autophagy*[s]. *J. Biol. Chem.* 282, 24131–24145. doi: 10.1074/jbc.M702824200

Park, J. A., Kim, A. J., Kang, Y., Jung, Y. J., Kim, H. K., and Kim, K. C. (2011). Deacetylation and Methylation at Histone H3 Lysine 9 (H3K9) Coordinate Chromosome Condensation During Cell Cycle Progression. *Mol. Cells.* doi: 10.1007/s10059-011-0044-4

Pasquinelli, V., Rovetta, A. I., Alvarez, I. B., Jurado, J. O., Musella, R. M., Palmero, D. J., et al. (2013). Phosphorylation of Mitogen-Activated Protein Kinases Contributes to Interferon γ Production in Response to Mycobacterium Tuberculosis. *J. Infect. Dis.* 207, 340–350. doi: 10.1093/infdis/jis672

Pennini, M. E., Pai, R. K., Schultz, D. C., Boom, W. H., and Harding, C. V. (2006). Mycobacterium Tuberculosis 19-kDa Lipoprotein Inhibits IFN- -Induced Chromatin Remodeling of MHC2TA by TLR2 and MAPK Signaling. *J. Immunol.* 176, 4323–4330. doi: 10.4049/jimmunol.176.7.4323

Pennini, M. E., Perrinet, S., Dautry-Varsat, A., and Subtil, A. (2010). Histone Methylation by NUE, a Novel Nuclear Effector of the Intracellular Pathogen Chlamydia Trachomatis. *PloS Pathog.* 6, 1–12. doi: 10.1371/journal.ppat.1000995

Philpott, D. J., Yamaoka, S., Israël, A., and Sansonetti, P. J. (2000). Invasive Shigella Flexneri Activates NF-κb Through a Lipopolysaccharide-Dependent Innate Intracellular Response and Leads to IL-8 Expression in Epithelial Cells. *J. Immunol.* 165, 903–914. doi: 10.4049/jimmunol.165.2.903

Præstholm, S. M., Siersbæk, M. S., Nielsen, R., Zhu, X., Hollenberg, A. N., Cheng, S., et al. (2020). Multiple Mechanisms Regulate H3 Acetylation of Enhancers in Response to Thyroid Hormone. *PloS Genet.* 16, e1008770. doi: 10.1371/journal.pgen.1008770

Rahman, S. A., Singh, Y., Kohli, S., Ahmad, J., Ehtesham, N. Z., Tyagi, A. K., et al. (2014). Comparative Analyses of Nonpathogenic, Opportunistic, and Totally Pathogenic Mycobacteria Reveal Genomic and Biochemical Variabilities and Highlight the Survival Attributes of Mycobacterium Tuberculosis. *MBio* 5, e02020. doi: 10.1128/mbio.02020-14

Rolando, M., Sanulli, S., Rusniok, C., Gomez-Valero, L., Bertholet, C., Sahr, T., et al. (2013). Legionella Pneumophila Effector RomA Uniquely Modifies Host Chromatin to Repress Gene Expression and Promote Intracellular Bacterial Replication. *Cell Host Microbe.* 13, 395–405. doi: 10.1016/j.chom.2013.03.004

Sethi, D., Mahajan, S., Singh, C., Lama, A., Hade, M. D., Gupta, P., et al. (2016). Lipoprotein LprI of Mycobacterium Tuberculosis Acts as a Lysozyme Inhibitor. *J. Biol. Chem.* 291, 2938–2953. doi: 10.1074/jbc.M115.662593

Seto, E., and Yoshida, M. (2014). Erasers of Histone Acetylation: The Histone Deacetylase Enzymes. *Cold Spring Harb. Perspect. Biol.* 6, a018713. doi: 10.1101/cshperspect.a018713

Singh, V., Prakhar, P., Rajmani, R. S., Mahadik, K., Borbora, S. M., and Balaji, K. N. (2017). Histone Methyltransferase SET8 Epigenetically Reprograms Host Immune Responses to Assist Mycobacterial Survival. *J. Infect. Dis.* 216, 477–488. doi: 10.1093/infdis/jix322

Tolg, C., Sabha, N., Cortese, R., Panchal, T., Ahsan, A., Soliman, A., et al. (2011). Uropathogenic E. Coli Infection Provokes Epigenetic Downregulation of CDKN2A (P16ink4a) in Uroepithelial Cells. *Lab. Investig.* 91, 825–836. doi: 10.1038/labinvest.2010.197

Večeřa, J., Bártová, E., Krejčí, J., Legartová, S., Komůrková, D., Rudá-Kučerová, J., et al. (2018). HDAC1 and HDAC3 Underlie Dynamic H3K9 Acetylation During Embryonic Neurogenesis and in Schizophrenia-Like Animals. *J. Cell. Physiol.* 233, 530–548. doi: 10.1002/jcp.25914

Vermeulen, L., Berghe, W., Vanden, Beck, I. M. E., De Bosscher, K., and Haegeman, G. (2009). The Versatile Role of MSKs in Transcriptional Regulation. *Trends Biochem. Sci.* 34, 311–318. doi: 10.1016/j.tibs.2009.02.007

Yaseen, I., Kaur, P., Nandicoori, V. K., and Khosla, S. (2015). Mycobacteria Modulate Host Epigenetic Machinery by Rv1988 Methylation of a non-Tail Arginine of Histone H3. *Nat. Commun.* 6, 1–13. doi: 10.1038/ncomms9922

Zarubin, T., and Han, J. (2005). Activation and Signaling of the P38 MAP Kinase Pathway. *Cell Res.* 15, 11–18. doi: 10.1038/sj.cr.7290257

Conflict of Interest: The authors declare that the research was conducted in the absence of any commercial or financial relationships that could be construed as a potential conflict of interest.

Publisher's Note: All claims expressed in this article are solely those of the authors and do not necessarily represent those of their affiliated organizations, or those of the publisher, the editors and the reviewers. Any product that may be evaluated in this article, or claim that may be made by its manufacturer, is not guaranteed or endorsed by the publisher.

frontiers in Cellular and Infection Microbiology

ORIGINAL RESEARCH
published: 25 March 2022
doi: 10.3389/fcimb.2022.827528

Novel Potential Diagnostic Serum Biomarkers of Metabolomics in Osteoarticular Tuberculosis Patients: A Preliminary Study

Ximeng Chen[1,2], *Jingyun Ye*[2], *Hong Lei*[3]* and *Chengbin Wang*[2]*

[1] Medical School of Chinese People's Liberation Army (PLA), Beijing, China, [2] Department of Clinical Laboratory Medicine, The First Medical Center, Chinese People's Liberation Army (PLA) General Hospital, Beijing, China, [3] Department of Clinical Laboratory Medicine, The Eighth Medical Center, Chinese People's Liberation Army (PLA) General Hospital, Beijing, China

OPEN ACCESS

Edited by:
Yi-Wei Tang,
Cepheid (United States), United States

Reviewed by:
Jianping Xie,
Southwest University, China
Yufeng Yao,
Shanghai Jiao Tong University, China
Deng Guofang,
Shenzhen Third People's Hospital, China

***Correspondence:**
Chengbin Wang
wangcbin301@163.com
Hong Lei
leihong_hospital@126.com

Specialty section:
This article was submitted to Clinical Microbiology, a section of the journal Frontiers in Cellular and Infection Microbiology

Received: *02 December 2021*
Accepted: *21 January 2022*
Published: *25 March 2022*

Citation:
Chen X, Ye J, Lei H and Wang C (2022) Novel Potential Diagnostic Serum Biomarkers of Metabolomics in Osteoarticular Tuberculosis Patients: A Preliminary Study. Front. Cell. Infect. Microbiol. 12:827528. doi: 10.3389/fcimb.2022.827528

Osteoarticular tuberculosis is one of the extrapulmonary tuberculosis, which is mainly caused by direct infection of *Mycobacterium tuberculosis* or secondary infection of tuberculosis in other parts. Due to the low specificity of the current detection method, it is leading to a high misdiagnosis rate and subsequently affecting the follow-up treatment and prognosis. Metabolomics is mainly used to study the changes of the body's metabolites in different states, so it can serve as an important means in the discovery of disease-related metabolic biomarkers and the corresponding mechanism research. Liquid chromatography tandem mass spectrometry (LC-MS/MS) was used to detect and analyze metabolites in the serum with osteoarticular tuberculosis patients, disease controls, and healthy controls to find novel metabolic biomarkers that could be used in the diagnosis of osteoarticular tuberculosis. Our results showed that 68 differential metabolites (p<0.05, fold change>1.0) were obtained in osteoarticular tuberculosis serum after statistical analysis. Then, through the evaluation of diagnostic efficacy, PC [o-16:1(9Z)/18:0], PC[20:4(8Z,11Z,14Z,17Z)/18:0], PC[18:0/22:5(4Z,7Z,10Z,13Z,16Z)], SM(d18:1/20:0), and SM[d18:1/18:1(11Z)] were found as potential biomarkers with high diagnostic efficacy. Using bioinformatics analysis, we further found that these metabolites share many lipid metabolic signaling pathways, such as choline metabolism, sphingolipid signaling, retrograde endocannabinoid signaling, and sphingolipid and glycerophospholipid metabolism; these results suggest that lipid metabolism plays an important role in the pathological process of tuberculosis. This study can provide certain reference value for the study of metabolic biomarkers of osteoarticular tuberculosis and the mechanism of lipid metabolism in osteoarticular tuberculosis and even other tuberculosis diseases.

Keywords: osteoarticular tuberculosis, metabolomics, biomarker (BM), lipid metabolism, tuberculosis

INTRODUCTION

Tuberculosis is a chronic infectious disease that is caused by *Mycobacterium tuberculosis (M.tb)* and takes the respiratory tract as the main route of transmission (Walzl et al., 2018). According to the Global Tuberculosis Report by the World Health Organization in 2021, 9.9 million new cases and 1.5 million deaths were caused by tuberculosis globally in 2020 (World Health Organization, 2021). Generally, tuberculosis is divided into two types: pulmonary tuberculosis (PTB) and extrapulmonary tuberculosis (EPTB). For the diagnosis of tuberculosis, clinical laboratory tests play an important role, although with the long culture time and the low positive rate, the culture of *Mycobacterium tuberculosis* is still the gold standard (Darton et al., 2017); the other common tests such as smear microscopy, purified protein derivative (PPD) test, interferon-gamma (IFN-γ) release assay (IGRA), *M.tb* nucleic acid test, and Xpert/MTB system are also widely used (Fan et al., 2012; Norbis et al., 2014; Fan et al., 2018).

Osteoarticular tuberculosis is a kind of extrapulmonary tuberculosis whose *M.tb* directly infects the bone and joint tissue or spreads to the bone and joint tissue from other parts, which accounts for about 3%–5% of the total incidence of EPTB (Norbis et al., 2014). The most common site for osteoarticular tuberculosis is spine, especially the thoracic and lumbar spine, and the pathological changes are mostly bone destruction and tuberculous granulation tissue formation. At the same time, tuberculous abscesses that do not show related inflammation are easily formed beside the bone, and in severe cases, sinus tracts may even be formed (Johansen et al., 2015). The early clinical manifestations of osteoarticular tuberculosis are atypical, and the specificity of laboratory tests and imaging examinations is low, resulting in a high rate of missed diagnosis for osteoarticular tuberculosis. Most patients are misdiagnosed during the advanced stage that affected the treatment and prognosis. Hence, there is an urgent need for accurate diagnosis methods of osteoarticular tuberculosis (Yi et al., 2018; Vinhaes et al., 2019).

Metabolomics is mainly used to study the changes of the body's metabolites in different states (Zhang et al., 2018); the main methods of metabolomics contained nuclear magnetic resonance (NMR) and mass spectrometry (MS) (Zhou and Yin, 2019). Numerous metabolites have been successfully discovered as biomarkers for the diagnosis of various diseases. What is more, the metabolites which are searched by metabolomics can be elucidating the pathological or functional mechanisms by bioinformatics analysis (Wheelock et al., 2013). In the aspect of tuberculosis, there were many metabolomics studies of PTB, including secondary pulmonary tuberculosis (Luies et al., 2017), active pulmonary tuberculosis (Cho et al., 2020), and drug-resistant pulmonary tuberculosis (Tuyiringire et al., 2018; Chen et al., 2020); however, for osteoarticular tuberculosis, because of the low incidence of this disease, the related metabolomics studies are rare.

According to this situation, we used LC-MS/MS to detect serum metabolites in osteoarticular tuberculosis patients (TB Group), osteoarthritis patients (DC Group, including rheumatoid arthritis and ankylosing spondylitis), and healthy controls (HC Group) (Dudka et al., 2021), aiming to find potential markers for early and accurate diagnosis of osteoarticular tuberculosis. We further compared and analyzed serum metabolites of the above three groups and selected differential metabolites by the bioinformatics method to analyze the corresponding pathogenesis (Zhang et al., 2019).

MATERIALS AND METHODS

Study Cohort

From November 2018 to November 2019, 30 serum samples of diagnosed osteoarticular tuberculosis patients (TB group), 30 serum samples of disease control containing rheumatoid arthritis patients and ankylosing spondylitis patients (DC group), and 30 serum samples of healthy control (HC group) were collected from the 1st and the 8th Medical Center of Chinese PLA General Hospital. The diagnosis of the TB group was based on the following criteria: (a) positive nucleic acid test of *M.tb*; (b) medical image (X-ray, CT scan, etc.) findings showed specific features of TB infection; (c) positive pathology diagnosis of TB in bone or joint specimens; and (d) effective response to antituberculosis treatments. The diagnosis of the DC group was based on the following criteria: (a) positive inflammatory protein test; (b) specific clinical manifestations (joint stiffness in the morning, bending change, etc.); (c) medical image (X-ray, CT scan, etc.) findings showed specific features; and (d) effective response to hormone treatments (glucocorticoid, etc.). The HC group included adults without any disease clinical diagnosis, and all the tests were negative or normal. Patients with any diagnosis of cancer, metabolic disease, autoimmunity disease, immunodeficiency disease, and other pathogen infections were excluded from this study. Patients who have other organs tuberculosis (e.g., pulmonary tuberculosis or other extrapulmonary tuberculosis) were excluded as well.

This research was carried out in strict accordance with the declaration of Helsinki and approved by the Ethics Committee of Chinese PLA General Hospital. All participants signed an informed consent and gave their permission to use their blood samples for this study.

For each patient, 5 ml peripheral blood was drawn under a vacuum vessel containing separation gel in the morning before any treatments. After blood coagulation and 2,370g centrifugation, the serum was divided into several EP tubes and stored in a -80°C refrigerator for subsequent metabolomics analysis.

Metabolomics Analysis

This study applied untargeted metabolomics, which included reversed-phase chromatography positive ion detection, reversed-phase chromatography anion detection, and hydrophilic chromatography positive ion detection. The types of metabolites detected by these three modes are positive ion lipid, negative ion lipid (e.g., fatty acid), and small polar molecules (e.g., amino acid), respectively. The analysis

contained three parts: serum pretreatment and separation, mass spectrometry detection, and data processing.

Serum Pretreatment and Separation

Serum samples were thawed at 4°C, 300 μl methanol and 1,000 μl methyl tert-butyl ether (reversed-phase chromatography ion) or 150 μl acetonitrile (hydrophilic chromatography ion) was added to get a mixture in a microcentrifuge tube. Then, the mixture was centrifuged at 4°C temperature, 12,000 rpm for 10 min, and 100 μl supernatant was taken for analysis. As for reversed-phase chromatography ion mode, 400 μl was first taken from the mixture to dry, and then 100 μl methanol was added to dissolve after centrifugation.

For reversed-phase chromatography ion separation, mobile phase A was acetonitrile/water (60/40) and mobile phase B was isopropanol/acetonitrile (90/10); both A and B contained 0.1% formic acid and 10 mmol/l ammonium acetate. The column was an HSS T3 column (2.1 × 100 mm, 1.8 μm) operated at 45°C. The flow rate was 300 μl/min, and the injection volume was 1 μl. For hydrophilic chromatography ion separation, mobile phase A was acetonitrile and mobile phase B was water; both A and B contained 0.1% formic acid and 10 mmol/l ammonium acetate. The column was a BEH Amide column (2.1 × 100 mm, 1.7 μm) operated at 40°C. The flow rate was 300 μl/min, and the injection volume was 1 μl.

Mass Spectrometry Detection

A Thermo Scientific™ Q Exactive™ Hybrid Quadrupole-Orbitrap Mass Spectrometer equipped with a HESI-II probe was employed. The positive and negative HESI-II spray voltages were 3.7 and 3.5 kV, respectively, the heated capillary temperature was 320°C, the sheath gas pressure was 30 psi, the auxiliary gas setting was 10 psi, and the heated vaporizer temperature was 300°C. Both the sheath gas and the auxiliary gas were nitrogen. The collision gas was also nitrogen at a pressure of 1.5 mTorr. The parameters of the full mass scan were as follows: a resolution of 70,000, an auto gain control target under 1×10^6, a maximum isolation time of 50 ms, and an m/z range 50–1500. The LC-MS system was controlled using Xcalibur 2.2 SP1.48 software (Thermo Fisher Scientific, Waltham, MA, USA), and data were collected and processed with the same software.

Data Processing

All data obtained from the four assays in the two systems in both positive and negative ion modes were processed using Progenesis QI data analysis software (Nonlinear Dynamics, Newcastle, UK) for imputing raw data, peak alignment, picking, and normalization to produce peak intensities for retention time (tR) and m/z data pairs. The ranges of automatic peak picking for C18 were between 1 and 16 min and between 1 and 12 min, respectively. Then, the adduct ions of each feature (*m/z*, tR) were deconvoluted, and these features were identified in the Human Metabolome Database (HMDB, http://www.hmdb.ca/) and LIPID MAPS (http://www.lipidmaps.org/).

To monitor the system's stability and performance and the reproducibility of the sample, quality control (QC) samples were prepared by pooling equal volumes of each serum sample. The pretreatment of serum QC samples was in accord with real samples. For repeatable metabolic analyses, three features of the analytical system must be stable: (1) retention time, (2) signal intensity, and (3) mass accuracy. In this study, three QCs were continuously injected at the beginning of the run. QC samples are then injected at regular intervals of six or eight samples throughout the analytical run-in order to provide data from which repeatability can be assessed.

The features were selected based on their coefficients of variation (CVs) with QC samples; features with CVs over 15% were eliminated.

Statistical Analysis

The chi-square test was used for the analysis of characteristics of the study participants, and the Kruskal–Wallis H test was used to determine the differences between groups. The data of metabolomics were normalized using Progenesis QI data analysis software (Nonlinear Dynamics, Newcastle, UK). SIMCA 14.1 software was used to analyze the metabolites using the orthogonal partial least squares (OPLS) model. MetaboAnalyst (http://www.metaboanalyst.ca/) was used to analyze the related pathways of specific metabolites. R^2X (the interpretability of the model for the categorical variable X) was obtained after cross-validation; R^2Y (the interpretability of the model for the categorical variable Y) and Q^2 (predictability of the model) were obtained after cross-validation to judge the validity of the model. The Variable Importance in the Projection (VIP) value and the *p* value of t-test were used for evaluating the difference metabolites between groups. Final results were shown with scatter plots, trend charts, and the receiver operator characteristic curve (ROC curve), and analyses of the AUC, sensitivity, and specificity of each different metabolites were made by GraphPad Prism 6.0 software. The establishment of diagnostic models which contained metabolic biomarkers was made by MedCalc software, including several different metabolites combination and its statistical analysis; meanwhile, logistic regression and ROC curve analysis were used for the establishment of diagnostic models.

RESULTS

Basic Data Preprocessing

There was no statistical difference in the age and gender between TB, DC, and HC groups ($p>0.05$). The positive rates of clinical laboratory tests and medical imaging features are shown in **Table 1**. After LC-MS/MS analysis and peak alignment, picking, and normalization of raw data, metabolites were obtained, while the QC results of three patterns showed good reproducibility, which indicated that the results were credible (**Supplementary Files**).

Metabolite Profile

The OPLS-DA models of three patterns showed that the metabolites in three groups were clearly separated (**Figure 1**),

TABLE 1 | Clinical information of the study cohort.

	TB Group (n = 30)	DC Group (n = 30)	HC Group (n = 30)	*p* value
Age (median, IQR)	46 (33–61)	53.5 (31.5–63.5)	48.5 (41–55)	>0.05
Gender (male/female)	16/14	14/16	17/13	>0.05
Xpert test positive no. (%)	17 (56.67%)	/	/	/
TB nucleic acid test positive no. (%)	13 (43.33%)	/	/	/
TB antibody test positive no. (%)	9 (30.0%)	/	/	/
IGRA positive no. (%)	25 (83.3%)	/	/	/
Cultivate positive no. (%)	2 (6.67%)	/	/	/
Imaging features positive no. (%)	24 (80.00%)	/	/	/
Pathology positive no. (%)	17 (56.67%)	/	/	/

which indicated that significant serum metabolites change in osteoarticular tuberculosis patients. Variable Importance in the Projection (VIP) is a factor that means to extend a variable contribute in the projection, and the p <0.05 of statistical tests between groups is also important to explain the differences. The R^2Y and Q^2 of each OPLS-DA model are shown in **Table 2**; as TB compared to HC, the R^2Y were 0.936, 0.945, and 0.906, respectively, and the Q^2 were 0.870, 0.898, and 0.877, respectively; as TB compared to DC, the R^2Y were 0.972, 0.976, and 0.941 respectively, and the Q^2 were 0.956, 0.965, and 0.690, respectively; and as DC compared to HC, the R^2Y were 0.824, 0.817, and 0.832, respectively, and the Q^2 were 0.620, 0.646, and 0.789, respectively.

According to the results of the LC-MS/MS analysis, 62 and 40 metabolites were obtained among TB vs. HC and TB vs. DC, respectively; the heat maps and volcano maps are shown in **Figure 2**. After screening by a difference standard, 68 differential metabolites were obtained among TB vs. HC and TB vs. DC, including 37 upregulated metabolites and 31 downregulated metabolites. Further, based on the Venn diagram of these two comparisons (**Figure 3**), 19 upregulated common metabolites and 15 downregulated common metabolites were found (**Table 3**). The upregulated metabolites were phosphatidylcholine (PC), phosphatidylethanolamine (PE), ceramide (Cer), sphingomyelin (SM), etc. The downregulated metabolites were amino acid, ceramide (Cer), and fatty acid. At the same time, we conducted basic information retrieval and statistical analysis of 34 differential metabolites.

KEGG Enrichment Analysis

For the differential metabolites screened out in the previous analysis, we conducted a bioinformatics analysis on the differential metabolites. We imported these metabolites one by one into the KEGG database for signal pathway analysis and performed further enrichment and statistical analysis of these results. After KEGG enrichment analysis, the main metabolic

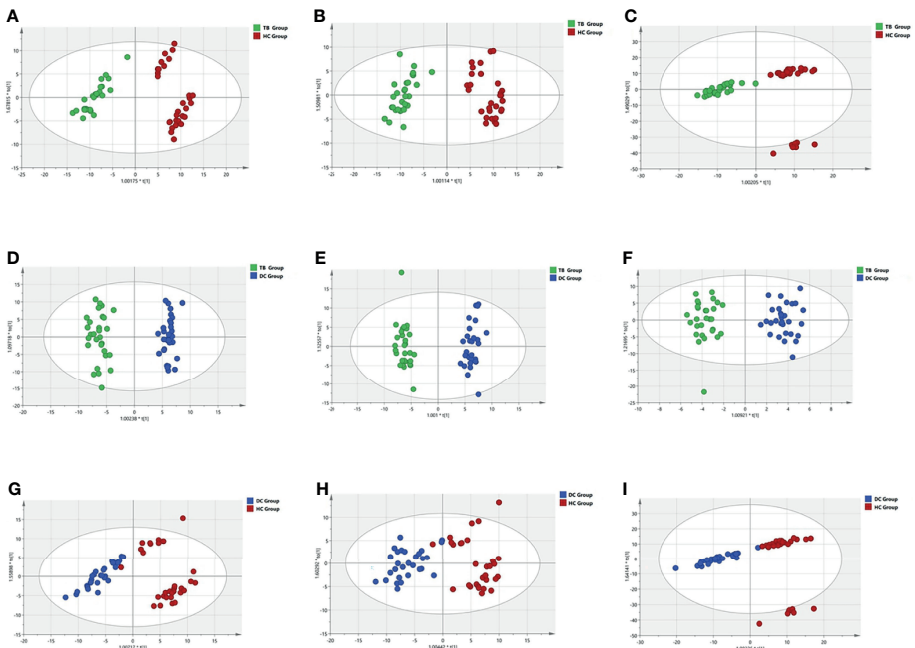

FIGURE 1 | OPLS-DA models of three patterns in three groups. **(A, D, G)** reversed-phase chromatography positive ion; **(B, E, H)** reversed-phase chromatography anion; **(C, F, I)** hydrophilic chromatography positive ion.

TABLE 2 | OPLS-DA models parameters.

	Reversed-phase chromatography Positive ion		Reversed-phase chromatography Anion		Hydrophilic chromatography Positive ion	
	R^2Y	Q^2	R^2Y	Q^2	R^2Y	Q^2
TB vs. HC	0.936	0.870	0.945	0.898	0.906	0.877
TB vs. DC	0.972	0.956	0.976	0.965	0.941	0.690
DC vs. HC	0.824	0.620	0.817	0.646	0.832	0.789

pathways in these differential metabolites are necroptosis, choline metabolism, sphingolipid signaling, retrograde endocannabinoid signaling, sphingolipid metabolism, and glycerophospholipid metabolism (**Figure 4**). According to the results of bioinformatics, it can be seen that the main signal pathways are concentrated in cell metabolism and lipid metabolism, which is in good agreement with the currently known pathogenic mechanisms of *Mycobacterium tuberculosis*.

Metabolites Diagnostic Efficiency Evaluation

We performed ROC curve analysis, 95% CI value calculation, sensitivity and specificity analyses on the differential metabolites in the TB group according to the aforementioned results to evaluate the diagnostic efficacy of each differential metabolite (**Table 4**). Based on clinical practicability and feasibility, for the diagnostic efficacy evaluation of each differential metabolite, we focus on the differential metabolites that specifically increase in osteoarticular tuberculosis. Generally, an AUC value greater than 0.7 indicates better diagnostic performance; according to this principle, SM(d18:0/24:1(15Z)) and SM(d18:1/14:0) were excluded from the evaluation. On the other hand, according to the comprehensive consideration of the AUC value, 95% CI, sensitivity, and specificity of each different metabolite, PC(o-16:1(9Z)/18:0), PC(20:4(8Z,11Z,14Z,17Z)/18:0), PC(18:0/20:3(5Z,8Z,11Z)), PC(18:0/22:5(4Z,7Z,10Z,13Z,16Z)), SM(d18:1/20:0), SM(d18:1/24:1(15Z)), SM(d18:0/16:1(9Z)), SM(d18:0/18:1(11Z)), and SM(d18:1/18:1(11Z)) were finally selected for further diagnostic efficacy evaluation and analysis.

After that, we drew scatter plots of the 9 selected differentially upregulated metabolites and performed a statistical analysis of their concentration in the three groups (**Figure 5**). As the scatter plots showed, PC(18:0/20:3(5Z,8Z,11Z)), SM(d18:1/24:1(15Z)), SM(d18:0/16:1(9Z)), and SM(d18:0/18:1(11Z)) also have a statistical difference between the DC group and HC group, which may disturb the diagnostic efficacy of osteoarticular tuberculosis. In contrast, the remaining five differential metabolites only have statistical difference between the TB group vs. DC group and TB group vs. HC group.

In summary, combining the AUC value of the ROC curve (**Figure 6**), 95% CI, sensitivity, and specificity, we finally considered that PC(o-16:1(9Z)/18:0), PC(20:4

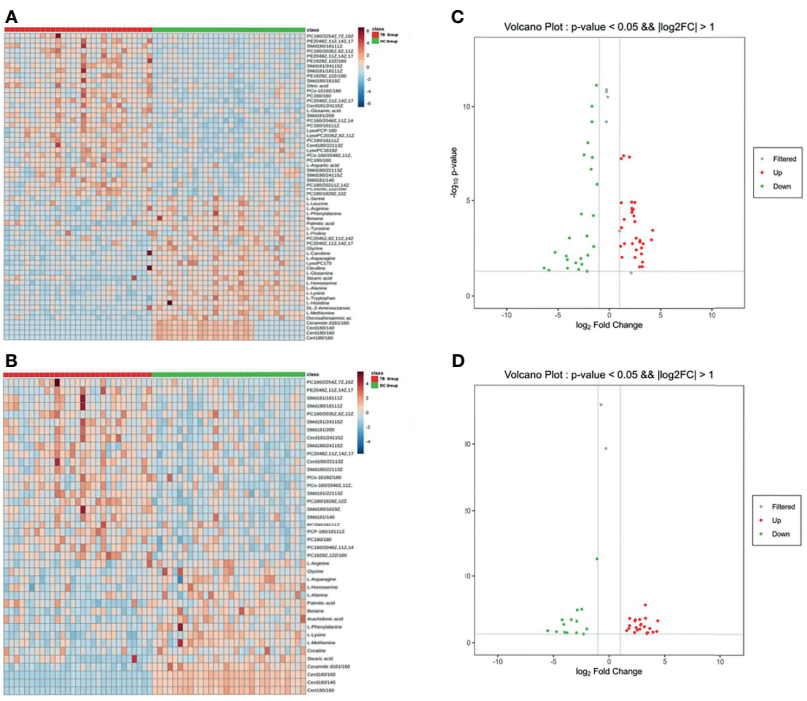

FIGURE 2 | Heat maps and volcano maps of metabolites. **(A)** Heat map of TB group vs. HC group; **(B)** volcano map of TB group vs. HC group **(C)** heat map of TB group vs. DC group; **(D)** volcano map of TB group vs. DC group.

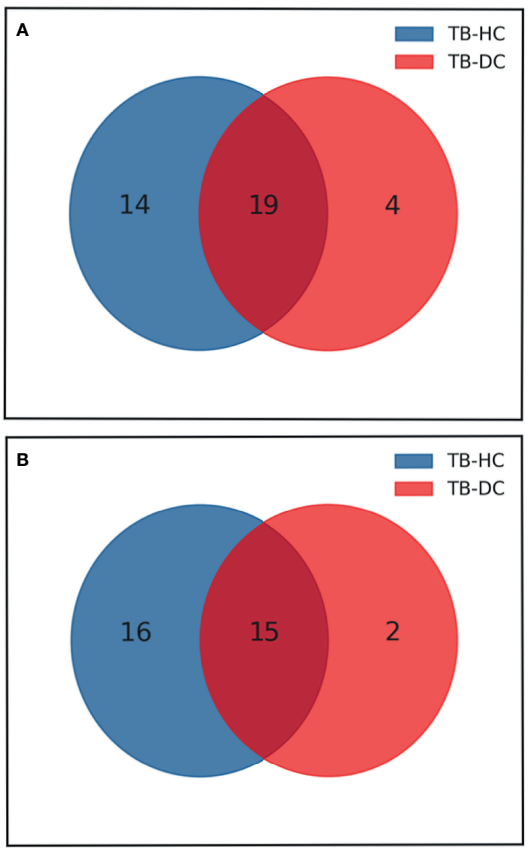

FIGURE 3 | Venn diagram of differential metabolites between TB group vs HC group and TB group vs DC group. **(A)** Up-regulated metabolites; **(B)** Down-regulated metabolites

(8Z,11Z,14Z,17Z)/18:0), PC(18:0/22:5(4Z,7Z,10Z,13Z,16Z)), SM (d18:1/20:0), and SM(d18:1/18:1(11Z)) may be potentially relevant metabolic biomarkers for the diagnosis of osteoarticular tuberculosis.

Establishment of Diagnostic Models Based on Five Potentially Metabolic Biomarkers

In order to improve the diagnostic efficiency of metabolites, diagnostic models are necessary to be considered. First of all, we combined two metabolites, PC and SM, respectively, to establish diagnostic models (Models A and B). After the combination of these metabolites, the AUC values of these two models were 0.8820 and 0.7940, respectively. However, the sensitivity of Model A and the specificity of Model B were more reasonable for the diagnosis, which were 96.67% and 83.33%, respectively. The data of Models A and B indicated that three PC biomarkers may be related to the sensitivity of models and two SM biomarkers may be related to the specificity of models. After that, for the improvement of the diagnostic efficiency, we added two SM biomarkers into PC combination respectively to establish new diagnostic models called Model C and Model D, which showed an ideal AUC value, 95% CI, sensitivity, and specificity (**Table 5**). What is more, the index of Model C is better than that of Model D comprehensively, indicating better diagnostic efficiency. Further, we also combined all the five biomarkers to establish Model E, although the AUC value, 95% CI, and sensitivity were similar to Model D, the specificity was improved to 86.67%. Also, the ROC curve of each diagnostic model was as shown in **Figure 7**. At last, based on the evaluation of these five diagnostic model indexes, we finally considered Model C as the most comprehensive diagnostic model in this study, consisting of PC(o-16:1(9Z)/18:0), PC(20:4 (8Z,11Z,14Z,17Z)/18:0), PC(18:0/22:5(4Z,7Z,10Z,13Z,16Z)), and SM(d18:1/20:0).

DISCUSSION

Tuberculosis is caused by *Mycobacterium tuberculosis*, one of the most widespread infectious diseases worldwide (Procop, 2016), which is always divided into two types: pulmonary tuberculosis (PTB) and extrapulmonary tuberculosis (EPTB). Because of its lower incidence rate, EPTB does not attract enough attention compared to PTB. Osteoarticular tuberculosis is one of EPTB, whose *M.tb* directly infects the bone and joint tissue or spreads to

TABLE 3 | Common metabolites between TB vs. HC and TB vs. DC.

Metabolite	HMDB ID	Log_2 fold change		Type
		TB vs. HC	TB vs. DC	
PC(o-16:1(9Z)/18:0)	HMDB13412	2.172	2.839	Up
PC(20:4(8Z,11Z,14Z,17Z)/18:0)	HMDB08464	2.192	2.745	Up
PC(16:0/20:4(8Z,11Z,14Z,17Z))	HMDB07983	2.383	4.281	Up
PC(18:0/18:2(9Z,12Z))	HMDB08039	4.213	3.249	Up
PC(18:2(9Z,12Z)/16:0)	HMDB08133	4.107	4.362	Up
PC(18:0/20:3(5Z,8Z,11Z))	HMDB08046	1.154	2.288	Up
PC(18:0/22:5(4Z,7Z,10Z,13Z,16Z))	HMDB08055	0.988	1.570	Up
PC(o-16:0/20:4(8Z,11Z,14Z,17Z))	HMDB13407	2.970	2.854	Up
SM(d18:1/20:0)	HMDB12102	2.317	2.354	Up
SM(d18:1/24:1(15Z))	HMDB12107	1.383	2.318	Up
SM(d18:0/16:1(9Z))	HMDB13464	1.953	3.265	Up
SM(d18:0/18:1(11Z))	HMDB12088	1.151	1.843	Up
SM(d18:0/24:1(15Z))	HMDB12095	3.213	2.527	Up
SM(d18:0/22:1(13Z))	HMDB12092	3.133	2.822	Up
SM(d18:1/18:1(11Z))	HMDB12100	1.436	1.840	Up
SM(d18:1/14:0)	HMDB12097	3.234	3.371	Up
Cer(d18:1/24:1(15Z))	HMDB04953	2.241	2.428	Up
Cer(d18:0/22:1(13Z))	HMDB11766	2.618	2.759	Up
PE(20:4(8Z,11Z,14Z,17Z)/18:0)	HMDB09420	1.174	1.773	Up
Glycine	HMDB00123	-2.730	-4.723	Down
L-Arginine	HMDB00517	-5.286	-5.514	Down
L-Alanine	HMDB00161	-1.708	-4.011	Down
L-Phenylalanine	HMDB00159	-4.203	-2.912	Down
L-Asparagine	HMDB00168	-2.475	-4.218	Down
L-Homoserine	HMDB00719	-1.781	-4.070	Down
L-Methionine	HMDB00696	-1.273	-2.458	Down
L-Lysine	HMDB00182	-1.706	-2.862	Down
Betaine	HMDB00043	-4.098	-3.404	Down
Cer(d18:0/14:0)	HMDB11759	-0.292	-0.719	Down
Cer(d18:0/16:0)	HMDB11760	-0.291	-0.752	Down
Cer(t18:0/16:0)	HMDB10697	-0.178	-0.305	Down
Cer(d18:1/16:0)	HMDB04949	-0.307	-1.077	Down
Palmitic acid	HMDB00220	-4.082	-3.782	Down
Stearic acid	HMDB00827	-2.099	-2.011	Down

the bone and joint tissue from other parts, and it is hard to distinguish with rheumatic immune arthritis and bone tumor at its early stage based on current clinical laboratory and clinical imaging methods (Fan et al., 2018). Metabolomics is one of the omics proposed together with proteomics and transcriptomics in recent years (Dutta et al., 2020). It is defined as the study of the complete set of metabolites inside cells, tissues, organs, and biological fluids. It represents a major and rapidly evolving component of systems biology—a new integrative approach to deciphering the complexity of biological systems (Preez et al., 2017). The metabolite changes associated with the specific phenotype being investigated may be classified as characteristics of the perturbation, which, in the context of investigating a disease, could be used toward better disease characterization, diagnostics, treatment, and other clinical applications. The methods of metabolomics include nuclear magnetic resonance (NMR) and mass spectrometry (MS) (Laíns et al., 2019). NMR is appropriate for the detection of all hydrogen-containing compounds, since it determines the magnetic resonance of nuclei in a molecule, and it is considered an unbiased, robust, reproducible, non-destructive, and selective analytical platform, which requires almost no sample pretreatment. On the other side, however, NMR has a low sensitivity and is short of an analyte separation element (Shin et al., 2011). MS is defined as the process of forming gaseous ions, with or without fragmentation, which are then characterized by their *m/z* ratios and respective relative abundances. Direct MS infusion is a high-throughput method, requiring short time for each sample analysis, and has been applied successfully in metabolomics studies, but it is not preferred for the analyses of complex biological samples such as blood and urine due to matrix interference (Schoeman et al., 2012). For TB, there are also more metabolomics studies focusing on colony culture, sputum specimens, blood specimens, urine specimens, tissue specimens, etc. (Parida and Kaufmann, 2010)

Zhou et al. (2015) and Albors-Vaquer et al. (2020) used NMR to detect differences in the expression of metabolites in the serum of PTB, healthy adults, lung-related benign lesions, and lung cancers; the results showed that some amino acids have been changed among these groups, such as alanine, lysine, glutamate, glutamine, ketone bodies, lactate, and pyruvate. Mendes Rˆego et al. (Rêgo et al., 2021) used MS to detect serum metabolites among drug-sensitive tuberculosis and drug-resistant tuberculosis; there were also some amino acids that were changed such as isoleucine, proline, hercynite, betaine, and pantothenic acid. On another aspect, Vrieling et al. (2019), Luo et al. (2020) and Chen et al. (2021) used MS to detect serum

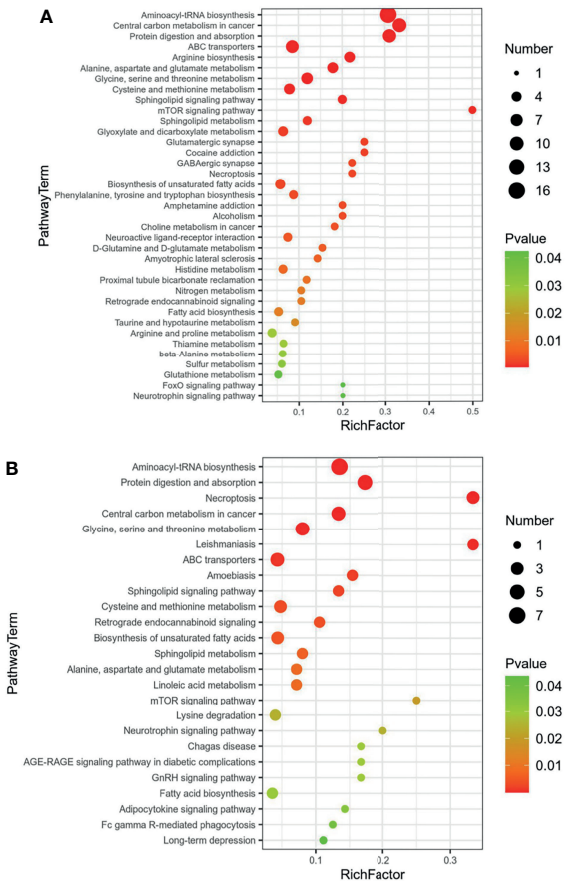

FIGURE 4 | KEGG enrichment of common regulated metabolites **(A)** Up-regulated metabolites; **(B)** down-regulated metabolites.

metabolites among PTB and healthy control, tuberculous pleuritis and malignancy, and PTB and PTB with type 2 diabetes, respectively. The results of these studies also showed some changes in amino acids, phospholipids, sphingolipids, etc., which are similar to other studies. According to other studies, amino acid levels such as alanine, lysine, glutamate, and glutamine in patients with tuberculosis infection have decreased significantly, which may be related to the uptake of glutamate, glutamate, and alanine by *Mycobacterium tuberculosis* for their corresponding life activities (Harth and Horwitz, 2003; Agapova et al., 2019). The body's immune process for tuberculosis is mainly the activation of T cells, which also changes the law of glucose metabolism. The disease process affects the metabolism of related immune cells and thus affects the secretion of cytokines such as IFN-γ, further leading to a decrease in immune effect (Lande et al., 2003).

According to the characteristics of *Mycobacterium tuberculosis*, in addition to the cell membrane and peptidoglycan of ordinary bacteria, there are also a large number of lipids and carbohydrates on its surface. These components have strong biological activity on eukaryotic cells, thus suggesting that it has a strong relationship with pathogenicity. For the mechanism of tuberculosis, lipid metabolism and lipid effector molecules play a vital role, such as regulating the production of cytokines, scavenging oxygen free radicals, and producing granulation inflammation and mitochondrial toxicity (Walpole et al., 2018). These related pathogenic components have also been reflected in other studies. Our study focuses on the blood specimens of osteoarticular tuberculosis, compared with PTB; this type of research is currently rarely reported. The results of our study showed that compared with healthy adults and rheumatoid arthritis patients, patients with osteoarticular tuberculosis also have significant changes in serum amino acid and lipid metabolism. Most amino acids such as glycine, L-arginine, and L-alanine were downregulated in osteoarticular tuberculosis patients' serum; in contrast, most lipids such as phosphatidylcholine, sphingomyelin, and phosphatidylethanolamine were upregulated in osteoarticular tuberculosis patients' serum.

Further, our study selected five potential serum metabolite biomarkers, namely, PC(o-16:1(9Z)/18:0), PC(20:4(8Z,11Z,14Z,17Z)/18:0), PC(18:0/22:5(4Z,7Z,10Z,13Z,16Z)), SM(d18:1/20:0), and SM(d18:1/18:1(11Z)), which belong to phosphatidylcholine (PC) and sphingomyelin (SM). On the aspect of KEGG enrichments, necroptosis, choline metabolism, sphingolipid signaling, retrograde endocannabinoid signaling, sphingolipid metabolism, and glycerophospholipid metabolism are

TABLE 4 | Diagnostic test information of metabolites between TB vs. HC and TB vs. DC.

Metabolites	AUC	95% CI	Sensitivity	Specificity
PC(o-16:1(9Z)/18:0)	0.8287	0.7235–0.9340	82.76%	76.67%
PC(20:4(8Z,11Z,14Z,17Z)/18:0)	0.7989	0.6858–0.9119	75.86%	73.33%
PC(16:0/20:4(8Z,11Z,14Z,17Z))	0.7770	0.6607–0.8933	68.97%	66.67%
PC(18:0/18:2(9Z,12Z))	0.7494	0.6251–0.8738	72.41%	66.67%
PC(18:2(9Z,12Z)/16:0)	0.7218	0.5924–0.8512	65.62%	66.67%
PC(18:0/20:3(5Z,8Z,11Z))	0.8529	0.7581–0.9477	79.31%	76.67%
PC(18:0/22:5(4Z,7Z,10Z,13Z,16Z))	0.8448	0.7423–0.9473	86.21%	76.67%
PC(o-16:0/20:4(8Z,11Z,14Z,17Z))	0.7195	0.5887–0.8504	65.52%	66.67%
SM(d18:1/20:0)	0.7989	0.6885–0.9092	75.86%	66.67%
SM(d18:1/24:1(15Z))	0.9057	0.8333–0.9782	82.76%	80.00%
SM(d18:0/16:1(9Z))	0.9107	0.8381–0.9833	85.71%	80.00%
SM(d18:0/18:1(11Z))	0.9506	0.9031–0.9980	82.76%	83.33%
SM(d18:0/24:1(15Z))	0.6529	0.5090–0.7968	62.07%	63.33%
SM(d18:0/22:1(13Z))	0.7189	0.5815–0.8484	72.41%	70.00%
SM(d18:1/18:1(11Z))	0.8138	0.7040–0.9235	72.41%	76.67%
SM(d18:1/14:0)	0.6621	0.5218–0.8023	82.76%	56.67%
Cer(d18:1/24:1(15Z))	0.7138	0.5811–0.8465	68.97%	66.67%
Cer(d18:0/22:1(13Z))	0.7195	0.5832–0.8559	72.41%	70.00%
PE(20:4(8Z,11Z,14Z,17Z)/18:0)	0.7690	0.6483–0.8896	72.41%	66.67%
Glycine	0.7954	0.6831–0.9077	72.41%	73.33%
L-Arginine	0.7402	0.6126–0.8679	68.97%	73.33%
L-Alanine	0.9172	0.8473–0.9872	86.21%	83.33%
L-Phenylalanine	0.6989	0.5658–0.8319	65.52%	63.33%
L-Asparagine	0.8989	0.8155–0.9822	82.76%	83.33%
L-Homoserine	0.9011	0.8226–0.9797	86.21%	86.67%
L-Methionine	0.9701	0.9309–1.0009	86.21%	93.93%
L-Lysine	0.9253	0.8620–0.9886	86.21%	86.67%
Betaine	0.6943	0.5595–0.8290	68.97%	63.33%
Cer(d18:0/14:0)	1	1	100%	100%
Cer(d18:0/16:0)	1	1	100%	100%
Cer(t18:0/16:0)	1	1	100%	100%
Cer(d18:1/16:0)	0.9782	0.9489–1.007	93.10%	96.67%
Palmitic acid	0.7115	0.5663–0.8567	68.97%	66.67%
Stearic acid	0.7678	0.6325–0.9032	72.41%	76.67%

maybe the main pathways. In most cases, these metabolites are related to lipid accumulation and obesity in the body (Wahl et al., 2012; Reinehr et al., 2015; Hellmuth et al., 2016). At the same time, some other pathological processes that cause enhanced lipid metabolism can also significantly increase these metabolites; for example, Wu et al. (2018) have reported that the sphingomyelinase/ceramide system, which has shown several times to be a crucial factor in the internalization, processing, and killing of diverse pathogens, also modulates the pro-inflammatory response and the state of mycobacteria in macrophages, which highlights the important role of lipid metabolism in the pathogenic mechanism of pathogens. For PTB, sphingosine-1 phosphate (S1P) and ceramide are central molecules and are decisive for sphingolipid signaling; otherwise, they are about the secretion of interferon (IFN)-γ during the course of infection and infiltration of pulmonary CD11b+ macrophages and expression of S-1P receptor-3 (S-1PR3) in the lungs during the course of infection (Braverman et al., 2016; Nadella et al., 2019). Takenami et al. (2018) have a research about the IgM and total IgG antibody response to cardiolipin (CL), phosphatidylcholine (PTC), phosphatidylethanolamine (PE), phosphatidylinositol (PI), and sulfatide (SL-I) as biosignatures that can be used to diagnose PTB and its applicability for monitoring the efficacy of antituberculosis treatment; the antibody concentrations of PTB patients were significantly higher than those of healthy control, which also indicates that lipids play a vital role in the process of *Mycobacterium tuberculosis* infection. Also, fatty acids can stimulate the activation of dormant *Mycobacterium tuberculosis* in liquid medium (Shleeva et al., 2013). Eicosanoids, lipid mediators derived from arachidonic acid, have been associated with the modulation of the host response to *Mycobacterium tuberculosis* infection (Bafica et al., 2005; Tobin et al., 2012). Moreover, it also reported increased eicosanoid ratios in plasma in tuberculosis patients compared to healthy control (Mayer-Barber and Sher, 2015). However, related research about the lipid in osteoarticular tuberculosis or even other extrapulmonary tuberculosis is rare; the results of our research, whether from the differential metabolites screened out or the signal pathways obtained from bioinformatics, are closely related to the results of pulmonary tuberculosis-related research (Huang et al., 2020; Han et al., 2021). It provides more reference value for future research on diagnostic biomarkers from the perspective of metabolomics and provides some hints for the establishment of subsequent auxiliary diagnostic methods for these differential metabolites.

In the future study, we will expand the scope of clinical serum samples, from the single-center collection to the multicenter collection in different regions, in order to minimize the limitations of the experimental results. At the same time, serum samples of different tuberculosis diseases such as pulmonary

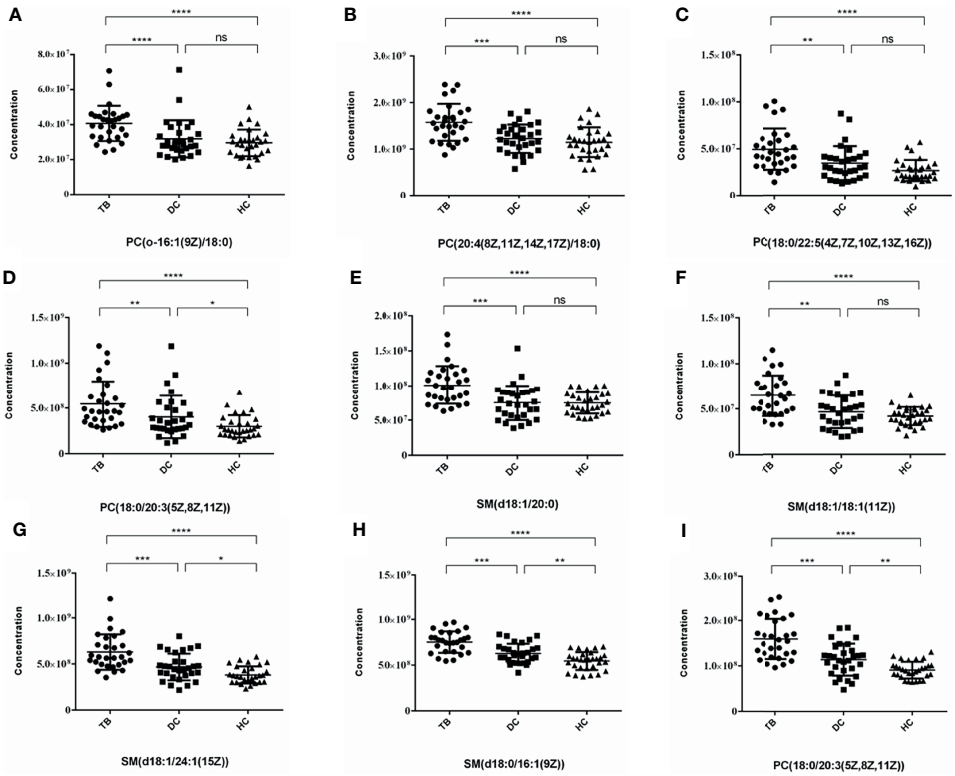

FIGURE 5 | Scatter plots of 9 selected differential metabolites among TB, DC and HC Group. **(A)** PC(o-16:1(9Z)/18:0); **(B)** PC(20:4(8Z,11Z,14Z,17Z)/18:0); **(C)** PC (18:0/22:5(4Z,7Z,10Z,13Z,16Z)); **(D)** PC(18:0/20:3(5Z,8Z,11Z)) **(E)** SM(d18:1/20:0); **(F)** SM(d18:1/18:1(11Z)); **(G)** SM(d18:1/24:1(15Z)); **(H)** SM(d18:0/16:1(9Z)); **(I)** PC (18:0/20:3(5Z,8Z,11Z)) (*p < 0.05, **p < 0.01, ***p < 0.001, ****p < 0.0001, ns, no statistical difference).

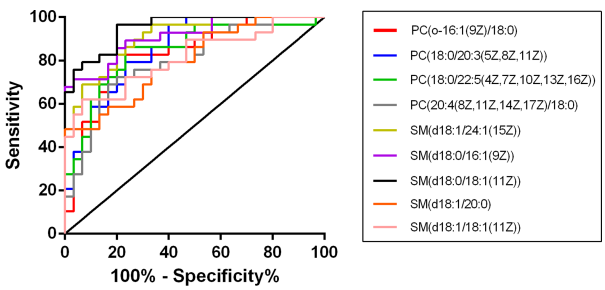

Metabolites	AUC	95%CI	Sensitivity	Specificity
PC(o-16:1(9Z)/18:0)	0.8287	0.7235-0.9340	82.76%	76.67%
PC(18:0/20:3(5Z,8Z,11Z))	0.8529	0.7581-0.9477	79.31%	76.67%
PC(18:0/22:5(4Z,7Z,10Z,13Z,16Z))	0.8448	0.7423-0.9473	86.21%	76.67%
PC(20:4(8Z,11Z,14Z,17Z)/18:0)	0.7989	0.6858-0.9119	75.86%	73.33%
SM(d18:1/24:1(15Z))	0.9057	0.8333-0.9782	82.76%	80.00%
SM(d18:0/16:1(9Z))	0.9107	0.8381-0.9833	85.71%	80.00%
SM(d18:0/18:1(11Z))	0.9506	0.9031-0.9980	82.76%	83.33%
SM(d18:1/20:0)	0.7989	0.6885-0.9092	75.86%	66.67%
SM(d18:1/18:1(11Z))	0.8138	0.7040-0.9235	72.41%	76.67%

FIGURE 6 | ROC curves of selected differential metabolites.

TABLE 5 | Diagnostic models based on five upregulated potential metabolic biomarkers.

Model	Components	AUC	95% CI	Sensitivity	Specificity
A	PC(o-16:1(9Z)/18:0) PC(20:4(8Z,11Z,14Z,17Z)/18:0) PC(18:0/22:5(4Z,7Z,10Z,13Z,16Z))	0.8820	0.796–0.940	96.67%	70.00%
B	SM(d18:1/20:0) SM(d18:1/18:1(11Z))	0.7940	0.696–0.872	63.33%	83.33%
C	PC(o-16:1(9Z)/18:0) PC(20:4(8Z,11Z,14Z,17Z)/18:0) PC(18:0/22:5(4Z,7Z,10Z,13Z,16Z)) SM(d18:1/20:0)	0.8960	0.813–0.950	90.00%	80.00%
D	PC(o-16:1(9Z)/18:0) PC(20:4(8Z,11Z,14Z,17Z)/18:0) PC(18:0/22:5(4Z,7Z,10Z,13Z,16Z)) SM(d18:1/18:1(11Z))	0.8890	0.805–0.945	80.00%	83.33%
E	PC(o-16:1(9Z)/18:0) PC(20:4(8Z,11Z,14Z,17Z)/18:0) PC(18:0/22:5(4Z,7Z,10Z,13Z,16Z)) SM(d18:1/20:0) SM(d18:1/18:1(11Z))	0.8890	0.805–0.945	80.00%	86.67%

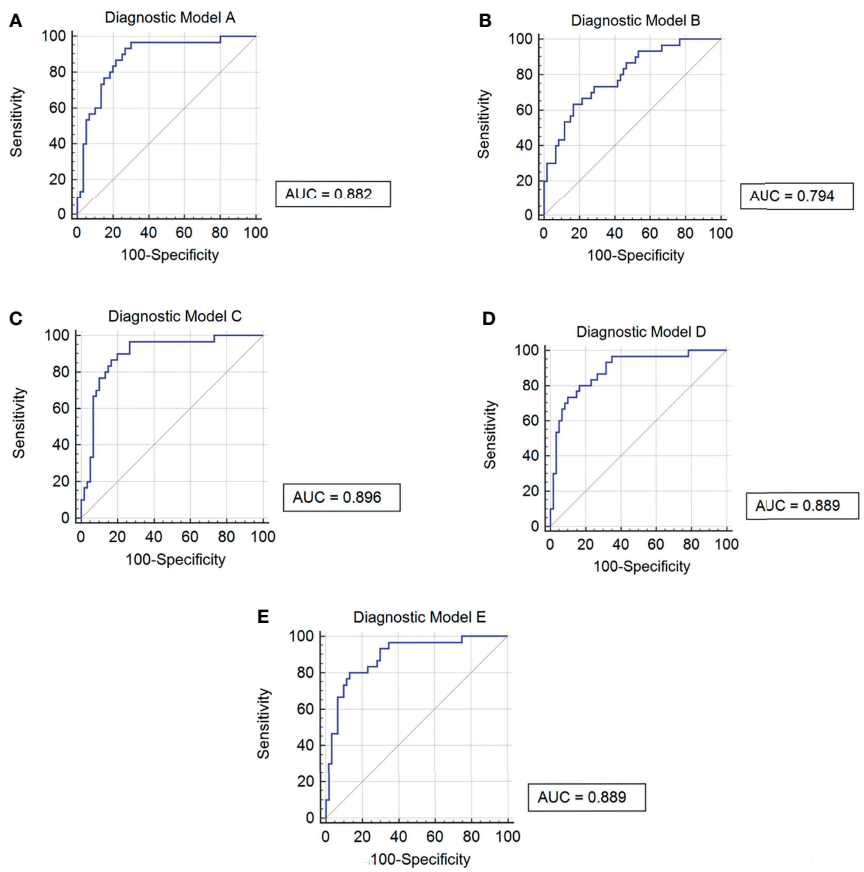

FIGURE 7 | ROC curves of 5 diagnostic models. **(A)** Diagnostic Model A contained PC(o-16:1(9Z)/18:0), PC(20:4(8Z,11Z,14Z,17Z)/18:0) and PC(18:0/22:5(4Z,7Z,10Z,13Z,16Z)). **(B)** Diagnostic Model B contained SM(d18:1/20:0) and SM(d18:1/18:1(11Z)). **(C)** Diagnostic Model C contained PC(o-16:1(9Z)/18:0), PC(20:4(8Z,11Z,14Z,17Z)/18:0), PC(18:0/22:5(4Z,7Z,10Z,13Z,16Z)) and SM(d18:1/20:0). **(D)** Diagnostic Model D contained PC(o-16:1(9Z)/18:0), PC(20:4(8Z,11Z,14Z,17Z)/18:0) , PC(18:0/22:5(4Z,7Z,10Z,13Z,16Z)) and SM(d18:1/18:1(11Z)). **(E)** Diagnostic Model E contained PC(o-16:1(9Z)/18:0), PC(20:4(8Z,11Z,14Z,17Z)/18:0), PC(18:0/22:5(4Z,7Z,10Z,13Z,16Z)), SM(d18:1/20:0) and SM(d18:1/18:1(11Z)).

tuberculosis can be added as follow-up controls to determine whether the relevant markers are widely related to tuberculosis, and then extended to not only the auxiliary diagnosis for osteoarticular tuberculosis but also the establishment of a new method of laboratory examination for tuberculosis for reference.

DATA AVAILABILITY STATEMENT

The data presented in the study are deposited in the MetaboLights repository, accession number MTBLS4187 with URL www.ebi.ac.uk/metabolights/MTBLS4187.

ETHICS STATEMENT

The studies involving human participants were reviewed and approved by the Ethics Committee of Chinese PLA General Hospital. The patients/participants provided their written informed consent to participate in this study.

AUTHOR CONTRIBUTIONS

CW and HL contributed to the research design. XC performed the experiments, coordinated the data modeling, and wrote the paper. JY performed the collection of serum samples and subjects' clinical data. All authors contributed to the article and approved the submitted version.

ACKNOWLEDGMENTS

This study did not receive any specific grants from funding agencies in the public, commercial, or not-for-profit sectors. We sincerely thank the staff of Beijing Omics Biotechnology Co., Ltd., for their help with LC-MS/MS analysis.

SUPPLEMENTARY MATERIAL

The Supplementary Material for this article can be found online at: https://www.frontiersin.org/articles/10.3389/fcimb.2022.827528/full#supplementary-material

REFERENCES

Agapova, A., Serafini, A., Petridis, M., Garza-Garcia, D. M., Sohaskey, M., de Carvalho, M., et al. (2019). Flexible Nitrogen Utilisation by the Metabolic Generalist Pathogen Mycobacterium Tuberculosis. *Elife* 8, e41129. doi: 10.7554/eLife.41129

Albors-Vaquer, A., Rizvi, A., Matzapetakis, M., Lamosa, P., Coelho, A. B., Patel, S. C., et al. (2020). Active and Prospective Latent Tuberculosis Are Associated With Different Metabolomic Profiles: Clinical Potential for the Identification of Rapid and Non-Invasive Biomarkers. *Emerging Microbes Infect.* 9 (1), 1131–1139. doi: 10.1080/22221751.2020.1760734

Bafica, A., Scanga, C. A., Serhan, C., Machado, F., White, S., Sher, A., et al (2005). Host Control of Mycobacterium Tuberculosis Is Regulated by 5-Lipoxygenase-Dependent Lipoxin Production. *J. Clin. Invest.* 115 (6), 1601–1606. doi: 10.1172/JCI23949

Braverman, J., Sogi, K. M., Benjamin, D., Nomura, D. K., and Stanley, S. A. (2016). HIF-1alpha Is an Essential Mediator of IFN-Gamma-Dependent Immunity to Mycobacterium Tuberculosis. *J. Immunol.* 197 (4), 1287–1297. doi: 10.4049/jimmunol.1600266

Chen, J., Han, Y. S., Yi, W. J., Huang, H., Li, Z. B., Shi, L. Y., et al. (2020). Serum Scd14, PGLYRP2 and FGA as Potential Biomarkers for Multidrug-Resistant Tuberculosis Based on Data-Independent Acquisition and Targeted Proteomics. *J. Cell. Mol. Med.* 24 (21), 12537–12549. doi: 10.1111/jcmm.15796

Chen, J. X., Han, Y. S., Zhang, S. Q., Li, Z. B., Chen, J., Yi, W. J., et al. (2021). Novel Therapeutic Evaluation Biomarkers of Lipid Metabolism Targets in Uncomplicated Pulmonary Tuberculosis Patients. *Signal Transduct. Target. Ther.* 6 (1), 22. doi: 10.1038/s41392-020-00427-w

Cho, Y., Park, Y., Sim, B., Lee, H., Cho, S. N., Kang, Y. A., et al. (2020). Identification of Serum Biomarkers for Active Pulmonary Tuberculosis Using a Targeted Metabolomics Approach. *Sci. Rep.* 10 (1), 3825. doi: 10.1038/s41598-020-60669-0

Darton, T. C., Zhou, L., Blohmke, C. J., Jones, C., Waddington, C. S., Baker, S., et al. (2017). Blood Culture-PCR to Optimise Typhoid Fever Diagnosis After Controlled Human Infection Identifies Frequent Asymptomatic Cases and Evidence of Primary Bacteraemia. *J. Infect.* 74 (4), 358–366. doi: 10.1016/j.jinf.2017.01.006

Dudka, I., Chachaj, A., Sebastian, A., Tański, W., Stenlund, H., Gröbner, G., et al. (2021). Metabolomic Profiling Reveals Plasma GlycA and GlycB as a Potential Biomarkers for Treatment Efficiency in Rheumatoid Arthritis. *J. Pharm. Biomed. Anal.* 197, 113971. doi: 10.1016/j.jpba.2021.113971

Dutta, N. K., Tornheim, J. A., Fukutani, K. F., Paradkar, M., Tiburcio, R. T., Kinikar, A., et al. (2020). Integration of Metabolomics and Transcriptomics Reveals Novel Biomarkers in the Blood for Tuberculosis Diagnosis in Children. *Sci. Rep.* 10 (1), 19527. doi: 10.1038/s41598-020-75513-8

Fan, L., Chen, Z., Hao, X. H., Hu, Z. Y., and Xiao, H. P. (2012). Interferon-Gamma Release Assays for the Diagnosis of Extrapulmonary Tuberculosis: A Systematic Review and Meta-Analysis. *FEMS Immunol. Med. Microbiol.* 65 (3), 456–466. doi: 10.1111/j.1574-695X.2012.00972.x

Fan, L., Li, D., Zhang, S., Yao, L., Hao, X., Gu, J., et al. (2018). Parallel Tests Using Culture, Xpert MTB/RIF, and SAT-TB in Sputum Plus Bronchial Alveolar Lavage Fluid Significantly Increase Diagnostic Performance of Smear-Negative Pulmonary Tuberculosis. *Front. Microbiol.* 9. doi: 10.3389/fmicb.2018.01107

Han, Y. S., Chen, J. X., Li, Z. B., Chen, J., Yi, W. J., Huang, H., et al. (2021). Identification of Potential Lipid Biomarkers for Active Pulmonary Tuberculosis Using Ultra-High-Performance Liquid Chromatography-Tandem Mass Spectrometry. *Exp. Biol. Med.* 246, 4, 387–399. doi: 10.1177/1535370220968058

Harth, G., and Horwitz, M. A. (2003). Inhibition of Mycobacterium Tuberculosis Glutamine Synthetase as a Novel Antibiotic Strategy Against Tuberculosis: Demonstration of Efficacy In Vivo. *Infect. Immun.* 71 (1), 456–464. doi: 10.1128/IAI.71.1.456-464.2003

Hellmuth, C., Kirchberg, F. F., Lass, N., Harder, U., Peissner, B., Koletzko, T., et al. (2016). Tyrosine Is Associated With Insulin Resistance in Longitudinal Metabolomic Profiling of Obese Children. *J. Diabetes Res.* 2016, 2108909. doi: 10.1155/2016/2108909

Huang, H., Han, Y. S., Chen, J., Shi, L. Y., Wei, L. L., Jiang, T. T., et al. (2020). The Novel Potential Biomarkers for Multidrug-Resistance Tuberculosis Using UPLC-Q-TOF-Ms. *Exp. Biol. Med.* 245, 6, 501–511. doi: 10.1177/1535370220903464

Johansen, I. S., Nielsen, S. L., Hove, M., Kehrer, M., Shakar, S., Wøyen, A. V., et al. (2015). Characteristics and Clinical Outcome of Bone and Joint Tuberculosis From 1994 to 2011: A Retrospective Register-Based Study in Denmark. *Clin. Infect. Dis.* 61 (4), 554–562. doi: 10.1093/cid/civ326

Laíns, I., Gantner, M., Murinello, S., Lasky-Su, J. A., Miller, J. W., Friedlander, M., et al. (2019). Metabolomics in the Study of Retinal Health and Disease. *Prog. retinal Eye Res.* 69, 57–79. doi: 10.1016/j.preteyeres.2018.11.002

Lande, R., Giacomini, E., Grassi, T., Remoli, M. E., Iona, E., Miettinen, M., et al. (2003). IFN-Alpha Beta Released by Mycobacterium Tuberculosis-Infected Human Dendritic Cells Induces the Expression of CXCL10: Selective

Recruitment of NK and Activated T Cells. *J. Immunol.* 170 (3), 1174–1182. doi: 10.4049/jimmunol.170.3.1174

Luies, L., du Preez, I., and Loots, D. T. (2017). The Role of Metabolomics in Tuberculosis Treatment Research. *Biomarkers Med.* 11 (11), 1017–1029. doi: 10.2217/bmm-2017-0141

Luo, P., Mao, K., Xu, J., Wu, F., Wang, X., Wang, S., et al. (2020). Metabolic Characteristics of Large and Small Extracellular Vesicles From Pleural Effusion Reveal Biomarker Candidates for the Diagnosis of Tuberculosis and Malignancy. *J. Extracell. Vesicles* 9 (1), 1790158. doi: 10.1080/20013078.2020.1790158

Mayer-Barber, K. D., and Sher, A. (2015). Cytokine and Lipid Mediator Networks in Tuberculosis. *Immunol. Rev.* 264 (1), 264–275. doi: 10.1111/imr.12249

Nadella, V., Sharma, L., Kumar, P., Gupta, P., Gupta, U. D., Tripathi, S., et al. (2019). Sphingosine-1-Phosphate (S-1p) Promotes Differentiation of Naive Macrophages and Enhances Protective Immunity Against Mycobacterium Tuberculosis. *Front. Immunol.* 10, 3085. doi: 10.3389/fimmu.2019.03085

Norbis, L., Alagna, R., Tortoli, E., Codecasa, L. R., Migliori, G. B., Cirillo, D. M., et al. (2014). Challenges and Perspectives in the Diagnosis of Extrapulmonary Tuberculosis. *Expert Rev. Anti-Infective Ther.* 12 (5), 633–647. doi: 10.1586/14787210.2014.899900

Parida, S. K., and Kaufmann, S. H. (2010). The Quest for Biomarkers in Tuberculosis. *Drug Discovery Today* 15 (3-4), 148–157. doi: 10.1016/j.drudis.2009.10.005

Preez, I. D., Luies, L., and Loots, D. T. (2017). Metabolomics Biomarkers for Tuberculosis Diagnostics: Current Status and Future Objectives. *Biomarkers Med.* 11 (2), 179–194. doi: 10.2217/bmm-2016-0287

Procop, G. W. (2016). Laboratory Diagnosis and Susceptibility Testing for Mycobacterium Tuberculosis. *Microbiol. Spectr.* 4 (6), 45–58. doi: 10.1128/microbiolspec.TNMI7-0022-2016

Rêgo, A. M., Alves da Silva, D., Ferreira, N. V., de Pina, L. C., Evaristo, J. A. M., Caprini Evaristo, G. P., et al. (2021). Metabolic Profiles of Multidrug Resistant and Extensively Drug Resistant Mycobacterium Tuberculosis Unveiled by Metabolomics. *Tuberc. (Edinburgh Scotland)* 126, 102043. doi: 10.1016/j.tube.2020.102043

Reinehr, T., Wolters, B., Knop, C., Lass, N., Hellmuth, C., Harder, U., et al. (2015). Changes in the Serum Metabolite Profile in Obese Children With Weight Loss. *Eur. J. Nutr.* 54 (2), 173–181. doi: 10.1007/s00394-014-0698-8

Schoeman, J. C., du Preez, I., and Loots du, T. (2012). A Comparison of Four Sputum Pre-Extraction Preparation Methods for Identifying and Characterising Mycobacterium Tuberculosis Using GCxGC-TOFMS Metabolomics. *J. Microbiol. Methods* 91 (2), 301–311. doi: 10.1016/j.mimet.2012.09.002

Shin, J. H., Yang, J. Y., Jeon, B. Y., Yoon, Y. J., Cho, S. N., Kang, Y. H., et al. (2011). (1)H NMR-Based Metabolomic Profiling in Mice Infected With Mycobacterium Tuberculosis. *J. Proteome Res.* 10 (5), 2238–2247. doi: 10.1021/pr101054m

Shleeva, M., Goncharenko, A., Kudykina, Y., Young, D., Young, M., Kaprelyants, A., et al. (2013). Cyclic AMP-Dependent Resuscitation of Dormant Mycobacteria by Exogenous Free Fatty Acids. *PloS One* 8 (12), e82914. doi: 10.1371/journal.pone.0082914

Takenami, I., de Oliveira, C. C., Petrilli, J. D., Machado, A., Riley, L. W., Arruda, S., et al. (2018). Serum Antiphospholipid Antibody Levels as Biomarkers for Diagnosis of Pulmonary Tuberculosis Patients. *Int. J. Tubercul. Lung Dis.* 22 (9), 1063–1070. doi: 10.5588/ijtld.17.0874

Tobin, D. M., Roca, F. J., Oh, S. F., McFarland, R., Vickery, T. W., Ray, J. P., et al. (2012). Host Genotype-Specific Therapies can Optimize the Inflammatory Response to Mycobacterial Infections. *Cell* 148 (3), 434–446. doi: 10.1016/j.cell.2011.12.023

Tuyiringire, N., Tusubira, D., Munyampundu, J. P., Tolo, C. U., Muvunyi, C. M., Ogwang, P. E., et al. (2018). Application of Metabolomics to Drug Discovery and Understanding the Mechanisms of Action of Medicinal Plants With Anti-Tuberculosis Activity. *Clin. Trans. Med.* 7 (1), 29. doi: 10.1186/s40169-018-0208-3

Vinhaes, C. L., Oliveira-de-Souza, D., Silveira-Mattos, P. S., Nogueira, B., Shi, R., Wei, W., et al. (2019). Changes in Inflammatory Protein and Lipid Mediator Profiles Persist After Antitubercular Treatment of Pulmonary and Extrapulmonary Tuberculosis: A Prospective Cohort Study. *Cytokine* 123, 154759. doi: 10.1016/j.cyto.2019.154759

Vrieling, F., Alisjahbana, B., Sahiratmadja, E., Crevel, R., Harms, A. C., Hankemeier, T., et al. (2019). Plasma Metabolomics in Tuberculosis Patients With and Without Concurrent Type 2 Diabetes at Diagnosis and During Antibiotic Treatment. *Sci. Rep.* 9 (1), 18669. doi: 10.1038/s41598-019-54983-5

Wahl, S., Yu, Z., Kleber, M., Singmann, P., Holzapfel, C., He, Y., et al. (2012). Childhood Obesity is Associated With Changes in the Serum Metabolite Profile. *Obes. Facts* 5 (5), 660–670. doi: 10.1159/000343204

Walpole, G. F. W., Grinstein, S., and Westman, J. (2018). The Role of Lipids in Host-Pathogen Interactions. *IUBMB Life* 70 (5), 384–392. doi: 10.1002/iub.1737

Walzl, G., McNerney, R., du Plessis, N., Bates, M., McHugh, T. D., Chegou, N. N., et al. (2018). Tuberculosis: Advances and Challenges in Development of New Diagnostics and Biomarkers. *Lancet Infect. Dis.* 18 (7), e199–e210. doi: 10.1016/S1473-3099(18)30111-7

Wheelock, C. E., Goss, V. M., Balgoma, D., Nicholas, B., Brandsma, J., Skipp, P. J., et al. (2013). Application of 'Omics Technologies to Biomarker Discovery in Inflammatory Lung Diseases. *Eur. Respir. J.* 42 (3), 802–825. doi: 10.1183/09031936.00078812

World Health Organization. (2021). *World Health Organization Global Tuberculosis Report*.

Wu, Y., Gulbins, E., and Grassmé, H. (2018). The Function of Sphingomyelinases in Mycobacterial Infections. *Biol. Chem.* 399 (10), 1125–1133. doi: 10.1515/hsz-2018-0179

Yi, L., Li, Z., Jiang, H., Cao, Z., Liu, J., Zhang, X., et al. (2018). Gene Modification of Transforming Growth Factor Beta (TGF-Beta) and Interleukin 10 (IL-10) in Suppressing Mt Sonicate Induced Osteoclast Formation and Bone Absorption. *Med. Sci. Monit.* 24, 5200–5207. doi: 10.12659/MSM.909720

Zhang, X., Chen, D., Yang, W., and Wu, J. (2019). Identifying Candidate Diagnostic Markers for Tuberculosis: A Critical Role of Co-Expression and Pathway Analysis. *Math. Biosci. Eng.: MBE* 16 (2), 541–552. doi: 10.3934/mbe.2019026

Zhang, P., Zhang, W., Lang, Y., Qu, Y., Chu, F., Chen, J., et al. (2018). Mass Spectrometry-Based Metabolomics for Tuberculosis Meningitis. *Clin. Chim. Acta* 483, 57–63. doi: 10.1016/j.cca.2018.04.022

Zhou, A., Ni, J., Xu, Z., Wang, Y., Zhang, H., Wu, W., et al. (2015). Metabolomics Specificity of Tuberculosis Plasma Revealed by (1)H NMR Spectroscopy. *Tuberc. (Edinburgh Scotland)* 95 (3), 294–302. doi: 10.1016/j.tube.2015.02.038

Zhou, J., and Yin, Y. (2019). Use of Liquid Chromatography-Mass Spectrometry-Based Metabolomics to Identify Biomarkers of Tuberculosis. *Methods Mol. Biol.* 1859, 241–251. doi: 10.1007/978-1-4939-8757-3_13

Conflict of Interest: The authors declare that the research was conducted in the absence of any commercial or financial relationships that could be construed as a potential conflict of interest.

frontiers | Frontiers in Cellular and Infection Microbiology

ORIGINAL RESEARCH
published: 11 July 2022
doi: 10.3389/fcimb.2022.885865

Analysis of Clinical Features and Risk Factors in Pregnant Women With Miliary Pulmonary Tuberculosis After *In Vitro* Fertilization Embryo Transfer

Siyuan Dong[1†], *Ruoyu Zhou*[1†], *Emin Peng*[2*‡] *and Ruoxi He*[1*‡]

[1] *Department of Respiratory Medicine, National Key Clinical Specialty, Branch of National Clinical Research Center for Respiratory Disease, Center of Respiratory Medicine, National Clinical Research Center for Geriatric Disorders, Xiangya Hospital, Central South University, Changsha, Hunan, China,* [2] *Xiangya International Medical Center, Xiangya Hospital, Central South University, Changsha, Hunan,China*

OPEN ACCESS

Edited by:
Natarajaseenivasan Kalimuthusamy, Bharathidasan University, India

Reviewed by:
Shashank Ganatra, Texas Biomedical Research Institute, United States
Muthu Prasad, Bharathidasan University, India
Anbarasu Kumarasamy, Bharathidasan University, India

***Correspondence:**
Ruoxi He
heruoxi@csu.edu.cn
Emin Peng
51318029@qq.com

[†]*These authors have contributed equally to this work and share first authorship*

[‡]*These authors have contributed equally to this work*

Specialty section:
This article was submitted to Bacteria and Host, a section of the journal Frontiers in Cellular and Infection Microbiology

Received: *28 February 2022*
Accepted: *26 May 2022*
Published: *11 July 2022*

Citation:
Dong S, Zhou R, Peng E and He R (2022) Analysis of Clinical Features and Risk Factors in Pregnant Women With Miliary Pulmonary Tuberculosis After In Vitro Fertilization Embryo Transfer. Front. Cell. Infect. Microbiol. 12:885865. doi: 10.3389/fcimb.2022.885865

Purpose: Miliary pulmonary tuberculosis (TB) among pregnant women after *in vitro* fertilization embryo transfer (IVF-ET) causes poor outcomes but is rarely reported. This study analyzed the clinical characteristics and risk factors of these patients to provide hints for further studies.

Method: The demographic characteristics, clinical manifestations, radiologic features, treatment, and outcomes of six patients diagnosed from May 2012 to August 2021 in Xiangya Hospital and 69 patients that were reported in English or Chinese literature from January 1980 to August 2021 were retrospectively analyzed. Continuous variables were compared between groups by *t*-test or *Mann–Whitney U* test, and categorical variables were compared between groups by *chi-square* test or *Fisher exact* test. *Univariate and multiple logistic regression* analyses were used to determine the predictors of respiratory failure.

Results: A total of 75 patients were included. The average age of patients was about 30 years. All patients had tubal obstruction; 5 of them were diagnosed with pelvic TB before. Thirteen cases had a history of pulmonary or extrapulmonary TB, six out of them without any antituberculosis treatment history. All patients were in their first or second trimester during the onset of symptoms. The average interval between onset of symptoms and radiologic examination was about 21 days. The most common abnormalities on chest computed tomography scan were multiple nodules, pulmonary infiltrate, and consolidation. Merely 10 patients obtained bacteriological diagnosis by *Mycobacterium tuberculosis* culture or polymerase chain reaction test. The other patients were clinically diagnosed. All the patients received antituberculosis treatment. Although 44% of patients had fatal complications, all cases were cured or improved after antituberculosis treatment. Unfortunately, only eight fetuses survived (10.6%). The most frequent and severe complication was type I respiratory failure (20%). Patients with expectoration, dyspnea, coarse breath sounds, ground-glass opacity, and pulmonary infiltrate or consolidation were more likely to have respiratory failure ($P < 0.05$). Ground-glass opacity (OR = 48.545, 95% CI = 2.366–995.974, $P = 0.012$) and pulmonary infiltrate or consolidation (OR = 19.943, 95% CI = 2.159–184.213, $P = 0.008$) were independent predictors for respiratory failure.

Conclusion: Tube infertility with underscreened or untreated TB is a risk factor for miliary TB during pregnancy after IVF-ET. Ground-glass opacity and pulmonary infiltrate or consolidation are predictors of respiratory failure. We demonstrate risk factors for incidence and complications to supply clues for future intervention and improve patient prognosis.

Keywords: miliary pulmonary tuberculosis, pregnant, infertility, *in vitro* fertilization, embryo transfer

INTRODUCTION

Tuberculosis (TB) is a communicable disease caused by the bacillus *Mycobacterium tuberculosis* which is a major cause of ill health and one of the leading causes of death globally. Worldwide, an estimated 9.9 million people fell ill with TB in 2020 (WHO, 2021a). Pregnancy is one of the risk factors for TB. The incidence rate ratio for TB in pregnant women is 1.4 and 1.9 times for postpartum compared with non-pregnant women (Jonsson et al., 2020). TB is a curable and preventable disease. However, the delay in the diagnosis and treatment of TB during pregnancy is associated with poor outcomes, including increased mortality in both fetuses and pregnant women (Sugarman et al., 2014). Pregnancy after *in vitro* fertilization and embryo transfer (IVF-ET) is a special and underestimated condition, which is susceptible to TB infection, especially miliary TB infection (Wang et al., 2022). However, the underlying reasons have not been clarified yet. IVF-ET is an effective technique to treat infertility with the process of *in vitro* fertilization of treated sperm and cultured mature ovum to form fertilized ovum and then implant early embryos into the uterine cavity. Genital TB (GTB) is a chronic inflammatory disease of reproductive organs involving the fallopian tubes, ovaries, pelvic peritoneum, and endometrium caused by *M. tuberculosis* with an approximately 3%–16% incidence rate in developing countries (Sharma, 2015), which is one of the most common causes of infertility (Muneer et al., 2019). Undetected and untreated GTB or other latent TB infections before IVF-ET is probably the main cause of miliary TB because the reactivation of a latent TB focus could cause miliary TB *via* hematogenous spread (Gai et al., 2021). After establishing a primary focus of infection in the lung, miliary TB affects multiple organs and systems, such as the liver, spleen, bone marrow, and brain. Miliary TB is associated with poor prognosis, which may induce not only fetal death but also life-threatening complications to patients such as respiratory failure and acute respiratory distress syndrome (ARDS) (Ma et al., 2021). Several case reports and case series referring to miliary TB after IVF-ET have been reported previously (Jacquemyn et al., 2012; Li and Zhao, 2015; Ye et al., 2019; Gai et al., 2021). Retrospective studies are rare. China is a developing country with high incidence as well as considerable burden of pregnancy TB (Sugarman et al., 2014). Most of the cases were published in Chinese by Chinese scholars without being included in previous analyses. This is a retrospective study of 69 cases that were previously reported both in the English and Chinese literatures combined with six cases diagnosed in Xiangya Hospital. The purpose of this study is to highlight the characteristics of pregnant cases with miliary pulmonary TB after IVF-ET and the probable risk factors.

MATERIALS AND METHODS

Research Subjects in Our Hospital

This study was performed at Xiangya Hospital, Central South University (China), a 3,500-bed tertiary-care center. Six pregnant patients with miliary pulmonary TB after IVF-ET from May 2012 to August 2021 were included through a systemic search of the database in our hospital. Demographic characteristics; past medical history; clinical presentations; radiologic, laboratory, and bronchoscopic findings; diagnostic approaches; treatments; and outcomes were retrospectively extracted from medical records using a standardized protocol. The studies involving human participants were approved by the Ethics Committee of Xiangya Hospital, Central South University (No. 201906766).

Literature Review and Data Acquisition

We conducted a MEDLINE (National Library of Medicine, Bethesda, Maryland) search with the MeSH terms ("Fertilization *in vitro*" or "embryo transfer" or "pregnancy") and "tuberculosis" to identify literature published between January 1980 and August 2021. We found 69 relevant literatures. After excluding irrelevant ones, a total of five relevant literatures were retrieved (Addis et al., 1988; Gull et al., 1995; Jacquemyn et al., 2012; Li and Zhao, 2015; Ye et al., 2019). The literature types were case reports and retrospective studies including 10 cases with valid variables. The same retrieval strategy was adopted to search in four Chinese databases, namely, China National Knowledge Infrastructure (CNKI), Chinese Biomedical Literature Database (CBM), VIP Database for Chinese Technical Periodicals, and Wanfang Database. In total, we found 168 relevant literatures. After excluding the literatures irrelevant to the subjects as well as those that lack clear diagnostic information and outcome, 23 relevant literatures were included with a total of 59 valid cases. All data shown here were extracted from these case reports and case series; some articles occasionally lacked relevant clinical data or treatment.

Definitions

The bacteriologically confirmed pulmonary TB is established by isolation of *M. tuberculosis* from a bodily secretion or fluid (e.g., culture of sputum, bronchoalveolar lavage fluid (BALF), or

pleural fluid) or tissue (e.g., pleural biopsy or lung biopsy) (Madhukar et al., 2016). A positive nucleic acid amplification test (NAAT) amplification of the genetic material uses the polymerase chain reaction (PCR) method in a person at risk for TB (who has no prior history of treatment for TB) who is considered sufficient for diagnosis of TB (WHO, 2021b). Clinically diagnosed pulmonary TB is based on symptoms, abnormalities on chest radiography/computed tomography (CT), suggestive histology, or the clinical and radiographic improvement after antituberculosis treatment (Deng et al., 2012; WHO, 2021b). The term miliary pulmonary TB was originally a pathologic and then a radiographic description. Patients are diagnosed with miliary pulmonary TB if they have a diagnosis of TB with the hallmark radiological appearance of the involved lung covered with firm small white nodules like numerous millet seeds.

Statistical Methods

The data were shown as mean ± standard deviation (SD) for quantitative variables and as absolute and relative frequencies (%) for qualitative variables. Continuous variables were compared between groups by *t*-test or *Mann–Whitney U* test, and categorical variables were compared between groups by *chi-square* or *Fisher exact* test. The independent risk predictors of respiratory failure were determined by *univariate and multivariate binary logistic regression* analyses. All significance tests were two-tailed tests. Statistical significance was set at $P < 0.05$. SPSS 22.0 software was used for statistical analysis.

RESULTS

The characteristics of six patients in our hospital are presented in **Table 1**. The average age was 30 years. The intervals from embryo transfer to the onset of symptoms were from 42 to 109 days. All six patients were diagnosed with fallopian tube obstruction before IVF-ET, and none of them underwent laparoscopy before. Two out of six patients had a history of TB infection; one of them did not accept treatment for pulmonary TB. Fever and dyspnea were complained by all the patients, which were the most common symptoms followed by cough. All patients had coarse breath sounds and moist rales on physical examination. Multiple nodules were presented among six patients, and half of the patients were illustrated with ground-glass opacity (GGO), pulmonary infiltrate or consolidation, and pleural effusion. All the patients had an elevated CRP level and neutrophil level in peripheral blood cell tests. The cultures of *M. tuberculosis* and PPD skin reaction were negative; however, T-cell enzyme-linked immunospot (T-SPOT) was positive. Patients were clinically diagnosed with pulmonary TB. Four out of six patients underwent bronchoscopy, but the changes were non-specific. Additionally, merely one patient was proved to be positive in acid-fast bacillus (AFB) smear of BALF. The primary diagnosis of patients was pneumonia, and patients were treated with broad-spectrum antibiotics as the initial treatment. Three out of them underwent respiratory failure and/or combined with ARDS. After being diagnosed, six patients received first-line antituberculosis treatments as recommended by the World Health Organization and were cured eventually. However, only one baby survived.

As **Table 2** shows, all the 75 patients were of childbearing age. The mean age of patients ranged from 21 to 39 years. The intervals between embryo transfer and the onset of symptoms varied from 28 to 240 days. All patients were in their first or second trimester when symptoms appeared. In available data, 53 patients were diagnosed with unilateral or bilateral fallopian tubal obstruction. Among them, five cases had been diagnosed with pelvic TB before they received IVF-ET, two out of them diagnosed by laparoscopy. Other patients with fallopian tubal obstruction did not exclude reproductive system TB by further examinations. There were 14.7% of patients with a history of diagnosed pulmonary TB or radiologic changes inferring to latent pulmonary TB; 10.7% of patients had extrapulmonary TB including pelvic TB, tuberculosis pleurisy, or tuberculosis peritonitis. Less than a third of patients with TB and one out of five patients with pelvic TB had been treated with antituberculosis drugs before.

As described in **Table 3**, the most common symptoms observed were fever (mainly high fever, ranging from 37.5°C to 40.0°C) (96.0%), cough (64.0%), dyspnea (46.7%), and vaginal bleeding (34.7%). Other symptoms suggestive of TB were uncommon, including night sweats (18.7%), decreased appetite (10.7%), fatigue (6.7%), and weight loss (4%). Besides fever, we found symptoms indicating intracranial TB infection, such as headache (18.7%) and disorders of consciousness (6.7%). Twenty-six of the 43 patients (60.5%) had positive physical findings. However, most of them were non-specific except neck stiffness (7%). A radiologic examination was done in all patients. The average interval time between the onset of symptoms and the first radiologic examination was about 21 days (range from 9 to 51 days). A percentage of 65.7% of the cases preferred to have X-ray examination other than CT scan initially; 12 of those patients (27.3%) were found to have miliary lesions in X-ray without further radiological examination. Thirty-two of 44 patients (72.7%) further underwent a CT scan for a certain diagnosis. Abnormal radiologic findings included multiple nodules (100%), pulmonary infiltrate or consolidation (32.7%), calcification (29.1%), pleural effusion (12.7%), GGO (9.1%), and fibrotic shadows (2.7%).

The laboratory and bronchoscopic findings are described in **Table 4**. In the aspect of inflammation examinations, 34 of 62 patients (54.8%) had normal blood tests, and 45.2% had elevated white blood cell (WBC) count and/or increased neutrophil percentage. The erythrocyte sedimentation rate (ESR) and C-reactive protein (CRP) level were observed to be elevated in most of the patients with available variables, 75% and 100% respectively. However, the two values had large variations. In the other aspect of examinations for TB, the most common test, PPD skin reaction test (24%), had a lower positive rate than T-spot assay (95.2%). Additionally, the positive ratios of *M. tuberculosis* culture and AFB smear were also very low, 24.1% in sputum and 28.6% in BALF for *M. tuberculosis* culture, and 33.3% in sputum and 40% in BALF for AFB smear. There were also some unexpected findings in unusual species like urine, cerebrospinal fluid,

TABLE 1 | Characteristics of six patients diagnosed with miliary pulmonary tuberculosis after IVF-ET in Xiangya Hospital.

Variables[a]	No. of patients N (%)/(mean ± SD)
Age, years [6]	30.33 ± 1.21 (29–32)
Time from received IVF-ET to onset of symptoms, days [6]	81.83 ± 25.56 (42–109)
Diagnosed with fallopian tube obstruction before IVF-ET [6]	6 (100)
Diagnosed with tuberculosis before and antituberculosis drugs treatment [6]	
Untreated pulmonary tuberculosis	1 (16.7)
Treated tuberculosis peritonitis	1 (16.7)
Clinical manifestations at diagnosis[6][b]	
Fever	6 (100)
High-grade fever	3 (50)
Moderate fever	3 (50)
Dyspnea	6 (100)
Cough	5 (83.3)
Productive cough	3 (50)
Non-productive cough	2 (33.3)
Decreased appetite	4 (66.7)
Vaginal bleeding	3 (50)
Headache	2 (33.3)
Fatigue	2 (33.3)
Night sweat	1 (16.7)
Disorders of consciousness	1 (16.7)
Weight loss	1 (16.7)
Physical examination findings [6][b]	
Coarse breath sounds	6 (100)
Moist rales	6 (100)
Radiologic examination methods [6]	
X-ray+ CT	5 (83.3)
Only CT	1 (16.7)
Interval between onset of symptoms to radiologic examination, days [6]	21.17 ± 6.91 (10–30)
Radiologic findings [6][b]	
Multiple nodules	6 (100)
Ground-glass opacity	3 (50)
Pulmonary infiltrate or consolidation	3 (50)
Pleural effusion	3 (50)
Calcification	1 (16.7)
Laboratory examination	
Elevated CRP [4]	4 (100)
CRP (mg/L)	89.75 ± 38.18 (55–132)
Elevated ESR [6]	4 (66.7)
ESR (mm/h)	53.17 ± 35.41 (6–83)
Elevated neutrophils in peripheral blood cells blood tests[6]	6 (100)
PPD skin reaction positive [2]	0
T-spot positive[5]	5 (100)
Acid-fast bacilli smear positive	
Sputum [6]	1 (16.7)
BALF[4]	1 (25)
Mycobacterium tuberculosis culture positive	
Sputum [4]	0
BALF [3]	0
Diagnosed method [6]	
Clinically diagnosed with pulmonary tuberculosis	6 (100)
Pathological diagnosis	1 (16.7)
Bronchoscopic descriptions[6]	4 (66.7)
Inflammation	2 (33.3)
Purulent secretion	1 (16.7)
Hyperemic mucosa	1 (16.7)
Primary diagnosis [6]	
Pneumonia	6 (100)
Type of initial pharmacological therapies [6]	
Broad-spectrum antibiotics	6 (100)
Type of antituberculosis treatments [6]	
Isoniazid + rifampicin + pyrazinamide + ethambutol	5 (83.3)
Isoniazid + rifampicin + pyrazinamide	1 (16.7)
Outcomes[6]	
Cured	6 (100)
Fetal condition[6]	
Spontaneous abortion	2 (33.3)
Artificial termination of pregnancy	1 (16.7)
Stillborn and curettage	1 (16.7)
Preterm delivery and death	1 (16.7)
Survivor	1 (16.7)
Complication [6][b]	
Type I respiratory failure	3 (50)
Tuberculosis meningitis	1 (16.7)
Acute respiratory distress syndrome	2 (33.3)

[a]*Values in brackets represent number of patients for whom data were available.*
[b]*Total number of patients may be less than the sum of clinical manifestations, physical examination findings, radiologic findings, and complications, because in some cases >1 variable was present in the same patient.*
IVF-ET, in vitro fertilization embryo transfer; CRP, C-reactive protein; ERS, erythrocyte sedimentation rate; BALF, bronchoalveolar lavage fluid; PCR, polymerase chain reaction.

and fetal chorionic. Ten patients in this study were microbiologically diagnosed with miliary pulmonary TB by *M. tuberculosis* culture (9.3%) or PCR assay (4%) without drug susceptibility testing. The rest of the patients (65 out of 75) were clinically diagnosed, four of whom had pathologic histology evidence with caseous necrosis in granulomas with/without positive AFB smear. Seven patients had the description of bronchoscopy examination (9.3%). Inflammation of the bronchus was the most common pathological change (57.1%) followed by purulent secretion (14.3%) and hyperemic mucosa (14.3%). One of them had a normal description under bronchoscopy.

Initially, all the patients were misdiagnosed with pneumonia and treated with broad-spectrum antibiotics (**Table 5**). The patients subsequently received antituberculosis therapy after being microbiologically or clinically diagnosed with pulmonary TB. Antituberculosis treatment regimens were slightly different from case to case. Overall, isoniazid (H), rifampicin (R), pyrazinamide (Z), and ethambutol (E) were the most frequently used first-line antituberculosis therapy (49.3%). After the treatment, all the patients had improvement or were cured. However, merely eight of 75 fetuses (10.6%) survived. The leading reason for fetal mortality was spontaneous abortion (46.7%), followed by artificial termination of pregnancy (32%), stillbirth (7.5%), and preterm delivery and death (4%). Twenty-five percent of patients had fatal complications including respiratory failure, ARDS, and shock. The most frequent and severe complication was type I respiratory failure (15 in 75 cases, 20%); the second was tuberculosis meningitis (13 cases, 17.3%), followed by ARDS (3 cases, 4%) (**Table 4**).

TABLE 2 | Demographic characteristics and past medical history in 75 patients diagnosed with miliary pulmonary tuberculosis after IVF-ET.

Variables[a]	No. of patients N (%)/(mean ± SD)
Age, years [75]	30.20 ± 3.54 (21–39)
Time from IVF-ET to onset of symptoms, days [63]	82.79 ± 40.86 (28–240)
Diagnosed with fallopian tube obstruction before IVF-ET [53]	53 (100)
Type of embryos for IVF-ET [18]	
Fresh embryos	14 (77.8)
Frozen-thawed embryos	4 (22.2)
Diagnosed with tuberculosis before [75]	
None	56 (74.7)
Extrapulmonary tuberculosis	8 (10.7)
Pelvic tuberculosis	5 (6.7)
Tuberculosis pleurisy	2 (2.7)
Tuberculosis peritonitis	1 (1.3)
Latent pulmonary tuberculosis diagnosed by X-ray/CT scan	6 (8)
Pulmonary tuberculosis	5 (6.7)
Treated with antituberculosis drugs [19]	
Extrapulmonary tuberculosis [8]	
Treated	5 (29.4)
Untreated	2 (11.8)
Latent pulmonary tuberculosis [6]	
Untreated	6 (35.3)
Pulmonary tuberculosis [5]	
Treated	2 (11.8)
Untreated	2 (11.8)

[a]*Values in brackets represent number of patients for whom data were available.*
IVF-ET, in vitro fertilization embryo transfer.

The dynamic imaging changes of a 30-year-old pregnant woman diagnosed with miliary pulmonary TB after IVF-ET at Xiangya Hospital are shown in **Figure 1**. The routine chest X-ray before the IVF-ET procedure was normal (**A**). Half a month after IVF-ET, the patient started to have fever and shortness of breath. X-ray showed a massive and symmetrical GGO in bilateral lungs 40 days after IVF-ET (**Figure 1B**). After antituberculosis treatment for a week, imaging showed a decrease in GGO (**C**). CT scan revealed diffuse GGO with partial fusion, multiple nodules, and a small amount of pleural effusion in the right thorax and a calcification nodule in the right middle lobe (**Figure 1D**). (**Figures 1E, F**) Resolution of miliary nodules was observed after 1 and 2 months of antituberculosis treatment, respectively. (**Figures 1G–I**) CT scan at 8 months and 1 and 3 years after therapy showed that nodules disappeared in the lungs.

Chest radiological images of six patients from Xiangya Hospital are presented in **Figure 2**. All images of six patients showed miliary and multiple nodules in the bilateral lungs. **Figure 2A** illustrates the extensive GGO. Multiple nodules were indiscernible against the background of ground-glass shadows in both lungs (**Figure 2B**). **Figure 2C** depicts diffuse random multiple nodules, which is a typical presentation of miliary pulmonary TB. **Figures 2D, E** show the symmetric distribution of pulmonary infiltrate and consolidation, accompanied by bilateral pleural effusion as shown in **Figure 2D**. GGO, pulmonary infiltrate, and consolidation were as presented in **Figure 2F**, and a fluid pneumothorax was found at the right thorax after mechanical ventilation.

The *chi-square* test showed that patients with expectoration, dyspnea, coarse breath sounds, GGO, and pulmonary infiltrate or consolidation were more likely to have respiratory failure ($P < 0.05$) (**Table 6**). Within 21 days of symptom onset, GGO was more possible to be detected by imaging ($P < 0.05$) (data not shown). *Logistic regression* analysis identified that pulmonary infiltrate and consolidation (odds ratio (OR) = 19.943, 95% confidence interval [CI] = 2.159–184.213, $P = 0.008$) and GGO (OR = 48.545, 95% CI = 2.366–995.974, $P = 0.012$) were independent predictors of respiratory failure (**Table 7**).

The characteristics of patients with successful pregnancies are presented in **Table 8** (Hou et al., 2005; Chu et al., 2011; Zhang, 2013; Liu et al., 2016; Wen et al., 2016; Zhang et al., 2017). When they were diagnosed with TB, three out of eight patients were in their first trimester, three patients were in the second trimester, and one patient was in the last trimester of pregnancy. Five patients had severe complications; three of them had tuberculosis meningitis, and two of them had respiratory failure. The antituberculosis treatment started immediately after diagnosis. Most patients received first-line antituberculosis therapy; only one patient was treated with p-aminosalicylic acid, one of second-line drugs. Four patients with complications were recorded using glucocorticoid accompanied by antituberculosis therapy. Merely three fetuses survived and were delivered by full-term cesarean section. The rest of the fetuses were delivered preterm, and one of them suffered from severe congenital TB. In accordance with our statistical analysis (data not shown), no significant difference was found between the patients with successful pregnancies and pregnancy termination.

DISCUSSION

Miliary TB is a potentially fatal form of TB. Approximately 15%–30% of patients with pulmonary TB during pregnancy exhibit hematogenous dissemination and suffer from miliary TB (Sobhy et al., 2017). It has been reported that the reasons for this phenomenon are associated with immune dysregulation (Mor and Cardenas, 2010), increased vascular permeability (Mali and Meena, 2018), or elevated blood lipid levels (Miele et al., 2020) during pregnancy, while miliary TB in pregnancy after IVF-ET is rare and the incidence has not been estimated. Our results reinforced previous findings that women during pregnancy after IVF-ET were more prone to miliary TB (Ye et al., 2019; Gai et al., 2021). Besides the waning of cellular immunity, latent TB infection and IVF-ET interventions were related to susceptibility to miliary TB (Singh and Perfect, 2007).

GTB is associated with 0.2% to 21% of infertility cases, mostly among women in resource-limited settings (Aliyu et al., 2004). Dam et al. detected 81 patients with unexplained infertility and repeated failure of *in vitro* fertilization in India by taking endometrial tissue or menstrual blood for *M. tuberculosis* PCR and found that 63 of them were positive (Dam et al., 2006). GTB is one of the most frequent etiologies of tubal infertility. Tubal infertility patients always present with failure to achieve a successful pregnancy after 12 months or more of regular unprotected intercourse in a woman

TABLE 3 | Clinical manifestations and radiologic findings.

Variables[a]	No. of patients N (%)/ (mean ± SD)
Clinical manifestations at diagnosis[75][b]	
Fever	72 (96)
High-grade fever	39 (67.2)
Moderate fever	15 (25.9)
Low-grade fever	4 (6.9)
Cough	48 (64)
Productive cough	27 (56.3)
Nonproductive cough	21 (43.7)
Dyspnea	35 (46.7)
Vaginal bleeding	26 (34.7)
Night sweat	14 (18.7)
Headache	14 (18.7)
Shiver	10 (13.3)
Decreased appetite	8 (10.7)
Fatigue	5 (6.7)
Disorders of consciousness	5 (6.7)
Weight loss	3 (4)
Physical examination findings[43][b]	
Coarse breath sounds	18 (41.9)
Moist rales	18 (41.9)
Peripheral edema	4 (9.3)
Low pitched breath sounds	3 (7)
Neck stiffness	3 (7)
Radiologic examination methods[67]	
X-ray+ CT	32 (47.8)
Only CT	23 (34.3)
Only X-ray	12 (17.9)
Interval between onset of symptoms to radiologic examination, days [67]	21.46 ± 10.81 (9-51)
Radiologic findings[55][b]	
Multiple nodules	55 (100)
Pulmonary infiltrate or consolidation	18 (32.7)
Calcification	16 (29.1)
Pleural effusion	7 (12.7)
Ground-glass opacity	5 (9.1)
Fibrotic shadows	2 (2.7)

[a]*Values in brackets represent number of patients for whom data were available.*
[b]*Total number of patients may be less than the sum of clinical manifestations, physical examination findings, and radiologic findings, because in some cases >1 variable was present in the same patient.*

combined with a history of tubal ligation or tubal changes including occlusion, hydrosalpinx, beading by hysterosalpingography, or laparoscopy (Briceag et al., 2015). *M. tuberculosis* can lead to fallopian tube inflammation, resulting in fallopian tube swelling, ponding, and intimal hyperplasia. In our study, most of the patients diagnosed with fallopian tube occlusion did not undergo laparoscopy or further examinations to exclude GTB. If IVF-ET is performed in GTB patients, *M. tuberculosis* in the original extrapulmonary lesions will spread to multiple systems through blood and lymph, resulting in miliary TB and fetal infection, even death (Ghosh et al., 2011). Extrapulmonary TB infections including GTB usually occur *via* hematogenous spread from the lungs (Aliyu et al., 2004; Moule and Cirillo, 2020). Pulmonary TB lesions such as calcification, fibrotic shadows, and pleural thickening were detected in routinely chest X-ray examination before IVF-ET in some cases here. The activation of latent *M. tuberculosis* may be the main reason for miliary TB in pregnant patients after IVF-ET.

As far as I know, there is lack of international guidelines and consensus on the TB screening procedures in patients with tubal occlusion before IVF-ET. Nowadays, tuberculosis is not uncommon in developed countries because of the increasing number of immigrants. However, TB screening is not part of the routine tests in infertility patients in developed countries (Jacquemyn et al., 2012). Laparoscopy was executed in all of three patients reported before in developed countries (Addis et al., 1988; Gull et al., 1995; Jacquemyn et al., 2012). It seems that laparoscopy is a usual examination not for TB screening but for infertility patients. In China, due to the high prevalence and burden of TB, TB screening by X-ray is the routine examination before IVF-ET nowadays. On the contrary, because of the limited medical and financial resources, only patients with risk factors for active TB infection will be asked to complete laparoscopy, including relevant clinical manifestations (pelvic or abdominal pain, and/or menstrual disorders) or classical changes under hysterosalpingography (fallopian tube constriction and/or uterine cavity adhesion or deformity, especially beaded tubal), as well as relevant epidemiologic factors (history of prior TB infection without antituberculosis treatment) and/or radiographic findings referring to active TB infection (Malhotra et al., 2020).

Another possible cause of miliary TB after IVF-ET is the interventions in IVF-ET. Artificial insemination requires progesterone to support luteal function and promote embryonic development. At the same time, estrogen, progesterone, and human chorionic gonadotropin *in vivo* are significantly higher than physiological levels. These hormones have a direct inhibitory effect on $CD4^+$ T lymphocytes and change the ratio of helper T lymphocyte cells (Th cells) to regulatory T cells (Treg cells) (Schumacher, 2017). $CD4^+$ T lymphocytes play an important role in the infection of *M. tuberculosis*. Th cells help to enhance immune function, while Treg cells can inhibit immune response (Ghosh et al., 2011). The imbalance of the proportion of these two cells will be conducive to the spread of *M. tuberculosis*. On the other hand, adrenocortical hormones will be used to improve endometrial receptivity in some conditions, which could inhibit the organic immune system as well (Plaks et al., 2006). Therefore, the changes in hormone levels in pregnant women during pregnancy easily lead to the new infection of TB, or the reactivation and diffusion of latent *M. tuberculosis*.

In general, it is recommended that patients with high prevalence and burden of TB regions should have more tests before assisted reproduction except X-ray to exclude latent TB infection and avoid TB dissemination. Tuberculin skin test (TST) is probably the most cost-effective test for latent TB screening. The combination of TST, interferon-gamma release assay (IGAR), or molecular WHO-recommended rapid diagnostic tests (WHO, 2021c), if available, is recommended among patients with latent lesions of TB on chest radiography as well. Tubal infertility patients with the abovementioned high-risk factors are still recommended to execute laparoscopy before IVF-ET. The guidelines or protocols for screening before IVF-ET should be formulated in the future.

TABLE 4 | Laboratory examinations and bronchoscopic descriptions.

Variables[a]	No. of patients N (%)/(mean ± SD)
Laboratory examinations	
Elevated CRP[29]	29 (100)
CRP (mg/L)	55.9 ± 35.6 (11.7–132.0)
Elevated ESR [44]	33 (75)
ESR (mm/h)	47 ± 29 (6–132)
Elevated neutrophils in peripheral blood cells blood tests[62]	28 (45.2)
PPD skin reaction positive[25]	6 (24)
T-spot positive[21]	20 (95.2)
Acid-fast bacilli smear positive	
Sputum[29]	7 (24.1)
BALF [7]	2 (28.6)
Urine[1]	1 (100)
Mycobacterium tuberculosis culture positive	
Sputum[16]	6 (37.5)
BALF[5]	2 (40)
Cerebrospinal fluid[1]	1 (100)
Fetal chorionic[1]	1 (100)
Urine[1]	1 (100)
Blood[1]	1 (100)
Antituberculosis drug susceptibility testing	0
Mycobacterium tuberculosis PCR positive	
Sputum[7]	2 (28.6)
BALF[1]	1 (100)
Fetal chorionic[1]	1 (100)
Diagnosed method[75]	
Microbiological diagnosis	7 (9.3)
Sputum culture	5 (6.7)
BALF culture	2 (2.7)
PCR test	3 (4.0)
Sputum	2 (2.7)
BALF	1 (1.3)
Clinically diagnosed with pulmonary tuberculosis	65 (86.7)
Pathological diagnosis	4 (5.3)
Bronchoscopic descriptions[7]	
Inflammation	4 (57.1)
Purulent secretion	1 (14.3)
Hyperemic mucosa	1 (14.3)
Normal	1 (14.3)

[a]*Values in brackets represent number of patients for whom data were available.*
CRP, C-reactive protein; ERS, erythrocyte sedimentation rate; BALF, bronchoalveolar lavage fluid; PCR, polymerase chain reaction.

The early clinical manifestations of miliary pulmonary TB are diverse and non-specific (Sharma and Mohan, 2017). The most common symptoms in this study were high-level fever, cough, and dyspnea which were consistent with studies before (Ye et al., 2019; Gai et al., 2021). The most common symptom was fever because miliary TB causes fulminant infection and systemic inflammatory response. Half or more cases had increased neutrophils in blood test, ESR, and CRP in this study. T-SPOT is one kind of IGRAs, which is not affected by Bacille Calmette-Guérin (BCG) vaccination or most *non-tuberculous mycobacteria* (Pai et al., 2008). The sensitivity of T-SPOT appears to be higher than TST (approximately 90% vs. 80%) (Pai et al., 2008). The higher sensitivity of T-SPOT may be useful for evaluating individuals with immunosuppressive conditions. In this study, the positive rate of T-SPOT was much higher than TST; the possible reason is that patients with miliary pulmonary TB after IVF-ET are in a relative anergy condition. The etiological examination is critical because it is the gold standard for the diagnosis of TB, but it may be less feasible in some circumstances (Pai et al., 2016). Of the 4.8 million people diagnosed with pulmonary TB worldwide in 2020, 59% were bacteriologically confirmed (WHO, 2021a). At least 15% to 20% of patients with clinical diagnosis of TB have never been identified by specific bacteriology (CDC, 2015). In our study, only 10 patients had confirmed diagnosis. None of the drug susceptibility tests had been reported in the cases. The possible reason is the unavailability of drug susceptibility tests. In China, due to pregnancy, those patients had been diagnosed mostly at general hospitals rather than at specialized tuberculosis hospitals which have laboratories to perform all tests relevant to TB including drug susceptibility tests. In the United States, not all laboratories perform all tests too. All United States jurisdictions require the submission of culture isolates identified as *M. tuberculosis* complex (MTBC) by any laboratory to their jurisdictional public health laboratory for identification and drug susceptibility testing. Another possible reason is that physicians had insufficient knowledge and did not pay attention to drug-resistant TB because most of the patients did not have risk factors for drug-resistant TB. Merely three patients were diagnosed by PCR assay here. How to get the microbiological detection of TB as early as possible is the trickiest problem. The amplification and detection of MTBC nucleic acids is a technology that has proven to be highly sensitive and specific. WHO recommended that Xpert MTB/RIF should be used as an initial diagnostic test for TB in sputum rather than smear microscopy/culture. However, the use of rapid tests remains far too limited because it is expensive and unreachable in some areas. Among the 49 countries in one of WHO's three global lists of high burden countries (for TB, HIV-associated TB and multidrug-resistant TB or rifampicin-resistant TB), only 21 countries reported that a WHO-recommended rapid diagnostic test had been used as the initial test for more than half of their notified TB cases (WHO 2021b). Seven cases in our series had reported bronchoscopic examination; six out of them had unspecific positive findings. Bronchoscopy is an option to obtain BALF or tissue specimens when the diagnosis is difficult and sputum is not available.

After establishing a focus of infection in the lung, bacilli can disseminate *via* the hematogenous to the most vascular organs, such as brain meningeal involvement, which was evident postmortem in 54% of cases of miliary TB (Mali and Meena, 2018). In our study, 14 out of 75 cases (18.7%) were complicated with TB meningitis and/or encephalitis. Two cases were diagnosed with endometrial TB after IVF-ET. Most clinical features of miliary TB have low specificity, which may lead to incorrect and delayed diagnosis of TB. All the patients were misdiagnosed with bacterial pneumonia and accepted antibodies therapy initially in our study. The probable reasons are non-specific presentation, elevated infection tests, and suspended radiological examination. This study reminds us that if a pregnant woman has high-grade fever and shortness of breath

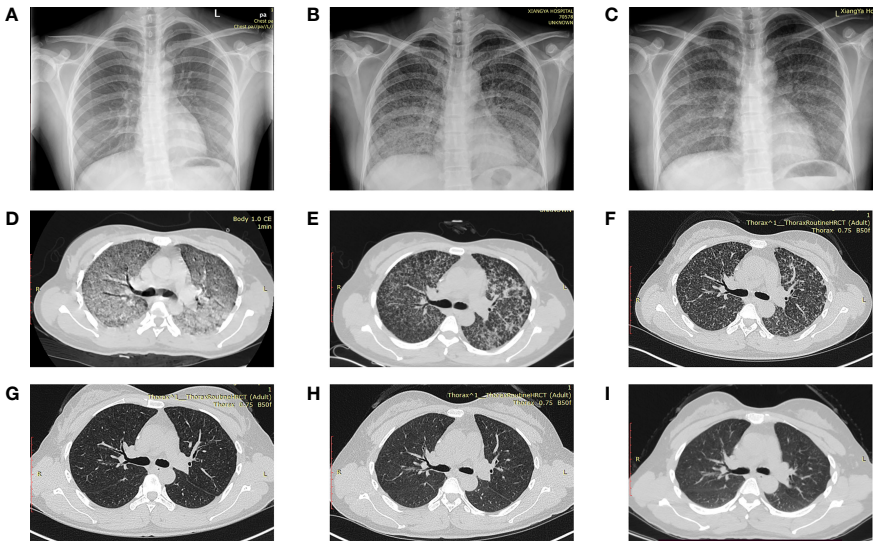

FIGURE 1 | Dynamic imaging changes of a 30-year-old pregnant woman diagnosed with miliary pulmonary tuberculosis after *in vitro* fertilization and embryo transfer **(A)** Normal chest X-ray in the routine exam before IVF-ET. **(B)** A massive and symmetrical ground-glass opacity in bilateral lungs 40 days after IVF-ET. **(C)** Decreased ground-glass opacity after antituberculosis treatment. **(D)** Diffuse ground-glass opacity and partial fusion, multiple nodules, and a small amount of pleural effusion in the right thorax and a calcification nodule in the right middle lobe. **(E, F)** Resolution of miliary nodules after 1 and 2 months of antituberculosis treatment, respectively. **(G–I)** Nodules disappeared at 8 months and 1 and 3 years after treatment. IVF-ET, *in vitro* fertilization and embryo transfer.

and does not respond to antibiotic treatment, pulmonary TB infection should be alerted and radiographic examination, TB screening, and even antituberculosis treatment should be started immediately. Since the sensitivity of culture and AFB smear is low, it suggests the need to utilize more sensitive assays like Xpert MTB/RIF and to obtain other sample sources as possible, such as urine, blood, and cerebrospinal fluid specimens.

Miliary pulmonary TB presents with acute onset and rapid clinical course. However, the delay of X-ray or CT examination among pregnant patients is common resulting from the fear of radiation exposure. Most of patients choose to accept chest X-ray instead of a more sensitive CT scan at first. Our study found that merely 27.3% of the 44 patients who underwent an X-ray examination showed typical miliary nodules. Previous research had shown that 50% of patients did not see typical manifestations on chest X-rays at the early onset, because it can be displayed under X-ray only in the presence of caseous material (Hunter, 2018). CT has a better distinguishability to the distribution of nodules than chest X-ray (Lee et al., 2014). All patients in this study were found to have miliary nodules in bilateral lungs by CT scan. GGO was discovered in 9.1% of patients here and 12.9% reported before (Han et al., 2009), indicating the beginning and

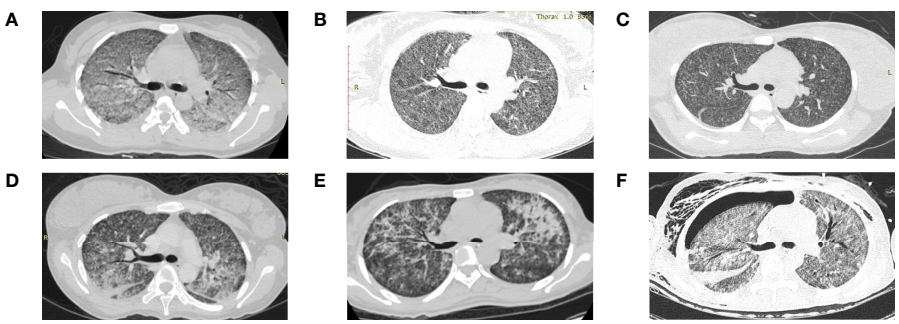

FIGURE 2 | Chest computed tomography scan of six patients from Xiangya Hospital diagnosed with miliary pulmonary tuberculosis after *in vitro* fertilization and embryo transfer **(A)** Extensive ground-glass opacity in both lungs. **(B)** Indiscernible multiple nodules against the background of ground-glass shadows in both lungs. **(C)** Diffuse random multiple nodules in bilateral lungs. **(D)** Symmetric distribution of pulmonary infiltrate and consolidation in both lungs and bilateral pleural effusion. **(E)** Multiple patchy high-density shadows in both lungs. **(F)** Ground-glass opacity, pulmonary infiltrate and consolidation in both lungs, and a fluid pneumothorax at the right thorax.

TABLE 5 | Treatment, outcomes, and complications.

Variables[a]	No. of patients N (%)/(mean ± SD)
Primary diagnosis[58]	
Pneumonia	58 (100)
Type of initial pharmacological therapies[58]	
Broad-spectrum antibiotics	58 (100)
Type of anti-tuberculosis treatments[75]	
Isoniazid+rifampicin+pyrazinamide+ethambutol	37 (49.3)
Isoniazid+rifampicin+pyrazinamide	4 (5.3)
Isoniazid+pyrazinamide+ethambutol+p-aminosalicylic acid	1 (1.3)
Isoniazid+ethambutol+streptomycin	1 (1.3)
Isoniazid+ethambutol	1 (1.3)
Outcomes[75]	
Improved	48 (64)
Cured	27 (36)
Fetal condition[75]	
Spontaneous abortion	35 (46.7)
Artificial termination of pregnancy	24 (32)
Survived	8 (10.6)
Stillborn and curettage	5 (6.7)
Preterm delivery and death	3 (4)
Complication[75][b]	
Type I respiratory failure	15 (20)
Tuberculous meningitis and/or encephalitis	14 (18.7)
Acute respiratory distress syndrome	3 (4)
Endometrial tuberculosis	2 (2.7)
Anemia	1 (1.3)
Hypoproteinemia	1 (1.3)
Shock	1 (1.3)

[a]*Values in brackets represent number of patients for whom data were available.*
[b]*Total number of patients may be less than the sum of complications, because in some cases >1 variable was present in the same patient.*

rapid progress of miliary pulmonary TB (Im et al., 1995). A study found that patients with GGO exceeding 50% of the area of bilateral lung had a higher level of acute inflammatory indexes and were more prone to dyspnea, even respiratory failure and ARDS (Lee et al., 2014). Numerous tiny granulomas overlapped by the exudative lesions TB are not easily distinguished at the early stages of miliary pulmonary TB (McGuinness et al., 1992). We found that GGO was more likely to be found by chest imaging within 3 weeks after the onset of symptom. This imaging change needs to be differentiated from many other diseases, such as pneumocystis carinii pneumonia, acute interstitial pneumonia, alveolar protein deposition, and diffuse alveolar hemorrhage. A ground-glass shadow can be used as a CT sign indicating cases with active TB infection with high amounts of *M. tuberculosis* and a strong delayed hypersensitivity response of the body (Im et al., 1993). Our results reinforce preceding observation by showing that the presentation of GGO is not only correlated with the presence of type I respiratory failure but also an independent risk prognostic factor of respiratory failure (Hashemian et al., 2015). Apart from that, pulmonary infiltrate or consolidation formed by the merge of vast granulomatous nodules is also an independent risk factor for respiratory failure (Herreros et al., 2018). When the imaging found a large area of GGO and pulmonary infiltrate or consolidation, we should be alert to the occurrence of ARDS and respiratory failure among miliary pulmonary TB patients. The incidence of miliary pulmonary TB in combination with ARDS is low, but the mortality rate is high, up to 47.06% (Kim et al., 2008).

Although all patients in our study survived and had a good response to antituberculous treatment combined with respiratory support including mask oxygen inhalation or mechanical ventilation, there were still some patients that died due to TB dissemination (Ma et al., 2021). Perhaps, women who survived from miliary TB can no longer conceive again. TB in pregnancy is associated with adverse fetal consequences like a roughly two-fold increased risk of premature birth, low birthweight, and intrauterine growth retardation, and a six-fold increased risk of perinatal death (WHO, 2021a). Only eight fetuses survived; the others had been spontaneous or induced abortions in this study. All the patients with successful pregnancies received first-line antituberculosis therapy, and one of them was treated with p-aminosalicylic acid. No deformity was found. Although the teratogenic risk of normal doses of antituberculosis drugs is very low, it may still cause some injury to the fetus, such as ototoxicity (Miele et al., 2020). No significant risk factors for fetal prognosis were identified in this study; intrauterine hypoxia will adversely affect the embryo. Early recognition of patients at high risk of respiratory failure and ARDS in disseminated TB infection is vital to improving the prognosis. Postnatal, one baby was reported with congenital TB. Similar cases with congenital TB after IVF-ET have been reported before (Zhang et al., 2018). The TB screening before IVF-ET is essential to decreasing the prevalence of congenital TB in neonates.

As far as we know, we have the largest sample size of pregnant patients with miliary pulmonary TB after IVF-ET. The strength of this study is that the characteristics of six patients of Xiangya Hospital were summarized and confirmed by the analysis of other patients included. In particular, the large extent of GGO in the early stage was found among patients with dyspnea in our hospital which had been proved to be an independent risk factor of respiratory failure, and the notion has not been reported before. Another highlight of this study is that the features of patients with successful pregnancies were analyzed, which could apply experiences to other doctor counterparts. The present study has several limitations. Firstly, this was a single-center

TABLE 6 | Differences between patients with respiratory failure and non-respiratory failure.

Variables (N = 75)	Respiratory failure (N = 15)	Non-respiratory failure (N = 60)	$\chi 2$	*P* value
Expectoration	9/15 (60.0)	18/60 (30.0)	4.688	0.030
Dyspnea	15/15 (100)	20/60 (33.3)	21.429	<0.001
Ground-glass opacity	4/10 (40.0)	1/45 (2.2)	14.129	<0.001
Pulmonary infiltrate or consolidation	8/10 (80.0)	10/45 (22.2)	12.406	<0.001

TABLE 7 | Univariate and multivariate binary logistic regression analysis showing independent radiologic predictors of respiratory failure in pregnant patients.

Variables (N = 75)	Univariate OR (95% CI)	*P* value	Multivariate OR (95% CI)	*P* value
Pulmonary infiltrate or consolidation	14.000 (2.554–76.744)	0.002	19.943 (2.159–184.213)	0.008
Calcification	1.833 (0.440–7.640)	0.405	–	–
Pleural effusion	4.393 (0.804–23.999)	0.088	–	–
Ground Ground-glass opacity	29.333 (2.793–308.027)	0.005	48.545 (2.366–995.974)	0.012

study; however, our hospital has cooperation with one of the largest reproductive specialty hospitals in China. Our patients come from all over the country and are representative. Secondly, the data for pooled analysis of retrospective studies are unavoidably incomplete in origin. We also acknowledge that not all the analyses could yield reliable results because of the relatively small sample size and missing data. However, pregnant patients with miliary TB after IVF-ET are rare and it is difficult to obtain a large multicenter series of cases for a prospective design. Therefore, our results should be considered as hypothesis-generating for future studies. Further studies are required to clarify whether complete screening of latent TB infection before IVF-ET could decrease the incidence of miliary TB during pregnancy and whether early awareness of the possibility of activation TB infection and accurate judgment of the severity of the condition could improve the maternal and fetal prognoses.

TABLE 8 | Characteristics of eight patients with successful pregnancies.

Case	Age, years	Time from received IVF-ET to onset of symptoms	History of tuberculosis	Clinical manifestations	Time from received IVF-ET to diagnosis of TB	Diagnosed method of pulmonary TB	Treatments	Complication	Fetal condition	References
Case 1	21	7 months	NA	Fever, cough, sputum, dyspnea, headache, disorders of consciousness	8 months	Clinically diagnosed	Isoniazid + rifampicin + pyrazinamide, hydrocortisone	Tuberculosis meningitis	Health baby, cesarean section at over 9 months	Liu et al., 2016
Case 2	31	69 days	None	Fever, dyspnea	90 days	Sputum PCR test positive	Isoniazid + rifampicin + pyrazinamide, prednisone	Type I respiratory failure	Health baby, cesarean section at term	Zhang et al., 2017
Case 3	29	70 days	None	Fever, headache	110 days	Clinically diagnosed	Isoniazid + rifampicin + pyrazinamide, prednisone	Tuberculosis meningitis	Health baby, preterm delivery at 32 weeks	Zhang et al., 2017
Case 4	34	3 months	None	Fever, cough, sputum, dyspnea, headache,	4 months	Clinically diagnosed	Isoniazid + rifampicin + pyrazinamide + ethambutol, dexamethasone	Tuberculosis meningitis, anemia, Hypoproteinemia	Health baby, preterm delivery at 7 months	Zhang, 2013
Case 5	21	13 weeks	NA	Cough, night sweat	NA	Sputum *Mycobacterium tuberculosis* culture positive	Isoniazid + pyrazinamide + ethambutol + p-Aminosalicylic acid	None	Baby diagnosed with severe congenital tuberculosis, cesarean section at term	Wen et al., 2016
Case 6	31	43 days	NA	Vaginal bleeding, dry cough, fever	60 days	Clinically diagnosed	Isoniazid + rifampicin + ethambutol,	None	Health baby, preterm delivery at over 7 months	Hou et al., 2005
Case 7	31	60 days	None	Vaginal bleeding, dry cough, fever	70 days	Clinically diagnosed	Isoniazid + rifampicin + pyrazinamide + ethambutol,	Type I respiratory failure	Health baby, preterm delivery at over 8 months	Chu et al., 2011
Case 8	29	109 days	None	Fever, cough, sputum, dyspnea	140 days	Clinically diagnosed	Isoniazid + rifampicin + pyrazinamide + ethambutol,	None	Health baby, cesarean section at term	-

CONCLUSION

After IVF-ET, patients with latent GTB or pulmonary TB are prone to the spread of *M. tuberculosis* resulting in miliary TB to the organs with rich blood supply including lung, brain, and the reproductive system due to the change of immune environment in pregnancy as well as the IVF-ET intervention. The coexistence of primary tube infertility and untreated pulmonary or extrapulmonary TB are risk factors for miliary TB. Screening patients with TB infection in high TB burden regions should be an important evaluation before IVF-ET. Unspecific manifestations, lack of awareness, and fear of radiation exposure could induce the delay of diagnosis and treatment of miliary pulmonary TB consequently leading to serious complications, poor prognosis, and even death. The appearance of specific radiographic findings especially GGO suggests that the patients are experiencing early stage and rapid progression of disease and are likely to suffer from respiratory failure. They need more attention and positive medication treatment and respiratory support therapy as well to improve the prognosis.

DATA AVAILABILITY STATEMENT

The original contributions presented in the study are included in the article/supplementary material. Further inquiries can be directed to the corresponding authors.

ETHICS STATEMENT

The studies involving human participants were reviewed and approved by the Ethics Committee of Xiangya Hospital, Central South University. The patients/participants in Xiangya Hospital provided their written informed consent to participate in the study. Informed consent was obtained from the individual(s) for the publication of any potentially identifiable images or data included in this article.

AUTHOR CONTRIBUTIONS

SD and RZ collected the data. SD and RZ wrote the draft of the manuscript. RH and EP designed and edited the manuscript. RH conducted the study. All authors contributed to the article and approved the submitted version.

FUNDING

This work was supported by the Natural Science Foundation of Hunan Province (grant numbers: 2020JJ5897, 2020JJ4904). The National Natural Science Foundation of China (grant number:81400022)

REFERENCES

Addis, G. M., Anthony, G. S., d'A Semple, P., and Miller, A. W. (1988). Miliary Tuberculosis in an *In-Vitro* Fertilization Pregnancy: A Case Report. *Eur. J. Obstetrics gynecol. Reprod. Biol.* 27 (4), 351–353. doi: 10.1016/0028-2243(88)90049-4

Aliyu, M. H., Aliyu, S. H., and Salihu, H. M. (2004). Female Genital Tuberculosis: A Global Review. *Int. J. fertil. Women's Med.* 49 (3), 123–136.

Briceag, I, Costache, A, Purcarea, VL, Cergan, R, Dumitru, M, Briceag, I, et al. (2015). Fallopian Tubes–Literature Review of Anatomy and Etiology in Female Infertility. *J Med Life*. 8 (2), 129–131.

CDC (2015). Reported Tuberculosis in the United States: Tuberculosis Cases and Percentages by Case Verification Criterion and Site of Disease: United States, 1993–2015. (Centers for Disease Control and Prevention).

Chu, J., Qian, G., Xuan, Y., and Li, G. (2011). Acute Millary Pulmonary Tuberculosis in Pregnant Women After *In Vitro* Fertilization Pre-Embryo Transfer: A Report of Two Cases. *Chin. J. Clin. Infect. Dis.* 4, 378–379. doi: 10.3760/ cma.j.issn.167-2397.2011.06.016

Dam, P., Shirazee, H. H., Goswami, S. K., Ghosh, S., Ganesh, A., Chaudhury, K., et al. (2006). Role of Latent Genital Tuberculosis in Repeated IVF Failure in the Indian Clinical Setting. *Gynecol. obstetric Invest.* 61 (4), 223–227. doi: 10.1159/000091498

Deng, W., Yu, M., Ma, H., Hu, L. A., Chen, G., Wang, Y., et al. (2012). Predictors and Outcome of Patients With Acute Respiratory Distress Syndrome Caused by Miliary Tuberculosis: A Retrospective Study in Chongqing, China. *BMC Infect. Dis.* 12, 121. doi: 10.1186/1471-2334-12-121

Gai, X., Chi, H., Zeng, L., Cao, W., Chen, L., Zhang, C., et al. (2021). Impact of Positive Interferon-Gamma Release Assay on IVF-ET Pregnancy Outcomes in Infertile Patients With Untreated Prior Tuberculosis: A Prospective Cohort Study. *Front. Med.* 8, 749410. doi: 10.3389/fmed.2021.749410

Ghosh, K., Ghosh, K., and Chowdhury, J. R. (2011). Tuberculosis and Female Reproductive Health. *J. Postgraduate Med.* 57 (4), 307–313. doi: 10.4103/0022-3859.90082

Gull, I., Peyser, M. R., Yaron, Y., Jaffa, A. J., Amit, A., and Lessing, J. B. (1995). The Effect of an *In-Vitro* Fertilization Pregnancy on a Woman With Genital Tuberculosis. *Hum. Reprod. (Oxford England)* 10 (11), 3052–3054. doi: 10.1093/oxfordjournals.humrep.a135846

Han, X., Gao, W., Huang, X., and Ma, Y. (2009). Analysis on 202 Adult Patients With Hematogenous Pulmonary Tuberculosis. *Chin. J. Antituberculosis* 31 (7), 425–429.

Hashemian, S. M., Tabarsi, P., Karam, M. B., Kahkouee, S., Marjani, M., Jamaati, H., et al. (2015). Radiologic Manifestations of Pulmonary Tuberculosis in Patients of Intensive Care Units. *Int. J. Mycobacteriol.* 4 (3), 233–238. doi: 10.1016/j.ijmyco.2015.05.008

Herreros, B., Plaza, I., García, R., Chichón, M., Guerrero, C., and Pintor, E. (2018). Miliary Tuberculosis Presenting With Hyponatremia and ARDS in an 82-Year-Old Immunocompetent Female. *Pathog. (Basel Switzerland)* 7 (3), 72. doi: 10.3390/pathogens7030072

Hou, X., Zhang, Z., and Liu, L. (2005). A Case of Twin Twins Complicated With Acute Miliary Pulmonary Tuberculosis Survived After IVF-ET. *Chin. J. Birth Health Heredity* 13, 92.

Hunter, R. L. (2018). The Pathogenesis of Tuberculosis: The Early Infiltrate of Post-Primary (Adult Pulmonary) Tuberculosis: A Distinct Disease Entity. *Front. Immunol.* 9, 2108. doi: 10.3389/fimmu.2018.02108

Im, JG, Itoh, H, and Han, MC. (1995). CT of Pulmonary Tuberculosis. *Semin Ultrasound CT MR*. 16(5):420–34. doi: 10.1016/0887-2171(95)90029-2

Im, J. G., Itoh, H., Shim, Y. S., Lee, J. H., Ahn, J., Han, M. C., et al. (1993). Pulmonary Tuberculosis: CT Findings–Early Active Disease and Sequential Change With Antituberculous Therapy. *Radiology* 186 (3), 653–660. doi: 10.1148/radiology.186.3.8430169

Jacquemyn, Y., Van Casteren, C., Luijks, M., and Colpaert, C. (2012). Disseminated Tuberculosis in Pregnancy Unknown to Doctors in Western Europe Case Presentation: 'Part of the Routine Study in Infertility'. *BMJ Case Rep.*, bcr2012006227. doi: 10.1136/bcr-2012-006227

Jonsson, J., Kühlmann-Berenzon, S., Berggren, I., and Bruchfeld, J. (2020). Increased Risk of Active Tuberculosis During Pregnancy and Postpartum: A

Register-Based Cohort Study in Sweden. *Eur. Respir. J.* 55 (3), 1901886. doi: 10.1183/13993003.01886-2019

Kim, Y. J., Pack, K. M., Jeong, E., Na, J. O., Oh, Y. M., Lee, S. D., et al. (2008). Pulmonary Tuberculosis With Acute Respiratory Failure. *Eur. Respir. J.* 32 (6), 1625–1630. doi: 10.1183/09031936.00070907

Lee, J., Lim, J. K., Seo, H., Lee, S. Y., Choi, K. J., Yoo, S. S., et al. (2014). Clinical Relevance of Ground Glass Opacity in 105 Patients With Miliary Tuberculosis. *Respir. Med.* 108 (6), 924–930. doi: 10.1016/j.rmed.2014.03.016

Liu, G., Ye, J., Sun, W., Bai, D., and Mei, Z. (2016). Clinical Analysis of Pregnant Women Complicated With Acute Hematogenous Disseminated Tuberculosis and ARDS After IVF-ET. *Contin. Med. Educ.* 30, 108–109. doi: 10.3969.j.issn.1004-6763.2016.05.064

Li, H., and Zhao, L. (2015). Miliary Tuberculosis After *In Vitro* Fertilization and Embryo Transplantation. *Afr. Health Sci.* 15 (2), 701–704. doi: 10.4314/ahs.v15i2.50

Madhukar, Pai, Amrita, Daftary, and Srinath, Satyanarayana. (2016). TB Control: Challenges and Opportunities for India. *Trans. R. Soc. Trop. Med. Hyg.* 110 (3):158–160. doi: 10.1093/trstmh/trw003

Malhotra, N., Singh, U. B., Iyer, V., Gupta, P., and Chandhiok, N. (2020). Role of Laparoscopy in the Diagnosis of Genital TB in Infertile Females in the Era of Molecular Tests. *J. Minimally Invasive Gynecol.* 27 (7), 1538–1544. doi: 10.1016/j.jmig.2020.01.005

Mali, P. C., and Meena, L. S. (2018). Triacylglycerol: Nourishing Molecule in Endurance of Mycobacterium Tuberculosis. *J. Biosci.* 43 (1), 149–154. doi: 10.1007/s12038-018-9729-6

Ma, H., Sun, J., Zhang, L., Liu, Y., Liu, H., Wu, X., et al. (2021). Disseminated Hematogenous Tuberculosis Following *In Vitro* Fertilization-Embryo Transfer: A Case Report. *Infect. Drug Resistance* 14, 4903–4911. doi: 10.2147/IDR.S332992

McGuinness, G., Naidich, D. P., Jagirdar, J., Leitman, B., and McCauley, D. I. (1992). High Resolution CT Findings in Miliary Lung Disease. *J. Comput. Assisted tomogr.* 16 (3), 384–390. doi: 10.1097/00004728-199205000-00009

Miele, K., Bamrah Morris, S., and Tepper, N. K. (2020). Tuberculosis in Pregnancy. *Obstetrics. Gynecol.* 135 (6), 1444–1453. doi: 10.1097/AOG.0000000000003890

Mor, G., and Cardenas, I. (2010). The Immune System in Pregnancy: A Unique Complexity. *Am. J. Reprod. Immunol. (New York N.Y.: 1989)* 63 (6), 425–433. doi: 10.1111/j.1600-0897.2010.00836.x

Moule, M. G., and Cirillo, J. D. (2020). Mycobacterium Tuberculosis Dissemination Plays a Critical Role in Pathogenesis. *Front. Cell. Infect. Microbiol.* 10. doi: 10.3389/fcimb.2020.00065

Muneer, A., Macrae, B., Krishnamoorthy, S., and Zumla, A. (2019). Urogenital Tuberculosis-Epidemiology, Pathogenesis and Clinical Features. *Nat. Rev. Urol.* 16 (10), 573–598. doi: 10.1038/s41585-019-0228-9

Pai, M., Nicol, M. P., and Boehme, C. C. (2016). Tuberculosis Diagnostics: State of the Art and Future Directions. *Microbiol. Spectr.* 4 (5). doi: 10.1128/microbiolspec.TBTB2-0019-2016

Pai, M., Zwerling, A., and Menzies, D. (2008). Systematic Review: T-Cell-Based Assays for the Diagnosis of Latent Tuberculosis Infection: An Update. *Ann. Intern. Med.* 149, 177. doi: 10.7326/0003-4819-149-3-200808050-00241

Plaks, V., Kalchenko, V., Dekel, N., and Neeman, M. (2006). MRI Analysis of Angiogenesis During Mouse Embryo Implantation. *Magnetic. resonance Med.* 55 (5), 1013–1022. doi: 10.1002/mrm.20881

Schumacher, A. (2017). Human Chorionic Gonadotropin as a Pivotal Endocrine Immune Regulator Initiating and Preserving Fetal Tolerance. *Int. J. Mol. Sci.* 18 (10), 2166. doi: 10.3390/ijms18102166

Sharma, J. B. (2015). Current Diagnosis and Management of Female Genital Tuberculosis. *J. Obstet. Gynaecol. India* 65, 362–371. doi: 10.1007/s13224-015-0780-z

Sharma, S. K., and Mohan, A. (2017). Miliary Tuberculosis. *Microbiol. Spectr.* 5 (2) 2071: TNMI7-0013-2016. doi: 10.1128/microbiolspec.TNMI7-0013-2016

Singh, N., and Perfect, J. R. (2007). Immune Reconstitution Syndrome and Exacerbation of Infections After Pregnancy. *Clin. Infect. dis.* 45 (9), 1192–1199. doi: 10.1086/522182

Sobhy, S., Babiker, Z., Zamora, J., Khan, K. S., and Kunst, H. (2017). Maternal and Perinatal Mortality and Morbidity Associated With Tuberculosis During Pregnancy and the Postpartum Period: A Systematic Review and Meta-Analysis. *BJOG: An Int. J. Obstetrics Gynaecol.* 124 (5), 727–733. doi: 10.1111/1471-0528.14408

Sugarman, J., Colvin, C., Moran, A. C., and Oxlade, O. (2014). Tuberculosis in Pregnancy: An Estimate of the Global Burden of Disease. *Lancet Global Health* 2 (12), e710–e716. doi: 10.1016/S2214-109X(14)70330-4

Wang, K., Ren, D., Qiu, Z., and Li, W. (2022). Clinical Analysis of Pregnancy Complicated With Miliary Tuberculosis. *Ann. Med.* 54, 71–79. doi: 10.1080/07853890.2021.2018485

Wen, X., Xia, L., Xi, X., Li, F., and Lu, S. (2016). Clinical Analysis of Seven Tuberculosis Patients in Pregnant Women After *In Vitro* Fertilization and Embryo Transfer. *J. Tuberc. Lung Health* 5, 135–139. doi: 10.3969/ j.issn.2095-3755.2016.02.017

WHO (2021a). *Global Tuberculosis Report 2021* (Geneva: World Health Organization).

WHO (2021b). *WHO Consolidated Guidelines on Tuberculosis. Module 3: Diagnosis – Rapid Diagnostics for Tuberculosis Detection 2021 Update* (Geneva: World Health Organization).

WHO (2021c). *WHO Consolidated Guidelines on Tuberculosis. Module 2: Screening – Systematic Screening for Tuberculosis Disease 2021 Update* (Geneva: World Health Organization).

Ye, R., Wang, C., Zhao, L., Wu, X., Gao, Y., and Liu, H. (2019). Characteristics of Miliary Tuberculosis in Pregnant Women After *In Vitro* Fertilisation and Embryo Transfer. *Int. J. Tuberc. Lung Dis.* 23, 136–139. doi: 10.5588/ijtld.18.0223

Zhang, W. (2013). One Case Report of Acute Miliary Tuberculosis Complicated With Tuberculous Meningitis After *In Vitro* Fertilization-Embryo Transfer. *Gansu Med. J.* 32, 79–80.

Zhang, P., Cao, W., Zheng, J., Fu, L., Ye, T., and Deng, G. (2017). Clinical Characteristics and Pregnant Outcome of 5 Women With Hematogenous Pulmonary Tuberculosis After *In Vitro* Fertilization and Embryo Transplant. *Electronic J. Emerging Infect. Dis.* 2, 231–233.

Zhang, X., Ren, Z., Xu, F., Zhang, Q., Yang, H., Chen, L., et al. (2018). Congenital Tuberculosis After *In Vitro* Fertilization: Suggestion for Tuberculosis Tests in Infertile Women in Developing Countries. *J. Int. Med. Res.* 46, 5316–5321. doi: 10.1177/0300060518808179

Conflict of Interest: The authors declare that the research was conducted in the absence of any commercial or financial relationships that could be construed as a potential conflict of interest.

Publisher's Note: All claims expressed in this article are solely those of the authors and do not necessarily represent those of their affiliated organizations, or those of the publisher, the editors and the reviewers. Any product that may be evaluated in this article, or claim that may be made by its manufacturer, is not guaranteed or endorsed by the publisher.

Advantages of publishing in Frontiers

OPEN ACCESS
Articles are free to read for greatest visibility and readership

FAST PUBLICATION
Around 90 days from submission to decision

HIGH QUALITY PEER-REVIEW
Rigorous, collaborative, and constructive peer-review

TRANSPARENT PEER-REVIEW
Editors and reviewers acknowledged by name on published articles

Frontiers
Avenue du Tribunal-Fédéral 34
1005 Lausanne | Switzerland

Visit us: www.frontiersin.org
Contact us: frontiersin.org/about/contact

REPRODUCIBILITY OF RESEARCH
Support open data and methods to enhance research reproducibility

DIGITAL PUBLISHING
Articles designed for optimal readership across devices

FOLLOW US
@frontiersin

IMPACT METRICS
Advanced article metrics track visibility across digital media

EXTENSIVE PROMOTION
Marketing and promotion of impactful research

LOOP RESEARCH NETWORK
Our network increases your article's readership